Expanding Human Gut Microbiome Diversity Beyond Western Populations: Methanogens and Helminths

Dissertation

der Mathematisch-Naturwissenschaftlichen Fakultät
der Eberhard Karls Universität Tübingen
zur Erlangung des Grades eines
Doktors der Naturwissenschaften
(Dr. rer. nat.)

vorgelegt von
Mirabeau Mbong Ngwese
aus Tombel, Kamerun

Tübingen
2026

Gedruckt mit Genehmigung der Mathematisch-Naturwissenschaftlichen Fakultät der Eberhard Karls Universität Tübingen.

Tag der mündlichen Qualifikation:	15.07.2026
Dekan:	Prof. Dr. Thilo Stehle
1. Berichterstatterin:	Prof. Dr. Ruth E. Ley
2. Berichterstatterin:	Prof. Dr. Nadine Ziemert

Summary

The human gut harbors a constantly changing community of microbes that influences the immune system and affects many aspects of host health. Within this community are not only bacteria, but also eukaryotic parasites and methanogenic archaea, whose contributions are important, yet often overlooked. Soil-transmitted helminths (STHs) are common and endemic in most parts of sub-Saharan Africa, thriving in poor sanitation and causing chronic illnesses such as anaemia. These STH infections modulate the host immune system and can substantially alter the host gut microbiome composition. In parallel, methanogens such as *Methanobrevibacter smithii* play a central role in hydrogen metabolism and support microbial fermentation through close interactions with bacterial communities. However, the relationships between parasites and microbiota, and the diversity of methanogens outside Western populations, are not well described. This thesis clarifies two main findings from a study of an African population: (1) metagenomic sequencing reliably detects STH infections and reveals their associations with specific shifts in gut microbial diversity, and (2) comparative genomics uncovers new diversity and geographical structuring of *Methanobrevibacter* species, revealing distinct evolutionary patterns for human-associated archaea across continents.

In the first part, I performed metagenomic and qPCR analyses of stool samples from 310 Gabonese individuals. I showed that k-mer counts from metagenomic sequencing strongly correlate with qPCR for some STH parasites, confirming the effectiveness of metagenomics in detecting both parasites and bacteria. I observed significant changes in microbial alpha and beta diversity associated with parasite burden, particularly across different locations and age groups. These findings show that geography plays a significant role in how STH parasites interact with the gut microbiome, and demonstrate that metagenomic sequence data provide an effective method for linking parasite detection to microbial ecology.

In the second part, I performed targeted enrichment and isolation of *Methanobrevibacter* species from Gabon, Germany, and Vietnam, which enabled the first cultivation of *M. intestini* from Central Africa. I expanded this cultivation effort to obtain 200 strains, predominantly of *M. smithii* and *M. intestini*, from Gabon, Germany, and Vietnam. Using both Average Nucleotide Identity (ANI) and phylogenetic analyses based on single-copy marker genes, we found that *M. smithii* and *M. intestini* are distinct, confirming that they are separate species. Using whole-genome

synteny analysis, we also identified hypervariable genomic regions enriched for adhesins, mobile-element–associated functions, and defense genes. Also, key to our findings is the observed evolutionary pattern of partial co-divergence between human hosts and *M. smithii*, supporting long-term host–archaea relationships shaped by environmental and host-biological factors.

This work integrates metagenomic detection of parasites, cultivation, and comparative genomics to bridge ecological and evolutionary perspectives of the human archaeome. Among others, this work's contributions include the first cultivation-based identification of *M. intestini* in Central Africa, the demonstration of the geographical structuring of *Methanobrevibacter* diversity, and evidence that integrating parasite and archaeal data advances understanding of gut ecosystem complexity.

Zusammenfassung

Der menschliche Darm beherbergt eine dynamische Gemeinschaft von Mikroorganismen, die das Immunsystem beeinflusst und zahlreiche Aspekte der Gesundheit des Wirts prägt. Zu dieser Gemeinschaft gehören nicht nur Bakterien, sondern auch eukaryotische Parasiten und methanogene Archaeen, deren Beiträge wichtig sind, jedoch häufig übersehen werden. Bodenübertragene Helminthen (soil-transmitted helminths, STH) sind in weiten Teilen Subsahara-Afrikas weit verbreitet und endemisch; sie gedeihen unter Bedingungen mangelhafter Sanitärversorgung und verursachen chronische Erkrankungen wie Anämie. STH-Infektionen modulieren das Immunsystem des Wirts und können die Zusammensetzung des intestinalen Mikrobioms erheblich verändern. Parallel dazu spielen Methanogene wie *Methanobrevibacter smithii* eine zentrale Rolle im Wasserstoffstoffwechsel und unterstützen mikrobielle Fermentationsprozesse durch enge Interaktionen mit bakteriellen Gemeinschaften. Die Wechselwirkungen zwischen Parasiten und Mikrobiota sowie die Diversität methanogener Archaeen außerhalb westlicher Populationen sind jedoch bislang nur unzureichend beschrieben. Diese Dissertation klärt zwei zentrale Ergebnisse aus der Untersuchung einer afrikanischen Population: (1) Metagenomische Sequenzierung ermöglicht eine zuverlässige Detektion von STH-Infektionen und deckt deren Assoziationen mit spezifischen Veränderungen der mikrobiellen Diversität im Darm auf, und (2) vergleichende Genomanalysen zeigen eine bislang unbekannte Diversität und geographische Strukturierung von *Methanobrevibacter*-Arten und offenbaren unterschiedliche evolutionäre Muster humanassoziierter Archaeen über Kontinente hinweg.

Im ersten Teil führte ich metagenomische Analysen und qPCR-Untersuchungen von Stuhlproben aus 310 gabunischen Individuen durch. Ich konnte zeigen, dass k-Mer-Zählungen aus metagenomischen Sequenzdaten für einige STH-Parasiten stark mit qPCR-Ergebnissen korrelieren, was die Eignung der Metagenomik zur Detektion sowohl von Parasiten als auch von Bakterien bestätigt. Zudem beobachtete ich signifikante Veränderungen der mikrobiellen Alpha- und Beta-Diversität in Abhängigkeit von der Parasitenlast, insbesondere zwischen verschiedenen geographischen Standorten und Altersgruppen. Diese Ergebnisse zeigen, dass die Geographie eine wesentliche Rolle bei den Interaktionen zwischen STH-Parasiten und dem Darmmikrobiom spielt, und belegen, dass metagenomische Sequenzdaten eine effektive Methode zur Verknüpfung von Parasitendetektion und mikrobieller Ökologie darstellen.

Im zweiten Teil führte ich eine gezielte Anreicherung und Isolierung von *Methanobrevibacter*-Arten aus Gabun, Deutschland und Vietnam durch, wodurch erstmals *M. intestini* aus Zentralafrika kultiviert werden konnte. Diese Kultivierungsarbeiten wurden erweitert und führten zur Gewinnung von insgesamt 200 Stämmen, überwiegend *M. smithii* und *M. intestini*, aus Gabun, Deutschland und Vietnam. Mithilfe von Analysen der durchschnittlichen Nukleotididentität (Average Nucleotide Identity, ANI) sowie phylogenetischen Analysen auf Basis von Single-Copy-Markergenen konnte gezeigt werden, dass *M. smithii* und *M. intestini* klar voneinander abgegrenzte Arten sind. Darüber hinaus identifizierten wir mittels Ganzgenom-Syntenieanalysen hypervariable genomische Regionen, die angereichert sind für Adhäsine, Funktionen im Zusammenhang mit mobilen genetischen Elementen sowie Abwehrmechanismen. Von zentraler Bedeutung ist zudem das beobachtete evolutionäre Muster einer partiellen Ko-Divergenz zwischen menschlichen Wirten und *M. smithii*, welches langfristige Wirt–Archaeen-Beziehungen unterstützt, die durch Umweltfaktoren und wirtsbiologische Eigenschaften geprägt sind.

Diese Arbeit integriert die metagenomische Detektion von Parasiten, Kultivierung und vergleichende Genomik, um ökologische und evolutionäre Perspektiven des humanen Archaeoms miteinander zu verbinden. Zu den wichtigsten Beiträgen dieser Arbeit zählen unter anderem die erste kultivierungsbasierte Identifikation von *M. intestini* in Zentralafrika, der Nachweis einer geographischen Strukturierung der *Methanobrevibacter*-Diversität sowie die Evidenz dafür, dass die Integration von Parasiten- und Archaeen-Daten das Verständnis der Komplexität des intestinalen Ökosystems wesentlich vertieft.

Acknowledgements

Every academic path carries its own challenges. Yet, when shared with the right people at the right time and place, the journey becomes not only manageable but deeply fulfilling. I feel genuinely privileged to have worked alongside such an enthusiastic, knowledgeable, and generous group of scientists.

I want to express my sincere gratitude to Ruth Ley for allowing me to join her research group and undertake this project despite my limited background in the field. She provided me with the freedom and flexibility to integrate my background as a parasitologist into microbiome research, allowing me to grow into a more mature and independent scientist.

I am deeply grateful to my supervisor, Nicholas Youngblut, whose guidance and patience were invaluable throughout this journey. He endured my countless questions and took on the challenge of introducing me to anaerobic culturing, helping to establish protocols and bioinformatic pipelines, and guiding me step by step toward the successful completion of this work. I could not have accomplished this without his continuous support.

My laboratory experience was greatly enriched by the support of Sophie Maisch, Silker Dauser, Alina Prokipchuk and Stephen Loum, who assisted me with the preparation of anaerobic culture media, stool enrichments, DNA extractions, library preparation, and sequencing. As my work increasingly shifted toward bioinformatics, I received tremendous support from Nicholas Youngblut, Jacobo de la Cuesta, Leonardo Moreno, Guillermo Luque, and Alexander Tyakht. I am especially grateful to Nicholas Youngblut and Alexander Tyakht, whose offices I frequently visited whenever I found myself stuck with bioinformatic analyses. I likely occupied more of their time than I deserved, and I truly appreciate their generosity and patience.

I also wish to thank my TAC committee members (Nadine Ziemert and Hassan Salem) for their constructive feedback, which was instrumental in strengthening this work. My sincere thanks go to Lara Berg, who began as my Master's student and did an outstanding job conducting growth curve experiments and generating scanning electron micrographs of some of our cultured strains. I am equally thankful to James Marsh, with whom I worked extensively on submitting our strain as a type strain variant, analysing data, and preparing two manuscripts.

I met Victor Schmidt and Liam Fitzstevens back in Gabon, even before the start of my PhD, and both of you played a crucial role in helping me settle in Tübingen and begin this new chapter of my life as a doctoral student. Beyond your friendship and support, your scientific contribution to this work was truly invaluable. The extensive sampling efforts you carried out

across three continents laid the foundation for this thesis, and much of the data I analyzed throughout my PhD was made possible by your dedication and hard work in the field. I am deeply grateful not only for the many fun memories we shared in Gabon and in Tübingen, but also for the fundamental role you both played in the success of this project.

Special thanks also go to our collaborators at the Centre de Recherches Médicales de Lambaréné and the Institute for Tropical Medicine Tübingen, in particular Akim Ayola and Peter Kremsner for their constructive comments and commitment. My gratitude extends to Karin Klein, Heike Budde and Stephanie Forthaus-Kurz for their invaluable administrative support. I feel indebted to the entire department for providing such a stimulating and supportive environment.

I am thankful for the encouragement and scientific feedback from Kelsey Huus, Stacey Heaver, Hagay Enav, Inbal Paz, Andrea Borbon, Megna Chatterjee, Jan Kisker, and for the shared jokes and small chit-chats with my office mates, Xiaoying Liu, Yihua Liu, Hagay Enav, and Tony Walters, and everyone else in the lab. Working with each of you was inspiring, enjoyable, and intellectually enriching.

Beyond the science, I cherish the friendships formed along the way, memories of laughter, and even playing midweek and Sunday morning football at SSC Tübingen with colleagues, a hobby I love.

I want to dedicate this thesis to my late father, who could not witness this milestone. I know you would be proud. To my mother, Anna Ahone, my siblings Samuel Ngwese, Liliane Ngwese, and Carolin Ngwese, thank you for your unwavering support. To my beloved wife, Dibora Mande, and our son, Nathan Ngwese: you have been my rock and my constant source of strength. Finally, I thank God for granting me the health, strength, and perseverance to complete this journey.

Table of Contents

List of Abbreviations

µL	Microliter
mM	Millimolar
mg/mL	Milligram per millilitre
BSA	Bovine Serum Albumin
nM	Nanomolar
DNA	Deoxyribonucleic Acid
PCR	Polymerase Chain Reaction
qPCR	Quantitative Polymerase Chain Reaction
Ct	Cycle Threshold
PhHV-1	Phocine Herpesvirus 1
STH	Soil Transmitted Helminths
WHO	World Health Organisation
MDA	Mass Drug Administration
%	Percentage
s.d.	Standard deviation
FDR	False Discovery Rate
χ^2	Chi-squared
RELMβ	Resistin-like molecule-beta
TFF1/2	Trefoil factor 1/2
IL	Interleukin
ME	Methanogen Enrichment
ANI	Average Nucleotide Identity
M.	*Methanobrevibacter*

List of figures

List of tables

List of publications

Published

Ngwese MN, Loum S, Berg L, Tyakht AV, Youngblut ND, Adegnika AA, Kremsner PG, Ley RE, Marsh JW. Genomic and phenotypic characterization of a human gut *Methanobrevibacter intestini* strain G0370_i3 isolated in Gabon. Future Microbiol. 2026 Feb; 21 (3): 265-277. doi: 10.1080/17460913.2026.2645510.

Ngwese MM, Adegbite BR, Zinsou JF, Fitzstevens JL, Schmidt VT, Moure PAN, Maloum MN, Tyakht AV, Huus KE, Youngblut ND, Kremsner PG, Adegnika AA, Ley RE. Infection with gut parasites correlates with gut microbiome diversity across human populations in Africa. Gut Microbes. 2025 Dec 31;17(1):2587966. doi: 10.1080/19490976.2025.2587966.

Suzuki TA, Fitzstevens JL, Schmidt VT, Enav H, Huus KE, **Ngwese MM**, Grießhammer A, Pfeiderer A, Adegbite BR, Zinsou JF, Esen M, Velavan TP, Adegnika AA, Song LH, Spector TD, Muehlbauer AL, Marchi N, Kang H, Maier L, Blekhman R, Ségurel L, Ko G, Youngblut ND, Kremsner PG, Ley RE. Codiversification of gut microbiota with humans.Science. 2022; 377:1328–32. http://dx.doi.org/10.1126/science.abm7759

Advanced manuscript awaiting submission to target journal

Ngwese MN, Berg L, Kisker JP, Enav H. Paz I, Tyakht AV, Heaver SL, Adegnika AA, Kremsner PG, Youngblut ND, Ley RE, Marsh JW. Strain-resolved metagenomics and phylogenomics of human gut *Methanobrevibacter* spp. reveals Africa–Eurasia biogeographic patterns.

Introduction

Context and Rationale

The human gut microbiota is a complex community of microorganisms, including bacteria, viruses, fungi, and archaea, each of which plays an important role in host physiology and immunity. Through microbiome studies, our understanding of how microbial interactions shape health and disease has dramatically improved. These findings prompted efforts to identify beneficial microbes for probiotics. Thanks to sequencing technologies and bioinformatics, research on the gut microbiota has expanded rapidly.

Despite progress, most research on the gut microbiota focuses on Western populations, overlooking regions like Africa. The lack of representation of non-Western populations leaves gaps in our understanding of global microbial diversity and its health relevance. Key interests include how the gut microbiota interact with other residents, such as soil-transmitted helminths (STH) and methanogenic archaea, such as *Methanobrevibacter*. Four worm species listed by the WHO as neglected tropical diseases cause STH infections: Ascaris lumbricoides, Trichuris trichiura, Strongyloides stercoralis, and hookworms (*Necator americanus* and *Ancylostoma duodenale*). The WHO estimates 1.5 billion people—mainly in sub-Saharan Africa—have STH infections (WHO, 2020). How STH infections affect the gut microbiota remains poorly understood, especially in endemic areas.

Methanobrevibacter is the main archaeal genus in the human gut and a key part of its ecology. Most research focuses on *Methanobrevibacter smithii*, mainly from Western isolates, while the diversity and history of other species, such as *M. intestini*, are less well known. Studying *Methanobrevibacter* diversity across populations sheds light on how these archaea evolve and interact with bacteria in different environments.

This thesis demonstrates the importance of geographical representation for understanding how STH parasites and methanogens interact with the gut microbiome. To address this, I analyzed samples from Gabon, Vietnam, and Germany—three countries spanning three continents—to move beyond the traditional Western focus of microbiome research. The thesis has three main overarching aims: an evaluation of gut STH parasite infections using metagenomic sequencing and an examination of their associations with gut microbial diversity and community composition in African populations where these parasites remain prevalent.

To isolate, sequence, and characterize *Methanobrevibacter* strains, including *M. intestini* obtained from non-Western microbiomes, thereby contributing new variants of reference genomes and expanding our knowledge of archaeal diversity.

To integrate cultivation and metagenomic surveys across different populations, this thesis examines how geography affects methanogen prevalence, bacterial co-occurrence, and evolutionary change.

By focusing on STH parasites and archaeal diversity, this thesis highlights the value of including diverse populations in microbiome studies. Recognizing these differences enriches our understanding of the global human microbiome and helps create representative models of host–microbe–parasite interactions. This section outlines the thesis structure and previews the five chapters that follow. I summarize key contributions and suggest future research.

Chapter 1: Background on Soil-Transmitted Helminths (STH) and the Gut Microbiome.

This chapter focuses on the biology and distribution of STH infections in endemic regions. The chapter also explores interactions between STH infections and the gut microbiome, highlighting the dynamic and often reciprocal relationships between parasites and resident microbes.

An important issue addressed here is the strong geographic bias in microbiome research. Most existing datasets come from Western populations, where STH exposure is rare. STH infections can alter microbiome composition, so the underrepresentation of endemic populations limits our understanding of parasite–microbiota interactions and their effects on host health. Associations between STH burden and the gut microbiome vary widely between studies. This variation is due to both biological differences and inconsistencies in study design, sample handling, sequencing, and parasite detection methods.

This chapter discusses the challenges outlined above and focuses on methodological improvements, including the need for robust and standardized detection strategies. It also describes the advantages of metagenomic approaches, which allow simultaneous profiling of parasites, bacteria, archaea, and other microbial groups. Together, the background presented in this chapter establishes the rationale for the empirical analyses that follow, which investigate STH prevalence, burden, and microbiome associations in underrepresented populations.

Chapter 2: Infection with gut parasites correlates with gut microbiome diversity across human populations in Africa.

This chapter addresses the limitations outlined in Chapter 1 by employing a metagenomic approach to detect STH parasites directly from sequencing data. Unlike traditional workflows that require separate parasite diagnostics followed by group comparisons, this approach enables simultaneous exploration of parasites and microbiota within the same dataset.

Gabon is located in central Africa and is endemic to STH parasites. Thus, I first focus on Gabon, a high-prevalence setting, comparing metagenomic parasite detection with qPCR as a reference. I observed strong agreement between qPCR results and k-mer counts from the metagenome. I then applied the same approach to additional African datasets to assess their performance across populations and to examine STH-microbiome relationship across different populations. This framework demonstrates how metagenomic data can simplify parasite detection, reduce diagnostic bottlenecks, and support scalable comparisons across studies.

Beyond identifying associations between STH burden and microbiome diversity, this approach also enables co-occurrence network exploration to examine the different cross-domain interactions, particularly between bacteria and archaea or bacteria and STH parasites, using standardized data.

This methodological innovation, using metagenomes for both parasite detection and microbiome profiling, bridges the diagnostic gap and sets up deeper investigation of archaea and their ecological roles in Chapters 3 to 5.

Chapter 3: Background on Human Gut Methanogens.

This chapter introduces methanogenic archaea as key, yet understudied, members of the human gut microbiome. Methanogens play central roles in anaerobic metabolism, including hydrogen turnover and methane production, yet much of what we know about their diversity, ecology, and function comes from studies of Western populations. As a result, the global diversity and population structure of human-associated methanogens remain incompletely resolved.

This chapter then provides an overview of the taxonomy of dominant gut methanogens, highlighting their reported prevalence across different human populations worldwide. It then focuses on *M. smithii*, the most dominant and most described human-gut-associated methanogen species, to describe its genome architecture, metabolic capacities, ecological roles, and reported clinical and physiological associations. The chapter also addresses evolutionary dynamics,

including heritability, host-microbe coevolution, ecological partitioning, and the emergence of *M. intestini* in human populations.

It also highlights the scarcity of cultivated isolates from diverse human populations, a gap that limits our ability to link genomic variation to ecological traits or host biology. These limitations form the foundation for the empirical studies in this thesis, which integrate metagenomics, phylogenomics, and cultivation to provide insights into methanogen diversity, distribution, and evolution.

Chapter 4: Genomic and phenotypic characterization of a human gut Methanobrevibacter intestini strain G0370_i3 isolated in Gabon.

This chapter builds on the metagenomic analysis presented in Chapter 2 by demonstrating that cultivation can uncover previously unknown diversity and further our understanding of archaeal diversity in the human gut. Here, I isolate a *Methanobrevibacter* species from human stool and confirm its identification as *Methanobrevibacter* intestini, in agreement with previous reports(Low et al., 2022; Weinberger et al., 2025). Although type strains/variants of *M. intestini* and other variants exist, this is the first from an African population, underscoring the importance of geographic representation in cultivation-based research.

Detailed characterization of the isolate includes its phylogenetic lineage, metabolic potential, and optimal growth requirements. This Gabonese isolate (*M. intestini* G0370_i3) has been submitted as a variant of the published type strain (*M. intestini* WWM1085), making it available for comparative and evolutionary analyses.

This work highlights the ecological and functional dimension of gut methanogens. Cultivation not only validates metagenomic observations but also enables experimental follow-up on metabolism and host interactions. By linking cultivation to questions of geography and function, this chapter provides a crucial foundation for the broader evolutionary and ecological comparisons undertaken in Chapter 5.

Chapter 5: Strain-resolved metagenomics and phylogeography of cultured human gut Methanobrevibacter spp. Reveals Africa–Eurasia biogeographic patterns.

Building on the single-isolate work in Chapter 4, I extended cultivation of human gut methanogens to three populations in Gabon, Germany, and Vietnam. Through sustained anaerobic culturing and sequencing, I assembled an extensive collection of over 200 *Methanobrevibacter*

isolates, comprising strains of both *M. smithii* and *M. intestini*. This effort represents one of the most extensive culture-based collections of human-associated methanogens assembled to date. It provides a unique opportunity to examine strain-level diversity at an unprecedented scale.

The breadth of this collection generated a set of evolutionary and ecological questions that extended beyond single-isolate characterization. Addressing these questions required complementary analytical expertise, and the work presented in this chapter reflects a collaborative effort among multiple researchers. Together, we combined cultivation-derived genomes with stool-derived metagenomes from the same populations to examine how geography, host association, and microbial context shape the evolution of *Methanobrevibacter* in the human gut.

We used metagenomic data to assess methanogen prevalence and to explore cross-domain associations between archaea and bacteria across populations. We further used cultured genomes to assess codon usage patterns in *M. smithii* and *M. intestini* and to explore their codon preferences, which may reflect how these two species, which share similar habitats, adapt to their host-specific environments. Using these isolates, we reconstructed maximum-likelihood phylogenies to resolve relationships at both species and strain levels. We conducted pangenome analyses using species representative strains (that is strains that were dereplicated based on 99.99% ANI) of both *M. smithii* and *M. intestini*, which allowed us to characterize the core genome (gene sets found in >99% of genomes) or the accessory genome (gene sets found in <15% of genomes) as well as pangenome openness which reflect gene gain/loss. We also performed functional enrichment analyses to identify gene functions and pathways over-represented in the accessory genome. Using this analysis, we could assess how functional differences among lineages may relate to adaptation to particular hosts, ecological niches, or environments.

In addition, we analysed genome architecture using Average Nucleotide Identity (ANI) and synteny. We then used cophylogenetic methods to test whether methanogen evolutionary relationships track patterns of human population structure. Finally, we used lipid quantification experiments to link genomic variation to differences in archaeal cell biology, thus providing an experimental bridge between genetic potential and phenotype.

In summary our results show that (i) *M. smithii* and *M. intestini* are prevalent and abundant members of the human gut microbiome across diverse populations; (ii) Both *M. smithii* and *M. intestini* exhibits evolutionary patterns that partially mirror human population structure; (iii) adaptation in both species appears to be shaped by geography and host-related factors; and (iv) the

observed reduced prevalence and abundance of *M. intestini* in more industrialized settings raises the possibility that human-associated methanogens are potentially progressively lost with ongoing lifestyle and environmental change.

Chapter 6: Discussion.

In this final chapter, I draw together the main themes of the thesis and consider their implications for research on the human gut microbiome. Geography emerges as a recurring influence throughout the work. It shapes patterns of soil-transmitted helminth infection in Gabon (Chapter 2), describes the isolation and description of the first African isolate of *M. intestini* (Chapter 4), and structures global diversity within *Methanobrevibacter* (Chapter 5).

The thesis also relies on integrating several methods to study both STH and methanogen ecology. The methods used in this thesis shift from chapter to chapter. In Chapter 2, I used metagenomic sequencing to both detect parasites and profile the microbiome, providing a proof-of-concept for other potential applications of metagenomic sequencing data. Chapter 4 marks a shift from genomic inference to experimentation. Here, my first cultivation effort led to the characterization of a Gabonese strain of *M. intestini*. I then used this cultured strain to perform phenotypic assays to test how well genomic predictions, such as the ability to utilize formate, hold up against an established *M. intestini WWM1085* type strain. Chapter 5 steps back to consider the broader evolutionary context, drawing on comparative genomics to relate genome variation to geography and to clarify the functional distinctions between the two species.

Across chapters, ecological interactions become visible only after stratifying the data, whether for soil-transmitted helminths or the gut microbiome itself. The evolutionary perspective developed in Chapter 5—spanning codon usage, pangenome structure, cophylogeny, and lipid biology—illustrates how methanogens diversify and adapt in response to both host association and microbial context.

This thesis goes beyond describing microbiome diversity and brings ecological, evolutionary, and experimental perspectives together to explore how human gut microbes interact across eukaryotes and prokaryotes. It also draws on geographically diverse populations to challenge Western-centred baselines and to highlight the need for broader global representation in microbiome research.

Chapter 1: Background on Soil-Transmitted Helminths (STH) and the Gut Microbiome

This chapter includes material adapted from a publication to which I contributed. I mainly drew the background on soil-transmitted helminths from the review:

Diagnostic Techniques of Soil-Transmitted Helminths: Impact on Control Measures.

Doi: 10.3390/tropicalmed5020093.

I contributed to the conceptualization, methodology, drafting, figure preparation and writing of the manuscript.

1.1. Introduction

Soil-transmitted helminths (STHs) are a group of intestinal nematodes that infect over 1.5 billion people globally, particularly in regions with poor sanitation and limited access to clean water. Most infected people are asymptomatic; however, people with high parasite loads can suffer severe infections that can lead to chronic health problems such as anemia, malnutrition, impaired cognitive development, intestinal obstruction, and reduced academic performance, especially in children(Sakti et al., 1999; WHO, 2023). As a poverty-associated disease, STH parasite infections cause a significant morbidity measured in Disability-Adjusted Life Years (DALYs) lost(WHO, 2015). The major STHs include *Ascaris lumbricoides*, *Trichuris trichiura*, *Strongyloides stercoralis* and the hookworms (*Necator americanus* and *Ancylostoma duodenale*). Most people are at risk of infection through their agricultural, domestic, and recreational activities, which expose them to contaminated soil. Numerous studies have examined the complex interactions between STH parasites and the human host's immune system, as well as between STH parasites and the gut microbiota. Understanding these relationships can make an important contribution to the development of improved control and treatment strategies and provide insights into the coevolution of host, microbes, and helminths.

1.2. STH prevalence and geographic distribution.

Soil-transmitted helminths (STHs) are endemic in tropical and subtropical regions, where they remain a significant public health concern. In many low and middle-income regions, including parts of sub-Saharan Africa, Southeast Asia, and Latin America, people still carry far heavier burdens of STH than in most high-income regions(WHO, 2023). Transmission rates are higher

due to poverty, poor sanitation, and limited access to clean water and health care(WHO, 2023). Preschool and school‐age children bear the most significant burden of soil‐transmitted helminth infections, often because they are repeatedly exposed while playing in contaminated soil and water. The World Health Organization estimates that more than 267 million preschool‐aged children and over 568 million school‐aged children live in areas of intense transmission and need preventive treatment(WHO, 2023). Global commitments to control STH and other neglected tropical diseases have grown over the years through the integration of control programs targeting multiple tropical diseases simultaneously(Brady et al., 2006; Brooker et al., 2006; Fenwick, 2006; Lammie et al., 2006; Molyneux et al., 2005). Another approach, large-scale or Mass Drug Administration (MDA), targeting high-risk groups, has been widely used to reduce worm burden. WHO recommends preventive chemotherapy, i.e., single-dose anthelminthic treatment given annually or biannually without a prior diagnosis as a public health intervention for all young children (12-23 months of age), preschool (24-59 months of age), and school-age children living in settings where baseline prevalence of STH is >= 20%(WHO, 2018). This strategy has already proven useful, although cure is often incomplete and depends on the type of anthelminthic drug used(Adegnika et al., 2015; Keiser & Utzinger, 2008). Despite these mass drug administration (MDA) efforts, reinfection rates are high in many areas, and disparities exist in surveillance data across regions.

1.3. Life cycle and transmission of STHs.

Soil-transmitted helminth infections have complete and direct life cycles and do not require an intermediate host. The infection cycle starts when uninfected individuals ingest embryonated eggs, as in *A. lumbricoides* and *T. trichiura*, or when infective filariform larvae penetrate the skin, as seen for hookworms and *S. stercoralis*. After ingestion, *A. lumbricoides* larvae hatch in the small intestine, migrate via the bloodstream to the lungs, ascend the trachea, and mature into adults in the small intestine once swallowed by the host. *T. trichiura* eggs hatch in the colon, where larvae embed into the mucosa and develop into adults. After skin penetration, hookworm and *S. stercoralis* larvae enter the bloodstream, migrate to the lungs, and subsequently reach the gastrointestinal tract after being swallowed, where they mature in the small intestine. Among the STHs, *S. stercoralis* is the only species capable of autoinfection, in which some larvae can develop into infective filariform stages within the host. In contrast, others continue a free-living cycle in soil(Cheesbrough, 2005). This flexibility allows infections to persist for long periods, even in the absence of repeated exposure (Fig. 1).

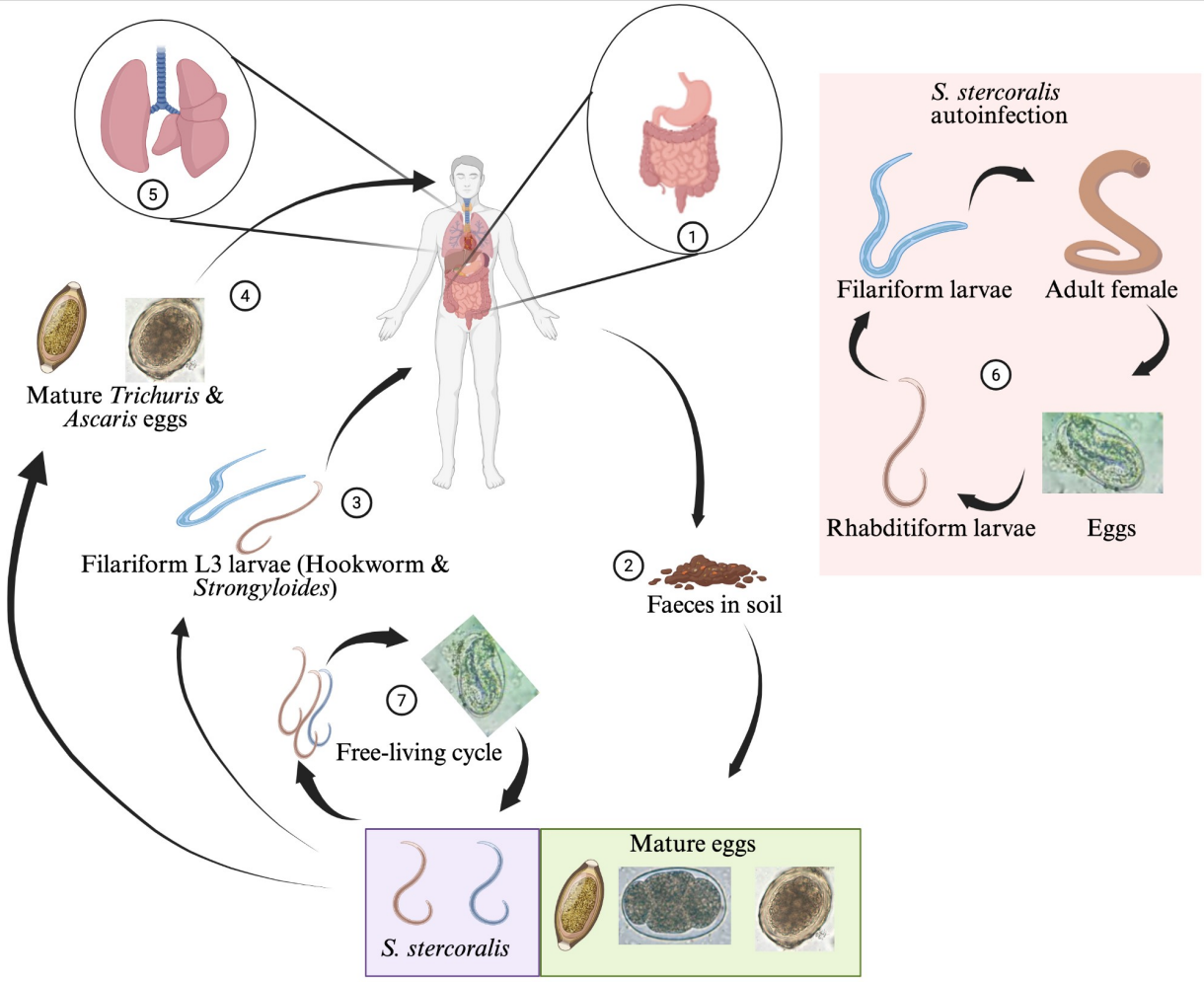

Figure 1. Life cycle of soil-transmitted helminths.

The major STHs (*A. lumbricoides, T. trichiura, hookworms,* and *S. stercoralis*) share a direct cycle linking intestinal establishment (1), shedding of eggs or larvae into the environment (2), and transmission via penetration by infective L3 larvae (3) or ingestion of embryonated eggs (4). Some species undergo pulmonary migration (5) before completing development in the intestine. *Strongyloides* can also sustain infection through autoinfection (6) and has a facultative free-living cycle in soil (7). Adapted from Gordon et al. (2017) and redrawn in BioRender.com.

Adult worms can produce large numbers of eggs every day, with *Ascaris* producing up to about 200,000 per day; *Trichuris* around 20,000; hookworms roughly 3,000–20,000, while *Strongyloides* produces larvae instead of eggs. These eggs or larvae leave the body in feces, and under warm, moist conditions, the eggs embryonate, or the larvae develop into infective stages within a few days to a few weeks. How long these free-living stages survive outside the host

depends strongly on local environmental conditions such as soil temperature and humidity, which can limit them to just days in some settings or allow them to persist for weeks in others. Once STHs establish infections in a host, adult worms can persist for one to several years. Together, these features help explain why co-infections are common in endemic regions and why transmission responds strongly to sanitation practices, human behaviour, and host immunity. Given the well-established life cycles of these STH parasites, the use of highly sensitive diagnostic tools can improve monitoring of infection intensity, prevalence, and the effectiveness of MDA(Mbong Ngwese et al., 2020).

1.4. Diagnosis of STHs

The evaluation of the efficacy, effectiveness, and disease elimination of interventions and control in the community and in endemic areas strongly depends on the accuracy of diagnostic tools, as defined by their sensitivity and specificity. Traditionally, methods for detecting parasitic elements have relied on microscopy. However, detecting parasites by microscopy in each sample is not always successful, even in heavily infected subjects. Several factors account for this difficulty, as we have discussed in this review(Mbong Ngwese et al., 2020), including the choice of diagnostic platform. In summary, these factors include, but are not limited to, possible methodological problems, uneven egg distribution within feces, low egg counts in stool, variation in stool sample volume, intermittent shedding of eggs or cysts, and suboptimal sample transport or storage(Anderson & Schad, 1985; Easton et al., 2017). Here, I provide an overview of two methods commonly used to detect or diagnose STH parasites.

Kato-Katz technique: The most widely used approach to assess the prevalence and infection intensity of STH is the Kato-Katz technique, also recommended by the WHO. Among the copro-microscopic methods, Kato-Katz is advantageous because it has higher sensitivity, the ability to quantify eggs, low operational cost, and feasibility in areas with minimal infrastructure(Katz et al., 1972). The Kato-katz method is also widely used to stratify infection intensities into classes based on egg counts and cut-off values. The Kato-Katz procedure starts with using a sieved fecal sample (approximately 41.7mg, 20mg, or 50mg, depending on the size of the template), which is placed on a slide and covered with a piece of cellophane soaked in glycerol. Subsequently, the slide is inverted and gently pressed to form a thin smear. The added glycerol 'clears' the fecal material from around the eggs. Hookworm eggs require about 30 minutes for this step, while for the other species, reading of the slide under the microscope can be done

after 1 to 24 hrs. A microscopist then counts the eggs under the microscope and expresses the results per gram of feces(Katz et al., 1972).

Polymerase Chain Reaction (PCR) Technique

Microscopy techniques require personnel expertise, multiple stool samples, and species-specific concentration and staining methods to improve performance. Limitations of these techniques include specificity, sensitivity, intra-specimen variability in egg counts, low infection intensities, and other factors mentioned earlier, which have led to increased use of PCR assays for intestinal parasite diagnosis(Taniuchi et al., 2011; ten Hove et al., 2009). Nucleic acid-based detection has had tremendous success in virology and bacteriology, and researchers are now increasingly applying it as a first-line diagnostic tool in clinical parasitology. There are, however, growing concerns that these techniques might replace microscopy and could have (possible) clinical drawbacks, and that the beauty of microscopy, which allows visualization of the different forms of parasitic elements, might be lost(van Lieshout & Roestenberg, 2015). Researchers have developed different protocols for PCR assays, including single PCR, nested PCR, real-time PCR, and multiplex PCR(Arndt et al., 2013; Verweij et al., 2004, 2007).

Irrespective of the protocol used, PCR usually involves repetitive cycles of DNA denaturation, primer annealing, and extension by a thermostable Taq DNA polymerase. PCRs are fast, easy to perform, and can be both sensitive and specific, but it also has drawbacks. Users need sequence information to design primers, and even small amounts of contamination can lead to misleading results(McKeand, 1998). Nevertheless, technicians now receive training in molecular diagnostics, and many PCR steps are automated, so labs now see fewer contamination-related issues as these workflows improve.

Although microscopy stool examination provides an acceptable measure of infection in highly endemic areas, its relevance in low-endemicity areas is limited, suggesting that microscopy may not be the most sensitive. However, it remains highly specific because it allows direct visualization and accurate identification of the parasite species in a sample. Sensitivity improves when skilled, experienced operators perform the procedure. False positives, which may occur due to artefacts, can be minimized by highly trained personnel, and low sensitivity may be improved using multiple samples. Molecular diagnosis with PCR, although initially deemed superior or more adequate for diagnosis, may be only marginally more sensitive than microscopic stool

examination. Overall, PCR offers slightly higher sensitivity and specificity than other techniques, but its cost and limited availability in resource-limited settings remain challenges.

1.5. Host immune responses to STHs.

STH infections typically induce type 2 (Th2) immune responses in their human host. These responses involve increased production of cytokines such as IL-4, IL-5, IL-9, and IL-13, eosinophilia, and IgE responses(Maizels et al., 2018). These responses help expel the parasites and limit tissue damage. Additionally, for STH infections to persist in humans, they dampen inflammation by shifting immune responses towards a protective, anti-inflammatory type 2 (Th2) response, by producing regulatory molecules like regulatory T cells (Tregs) and cytokines such as IL-10 and TGF-β(Gazzinelli-Guimaraes & Nutman, 2018; Mahanty & Nutman, 1995; Satoguina et al., 2005). In places where these infections are common, this kind of immune regulation often goes along with milder inflammatory responses and, in some groups, fewer or less severe allergy and autoimmune problems. Because of these effects, researchers have become increasingly interested in using helminths, or their products, as potential treatments for inflammatory diseases(Maizels & McSorley, 2016).

1.6. Mechanisms of immune evasion by STHs.

STH parasites also use different strategies to evade host immunity. These include secretion of excretory-secretory (ES) products that interfere with antigen presentation, T cell activation, and cytokine signaling(Maizels et al., 2018; McSorley et al., 2014). Molecules such as cysteine protease inhibitors, glycan-binding proteins, and TGF-β-like ligands help modulate host immune pathways(Donnelly et al., 2010).

To ensure survival and establish persistence, these parasites can skew immune responses toward regulatory or Th2 dominance. An example is Heligmosomoides polygyrus, which secretes molecules that mimic host cytokines and suppress in vitro effector cell proliferation(Grainger et al., 2010; Reynolds et al., 2015).

1.7. STH–gut microbiome and host immunity.

As inhabitants of the human intestine, STH infections can have effects that extend far beyond the classic pathologies associated with them and also influence the composition of the intestinal microbiome. Helminth colonization disrupts established gut niches by altering both the local immune response and intestinal barrier. In experimental mouse models, infections with

Trichuris muris lead to goblet cell hyperplasia and increased production of mucins such as Muc2 and Muc5ac, which thicken and remodel the mucus layer(Glover et al., 2019; Hasnain et al., 2011; Turner et al., 2013). Type 2 cytokines, including IL-13 and IL-22, help drive these epithelial responses and induce effector molecules such as RELM-β and trefoil factors (TFF1/2)(Herbert et al., 2009). RELM-β can impair worm feeding, promote their trapping in mucus, and support epithelial turnover, thereby contributing directly to luminal worm expulsion, while trefoil factors aid mucosal repair and support type 2 immunity, further improving barrier function during helminth infection(Mules et al., 2024; Wolff et al., 2012).

These helminth-induced changes often accompany shifts in bacterial communities, and several studies have reported alterations in both the diversity and composition of the gut microbiota during helminth infection(Houlden et al., 2015; Jenkins et al., 2017; Su et al., 2018). For example, a study showed that people with multi-helminth infections frequently showed higher alpha and beta diversity than those with single or no infections, and some cohorts showed a relative enrichment of Firmicutes (including Clostridia) compared with Bacteroidetes(Kupritz et al., 2021). Similar shifts have been observed in humans and animal models, particularly in the context of heavy Trichuris infections(Easton et al., 2019; Kupritz et al., 2021). Other studies have shown that enrichment of short-chain fatty acid (SCFA)–producing bacteria occurs during STH infections(Bhaskaran et al., 2018; Kupritz et al., 2021). These SCFAs, such as acetate, propionate, and butyrate, contribute to epithelial integrity, the induction of regulatory T cells (Tregs), and the suppression of pro-inflammatory responses. In addition to enrichment of specific SCFA-producing bacteria, genera such as Olsenella, Allobaculum, and Flavonifractor have been consistently associated with STH infection status across geographic settings(Rosa et al., 2018).

The mammalian immune system can cope with commensal microbes as well as pathogenic bacteria, viruses, and helminths. However, both bacteria and helminths can weaken the host's immune system to ensure their survival, but they suppress different T helper mechanisms (Th1 and Th2). A review by Reynolds et al. (2015) highlights the mechanisms by which helminths and the bacterial microbiota suppress host immunity. One key mechanism is that both helminths and commensal microbes can activate overlapping regulatory circuits, particularly those that induce Treg cells(Reynolds et al., 2015), thereby creating a tolerogenic intestinal environment, or through the excretion or secretion of extracellular vesicles, which directly modulate both the structure of the microbial community and the host's immune signals by influencing the production of antimicrobial peptides, the activation of macrophages, and the expansion of Foxp3+ Treg

cells(Rooney et al., 2022; Zou et al., 2025). Together, these findings underscore that the interactions among helminths, the microbiome, and host immunity are complex, limiting our understanding of them, particularly in areas where STH are endemic.

1.8. Future perspectives and knowledge gaps.

Our understanding of the relationships between STH and the microbiome is primarily based on cross-sectional data, leaving the causal and temporal dynamics unclear. The challenges associated with such data are manifold. First, STH prevalence differs between different population groups and age groups (adults vs. children). Second, transmission of most STH parasites is seasonal, so studies conducted during the peak transmission season for certain STH parasites may exaggerate any microbiome signals. Third, multi-parasitism is the rule rather than the exception in most highly endemic areas, making it difficult to discern the specific effects of a single STH on the microbiome in the context of co-infection. Fourth, different studies use different methods for detecting and quantifying parasites (microscopy vs. PCR) or for sequencing (16S RNA vs. shotgun metagenomics), and different reference databases for creating microbiome profiles.

Additionally, our knowledge of how microbial metabolites, helminth-secreted molecules, and host genetics each shape these interactions is minimal. Additionally, researchers have used longitudinal, integrative multi-omics approaches only rarely to tackle this. Of particular interest are the limited reports of how deworming to eliminate STH infections can influence the microbiome composition and immune development in infected subjects. Given these challenges, there is a need to harmonize microbiome studies related to STH infections by using standardized sampling frameworks, multi-cohort designs, longitudinal studies to account for seasonal variations in STH prevalence, and stratified analyses to account for demographic and environmental factors.

Methodological innovations offer a promising approach to closing these gaps. Researchers currently use microscopy or qPCR as the gold standard for parasite detection, both of which are resource-intensive and require technical expertise, especially in large-scale field studies. Metagenomic sequencing can profile both bacteria and multicellular eukaryotes, such as STH parasites, but most microbiome studies do not routinely use it. There are a few reports of its use in veterinary studies(Fu et al., 2023; Kirstahler et al., 2022), although it remains limited in human studies, with just one study reporting its use to quantify protozoan parasites(Lokmer et al., 2019). Establishing the accuracy of using metagenomes to quantify/detect STH parasites, especially relative to qPCR, is essential before researchers can adopt them as a scalable epidemiological tool.

In the next chapter, I present a proof-of-concept evaluation of metagenomic sequencing to simultaneously profile human STH infections and microbiome composition and correlate these infections with gut microbiome diversity in African populations. This work aims to contribute to a more standardized, context-specific basis for retrospective and future studies of the associations between STH and the microbiome.

Chapter 2: Infection with gut parasites correlates with gut microbiome diversity across human populations in Africa

This chapter is adapted from a manuscript of the same title, originally published in *Gut Microbes* (doi: 10.1080/19490976.2025.2587966).

Only changes to formatting have been made; main figures and tables have been renumbered to ensure consistency with chapter organization.

Authors are listed in publication order:

Mirabeau M. Ngwese[a, b, c], Bayode R. Adegbite[b, c], Jeannot F. Zinsou[b, c], J. Liam Fitzstevens[a], Victor T. Schmidt[a], Paul Alvyn N. Moure[b, c], Moustapha N. Maloum[b, c], Alexander V. Tyakht[a], Kelsey E. Huus[a], Nicholas D. Youngblut[a], Peter G. Kremsner[b,c,d,e], Ayola A. Adegnika[b, c, d], and Ruth E. Ley[a, e#]

[a]Department of Microbiome Science, Max Planck Institute for Biology, Tübingen, Germany

[b]Centre de Recherches Médicales de Lambaréné (CERMEL), Lambaréné, Gabon

[c]Institut für Tropenmedizin, Eberhard-Karls-Universität Tübingen, Germany

[d]German Center for Infection Research (DZIF), Tübingen, Germany

[e]Cluster of Excellence EXC 2124 Controlling Microbes to Fight Infections, University of Tübingen, Germany

#: Corresponding author

This chapter also makes use of data (extracted DNA from stool and metagenomes) from the following paper "Codiversification of gut microbiota with humans", published in Science (doi: 10.1126/science.abm7759).

Manuscript contributions: In the manuscript "Infection with gut parasites correlates with gut microbiome diversity across human populations in Africa," reported here, I contributed to the study conceptualization alongside N.D.Y and R.E.L. I designed the methodology to quantify soil-transmitted helminth (STH) parasites using metagenomes described in the "Codiversification of gut microbiota with humans" study, in collaboration with N.D.Y. I performed all the qPCRs of STH species using DNA extractions provided by J.L.F and V.T.S. I conducted all formal analyses, including metagenome profiling of additional samples not included in the "Codiversification" study, as well as the identification and integration of metagenome datasets from five additional

African cohorts and one USA cohort under the supervision of N.D.Y and R.E.L. I generated all figure visualizations and wrote the original draft alongside N.D.Y, A.V.T, K.E.H, and R.E.L.
For the data generated and used in "Codiversification of gut microbiota with humans," I conducted the field investigation at the Gabon sampling site alongside, carried out sample processing (including preliminary STH and other parasites assessment via microscopy), and performed data curation.

2.1. Abstract

Soil-transmitted helminths (STH) are common in (sub)tropical regions and primarily affect impoverished populations. These parasites reside in the gut, where they interact with both the microbiota and host immunity. Clinical STH detection is laborious and often not performed within the context of gut microbiome studies. Here, we present a proof-of-concept study assessing whether fecal metagenome data could be used to assess STH infection, and to relate STH infection to microbiome features. We leveraged 310 gut metagenomes obtained from mother-child pairs in two different locations in Gabon: one rural and one semi-urban, and assessed the presence of four STH species (*Ascaris lumbricoides*, *Strongyloides stercoralis*, *Trichuris trichiura*, and *Necator americanus*) using qPCR. Sequence data were used to characterize the microbiomes and to detect these parasites. Metagenomic read mapping and genome coverage metrics closely matched qPCR detection patterns. Within-location analyses revealed that parasite species richness was associated with microbiome diversity and taxonomic composition, with the strongest associations observed in children from the rural site. Applying this approach to published data from five additional African cohorts identified context-specific parasite-microbiome associations, as well as a modest but reproducible association between microbiome alpha diversity and parasite infection. These findings highlight the potential of shotgun metagenomics for concurrent parasite detection and microbiome profiling across diverse geographic and demographic contexts.

2.2. Introduction

Soil-transmitted helminth infections are endemic in developing countries, with over 1.5 billion people - representing 24% of the global population - affected by soil-transmitted helminths (STH)[1]. These infections are predominantly found in tropical and subtropical regions, particularly sub-Saharan Africa[2,3]. Transmission occurs through oral-fecal contact via contaminated soil and transcutaneously through larval penetration of the skin. Infections can spread within and between communities through shared environments. The prevalence of STHs in rural communities is often

poorly documented, especially in countries with limited resources and lacking mass drug administration (MDA) programs. MDA strategies, including deworming of high-risk populations and the widespread administration of anthelmintic drugs, are essential for controlling and reducing the morbidity associated with worm infections[4].

The World Health Organization (WHO) classifies the STH species *Ascaris lumbricoides*, *Trichuris trichiura*, Hookworms (*Necator americanus* and *Ancylostoma duodenale)* and *Strongyloides stercoralis* as neglected tropical diseases. These first three STHs contributed to an estimated 1.9 million disability-adjusted life years worldwide in 2019[5–7]. Strongyloidiasis, caused by *S. stercoralis*, further affects an estimated 30 to 100 million people worldwide[8]. At-risk groups include young children, preschool and school-age children, adolescent girls, women of reproductive age, pregnant women and adults with certain high-risk jobs such as tea-pickers or miners[5,9]. STH parasites often cause significant nutritional deficiencies, affecting growth and cognitive development in children [10]. They can also impact the behavior of the patient, as STH infections have been associated with reduced attention, memory, and learning abilities in children[10,11], and experimental infection models have demonstrated impairments in spatial memory [12]. In addition, they can lead to intestinal inflammation and malabsorption[13–15].

STHs are members of the gut microbiome. As such, they interact with other components of the microbiome such as Bacteria and Archaea, and these interactions can impact the success of parasite colonization and the outcome of parasitic infections[16]. Conversely, parasite colonization can affect the host's interaction with the microbiome[17–19]. When parasites colonize the gut, changes occur in the gut barrier, such as the epithelial mucus layers, which can subsequently alter the composition of microbiota[20,21]. Helminths can influence host-microbiome interactions by modulating immune signaling pathways and altering nutrient availability, thereby creating conditions that support their persistence within the gut ecosystem[22]. Furthermore, helminth-induced immunomodulation fosters a tolerogenic environment, which may encourage the growth of specific microbial taxa, indicating a potential mutualistic relationship between helminths and certain microbial communities[23]. Therefore, interactions between parasites and microbes may play significant roles in modifying host physiology and influencing disease outcomes[24].

The investigation of parasite-microbiome relationships across diverse populations has been limited in part because quantifying STH load is laborious and time-intensive and is not always done in conjunction with microbiome studies. Recently, a number of groups have reported the

possibility of detecting parasite presence by metagenomic sequencing in livestock stool[25,26] and the detection of unicellular parasites, such as Blastocystis, in human fecal metagenomes[27]. Although metagenomic sequencing shows promise for detecting a wide range of pathogens including STH, its diagnostic performance has not yet been fully validated against traditional diagnostic methods such as microscopy and PCR[28], highlighting the need for further standardization and targeted validation studies.

Here, we examined STH load in subjects sampled in Gabon using qPCR to compare with estimates generated from gut metagenomes. We then examined the relationship between STH infection with gut microbiome diversity from the same individuals. Subjects consisted of mother-child pairs from two different communities: the semi-urban region of Lambaréné, where parasite prevalence is well-documented[29,30], and the rural "Ikobey" region, which lacks parasite distribution data. We then expanded our analysis by leveraging publicly available metagenomic data from five additional studies in diverse African populations. Our results indicate that metagenome data can be used to assess STH richness, revealing reproducible patterns in microbiome-parasite associations across populations.

2.3. Results

2.3.1. Prevalence of parasites in samples from Gabon.

We collected 310 human stool samples from mothers and their children in Gabon (Fig. 2.1A) as described in[31]. This dataset comprises matched mother-child pairs from two distinct regions, the rural Ikobey (n=40 pairs) and the semi-urban Lambaréné (n=115 pairs). While the original study [31] was designed to investigate microbial strain transmission and cophylogeny, we leveraged this well-characterized cohort to address a complementary research question focused on parasite-microbiome associations. A total of 230 samples from Lambaréné and 80 from Ikobey were shipped to Germany for metagenomic sequencing and for qPCR-based detection of STHs. 259 were previously reported[31] and 51 were newly generated for this study. The average age of adults was 27 ± 6.7 (s.d.) years (Lambaréné = 26.3, Ikobey = 30.7), while that of children was 40 ± 45 (s.d.) weeks (Lambaréné = approximately 26 weeks [0.5 years], Ikobey = approximately 73 weeks [1.4 years]). Adults and children tended on average to be older in Ikobey compared to Lambaréné (Wilcoxon rank sum test, p = 6e-04 and p = 0.0032, respectively; Table 1).

Table 1: Age distribution and proportions of infection with one or more STH parasites (by qPCR: ct < 36) between groups in the Lambaréné and Ikobey sample populations

	Sampling site				
Category	Lambaréné		Ikobey		p-values
Mean age (years)	mothers: 26.3		mothers: 30.7		$p = 6e^{-04}$
	Children: 0.5		Children: 1.4		p = 0.0032
Proportion of infection n (%)	Mothers: 22 (19.1)		Mothers: 38 (95)		
	Children: 2 (1.9)		Children: 35 (87.5)		
Multiparasitism	Mothers (n = 115) Single infections (14)		Mothers (n = 40) Single infections (3)		
	Children (n = 115) Single infections (2)		Children (n = 40) Single infections (11)		
	Mothers: Double infections (7)		Mothers: Double infections (5)		
	Children: Double infections (0)		Children: Double infections (11)		
	Mothers: Triple infections (1)		Mothers: Triple infections (16)		
	Children: Triple infections (0)		Children: Triple infections (8)		
	Mothers: Quadruple infections (0)		Mothers: Quadruple infections (14)		
	Children: Quadruple infections (0)		Children: Quadruple infections (5)		
Individual parasite prevalence (%)	**Location**				
	Adults	Children	Adults	Children	
A. lumbricoides	5.2	0.0	82.5	37.5	
T. trichiura	9.6	0.9	95.0	60.0	
N. americanus	6.1	0.0	72.5	35.0	
S. stercoralis	6.1	0.9	42.5	60.0	

A. lumbricoides = Ascaris Lumbricoides, T. trichiura = Trichuris trichiura,
N. americanus = Necator americanus, S. stercoralis = Strongyloides. Stercoralis.

We focused on the four STH species previously reported as prevalent in this population *(i.e.*, *A. lumbricoides*, *T. trichiura*, *N. americanus* and *S. stercoralis*)[32,33]. To characterize the

distribution of intestinal parasites in this cohort, we first examined parasite counts per individual across age groups within each location. Linear models revealed significant differences by age in both settings. In both semi-urban Lambaréné and rural Ikobey, children had significantly lower parasite counts than adults (Linear model: $p = 2.3 \times 10^{-5}$ and $p = 2.8 \times 10^{-4}$; respectively; Table S1a). Post-hoc Tukey multiple comparisons confirmed these differences after false discovery rate (FDR) correction (Lambaréné: FDR-adjusted $p = 2.3 \times 10^{-5}$; Ikobey: FDR-adjusted $p = 2.8 \times 10^{-4}$; Table S1b), indicating that adults generally harbored more parasites per individual than children (Fig. 2.1B-D). These findings establish the baseline patterns of parasite burden necessary for subsequent analyses of infection risk and prevalence.

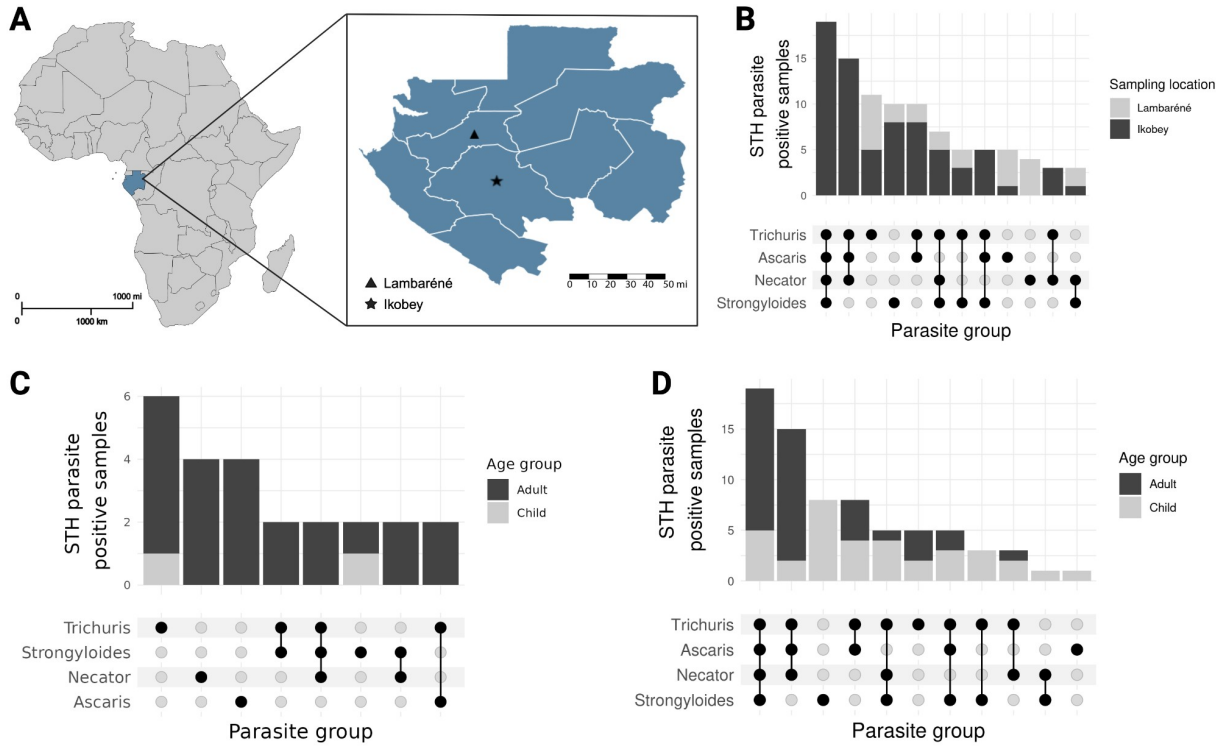

Figure 2.1: Sampling sites and prevalence of four STH species in Lambaréné and Ikobey. **A)** Map of Gabon showing the sampling locations (★ = Ikobey villages, ▲ = Lambaréné). **B)** Total number of STH-positive samples based on combined microscopy and qPCR data, displayed by sampling location. **C)** Total number of STH-positive samples by qPCR data, displayed by age group (Lambaréné). **D)** Total number of STH-positive samples from Ikobey, determined by qPCR data.

To assess whether age influenced the likelihood of being infected, we applied logistic regression models to parasite presence/absence data. In Lambaréné, children had significantly

lower odds of infection than adults (odds ratio = 0.075, $p = 5.6 \times 10^{-4}$). In Ikobey, the same trend was observed, but it did not reach statistical significance (odds ratio = 0.37, $p = 0.25$; Table S1c), reflecting the overall high prevalence of infection in this rural community. These models indicate that age is an important determinant of infection in the semi-urban population, whereas in high-prevalence rural settings, age-related differences are less pronounced.

To quantify infection prevalence and evaluate age-related differences within each location, we performed chi-squared tests for each parasite species. In Lambaréné, adults were more likely than children to be infected with *A. lumbricoides* ($p = 0.0515$), *T. trichiura* ($p = 0.0152$), and *N. americanus* ($p = 0.0340$), while *S. stercoralis* prevalence did not differ significantly by age ($p = 0.0822$). Similarly, in Ikobey, significant age differences were observed for *A. lumbricoides* ($p = 0.000837$), *T. trichiura* ($p = 0.002$), and *N. americanus* ($p = 0.00452$), but not for *S. stercoralis* ($p = 0.18$). All p-values were FDR-adjusted for multiple comparisons. These results confirm that age-related differences in parasite infection are evident for most species, though the effect is more pronounced in the semi-urban Lambaréné population.

To evaluate whether STH infection status was more similar within mother–child pairs than expected by chance, we performed a permutation-based concordance analysis stratified by location and parasite species. Across all species and locations, observed concordance did not differ from the null distribution generated by randomizing child infection status within locations (all $P > 0.05$; results not shown). These findings suggest no evidence that mothers with STH infection were more likely to have children infected with the same parasites, or vice versa.

Finally, to summarize overall parasite prevalence, we examined age-stratified infection rates for each species in both locations. In Ikobey, prevalence in adults versus children was 82.5% versus 37.5% for *A. lumbricoides*, 72.5% versus 35% for *N. americanus*, 42.5% versus 60% for *S. stercoralis*, and 95% versus 60% for *T. trichiura*. In Lambaréné, prevalence was substantially lower, with adults showing 5.2% versus 0% for *A. lumbricoides*, 6.1% versus 0% for *N. americanus*, 6.1% versus 0.9% for *S. stercoralis*, and 9.6% versus 0.9% for *T. trichiura* (Table 1). These findings highlight both the higher parasite burden in the rural Ikobey region and the marked age-related differences in infection risk within the semi-urban population. Together, these results provide a view of how parasite prevalence and burden vary with both geography and age, establishing a foundation for subsequent analyses of parasite–microbiome associations.

2.3.2. Associations of gut microbiome alpha and beta diversity with the number of STH species.

We next sought to investigate associations between the microbiome and parasite burden (richness) estimated by qPCR (n=310). To evaluate gut microbiome diversity at the species level, we employed metagenomic profiling against a custom database created from the Genome Taxonomy Database (GTDB Release 202)[34]. This approach significantly improved the classification of reads compared to the standard Kraken database, increasing the percentage of classified reads from 38.0% ± 26.4 (s.d.) to 81.8% ± 5.6 (s.d.).

To assess within-sample (alpha) diversity, and better account for the impact of age and parasite richness, we modelled Shannon entropy and Faith's phylogenetic diversity (PD), using linear models stratified by sampling location and age group (n = 307 samples with age data). These models included parasite species richness (parasite count) and standardized age (z-scores, Fig. S1A,B) as predictors (Table S2a-b). Among children in Ikobey, parasite richness was significantly and positively associated with Shannon diversity (estimate = 0.33, FDR-adjusted p = 0,030). Age was also strongly associated with both Shannon diversity and Faith's PD in this group (FDR-adjusted $p = 1.44 \times 10^{-3}$ and 4.1×10^{-5}, respectively). In contrast, no significant association with parasite richness was observed in Ikobey adults or in either age group from Lambaréné, although weak trends were noted in adults (Fig. 2.2A,B; Table S2a-b). Faith's PD was not associated with parasite richness in any group, but remained positively correlated with age in children from both locations (Ikobey: FDR-adjusted $p = 4.1 \times 10^{-5}$; Lambaréné: FDR-adjusted $p = 6.4 \times 10^{-3}$), but not in adults (Table S2a-b). These findings suggest that both parasite diversity and bacterial diversity increase with age in children, particularly those in Ikobey, but that there is little relationship between microbiome diversity and parasite burden in Gabonese adults.

We then assessed between-sample (beta) diversity using four distance metrics: Bray-Curtis, Jaccard, weighted UniFrac (Fig. 2.2C,D), and unweighted UniFrac (Fig. S1C,D), followed by PERMANOVA models stratified by sampling location (Lambaréné and Ikobey). In Lambaréné, age group explained the largest share of variance in microbiome composition across all metrics (R^2 = 0.138 to 0.198), while parasite richness accounted for substantially less (R^2 = 0.024 to 0,027). In Ikobey, the pattern was reversed: parasite richness explained the most variation across all four metrics (R^2 = 0.107 to 0.225), exceeding the contribution of the age group (R^2 = 0.061 to 0.073) (Table S2c; Fig. 2.2E).

These findings show that parasite richness contributes to variation in microbiome composition, particularly in Ikobey children where overall parasite prevalence is higher. In contrast, in the more urban setting of Lambaréné, age group is the dominant structuring factor. Together, these analyses reveal that both age and parasite burden can contribute to microbiome diversity in children, but their relative role depends on ecological context and exposure.

To assess these patterns in the pooled dataset while explicitly accounting for geography (sampling location), we ran PERMANOVA models including location as a covariate. Parasite burden remained significantly associated with beta diversity across all metrics (R^2 = 0.047-0.063, FDR-adjusted $p \leq 0.0015$). Age explained the largest share of variance (R^2 = 0.101–0.152), while location contributed comparatively little (R^2 = 0.005–0.008) but reached significance for unweighted UniFrac, Bray–Curtis, and Jaccard (FDR-adjusted p = 0.006–0.015). Using age group instead of continuous age yielded consistent results and slightly higher explanatory values, while avoiding sample loss from missing age data. These pooled analyses reinforce that age and parasite burden are stronger drivers of microbial community structure than geography in this cohort.

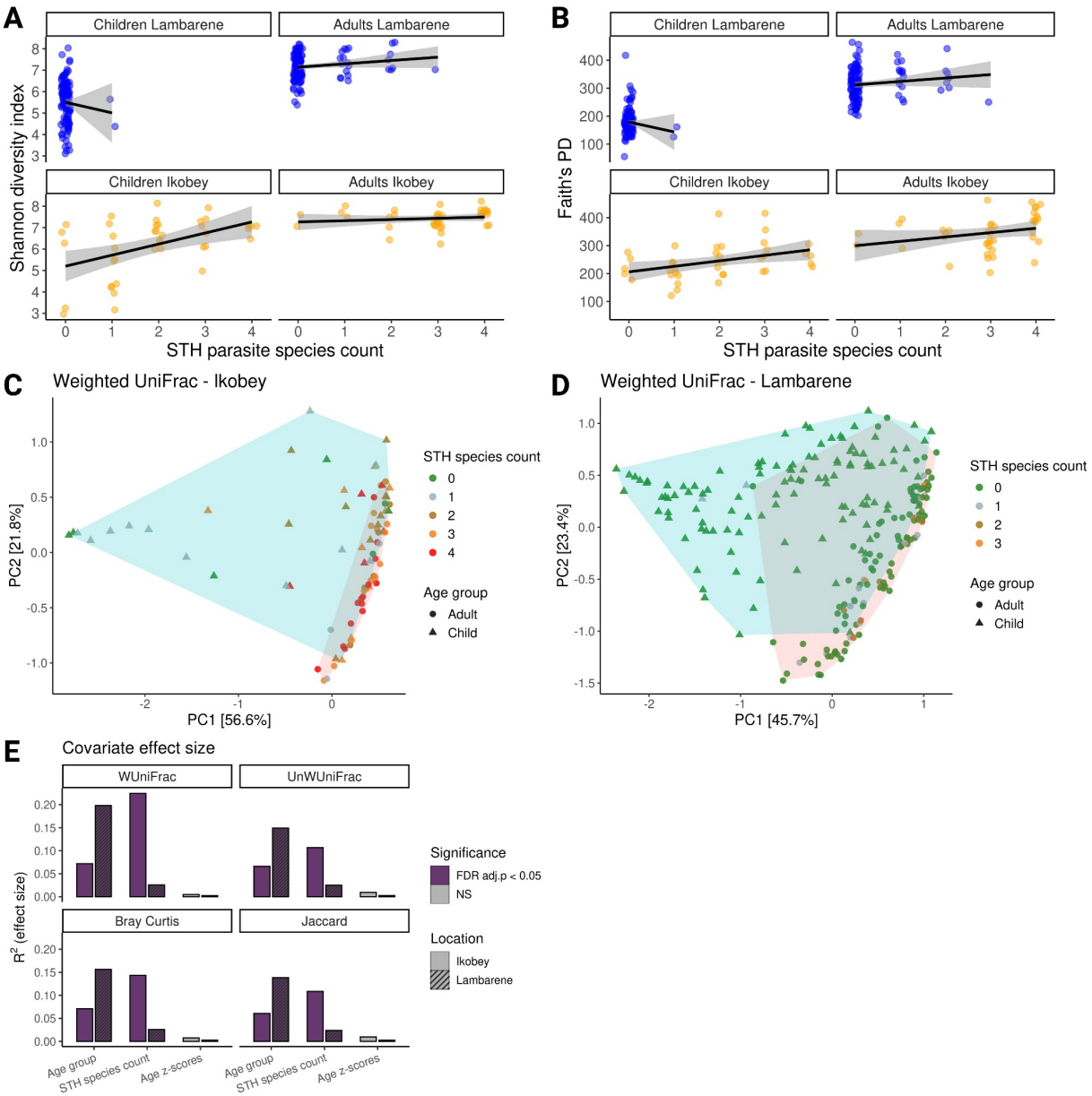

Figure 2.2: Gut Microbiome Diversity in Relation to STH species count, Age Group, and Location.

A) Correlation between gut microbiome Shannon diversity index and STH species count for adults and children by location (correlation method: LM). For children, $R^2 = 0.23$ in Ikobey and $R^2 = 0$ in Lambaréné; for adults, $R^2 = 0.02$ in both Ikobey and Lambaréné. **B)** Correlation between Faith's Phylogenetic Diversity (PD) and STH species count for adults and children by location (correlation method: LM). For children, $R^2 = 0.15$ in Ikobey and $R^2 = 0.01$ in Lambaréné; for adults, $R^2 = 0.07$ in Ikobey and $R^2 = 0.02$ in Lambaréné. **C)** Principal Coordinates Analysis (PCoA) of weighted UniFrac values for Ikobey samples (n = 80), colored by STH species count and shaped by age group (Adults = circles, children = triangles). **D)** PCoA of weighted UniFrac values for Lambaréné samples (n = 230), colored by STH species count and shaped by age group (Adults = circles,

children = triangles). **E)** Effect size (R^2) of each covariate plotted against significance (FDR-adjusted $p < 0.05$ = *, ns = non-significant) for all samples in both locations.
Effect sizes were calculated using four beta diversity metrics: Bray-Curtis, Jaccard, Weighted UniFrac, and Unweighted UniFrac.
Abbreviations: WUniFrac = Weighted UniFrac, UnWUniFrac = Unweighted UniFrac.

2.3.3. Specific microbial taxa are differentially abundant by STH species richness.

Having observed significant differences in microbiome diversity by parasite richness, we next sought to identify specific microbial taxa associated with the number of STH species. To account for substantial geographic variation in microbiome composition, we conducted separate differential abundance analyses for each sampling location (Lambaréné and Ikobey), while accounting for age group. We applied three complementary methods, DESeq2, MaAsLin2, and ANCOM-BC, each with distinct normalization strategies, to ensure robustness[35–37]. Because individual differential-abundance tools can yield variable results and differ in their susceptibility to false positives, we focused on taxa consistently identified across methods, thereby emphasizing signals most likely to represent biologically robust associations rather than method-specific artifacts. In Lambaréné, DESeq2 identified 108 species significantly associated with parasite richness, while MaAsLin2 and ANCOM-BC identified 29 and 37 species, respectively (FDR-adjusted $p < 0.05$), yielding a combined total of 174 unique species. Of these, 34 (19.5%) were detected by at least two methods (Table S3a), while 140 were method-specific. In Ikobey, DESeq2, MaAsLin2, and ANCOM-BC identified 252, 633, and 127 significant species, respectively, with 182 (18%) overlapping species and 830 method-specific (Table S3b). The top 30 overlapping species per location are shown in Fig. 2.3A,B. Relative abundance profiles for overlapping species are visualized in Fig. 2.3C,D, displaying the 23 most abundant species individually and grouping the remainder as "Other." Proportions are scaled within the subset and do not reflect total community composition. Ten consistently significant species were shared across both locations, primarily from Bacteroidaceae (n = 4), Lachnospiraceae (n = 5), and Anaerovoracaceae (n = 1).

Focusing on species identified by at least two methods, we observed contrasting patterns of association across locations. In Lambaréné, most overlapping species were negatively associated with parasite richness, particularly within Bacteroidaceae (n = 13), Bifidobacteriaceae (n = 10), and Lachnospiraceae (n = 2). Fewer species were positively associated, including members of Lachnospiraceae (n = 4) and one species each from Bacteroidaceae, Anaerovoracaceae, Borkfalkiaceae, and Erysipelotrichaceae (Fig. 2.3A, Table S3a). In contrast,

Ikobey exhibited a dominance of positive associations, particularly from Lachnospiraceae (n = 23), Bacteroidaceae (n = 20), UBA932 (n = 14), and Oscillospiraceae (n = 12), as well as other families including Acutalibacteraceae, UBA660, Ruminococcaceae, Streptococcaceae, Muribaculaceae, Campilobacteraceae, and Erysipelotrichaceae (3–8 species each). Negative associations were found mainly in Bacteroidaceae (n = 13), Lachnospiraceae (n = 9), and Coriobacteraceae (n = 9), with smaller contributions from Bifidobacteriaceae (n = 2) and others (Fig. 2.3B, Table S3b).

To identify taxonomic families enriched among differentially abundant species, we applied fast gene set enrichment analysis (FGSEA) using ranked association statistics[38]. In Lambaréné, 16 families were significantly enriched (padj < 0.05), primarily from the classes Clostridia (n = 6), Bacteroidia (n = 3), Bacilli (n = 2), and Gammaproteobacteria (n = 2), with one family each from Actinomycetia, Coriobacteriia, and Negativicutes (Fig. 2.3E, Table S3c). Most of these families had positive normalized enrichment scores (NES), suggesting that their constituent species tended to be positively associated with parasite richness. A smaller number showed negative NES values, indicating the opposite trend. In Ikobey, 26 families were enriched (FDR-adjusted $p < 0.05$), most with positive NES values, including members of Clostridia (n = 6), Bacilli (n = 4), Gammaproteobacteria (n = 2), and Negativicutes (n = 2), with additional contributions from several other classes (Fig. 2.3F, Table S3d). Families with negative NES values included Actinomycetia (n = 2), Negativicutes (n = 2), and one family each from Clostridia, Bacilli, Gammaproteobacteria, Bacteroidia, and Coriobacteriia.

Across both sites, 12 families were significantly enriched by FGSEA. Of these, nine families—Anaerovoracaceae, CAG-272, Oscillospiraceae, Erysipelotrichaceae, Streptococcaceae, UBA932, Veillonellaceae, Lachnospiraceae, and Pasteurellaceae—were generally associated with higher parasite richness, with most constituent species showing positive associations in at least one dataset. For instance, Anaerovoracaceae and Erysipelotrichaceae were positively associated in both locations, whereas Pasteurellaceae, Veillonellaceae, CAG-272, and UBA932 showed predominantly positive associations in Ikobey but not in Lambaréné. Bifidobacteriaceae, by contrast, exhibited only negative associations at both sites. Families such as Lachnospiraceae, Oscillospiraceae, and Streptococcaceae displayed mixed patterns, with more positive than negative associations across both locations. For example, Lachnospiraceae included 4 positively and 2 negatively associated species in Lambaréné, and 23 positives vs. 9 negatives in Ikobey.

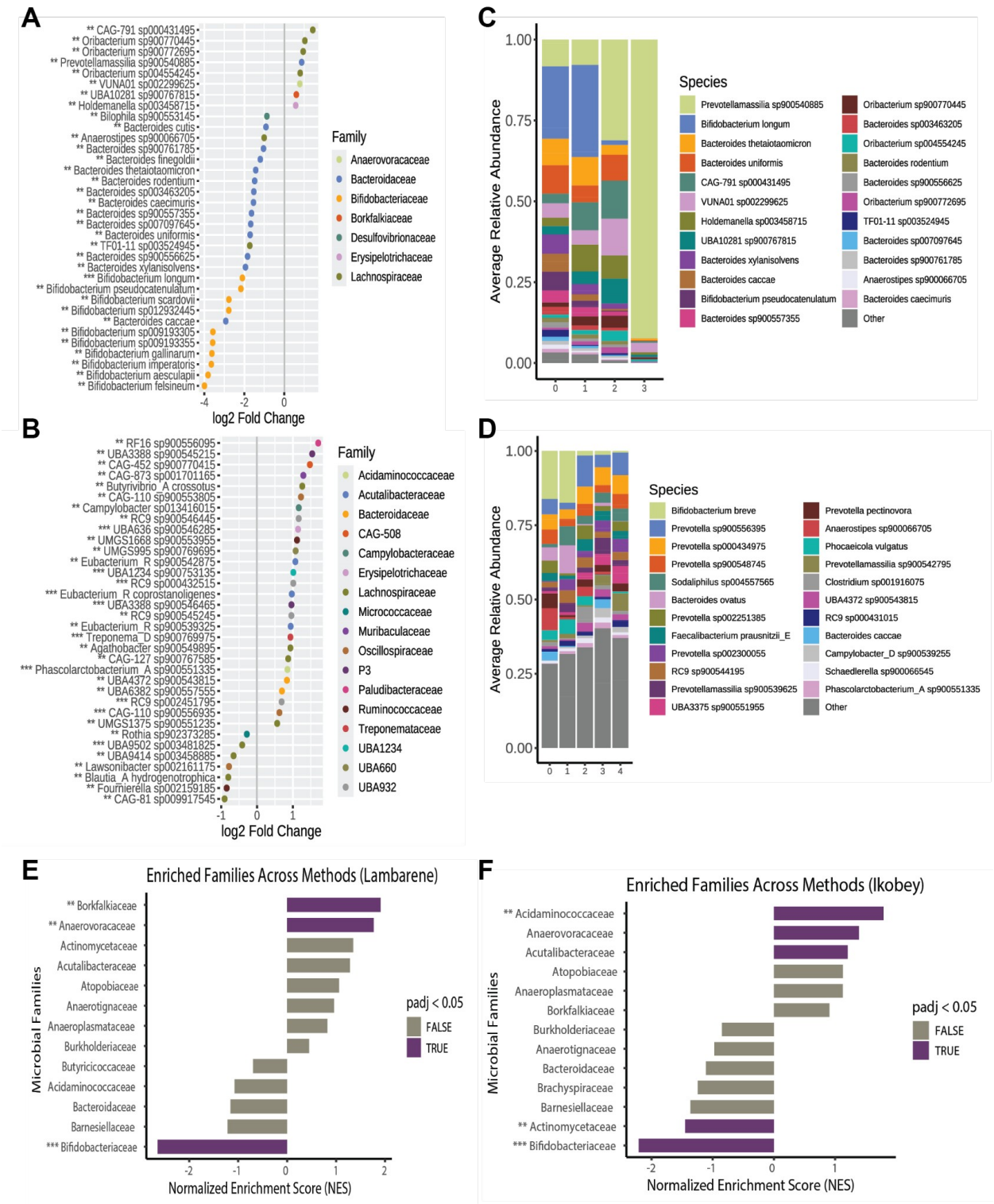

Figure 2.3: Differentially abundant microbial species and enriched bacterial families by STH parasite species richness across sampling locations.

A-B) Log2 fold changes in microbial species abundance associated with STH parasite count, separately for Lambaréné (A), and Ikobey (B), identified using DESeq2, MaAslin2, and ANCOM-

BC, while adjusting for age group (Adult vs. Child). Shown are the top 30 species found significant (FDR-adjusted $p < 0.05$) in at least two of the three methods. **C-D)** Relative abundances of the top all differentially abundant species in Lambaréné (C), and Ikobey (D), based on overlap across at least two methods. The top 23 species are colored by bacterial family; remaining species are grouped as "Other". **E-F)** Normalised enrichment scores of bacterial families significantly overrepresented in the differentially abundant species in Lambaréné (E), and Ikobey (F), based on fast gene set enrichment analysis (FGSEA).
Species-level abundances were pre-filtered to retain only those present in >50% of samples from both locations. The log2 fold changes are shown from the method reporting the highest effect size per species. Species identified by all three methods are annotated with ***, and those by two methods with **).

These results suggest that parasite–microbiota associations vary by geographic location, taxonomic composition, and direction of association. The recurrent enrichment of certain families across sites may reflect shared microbial responses to STH exposure, although the specific functional contributions of these taxa remain to be elucidated.

2.3.4. Functional pathway shifts in relation to parasite burden.

Given that microbial taxon differing by parasite burden often cluster within functionally coherent groups, we investigated whether gut microbial metabolic pathways also differed between parasite-positive and parasite-negative individuals. We applied the same three statistical frameworks used for taxonomic differential abundance (DESeq2, MaAsLin2, ANCOM-BC) to HUMAnN3-derived unnormalized, unstratified pathway abundance profiles, stratified by sampling location (Lambaréné, Ikobey) and adjusting for age group. Analyses were performed with both continuous age and age group; using age group retained all pathways identified with continuous age and additionally detected more, as it reduced sample loss from missing age values and increased statistical power in the stratified analyses. For pathway analyses, significance was defined as FDR-adjusted $p < 0.1$, and only pathways detected by at least two methods were considered robust. In Lambaréné, DESeq2 identified one differentially abundant pathway (PWY-622: starch biosynthesis), MaAsLin2 identified four (PWY-6641: superpathway of sulfolactate degradation, PWY-6148: tetrahydromethanopterin biosynthesis, PWY-6595: superpathway of guanosine nucleotides degradation plants, PWY-6478: GDP-D-glycero-α-D-manno-heptose biosynthesis), and ANCOM-BC identified none. No pathway overlapped between the three methods (Table S3e). Of the MaAsLin2 results, PWY-664: superpathway of sulfolactate degradation and PWY-6148: tetrahydromethanopterin biosynthesis were enriched in parasite-

positive individuals (positive $\log_2$ fold change), while the others, including PWY-622: starch biosynthesis, were depleted.

In Ikobey, where parasite prevalence was higher, DESeq2 identified 25 pathways, MaAsLin2 identified 76, and ANCOM-BC identified 35, with 27 pathways overlapping between all three methods. Of these, only PWY66-409: superpathway of purine nucleotide salvage and PWY-7323: superpathway of GDP-mannose derived O-antigen building blocks biosynthesis were enriched, while the remaining 25 were depleted (Fig. S2; Table S3f). No differentially abundant pathways overlapped between locations, although several amino acid biosynthesis pathways that were significantly depleted with STH in Ikobey showed a similar, non-significant trend to depletion in Lambaréné.

Overall, functional pathway differences were minimal in Lambaréné but pronounced in Ikobey, echoing patterns observed in the taxonomic profiles and aligning with the higher parasite prevalence in Ikobey. These findings suggest that helminth-associated microbiome changes in high-prevalence settings extend beyond taxonomic shifts to include broad alterations in predicted metabolic capacity.

2.3.5. Quantification of parasites by qPCR correlates with metagenome sequence data.

Next, we explored the feasibility of detecting and quantifying STH parasites directly from shotgun metagenome data. After filtering out bacterial and archaeal sequences, we employed KrakenUniq[39] to classify the remaining sequences against a custom database of the four target STH species, obtaining k-mer counts for each reference genome. To complement the k-mer based abundance estimates, genome coverage was assessed for the same species (Table S10) by mapping Kraken2-unclassified reads from a subset of 30 Gabonese samples to the corresponding reference genomes. The 30 samples were selected to include individuals with the highest k-mer counts per species, spanning both adults and children.

Mapped contigs ranged in length from 134 bp (*N. americanus*) to 29.16 Mb (*T. trichiura*), with median coverage values varying substantially between species (Fig. S3A). Minimum average per-contig coverage ranged from 0.000077x (*T. trichiura*) to 0.00244x (*S. stercoralis*), while maximum values ranged from 0.0386x (*T. trichiura*) to 632x (*A. lumbricoides*). For all four species, high-coverage contigs tended to be shorter fragments, whereas long contigs generally showed lower average coverage. This pattern is consistent with expectations for genome mapping from metagenomics reads, where GC content, repetitive or less well-represented regions often

assemble into longer contigs with lower or uneven read depth[40–42]. These patterns further illustrate the variability of eukaryotic genome recovery from metagenomic stool data, but also confirm that substantial genomic regions can be recovered in high-signal samples (Fig. S3B).

We next compared metagenomic detection with qPCR. Out of the 310 samples, the k-mer-based method identified 97 positives and 213 negatives, corresponding to a sensitivity of 82,47% and a specificity of 87,32% relative to qPCR (Table S11). The qPCR cycle threshold (Ct)(Fig. S3C) values were strongly and significantly negatively correlated with metagenomic k-mer counts for *A. lumbricoides* in both adults ($R^2 = 0.88$, $p = 2.2 \times 10^{-12}$) and children ($R^2 = 0.95$, $p < 2.2 \times 10^{-16}$), and similar trends were observed for *N. americanus* (adults: $R^2 = 0.56$, $p = 0.0013$; children: $R^2 = 0.88$, $p = 0.00067$) and *S. stercoralis* (adults: $R^2 = 0.77$, $p = 0.0056$; children: $R^2 = 0.92$, $p = 0.0001$). For *T. trichiura,* correlations were weaker and non-significant in children ($R^2 = 0.26$, $p = 0.21$) but moderate and significant in adults ($R^2 = 0.37$, $p = 0.008$) (Fig. 2.4).

Although both qPCR and metagenomics sequencing ultimately detect parasite DNA in stool, they do so via different mechanisms, qPCR amplifies species-specific genetic markers, whereas metagenomics classifies sequence fragments within the total read pool. Consequently, differences in detection, particularly for *T. trichiura*, may arise from biological and technical factors, including variable DNA yield due to egg morphology or wall composition, uneven distribution of parasite material in stool, inefficient lysis during DNA extraction, intermittent egg shedding, or stage-specific DNA content. Cross-reactivity of qPCR primers with non-target nematodes could further contribute to discordance between methods. Taken together, these results show that combining k-mer-based classification with genome coverage assessment offers a practical proof-of-concept approach for detecting STH parasites from metagenomic stool data. Performance was consistent for most species, and coverage profiles support the reliability of detection in high-signal samples. Notably, this approach outperformed the reference-based tool EukDetect[43], which failed to detect the prevalent *A. lumbricoides*, *T. trichiura*, and *N. americanus* in our dataset (Fig. S3D).

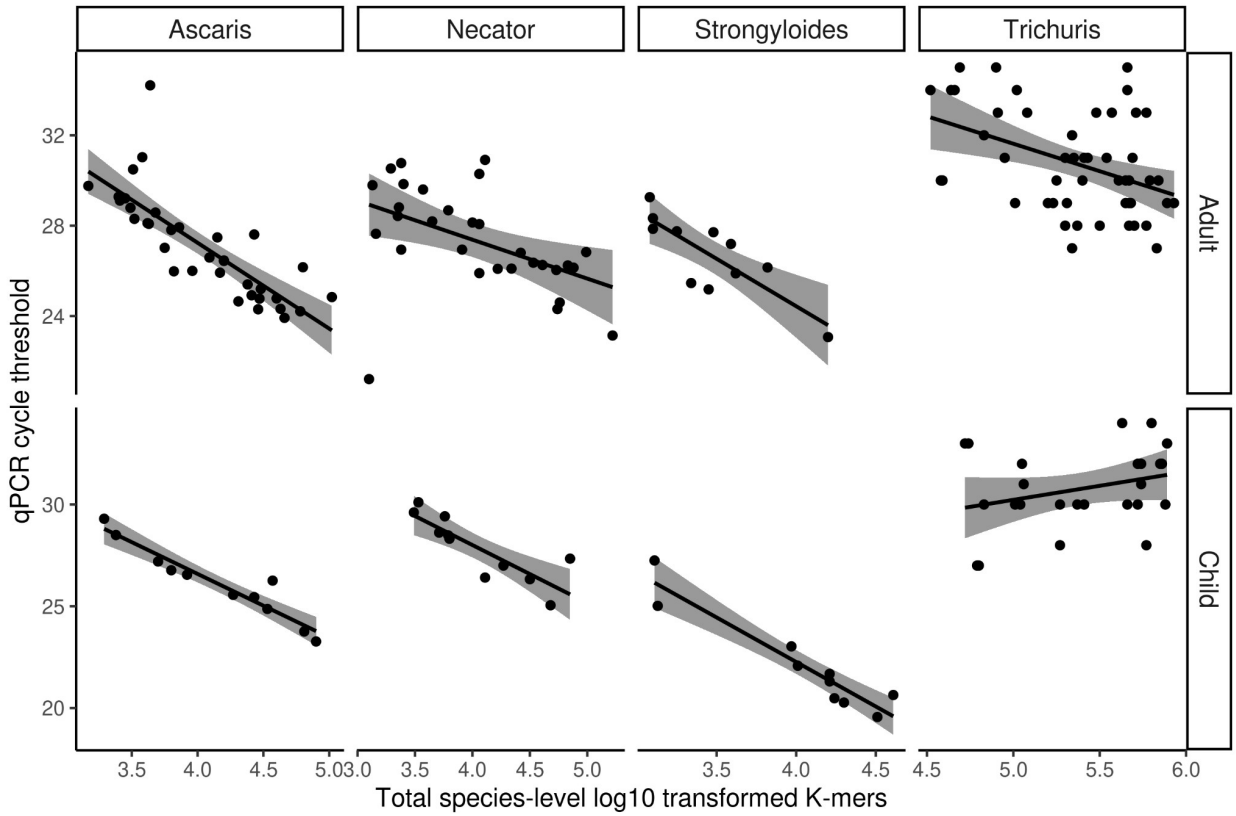

Figure 2.4: Correlation between metagenome-quantified STH parasite abundances and qPCR.

Spearman's rank correlation between qPCR cycle threshold (Ct) values and log10-transformed species-specific k-mer counts from metagenomic profiling was assessed separately for adults and children. For *Ascaris lumbricoides*, correlations were strong and significant (Adults: $R^2 = 0.88$, $p = 2.2 \times 10^{-12}$; Children: $R^2 = 0.95$, $p < 2.2 \times 10^{-16}$). For *Necator americanus*, significant correlations were also observed (Adults: $R^2 = 0.56$, $p = 0.0013$, Children: $R^2 = 0.88$, $p = 0.00067$). *Strongyloides stercoralis* showed moderate to strong correlations (Adults: $R^2 = 0.77$, $p = 0.0056$, Children: $R^2 = 0.92$, $p = 0.0001$). For *Trichuris trichiura*, the correlation was weaker and only significant in adults (Adults: $R^2 = 0.37$, $p = 0.008$, Children: $R^2 = 0.26$, $p = 0.21$). Ct values are inversely related to parasite load. Only correlations with $p \leq 0.005$ were considered significant.

2.3.6. Co-occurrence of the gut microbiome and STH parasites.

Using probabilistic models based on metagenomic data, we inferred co-occurrences between microbes and STH parasites presence/absence. Presence/absence data were used as required by the cooccur R package, which implements a probabilistic model of species co-occurrence based on binary input. In adults, all 4 STH parasites showed co-occurrences with specific microbial species (Fig. 2.5 A&B), while in children, only 3 parasites (excluding *T. trichiura*) exhibited such co-occurrences (Fig. 2.5C,D).

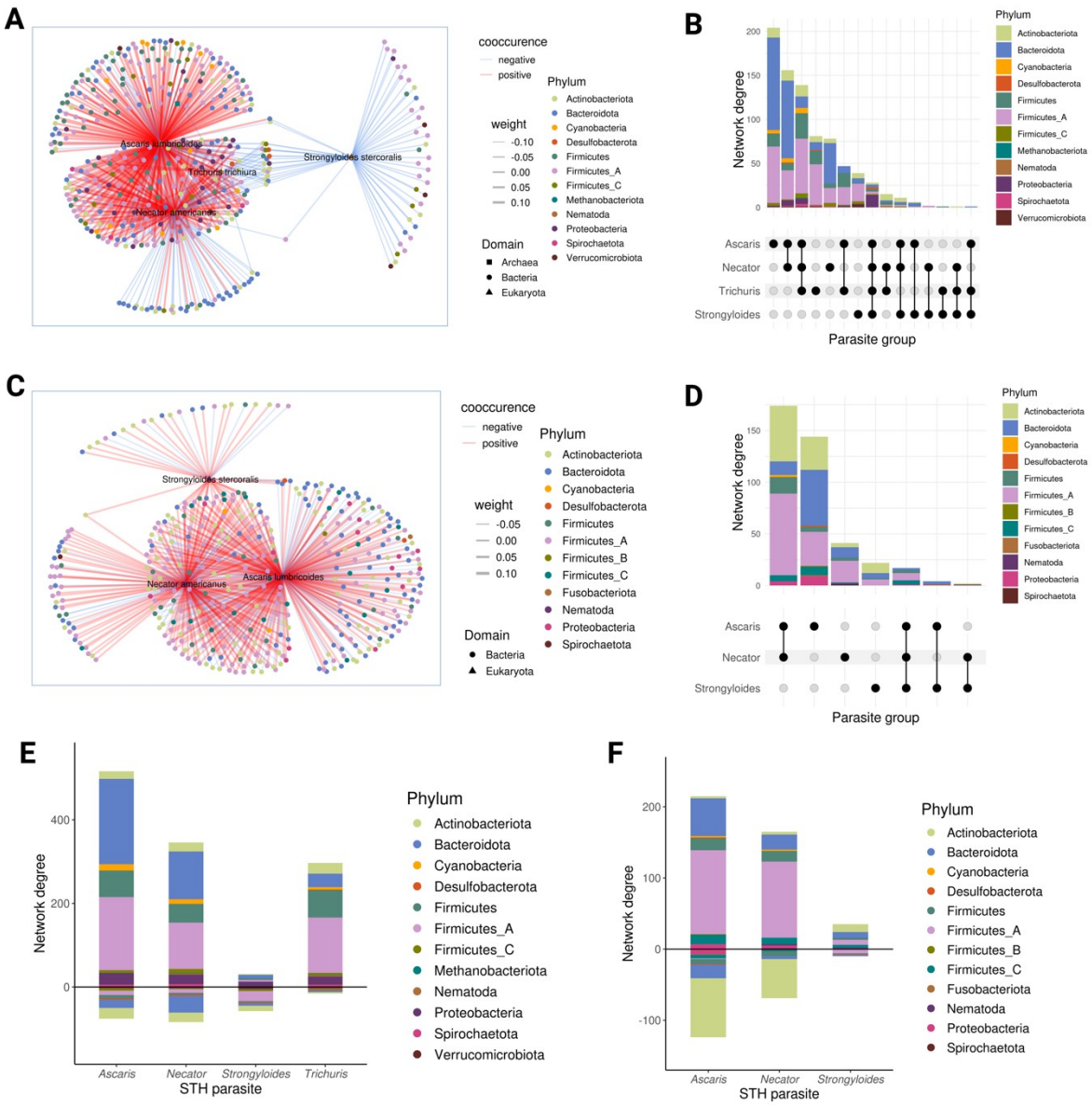

Figure 2.5: Co-occurrence network plots for adults and children in the Gabon dataset.
A) Co-occurrence network for adults, displaying species with significant co-occurrence probabilities. **B)** Network degree (number of connections per node) within the adult co-occurrence network. **C)** Upset plot showing parasites linked to similar bacteria/archaea in the adult network. **D)** Co-occurrence network for children, displaying species with significant co-occurrence probabilities. **E)** Network degree (number of connections per node) within the children's co-occurrence network. **F)** Upset plot showing parasites linked to similar bacteria/archaea in the children's network. Nodes represent species with significant co-occurrence probabilities, with red indicating positive co-occurrence and blue indicating negative co-occurrence. Only species associations with weights between -0.14 and -0.01 (negative) and 0.05 to 0.15 (positive) are shown for visualization.

Consistent with the association between parasite species count and increased microbial diversity, parasite species presence tended to be positively associated with bacterial presence, especially in adults (Fig. 2.5B,E). Ascaris had the highest number of unique co-occurrences with microbes in both adults and children (Fig. 2.5E,F). Positive associations were frequently observed between parasites and Firmicutes or Bacteroidota, while negative associations were observed between parasites and Actinobacteriota (Fig. 2.5E,F). Furthermore, analysis of random co-occurrence graph subsets indicated a low probability of associations between parasites or bacteria with similar properties (Fig. S3E). Overall, our findings support the associations of microbial species with parasite richness and suggest that these STH parasites may help shape specific microbial niche compositions.

2.3.7. Consistent parasite-microbiome associations across African datasets.

We leveraged publicly available metagenomic datasets to assess whether associations between STH parasites and gut microbiome are consistent across African populations. Using parasite species counts inferred from k-mer matches to parasite reference genomes, we conducted a meta-analysis across five metagenome datasets from Gabon (this study), Cameroon[27,44] , Burkina Faso[45], Ethiopia[46], and Madagascar[47], along with an American reference cohort[48]. Due to limited representation of young children in these metagenomic studies, we focused our analysis on adult women (mean age = 32), aligning with our primary cohort from Gabon. In total, 466 samples were included in the meta-analysis (410 from African cohorts; 405 with Age data; Fig. 2.6A).

We first examined the prevalence of four STHs based on metagenomic detection. *A. lumbricoides* was the most prevalent species, particularly in Burkina Faso (100%) and Ethiopia (95.8%), with lower detection in Gabon (38.3%), Cameroon (17.1%), Madagascar (16.7%), and USA (1.8%). *S. stercoralis* prevalence ranged from 64.3% in Burkina Faso to 0% in several populations, including Ethiopia and the USA. Prevalence differences for all four STHs were statistically significant across populations (χ^2 tests, FDR-adjusted $p < 0.001$; Fig. 2.6B; Fig. S3F), with STHs largely undetectable in the American dataset. Across datasets, we observed that higher parasite species richness was significantly associated with increased microbial alpha diversity. Specifically, Shannon entropy was positively associated with parasite richness (estimate = 0.14, FDR-adjusted $p = 0.00124$; Table S4a), while Faith's phylogenetic diversity also increased with

parasite richness (estimate = 31.5, FDR-adjusted p = 2.08 x 10^{-10}; Table S4b; Fig. 6C,D).

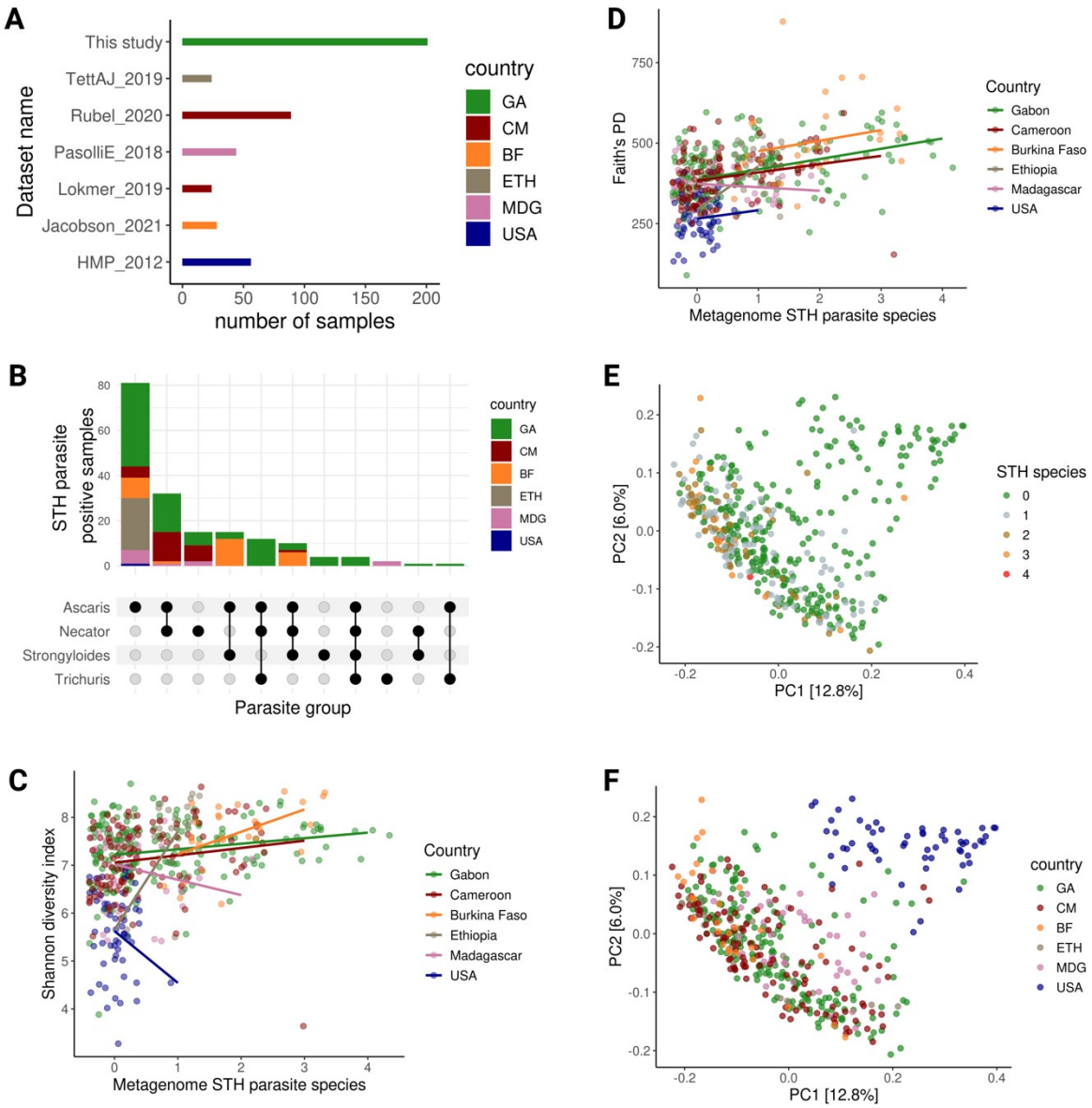

Figure 2.6: Meta-analysis of soil-transmitted helminth (STH) burden and gut microbiome diversity across multiple African cohorts.
A) The distribution of samples based on the STH parasites detected, categorized by datasets (GA = Gabon, CM = Cameroon, ETH = Ethiopia, GHA = Ghana, MDG = Madagascar, TZA = Tanzania, and USA). **B)** Upset plot showing STH parasites detected from metagenomes across datasets, with colours representing the country of origin. **C)** Correlation between Shannon diversity index and the number of STH parasites across datasets, using a generalized linear model (GLM). **D)** Same as panel C, showing correlation between Faith's PD and the number of STH parasite counts across datasets (GLM). **E)** Principal Coordinate Analysis (PCoA) of unweighted UniFrac values, with samples coloured based on the number of STH parasites detected. **F)** PCoA of unweighted UniFrac values, with samples coloured by country.

In contrast, neither age nor GDP per capita showed significant associations with alpha diversity after FDR correction (all FDR-adjusted $p > 0.8$). These associations remain significant after accounting for between dataset differences (random intercept), which predominantly, but not exclusively, corresponded to sampling country and protocols.

We also observed weak clustering by parasite species richness and dataset in the PCoA analyses (Fig. 2.6E,F). PERMANOVA confirmed that parasite species richness was significantly associated with beta diversity in Burkina Faso, Cameroon, Ethiopia, Gabon, and Madagascar across multiple distance metrics. Effect sizes were modest, generally ranging from $R^2 = 0.01–0.07$, but reproducible across sites (Table S4C). When pooling all datasets, parasite richness explained a consistent and statistically significant proportion of variance across metrics ($R^2 = 0.017–0.020$). Age contributed a smaller effect ($R^2 = 0.007–0.012$), while socioeconomic context (GDP per capita) explained a comparable amount ($R^2 = 0.019–0.029$). Geography (country) had the strongest effect, ranging from $R^2 = 0.035–0.087$ depending on the distance metric (Table S4c). These results show that parasite richness makes a reproducible but modest contribution to gut microbiome composition across African cohorts, with effects consistently smaller than those of geography or socioeconomic context.

To identify microbial species consistently associated with parasite richness, we used the intercept of the results from DESeq2, MaAslin2 and ANCOM-BC after filtering for species prevalence (FDR-adjusted $p < 0.05$) and controlling for geography and age. This yielded 665, 1050 and 1110 significantly associated species respectively, with 1072 overlapping across methods (Fig. 2.7A,B, Table S5a).

Using FGSEA, we identified 20 bacterial families overrepresented among the differentially abundant species. These included members of Clostridia (n = 5), Bacteroidia (n =5), Gammaproteobacteria (n = 2), Coriobacteria (n = 2) and one family each from Actinomycetia, Bacilli, Desulfovibrionia, Negativicutes, Spirochaetia and Vampirovibrionia. Most of these showed positive normalized enrichment scores (NES), suggesting an enrichment of taxa positively associated with parasite richness (e.g., all five Clostridia families, two Gammaproteobacteria and others). In contrast, a smaller number of families, including Bacteroidia (n = 4) and one each from Actinomycetia and desulfovibrionia, had negative NES values, indicating depletion (FDR-adjusted $p < 0.05$; Fig. 2.7C, Table S5b).

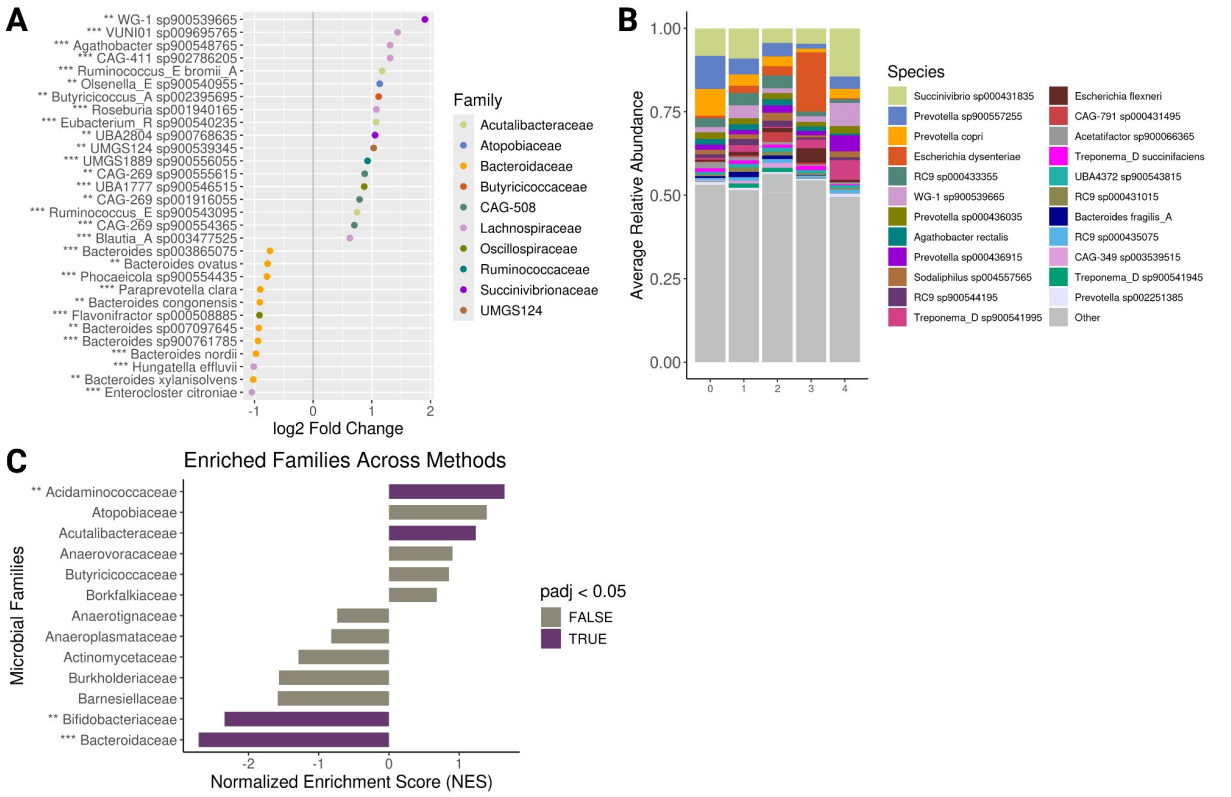

Figure 2.7: **Differential abundance of microbial species by STH parasite burden across countries**

A) Log2 fold changes in microbial species abundance associated with the number of STH (0-4) species based on DESeq2, MaAslin2, and ANCOM-BC. Shown are the top 30 species identified as significant (FDR-adjusted $p < 0.05$), by at least two of the three methods. Species detected by all three methods are marked with ***, and those by two methods with **. Analysis accounted for country as design factor and p-values were corrected using the Benjamini-Hochberg method. **B**) Relative abundances of all differentially abundant species by ≥ 2 methods. The top 23 species are coloured by the bacterial family; remaining are grouped as "Other". **C**) Normalised enrichment scores of bacterial families significantly overrepresented among differentially abundant species, based on fast gene set enrichment analysis (FGSEA).

Together, these findings indicate that associations between STH richness and gut microbiome diversity and composition, initially identified in Gabon, are also observed in other African populations using metagenomic data. While these patterns do not imply causality, they suggest that STH infections may be consistently linked with microbial diversity and compositional shifts in diverse African adult populations.

2.4. Discussion

Infection with STH is a neglected tropical disease that exerts complex, context-dependent effects on the human gut ecosystem. In this proof-of-concept study, we integrated molecular detection of STH with shotgun metagenomics to explore the relationship between STH infection and gut microbiota in 155 mother-child pairs from rural and semi-urban Gabonese communities. By combining qPCR assays with k-mer based detection from metagenomic data, we provide insights for the ecological interplay between STH parasites and the human gut microbiome.

One of the key methodological strengths of this study is the dual use of qPCR and shotgun metagenomics for STH detection. While traditional microscopy remains the clinical standard, it is laborious and often impractical in metagenomic studies. Our approach showed good concordance between molecular methods, with qPCR offering high sensitivity and metagenomic detection yielding > 80% sensitivity and specificity. Additionally, our validation of shotgun metagenomics against qPCR revealed robust correlations for most STH species. Notably, *T. trichiura* detection remained challenging, reflecting issues with primer specificity, egg shedding dynamics and DNA extraction efficiency. STH prevalence in our Gabonese cohort was high, particularly among mothers, which aligns with prior surveys from Gabon reporting adult STH prevalence > 20%[49,50], with STH infections in children reported between 20 to 33%[51,52]. In Lambaréné, where healthcare access is more established, this high maternal burden relative to children may reflect age-and behaviour-related reinfection dynamics, occupational exposures, or patterns of treatment uptake. In contrast, in the more remote Ikobey region, similarly high infection rates across mother-child pairs suggest persistent community transmission driven by limited sanitation and reduced access to preventive care.

The observed context-specific associations between STH burden and gut microbiome diversity likely reflects differences in environmental exposure, host development, and the stability of the microbial ecosystem across age groups. In rural Ikobey, where parasite exposure is widespread, increased parasite richness may promote or reflect a more heterogeneous microbial environment, particularly in children whose immune systems are still maturing. This may arise from immunomodulatory effects of helminths that enable colonization by a broader array of microbes, or from shared transmission routes linking parasite and microbial exposure via contaminated environments. In contrast, the absence of clear associations in adults or in the urban setting of Lambaréné suggests that the mature adult microbiome is more resistant to perturbations

and that hygiene infrastructure and periodic anthelminthic treatment may buffer parasite-microbiota interactions in this community. The strong influence of age group on microbial structure in Lambaréné, where parasite prevalence is lower, further underscores the importance of developmental transitions, potentially including diet, diversification, or immune maturation, in shaping the microbiota independently of STH exposure. The observed positive associations between parasite richness and microbiome diversity in Ikobey children, aligns with a previous study from Cameroon, where an increase in alpha diversity was associated with the number of parasites, although no differentiation between children and adults was made[44], and other global reports indicating increased microbial richness in helminth-infected individuals[53,54]. In contrast, a study conducted in Tanzania reported increased alpha diversity in parasite-infected mothers, whereas in children the effect was more limited, with only bacterial richness (Chao 1) increasing while other diversity measures did not show significant differences[55]. These discrepancies may be attributed to regional differences in parasite species and host responses. Nevertheless, the associations between parasite richness and microbial richness in this study are modest compared to the variance explained by age and location, highlighting that microbial community structure remains largely shaped by local environmental factors. Together, these patterns support a model in which parasite-microbiota associations are modulated by both host age and ecological context.

We observed specific microbial taxa associated with parasite infections. Notably, species from the Bacteroidaceae, Bifidobacteriaceae, and Lachnospiraceae families showed negative associations with parasites, in both locations in Gabon and the meta-analysis dataset. *Bifidobacterium* is a taxonomic group often associated with infant gut microbiota and may reflect developmental differences or microbiome maturity stages, rather than a direct link with parasitism. Conversely, the majority of species with a positive parasite association were Bacteroidales. Previous studies in humans have reported an increased abundance of Bacteroidales in parasite-infected samples[44,56], while mouse models of helminth infection have shown a decrease in Bacteroidales[20]. These results suggest that Bacteroidales may interact differently with helminth infections across host species, as human studies tend to report increases while mouse models often show decreases. Such apparent contradictions in literature may therefore arise from both biological differences between hosts and from limited taxonomic resolution in earlier analyses. Previous reports have also described an increase in the relative abundance of Clostridiales in the presence of STH parasites, often accompanied by a shift in relative proportions from Bacteroidota to Firmicutes[55,57–59]. However, these findings are based on compositional data, where increase in one

group necessarily implies decrease in another, and thus should be interpreted with caution. Additionally, it is important to emphasize that most differential taxa were method- and context-specific, with only a small subset reproducibly detected across locations and methods, highlighting the challenges of robust biomarker identification in microbiome–parasite studies.

It is important to also note that various species within these families associate differently with parasite infections, which may also result from analysis of compositional data. Interestingly, several of the bacterial taxa that correlated positively with parasite species richness in our data and meta-analysis are known mucus degraders[60]. Studies on mice have demonstrated that the absence of mucin production impairs their resistance to infection by *Trichuris muris*, a common mouse parasite[61]. It is plausible that when STH parasites colonize the gut, the bacterial mucin degradation dynamics are altered, resulting in shifts within the mucin-associated microbial communities.

In addition to taxonomic insights, functional profiling revealed metabolic associations tied to parasite status. In Lambaréné (low STH prevalence), only minimal functional differences were detected, indicating limited alteration to microbial metabolic capacity. However, in Ikobey (higher prevalence), we identified 27 pathways consistently associated with parasite positivity across the three statistical methods. Most of these pathways, particularly those involved in amino acid biosynthesis (e.g., threonine, methionine, lysine, histidine, valine, arginine) and central carbon metabolism (TCA cycle, pyruvate fermentation, coenzyme A biosynthesis), were depleted in parasite-positive individuals. These patterns echo reports of diminished microbial biosynthetic activity and shifts in energy metabolism during helminth infections in animal studies[62–64].

Only two pathways were enriched in parasite-positive samples: the purine nucleotide salvage superpathway and GDP-mannose–derived O-antigen biosynthesis. Both play critical roles in microbial adaptation to stress. The purine nucleotide salvage superpathway conserves cellular resources by recycling existing purine nucleotides, such as adenine and guanine, rather than relying on energy-intensive de novo synthesis, a particularly advantageous strategy under nutrient limitation or metabolic stress[65]. Meanwhile, GDP-mannose–derived O-antigen biosynthesis[66] is essential for maintaining bacterial cell-envelope integrity. GDP-mannose serves as a key precursor for the synthesis of O-antigen structures that reinforce the outer membrane. In a recent study, disruption of O-antigen biogenesis in *Escherichia coli* was shown to increase susceptibility to bile salts, a physiologically relevant gut stressor, highlighting its role in stress protection[67].

Depletion of the Bifidobacterium shunt, an obligate fermentative route in *Bifidobacterium* spp. characterized by fructose-6-phosphate phosphoketolase (F6PPK), was also consistently observed to be depleted in parasite-positive individuals in Ikobey. This pathway facilitates efficient carbohydrate fermentation into acetate and lactate, contributing to gut barrier maintenance[68] and immune modulation[69]. Importantly, both Bifidobacterium taxa and the shunt pathway were depleted even after adjusting for age group, suggesting that in addition to normal developmental variation parasite infections may also contribute to these changes. Supporting this, in a pig model of *Ascaris suum* infection, administration of *Bifidobacterium animalis* subsp. *lactis* (Bb12) helped mitigate infection-induced impairments in glucose absorption and localized immune responses[70]. Together, these functional findings align with and extend the taxonomic shifts we observed, demonstrating that higher parasite burden is associated with coordinated metabolic changes in the gut microbiome, particularly reductions in biosynthetic and fermentative capacity and selective enrichment of stress-responsive pathways.

The co-occurrence network analysis provided further insights into the ecological relationships between STH parasites and the gut microbiota. We observed significant associations between specific bacterial species and STH parasites, particularly in adults where all four STH species showed distinct co-occurrences with microbial taxa. Ascaris showed the highest number of unique co-occurrences, often with Firmicutes and Bacteroidota, indicating potential niche preferences and microbial community adaptations in response to parasitic colonization. These results suggest that STHs do not induce a uniform shift in microbiome composition, highlighting the nuanced nature of parasite-microbiota interactions in the gut ecosystem.

Expanding beyond Gabon, our cross-cohort meta-analysis indicates that helminth infections are associated with reproducible but modest shifts in gut microbial diversity across African populations. Although the effect sizes were small relative to geography and socioeconomic context, the consistent increase in alpha diversity and enrichment of certain Clostridia taxa suggest a consistent relationship between helminth and bacteria within the gut microbiome. One possible interpretation is that common environmental exposures, such as contamination, simultaneously shape parasite prevalence and microbial diversity; alternatively, helminth colonization itself may create ecological niches that favor specific microbial groups. Experimental work supports that helminth-induced immune modulation and altered microbial metabolism can reshape the gut microbiome. For example, murine infection with *Heligmosomoides polygyrus* increased short-

chain fatty acid (SCFA) production and conferred anti-inflammatory effects, changes that were transferred via fecal microbial transplantation and dependent on host GPR41 signaling[71]. At the same time, the strong influence of geography highlights that helminth–microbiome interactions are embedded within local ecological and cultural contexts, cautioning against broad generalizations across populations[44,72].

Despite the strengths of our study, such as high-depth metagenomic sequencing and robust validation techniques, there are limitations that warrant consideration. The observational and cross-sectional nature of the data limits our analyses to only infer associations. While metagenomic detection methods were carefully validated against qPCR, and read mapping, inherent biases related to DNA extraction, sequencing depth, and reference genome representation remain. Geographic and socioeconomic variation also contributes substantially to microbiome structure, sometimes more than parasites alone, and complicates cross-cohort comparisons. For instance, while parasite-microbiome associations were reproducible across African datasets, they remained modest relative to geographic structuring. This study is further limited by its focus on mothers and young children in only two Gabonese locations, with different lifestyles and parasite prevalence. Additionally, the lack of detailed deworming histories, dietary assessments, and environmental microbiota exposure limits our ability to account for confounding variables. Furthermore, because analyses were stratified by location to account for geographic and demographic heterogeneity, some parasite-microbiome associations were site-specific in direction or magnitude. This context dependence likely reflects genuine ecological variation rather than analytical inconsistency, and emphasizes the need for larger, harmonized datasets to disentangle environmental from parasitic effects. Despite these limitations, our findings highlight the value of combining molecular parasite detection with metagenomic microbiome profiling in underrepresented populations. The use of multiple detection platforms and analytical methods bolsters confidence in the robustness of observed patterns.

In summary, our study presents the first assessment of correlations between STH parasite infections and gut microbiota associations in rural communities in Gabon. By including stool samples from villages in a remote community in southern Gabon, we expand the epidemiological understanding of STH and their associations with the microbiome in these populations. Furthermore, our research enhances our comprehension of parasite-microbiome associations across diverse populations in Africa. Overall, our findings underscore the significance of parasite-microbiota associations, particularly in children who are commonly targeted for control

interventions through mass drug administration (MDA). According to the most recent WHO data (2022), an estimated 465,348 children in Gabon were in need of preventive chemotherapy against STH infections, including 321,403 school-aged children (SAC) and 143,945 preschool-aged children (Pre-SAC). However, coverage remains suboptimal: only 120,989 SAC (37.6%) received treatment, and just 25.5% of implementation units achieved the effective coverage threshold (≥75%). National coverage of SAC was only 37.6%[73], and the low treatment uptake underscores persistent challenges in MDA programs. One important factor contributing to hesitancy is the high burden of *Loa loa* infection in Gabon, particularly in regions such as Lambaréné, where co-endemicity with malaria, schistosomiasis, and other filarial infections is well documented[50,52,74]. Because *Loa loa* microfilaremia increases the risk of severe adverse events, including encephalopathy following albendazole treatment, health authorities and communities often approach deworming campaigns with caution.

Collectively, this proof-of-concept framework demonstrates how integrating metagenomic parasite detection with microbiome profiling across multiple African cohorts can uncover both shared and context-specific patterns of parasite-microbiome interactions. While geographic and demographic variables remain major determinants of gut microbiome structure, our findings establish a methodological and analytical baseline for future comparative studies aiming to disentangle environmental from parasitic influences on microbiome composition in global health context.

Our findings have significant implications for public health strategies, particularly in the design of deworming programs targeting vulnerable populations, such as children in endemic areas. By elucidating the association of STH infections with gut microbiome diversity and community structure, our study highlights the potential role of microbiota modulation in enhancing host resilience against parasitic infections. Further research is needed to explore the mechanistic underpinnings of parasite-microbiota interactions and their implications for host health and disease susceptibility in diverse epidemiological contexts. Future studies would benefit from integrating detailed sociodemographic and lifestyle information, including socioeconomic status, medication use, occupation, housing conditions, to better contextualize observed microbiome-parasite associations.

2.5. Materials and Methods

Study Populations - The study was conducted at the Centre de Recherches Médicales de Lambaréné (CERMEL), Gabon between November 2017 and February 2018. Study participants were mother and child pairs from multiple ethnic groups living in Lambaréné in the vicinity of CERMEL and those living in 5 Ikobey villages including; villages surrounding Tchibanga, Tranquille, Soga, Erouba, and Ikobey of the Southern part of the country (Fig. 1A). Given their similar lifestyles, all participants from the 5 villages are grouped as one community and labeled "Ikobey". Their subsistence practices are centered around hunting, agricultural crop cultivation, and livestock rearing[75,76]. In contrast, participants from and within the vicinity of Lambaréné, a semi-urban town in the Moyen-Ogooue province of Gabon, mostly practice fishing, farming, and a semi-westernized lifestyle. The metadata associated with samples in this study is shown in Table S6.

Approval and Informed consent - The study was reviewed and approved by the "Comité National d'Ethique " of Gabon with registration number PROT N˚0025/2017/SG/CNE. Stool samples were collected after participants provided written informed consent or assent.

Sample collection - Stool samples were collected in sterile plastic containers from both mothers and their children. Stool samples collected on-site (CERMEL) were aliquoted and stored at -20 °C within 2 hours of sample collection. Samples collected in the field (Ikobey) were transported in cold boxes to CERMEL and later stored at -20 °C. Samples were later transported to Germany on dry ice where they were stored at -80 °C before DNA extraction, qPCR, and sequencing.

Publicly available datasets - We utilized publicly available African gut metagenome datasets for studies performed in Cameroon[27,44], Burkina Faso[45], Ethiopia[46], and Madagascar[47]. The two Cameroon cohorts were sampled from ethnically diverse populations that practiced pastoralist, agropastoralist, or hunter-gatherer lifestyles[44], or from hunter-gatherers, farmers, or fishing populations in Southwest Cameroon[27]. The Burkina Faso cohort comprised samples collected from healthy volunteers in a single village in Burkina Faso[45]. The Madagascar cohort comprised samples collected from two ethnic groups in a remote rainforest region of north-eastern Madagascar[47] and the Ethiopia cohort included samples from healthy adult females[46]. We also included one USA cohort, which is a subset of the Human Microbiome Project (HMP) dataset[48]. Only female subjects who were described as healthy (mostly self-report) and ≥17 years old were included. The combined dataset used for our meta-analysis comprised 466 metagenome samples. The metagenomes from

the 5 African and one USA cohorts were sequenced on the Illumina platform at an average depth of 45 M read pairs. These metagenomes were retrieved from Sequence Read Archive (SRA) and processed as described here[77] and here[44]. The USA cohort was not included in the statistical analysis and was used for illustrative purposes only. The metadata associated with samples in the public datasets is shown in Table S8 and Table S9.

Detection of parasites by quantitative PCR - Diagnosis of STH parasites was performed by multiplex qPCR using protocols as described elsewhere[78,79]. The target species were *A. lumbricoides*, *T. trichiura*, *S. Stercoralis*, and the hookworm species *N. americanus*. The primers, probes, and reaction conditions for amplification were based on published protocols[79,80] with minor modifications. Primer sequences are given in Table S12. An internal control DNA from Phocine Herpesvirus 1 (PhHV-1) was added into the master mix to control for DNA amplification inhibition. The PCRs were split into two multiplex assays combining *A. lumbricoides, T. trichiura*, and PhHV-1 as targets (assay 1) and *S. stercoralis, N. americanus*, and PhHV-1 as targets (assay 2). The positive controls were plasmids carrying the targeted regions of the four target parasites, kindly provided by the Institute of Tropical Medicine (University of Tübingen). The target genes inserted in these plasmids were an 87 -bp fragment of the ITS1 sequence of *A. lumbricoides*, a 101-bp fragment of the 18S rRNA gene sequences of *S. stercoralis* and *T. trichiura,* and a 101-bp fragment of the ITS2 gene sequence of *N. americanus.* Wells without any template served as negative controls, and all samples, including controls, were tested in duplicate. The total reaction volume was 12.5 µL, which included: 6.25 µL Qiagen HotStarTaq Master Mix (QIAGEN GmbH, Hilden, Germany), 1 µL of 25 mM $MgCl_2$, 0.25 µL of 5 mg/ml BSA, 0.1 µL species-specific primers (final concentration of 800 nM), 0.0625 µL of probes (final concentration of 500 nM), 1.5 µL of PhHV-1 plasmid DNA (diluted to 10^{-7}), 2 µL of template DNA, 0.2125 µL of PCR-grade water (Sigma-Aldrich, Darmstadt, Germany). The qPCRs were conducted for 40 cycles using a Bio-Rad CFX284 Touch Real-Time PCR Detection System (Bio-Rad laboratories, Germany). Only samples with cycle threshold (Ct) values < 36 were considered positive (samples with Ct > 35 but < 36 were still considered positive). All negative controls had Ct values above 36 (qPCR values are shown in Table S6).

DNA extraction and shotgun metagenomic sequencing - Total DNA from fecal samples was extracted from approximately 250 mg of frozen stool aliquots. DNA extractions were performed using the Qiagen DNeasy PowerSoil HTP 96 kit (QIAGEN GmbH, Hilden, Germany)

following the manufacturer's instructions. Extraction blanks were included to control for reagents and environmental contamination. Extractions were performed under sterile conditions in a laminar flow hood, and the eluted DNA was stored at -20 °C following quantification with Qubit 4 fluorometer (Fisher Scientific GmbH, Schwerte, Germany). Genomic DNA libraries were constructed using the Nextera protocol[81] with in-house produced Tn5 enzyme[82]. Briefly, DNA was diluted to 5 ng/µL and tagmented with the Tn5 transposase, followed by amplification using a combination of paired-barcoded primers for 12 cycles. Libraries were pooled and quantified with a Qubit, followed by size selection for the 300-700 bp range on a BluePippin. The resulting libraries were then sequenced on an Illumina HiSeq3000 at the Max Planck Institute for Biology in Tübingen.

Processing of sequences and taxonomic profiling - All Illumina shotgun raw sequences were processed similarly to Youngblut and colleagues[77]. Briefly, raw reads were validated with fqtools v.2.0[83] and de-duplicated with the "clumpify" command from bbtools v37.78 (https://jgi.doe.gov/data-and-tools/bbtools/). Adapters were trimmed and quality controlled with Skewer v0.2.2[84], and the "bbduk" command from bbtools. Human genome reads mapped to the hg19 assembly were filtered with the "bbmap" command from bbtools.

Quality control (QC) reports for all reads were generated with fastqc v0.11.7 (https://github.com/s-andrews/FastQC) and multiQC v.1.5a[85]. The filtered reads were then subsampled to 5 million reads per sample, and a combination of Kraken 2[86] and Bracken v2.2[87] was used to classify filtered, quality-controlled reads with a custom database build from Genome Taxonomy Database (GTDB, Release 202; https://gtdb.ecogenomic.org/). Parasite profiling from metagenomic data was performed using KrakenUniq[39] with a custom database containing the reference genomes of the four target STH species, *A. lumbricoides*, *S. stercoralis*, *N. americanus*, and *T. trichiura* (accessions in Table S10). Raw reads were first classified with Kraken2 to identify and remove Bacterial and Archaeal sequences; the remaining unclassified reads were then queried against the STH database[34]. Bacteria and Archaea classification with Kraken2 were resolved to species level. KrakenUniq assignments were resolved at the species level based on unique k-mers. To reduce spurious assignments from low-complexity or contaminant sequences, we applied a minimum detection threshold of 1000 unique k-mers per species per sample, as recommended by the tool's authors. Counts below this threshold were set to zero (k-mer counts are shown in Table S7). The resulting k-mer counts were used both as abundance estimates and, when binarized, as

presence/absence calls. This approach was intended as a proof-of-concept for direct STH detection from shotgun metagenomes, with further validation performed through reference-based mapping and coverage analysis (described below).

Assessing parasite genome assembly quality and coverage - Reference genomes for all four target STH species were downloaded from NCBI and indexed with bowtie2-build (Bowtie2 v2.3.5)[88]. Metagenomic reads classified as "unclassified" by Kraken2 were mapped to these references using Bowtie2, and per-base coverage was calculated across each contig. Coverage metrics were summarized in R[89], including contig length, median coverage, minimum/maximum average converge per contig. BLASTn searches of high-coverage contigs confirmed sequence identity to the respective target parasite species. The overall sample processing workflow is shown in Fig. S4.

Statistical Analysis - The mean ages and proportions of STH parasite infections were compared between groups using the Wilcoxon test. The assessment whether STH infection status was more similar within mother–child pairs than expected by chance was performed separately for each sampling location (Ikobey and Lambaréné). For each parasite species (*A. lumbricoides, T. trichiura, N. americanus*, and *S. stercoralis*), as well as for any-parasite positivity, binary infection status was defined using qPCR cycle threshold values <36. For each location, parasite combination, mother–child concordance was calculated as the proportion of pairs where mother and child had the same infection status. The null distribution was generated from 10,000 permutations in which child infection statuses were randomly shuffled across pairs within the same location, preserving the number of positive and negative children. The P-value was defined as the proportion of permuted concordance values greater than or equal to the observed concordance.

All diversity measures were obtained from shotgun metagenomic data. Reads were randomly subsampled to 5000000. Diversity was assessed using QIIME 2[90] at a rarefaction depth of 300000 reads. The alpha diversity measures assessed include Shannon's index (which takes into account the abundances and evenness of species), and Faith's PD (which takes into account the phylogenetic relatedness of species). Beta diversity was assessed using Bray Curtis (takes into account species abundances) and Jaccard (measures presence/absence of species) dissimilarity indices. For the Gabon-only cohort, metadata variables tested with alpha and beta diversity in R include the number of parasites, age group, age z-scores and location. We accounted for potential familial clustering in microbial diversity analyses by including *FamilyID* (linking mother-child

pairs within households) as a random effect in linear mixed-effects models for alpha diversity, and as a stratification variable in PERMANOVA for beta diversity. In both cases, however, *FamilyID* explained negligible variance, and in the mixed models this resulted in singular fits. Given this, and consistent with prior work in the same population showing both intra-household and inter-household strain sharing[31], we proceeded with linear models that did not include a family-level effect.

Linear models were used to assess the relationships between alpha diversity and parasite species count, stratified by sampling location (Lambaréné and Ikobey), with age (z-scores) included as a covariate. For beta diversity, PERMANOVA was performed in R using the *adonis* function of the vegan package[91], on Bray-Curtis, Jaccard, Weighted, and Unweighted UniFrac distance matrices. In stratified analysis, models included parasite species count, age group, and standardized age (z-scores) as fixed effects. In addition, a pooled PERMANOVA model (without stratification) was run to estimate the effect of location on microbiome composition, where parasite species count, age, and location were included as fixed effects. Similar measures of alpha and beta diversity were employed in the meta-analysis. Linear mixed models were used to assess the relationship between the number of parasites and alpha diversity while accounting for non-independence of samples within the same dataset (random intercept: dataset_name). Since most of the datasets mapped uniquely to sampling countries (1.1), this random effect also adjusted for geographic differences in sampling context. The only exception was Cameroon, which included two independent datasets. PERMANOVA was also performed on beta diversity measures with 999 permutations constrained by dataset ID (dataset_name).

Differential abundance analysis was performed using three complementary methods: DESeq2[35], MaAslin2[36], and ANCOM-BC[37]. These analyses were applied to both the Gabon-only dataset and the broader African meta-analysis cohort to identify microbial species associated with parasite species richness. While DESeq2 remains widely used in RNA-seq studies and some microbiome analysis, it can be prone to inflated false positives when applied to compositional microbiome data, such as those derived from 16S rRNA, gene sequencing or metagenomic shotgun sequencing. These data types often exhibit characteristics like high sparsity, zero inflation, and compositional constraints, which DESeq2 was not originally designed to accommodate[92]. To mitigate such biases, we employed a consensus overlap approach, reporting only taxa consistently detected by multiple methods. This strategy reduces method-specific noise and highlights reproducible associations across differential-abundance tools[93,94]. For DESeq2, unnormalized

microbial species counts were used as input, with singleton reads removed to minimize the influence of sequencing errors. Geometric means were calculated before estimating size factors, and apeglm[95] was used for log fold changes shrinkage. The design formula included parasite species richness and location for the Gabon cohort, and parasite species richness, country, and age for the meta-analysis. In MaAslin2, species counts were log-transformed and normalized using total sum scaling (TSS). Both minimum abundance and minimum prevalence thresholds were set to 0.0. A linear model was used for the analysis, and continuous variables including age and parasite species richness were standardized using z-scores. The same design variables as in DESeq2 were applied. ANCOM-BC was run using the ancombc() function from the ANCOMBC R package. Parameters included a zero cutoff of 0.90, library size cutoff of 1000, and use of structural zeros, bias correction (neg_Ib = TRUE), and conserve = TRUE setting for conservative inference. The significance threshold was set at $\alpha = 0.05$ with Benjamini-Hochberg correction (p_adj_method = "BH"). The formula used for the Gabon-only dataset was "parasite_count + location", while for the meta-analysis it was "parasite_count + country + Age". In both cases, raw unnormalized counts (with singleton reads removed) were used as input, consistent with the other two methods.

For all three methods, microbial species were filtered for prevalence (>50% of samples) prior to analysis, with this step performed separately for Gabon and meta-analysis datasets. Multiple testing correction was performed using Benjamini-Hochberg method, and FDR-adjusted p-values below 0.05 were considered significant. Entries with missing values (NA), were removed prior to downstream analyses. To assess whether differentially abundant microbial taxa were enriched at higher taxonomic levels, we applied gene set enrichment analysis GSEA[38],using the R package *fgsea*[96]. All species evaluated in each method (not only those passing the significant threshold) were grouped by family, and their corresponding log2 fold changes were used to rank species. The minimum number of species required per family was set to 2, while the maximum number of species per family was set to 600 for the Gabon dataset and 800 for the meta-analysis dataset, reflecting the large number of DA species identified in the latter. To improve accuracy in p-value estimation, the eps parameter in FGSEA was set to zero.

Differential pathway abundance was assessed using HUMAnN3-derived, unnormalized, unstratified pathway abundance profiles. We applied the same three statistical frameworks used for taxonomic differential abundance, DESeq2, MaAsLin2, and ANCOM-BC, stratified by sampling location (Lambaréné and Ikobey). Parasite species count and age group were included

as fixed effects. Pathways were considered differentially abundant if they passed an FDR-adjusted p-value threshold of 0.1. In general, only pathways identified by at least two of the three methods were considered robust for interpretation. For the HUMAnN3 functional analysis stratified by location, this approach was applied as follows: in the Lambaréné cohort, DESeq2 and MaAsLin2 identified differentially abundant pathways with no overlap between the two methods, while ANCOM-BC did not detect any significant features; in this case, the pathways detected by DESeq2 and MaAsLin2 were reported individually. In the Ikobey cohort, all three methods identified overlapping pathways, and only the intersecting results were reported. This strategy ensures clarity, while emphasizing reproducible functional signals and mitigating method-specific false positives. For visualization, $\log_2$ fold change estimates were plotted against pathway identity, with overlapping pathways highlighted with stars (*** when detected by all 3 methods and ** when detected by 2 methods).

Co-occurrence abundance analysis was performed with the R package cooccur[97]. First, the microbiota species abundance counts were split between adults and children. Species counts were then transformed to relative abundances, filtered to a >50% prevalence, and then converted to presence/absence (1/0) in separate datasets. Similarly, the number of parasites from KrakenUniq was converted to presence/absence and then joined to the microbiota presence/absence table in the separate datasets. Probabilities of co-occurrence between microbiota and STH parasites were defined as negative if p_lt < 0.05, or positive if p_gt < 0.05, where p_lt and p_gt are probabilities that two species do not co-occur less or more frequently than expected. Only the species with significant probabilities of cooccurrences with the 4 STH parasites were included in the network graphs. The weights are the differences between the observed and expected frequencies of co-occurrence normalized by the sample size (n=155) for adults and children respectively.

Summary of statistical thresholds and multiple testing correction. Unless otherwise specified, all tests were two-sided. Multiple testing correction using the Benjamini-Hochberg false discovery rate (FDR) procedure was applied to analyses involving multiple comparisons, including alpha and beta diversity models (both within the Gabon cohort and in the meta-analysis), chi-square tests of parasite prevalence across sampling locations and countries, and all differential abundance and pathway analyses (DESeq2, MaAsLin2, and ANCOM-BC). FDR-adjusted p-values < 0.05 were considered significant, except for pathway-level analyses where a threshold of 0.1 was used. For analyses involving a limited number of comparisons, such as tests for mother-child concordance, linear and logistic models of parasite richness or presence/absence, and

comparisons of age or infection prevalence between sampling locations, unadjusted p-values are reported.

The following R[89] packages were used for data processing and visualizations: phyloseq[98], microbiome[99], dplyr[100], tidytable[101], tidygraph[102], broom[103], igraph[104], ggplot2[105], ggraph[106], UpsetR[107], complexUpset[108], fgsea[96], MaAsLin2[36], concur[97].

2.6. Acknowledgments

We are grateful to the laboratory personnel of CERMEL-Gabon and members of the Department of Microbiome Science at the MPI for Biology, in particular Silke Dauser, for technical assistance. This work was funded by the Max Planck Society.

Disclosure statement

The authors declare that there are no conflicts of interest related to this work.

2.7. Author contributions

Conceptualization, Methodology, Writing – Original Draft, and Visualization: M.M.N., N.D.Y., A.V.T., K.E.H., and R.E.L.

Formal Analysis: M.M.N., N.D.Y., and A.V.T.

Investigation: B.R.A., J.F.Z., V.T.S., J.L.F., M.M.N., and A.A.A

Sample Processing, and Data Curation: P.A.N.M., M.N.M., and M.M.N.

Supervision: A.A.A., N.D.Y., and R.E.L.

Funding Acquisition: P.G.K., and R.E.L.

2.7. Data availability statement

The authors confirm that all data supporting the findings of this study are included within the article and its supplementary materials. The raw sequence data for the Gabon cohort can be accessed from the European Nucleotide Archive under the study accession numbers PRJEB46788 and PRJEB86954. Additionally, the meta-analysis dataset and references are provided in the supplementary tables.

The supplementary tables associated with this manuscript are available online through the following PubMed link (PMID: 41358671).

2.8. Supplementary Figures

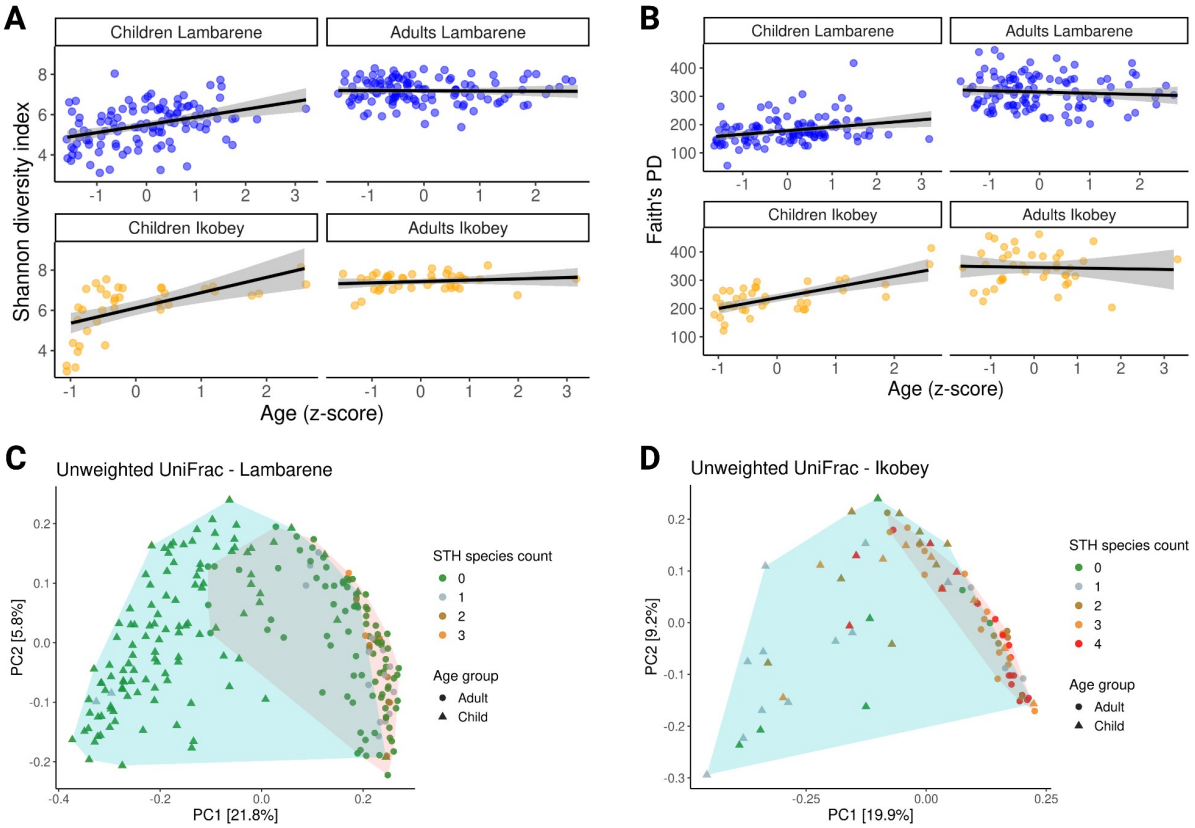

Figure S1: **Gut Microbiome Diversity by Age Group and Location**

A) Correlation between gut microbiome Shannon diversity index and age z-scores for adults and children by location (correlation method: LM). For children, $R^2 = 0.33$ in Ikobey and $R^2 = 0.15$ in Lambaréné; for adults, $R^2 = 0.02$ in both Ikobey and $R^2 = 0$ in Lambaréné. **B)** Correlation between Faith's Phylogenetic Diversity (PD) and age z-scores for adults and children by location (correlation method: LM). For children, $R^2 = 045$ in Ikobey and $R^2 = 0.08$ in Lambaréné; for adults, $R^2 = 0$ in both Lambaréné and Ikobey. **C)** Principal Coordinates Analysis (PCoA) of unweighted UniFrac values for Lambaréné samples (n = 230), colored by STH species count and shaped by age group (Adults = circles, children = triangles). **D)** PCoA of unweighted UniFrac values for Ikobey samples (n = 80), colored by STH species count and shaped by age group (Adults = circles, children = triangles).

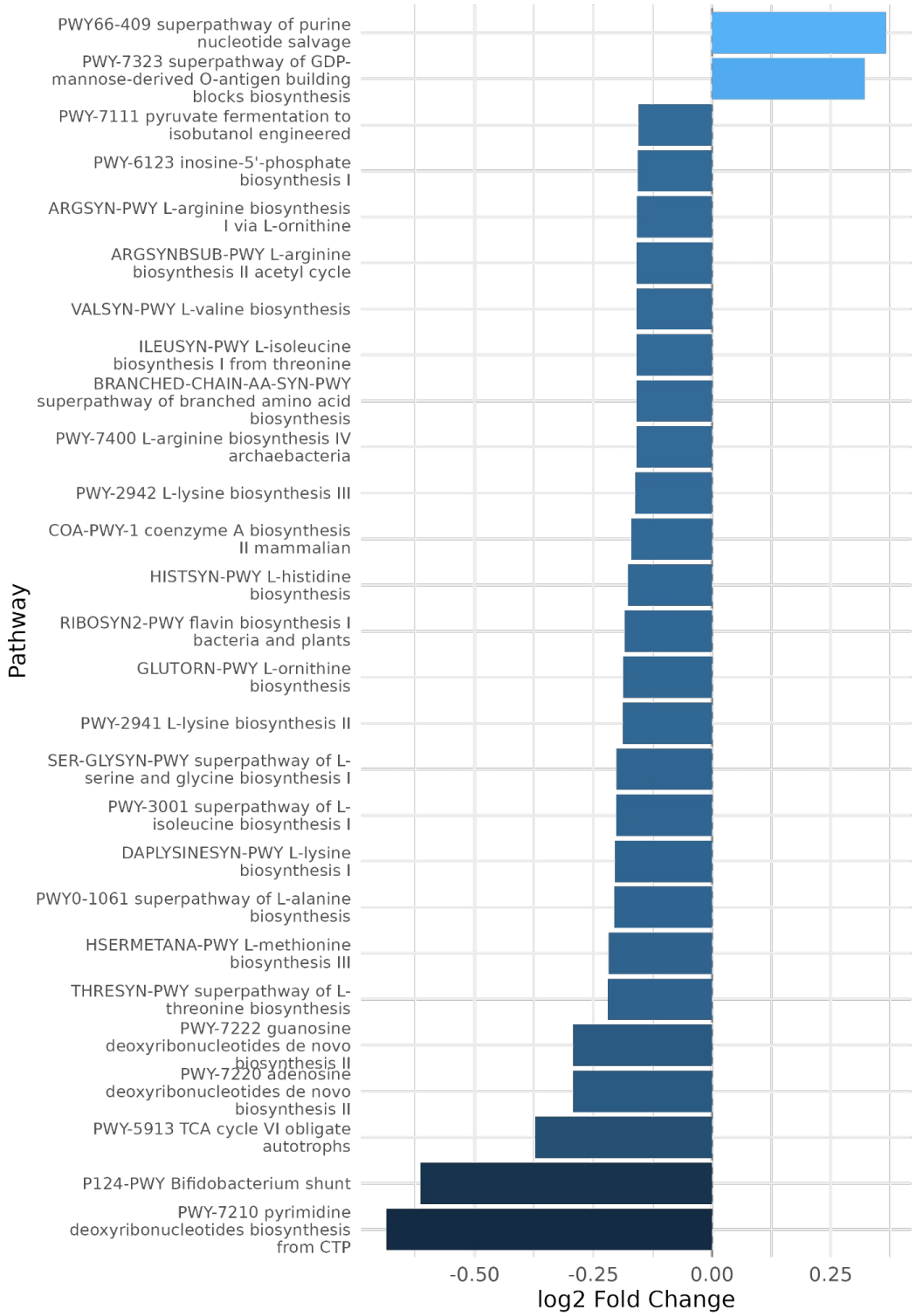
PWY66-409 superpathway of purine nucleotide salvage
PWY-7323 superpathway of GDP-mannose-derived O-antigen building blocks biosynthesis
PWY-7111 pyruvate fermentation to isobutanol engineered
PWY-6123 inosine-5'-phosphate biosynthesis I
ARGSYN-PWY L-arginine biosynthesis I via L-ornithine
ARGSYNBSUB-PWY L-arginine biosynthesis II acetyl cycle
VALSYN-PWY L-valine biosynthesis
ILEUSYN-PWY L-isoleucine biosynthesis I from threonine
BRANCHED-CHAIN-AA-SYN-PWY superpathway of branched amino acid biosynthesis
PWY-7400 L-arginine biosynthesis IV archaebacteria
PWY-2942 L-lysine biosynthesis III
COA-PWY-1 coenzyme A biosynthesis II mammalian
HISTSYN-PWY L-histidine biosynthesis
RIBOSYN2-PWY flavin biosynthesis I bacteria and plants
GLUTORN-PWY L-ornithine biosynthesis
PWY-2941 L-lysine biosynthesis II
SER-GLYSYN-PWY superpathway of L-serine and glycine biosynthesis I
PWY-3001 superpathway of L-isoleucine biosynthesis I
DAPLYSINESYN-PWY L-lysine biosynthesis I
PWY0-1061 superpathway of L-alanine biosynthesis
HSERMETANA-PWY L-methionine biosynthesis III
THRESYN-PWY superpathway of L-threonine biosynthesis
PWY-7222 guanosine deoxyribonucleotides de novo biosynthesis II
PWY-7220 adenosine deoxyribonucleotides de novo biosynthesis II
PWY-5913 TCA cycle VI obligate autotrophs
P124-PWY Bifidobacterium shunt
PWY-7210 pyrimidine deoxyribonucleotides biosynthesis from CTP
Pathway
-0.50
-0.25
0.00
0.25
log2 Fold Change

Figure S2: Differentially abundant pathways in Ikobey

Log_2 fold change estimates for the 27 pathways identified by all three methods (DESeq2, MaAsLin2, ANCOM-BC). Pathways enriched in parasite-positive individuals are shown with positive values; depleted pathways have negative values. Pathway IDs correspond to MetaCyc identifiers.

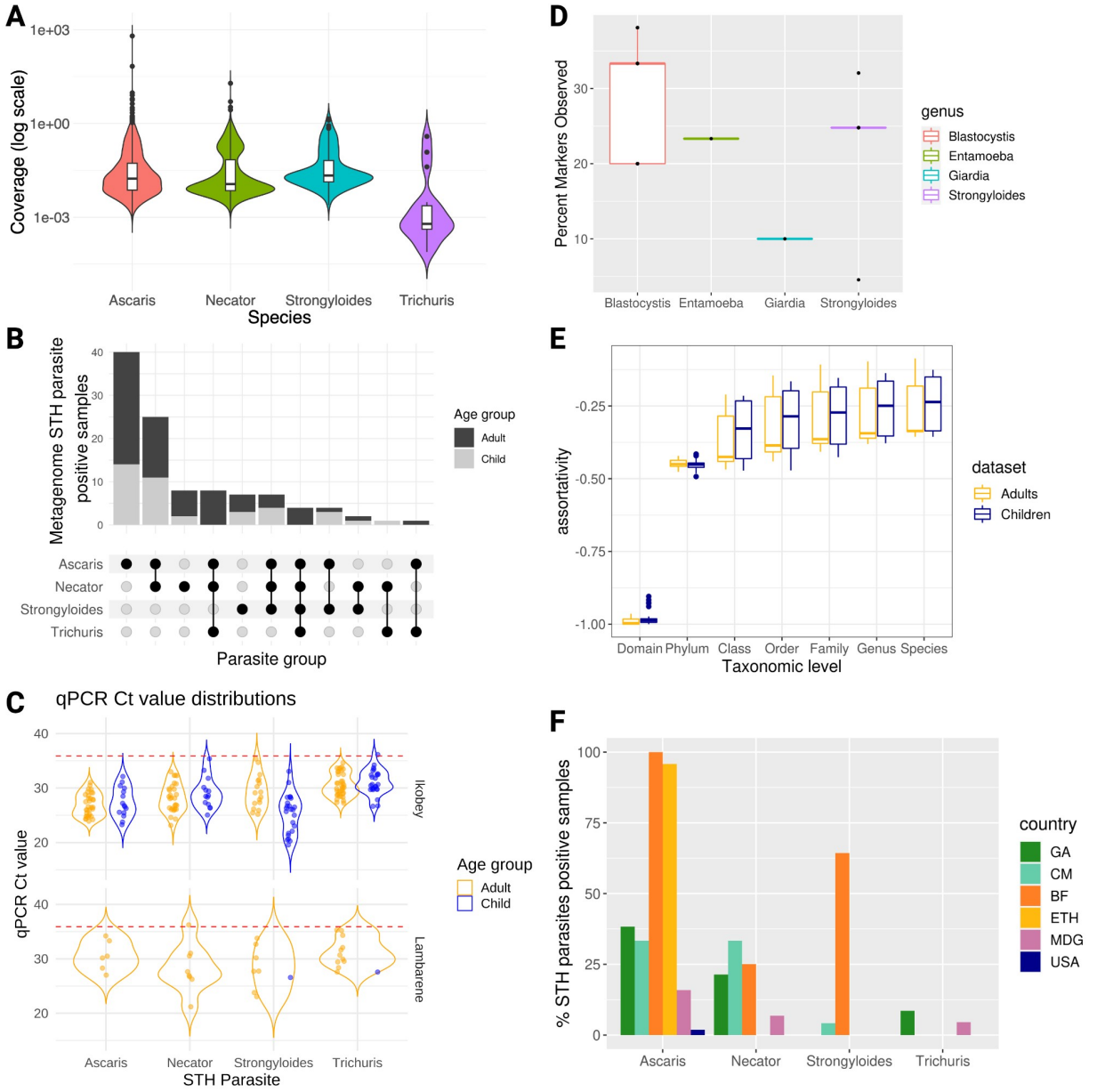

Figure S3: Detection and characterization of soil-transmitted helminths (STHs) in African gut metagenomes.

A) Boxplots of average coverage depth (log_{10} scale) for contigs from the reference genomes of *A. lumbricoides*, *N. americanus*, *S. stercoralis* and *T. trichiura*, based on mapping Kraken2-unclassified reads with Bowtie2. Each point is a contig; contigs without mapped reads were excluded. **B**) Upset plots showing co-detection patterns of the four STHs in Gabonese mother-

child metagenomes. **C**) Distribution of qPCR Ct values for the four STHs in Lambaréné and Ikobey samples. Points = positive samples; violins = density. Lower Ct = higher parasite DNA. Dashed red line = positivity threshold. **D**) Percentage of STH-associated markers detected in Gabonese mother-child metagenomes using the Eukdetect database. **E**) Boxplots of assortativity coefficients (node connections) across taxonomic levels in co-occurrence networks. For each network, 100 random subsets of 230 nodes were analyzed, and assortativity values calculated per taxonomy level. **F**) Bar plots showing the percentage of STH-positive samples detected from metagenomes across different datasets, colored by country of origin.

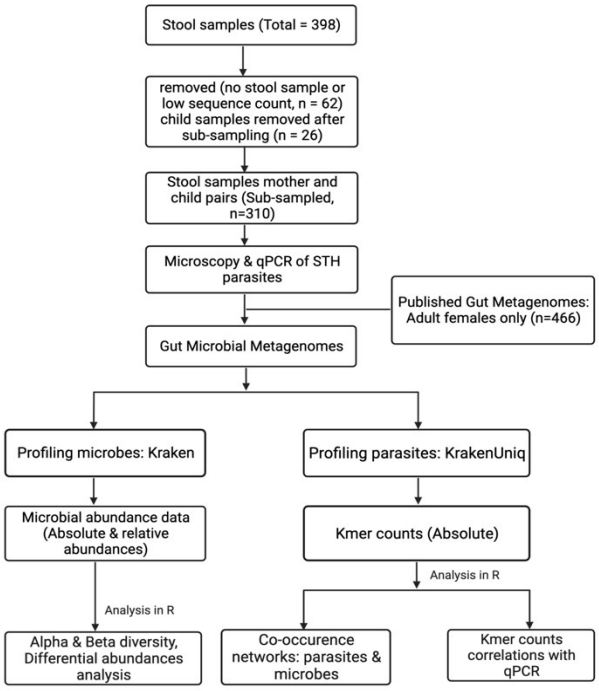

Figure S4: **Sample Processing Workflow**

Participants without stool samples and samples with low sequencing counts (<100,000 reads) were excluded from downstream analysis (n = 62). An additional 26 samples were removed to focus on mother-child pairs. Publicly available metagenomes from adult women in studies conducted across four African countries (n = 265) and this study's cohort (n = 201) were included in the meta-analysis.

2.9. References

1. Soil-transmitted helminth infections. https://www.who.int/news-room/fact-sheets/detail/soil-transmitted-helminth-infections.
2. Sartorius B, Cano J, Simpson H, Tusting LS, Marczak LB, Miller-Petrie MK, Kinvi B, Zoure H, Mwinzi P, Hay SI, et al. Prevalence and intensity of soil-transmitted helminth infections of children in sub-Saharan Africa, 2000–18: a geospatial analysis. The Lancet Global Health. 2021; 9:e52–60. https://doi.org/10.1016/S2214-109X(20)30398-3

3. Pullan RL, Smith JL, Jasrasaria R, Brooker SJ. Global numbers of infection and disease burden of soil transmitted helminth infections in 2010. Parasit Vectors. 2014; 7:37. http://dx.doi.org/10.1186/1756-3305-7-37
4. Bronzan RN, Dorkenoo AM, Agbo YM, Halatoko W, Layibo Y, Adjeloh P, Teko M, Sossou E, Yakpa K, Tchalim M, et al. Impact of community-based integrated mass drug administration on schistosomiasis and soil-transmitted helminth prevalence in Togo. PLoS Negl Trop Dis. 2018; 12:e0006551. http://dx.doi.org/10.1371/journal.pntd.0006551
5. Geneva: World Health Organization, Licence: C C By-Nc-Sa 3. Guideline: Preventive chemotherapy to control soil-transmitted helminth infections in at-risk population groups. World Health Organization 2017. http://apps.who.int/iris/bitstream/10665/258983/1/9789241550116-eng.pdf?ua=1
6. Savioli L, Albonico M, Daumerie D, Lo NC, Russell Stothard J, Asaolu S, Tchuenté LAT, Anderson RM. Review of the 2017 WHO Guideline: Preventive chemotherapy to control soil-transmitted helminth infections in at-risk population groups. An opportunity lost in translation. PLOS Neglected Tropical Diseases. 2018; 12:e0006296. http://dx.doi.org/10.1371/journal.pntd.0006296
7. Montresor A, Mwinzi P, Mupfasoni D, Garba A. Reduction in DALYs lost due to soil-transmitted helminthiases and schistosomiasis from 2000 to 2019 is parallel to the increase in coverage of the global control programmes. PLoS Negl Trop Dis. 2022; 16:e0010575. http://dx.doi.org/10.1371/journal.pntd.0010575
8. Krolewiecki A, Nutman TB. Strongyloidiasis: A Neglected Tropical Disease. Infect Dis Clin North Am. 2019; 33:135–51. http://dx.doi.org/10.1016/j.idc.2018.10.006
9. Adegnika AA, Agnandji ST, Chai SK, Ramharter M, Breitling L, Kendjo E, Issifou S, Yazdanbakhsh M, Kombila M, Kremsner PG. Increased prevalence of intestinal helminth infection during pregnancy in a Sub-Saharan African community. Wien Klin Wochenschr. 2007; 119:712–6. http://dx.doi.org/10.1007/s00508-007-0907-z
10. Kvalsvig JD, Cooppan RM, Connolly KJ. The effects of parasite infections on cognitive processes in children. Ann Trop Med Parasitol. 1991; 85:551–68. http://dx.doi.org/10.1080/00034983.1991.11812608
11. Pabalan N, Singian E, Tabangay L, Jarjanazi H, Boivin MJ, Ezeamama AE. Soil-transmitted helminth infection, loss of education and cognitive impairment in school-aged

children: A systematic review and meta-analysis. PLoS Negl Trop Dis. 2018; 12:e0005523. http://dx.doi.org/10.1371/journal.pntd.0005523

12. Pan SC, Ward DV, Yin Y, Hu Y, Elfawal MA, Clark RE, Aroian RV. Cognitive and microbiome impacts of experimental Ancylostoma ceylanicum hookworm infections in hamsters. Sci Rep. 2019; 9:7868. http://dx.doi.org/10.1038/s41598-019-44301-4
13. Hagel I, Cabrera M, Puccio F, Santaella C, Buvat E, Infante B, Zabala M, Cordero R, Di Prisco MC. Co-infection with Ascaris lumbricoides modulates protective immune responses against Giardia duodenalis in school Venezuelan rural children. Acta Trop. 2011; 117:189–95. http://dx.doi.org/10.1016/j.actatropica.2010.12.001
14. Weatherhead J, Cortés AA, Sandoval C, Vaca M, Chico M, Loor S, Cooper PJ, Mejia R. Comparison of cytokine responses in Ecuadorian children infected with Giardia, Ascaris, or both parasites. Am J Trop Med Hyg. 2017; 96:1394–9. https://ajtmh.org/doi/10.4269/ajtmh.16-0580
15. Trelis M, Taroncher-Ferrer S, Gozalbo M, Ortiz V, Soriano JM, Osuna A, Merino-Torres JF. Giardia intestinalis and Fructose Malabsorption: A Frequent Association. Nutrients. 2019; 11. http://dx.doi.org/10.3390/nu11122973
16. Rosa BA, Supali T, Gankpala L, Djuardi Y, Sartono E, Zhou Y, Fischer K, Martin J, Tyagi R, Bolay FK, et al. Differential human gut microbiome assemblages during soil-transmitted helminth infections in Indonesia and Liberia. Microbiome. 2018; 6:33. http://dx.doi.org/10.1186/s40168-018-0416-5
17. Leung JM, Graham AL, Knowles SCL. Parasite-Microbiota Interactions With the Vertebrate Gut: Synthesis Through an Ecological Lens. Front Microbiol. 2018; 9:843. http://dx.doi.org/10.3389/fmicb.2018.00843
18. Rafaluk-Mohr C, Gerth M, Sealey JE, Ekroth AKE, Aboobaker AA, Kloock A, King KC. Microbial protection favors parasite tolerance and alters host-parasite coevolutionary dynamics. Curr Biol. 2022; 32:1593–8.e3. https://www.sciencedirect.com/science/article/pii/S0960982222001257
19. White EC, Houlden A, Bancroft AJ, Hayes KS, Goldrick M, Grencis RK, Roberts IS. Manipulation of host and parasite microbiotas: Survival strategies during chronic nematode infection. Science Advances. 2018; 4:eaap7399. https://www.science.org/doi/abs/10.1126/sciadv.aap7399
20. Ramanan D, Bowcutt R, Lee SC, Tang MS, Kurtz ZD, Ding Y, Honda K, Gause WC,

Blaser MJ, Bonneau RA, et al. Helminth infection promotes colonization resistance via type 2 immunity. Science. 2016; 352:608–12. http://dx.doi.org/10.1126/science.aaf3229

21. McKay DM, Shute A, Lopes F. Helminths and intestinal barrier function. Tissue Barriers. 2017; 5:e1283385. http://dx.doi.org/10.1080/21688370.2017.1283385
22. Loke P 'ng, Harris NL. Networking between helminths, microbes, and mammals. Cell Host Microbe. 2023; 31:464–71. https://www.sciencedirect.com/science/article/pii/S1931312823000781
23. Loke P 'ng, Lee SC, Oyesola OO. Effects of helminths on the human immune response and the microbiome. Mucosal Immunol. 2022; 15:1224–33. https://pubmed.ncbi.nlm.nih.gov/35732819/
24. Croese J, Giacomin P, Navarro S, Clouston A, McCann L, Dougall A, Ferreira I, Susianto A, O'Rourke P, Howlett M, et al. Experimental hookworm infection and gluten microchallenge promote tolerance in celiac disease. J Allergy Clin Immunol. 2015; 135:508–16. http://dx.doi.org/10.1016/j.jaci.2014.07.022
25. Fu Y, Zhang K, Yang M, Li X, Chen Y, Li J, Xu H, Dhakal P, Zhang L. Metagenomic analysis reveals the relationship between intestinal protozoan parasites and the intestinal microecological balance in calves. Parasit Vectors. 2023; 16:NA. https://go.gale.com/ps/i.do?id=GALE%7CA759214574&sid=sitemap&v=2.1&it=r&p=HRCA&sw=w
26. Kirstahler P, Aarestrup FM, Pamp SJ. Detection of Parasites in Microbiomes using Metagenomics. bioRxiv. 2022; 2022.03.27.485979. https://www.biorxiv.org/content/10.1101/2022.03.27.485979v1.full
27. Lokmer A, Cian A, Froment A, Gantois N, Viscogliosi E, Chabé M, Ségurel L. Use of shotgun metagenomics for the identification of protozoa in the gut microbiota of healthy individuals from worldwide populations with various industrialization levels. PLoS One. 2019; 14:e0211139. http://dx.doi.org/10.1371/journal.pone.0211139
28. Miller RR, Montoya V, Gardy JL, Patrick DM, Tang P. Metagenomics for pathogen detection in public health. Genome Med. 2013; 5:81. https://genomemedicine.biomedcentral.com/articles/10.1186/gm485
29. Adegnika AA, Ramharter M, Agnandji ST, Ateba Ngoa U, Issifou S, Yazdanbahksh M, Kremsner PG. Epidemiology of parasitic co-infections during pregnancy in Lambaréné,

Gabon. Trop Med Int Health. 2010; 15:1204–9. http://dx.doi.org/10.1111/j.1365-3156.2010.02598.x

30. Dejon-Agobé JC, Honkpehedji YJ, Zinsou JF, Edoa JR, Adégbitè BR, Mangaboula A, Agnandji ST, Mombo-Ngoma G, Ramharter M, Kremsner PG, et al. Epidemiology of Schistosomiasis and Soil-Transmitted Helminth Coinfections among Schoolchildren Living in Lambaréné, Gabon. Am J Trop Med Hyg. 2020; 103:325–33. http://dx.doi.org/10.4269/ajtmh.19-0835
31. Suzuki TA, Fitzstevens JL, Schmidt VT, Enav H, Huus KE, Mbong Ngwese M, Grießhammer A, Pfleiderer A, Adegbite BR, Zinsou JF, et al. Codiversification of gut microbiota with humans. Science. 2022; 377:1328–32. http://dx.doi.org/10.1126/science.abm7759
32. M'bondoukwé NP, Kendjo E, Mawili-Mboumba DP, Koumba Lengongo JV, Offouga Mbouoronde C, Nkoghe D, Touré F, Bouyou-Akotet MK. Prevalence of and risk factors for malaria, filariasis, and intestinal parasites as single infections or co-infections in different settlements of Gabon, Central Africa. Infect Dis Poverty. 2018; 7:6. http://dx.doi.org/10.1186/s40249-017-0381-4
33. Edoa JR, Adégbitè BR, Honkpéhèdji YJ, Zinsou JF, Boussougou-Sambe ST, Woldearegai TG, Mordmüller B, Adegnika AA, Dejon-Agobé JC. Epidemiology of soil-transmitted helminth infections and the differential effect of treatment on the distribution of helminth species in rural areas of Gabon. Trop Med Health. 2024; 52:3. https://tropmedhealth.biomedcentral.com/articles/10.1186/s41182-023-00567-z
34. de la Cuesta-Zuluaga J, Ley RE, Youngblut ND. Struo: a pipeline for building custom databases for common metagenome profilers. Bioinformatics. 2020; 36:2314–5. http://dx.doi.org/10.1093/bioinformatics/btz899
35. Love MI, Huber W, Anders S. Moderated estimation of fold change and dispersion for RNA-seq data with DESeq2. Genome Biol. 2014; 15:550. http://dx.doi.org/10.1186/s13059-014-0550-8
36. Mallick H, Rahnavard A, McIver LJ, Ma S, Zhang Y, Nguyen LH, Tickle TL, Weingart G, Ren B, Schwager EH, et al. Multivariable association discovery in population-scale meta-omics studies. PLoS Comput Biol. 2021; 17:e1009442. http://dx.doi.org/10.1371/journal.pcbi.1009442
37. Lin H, Peddada SD. Analysis of compositions of microbiomes with bias correction. Nat

Commun. 2020; 11:3514. http://dx.doi.org/10.1038/s41467-020-17041-7

38. Subramanian A, Tamayo P, Mootha VK, Mukherjee S, Ebert BL, Gillette MA, Paulovich A, Pomeroy SL, Golub TR, Lander ES, et al. Gene set enrichment analysis: A knowledge-based approach for interpreting genome-wide expression profiles. Proceedings of the National Academy of Sciences. 2005; 102:15545–50. https://www.pnas.org/doi/abs/10.1073/pnas.0506580102
39. Breitwieser FP, Baker DN, Salzberg SL. KrakenUniq: confident and fast metagenomics classification using unique k-mer counts. Genome Biol. 2018; 19:198. http://dx.doi.org/10.1186/s13059-018-1568-0
40. Douglass AP, O'Brien CE, Offei B, Coughlan AY, Ortiz-Merino RA, Butler G, Byrne KP, Wolfe KH. Coverage-versus-length plots, a simple quality control step for de Novo yeast genome sequence assemblies. G3 (Bethesda). 2019; 9:879–87. http://dx.doi.org/10.1534/g3.118.200745
41. Ekblom R, Smeds L, Ellegren H. Patterns of sequencing coverage bias revealed by ultra-deep sequencing of vertebrate mitochondria. BMC Genomics. 2014; 15:467. http://dx.doi.org/10.1186/1471-2164-15-467
42. Li D, Liu C-M, Luo R, Sadakane K, Lam T-W. MEGAHIT: an ultra-fast single-node solution for large and complex metagenomics assembly via succinct de Bruijn graph. Bioinformatics. 2015; 31:1674–6. http://dx.doi.org/10.1093/bioinformatics/btv033
43. Lind AL, Pollard KS. Accurate and sensitive detection of microbial eukaryotes from whole metagenome shotgun sequencing. Microbiome. 2021; 9:58. http://dx.doi.org/10.1186/s40168-021-01015-y
44. Rubel MA, Abbas A, Taylor LJ, Connell A, Tanes C, Bittinger K, Ndze VN, Fonsah JY, Ngwang E, Essiane A, et al. Lifestyle and the presence of helminths is associated with gut microbiome composition in Cameroonians. Genome Biol. 2020; 21:122. http://dx.doi.org/10.1186/s13059-020-02020-4
45. Jacobson DK, Honap TP, Ozga AT, Meda N, Kagoné TS, Carabin H, Spicer P, Tito RY, Obregon-Tito AJ, Reyes LM, et al. Publisher Correction: Analysis of global human gut metagenomes shows that metabolic resilience potential for short-chain fatty acid production is strongly influenced by lifestyle. Sci Rep. 2021; 11:10114. http://dx.doi.org/10.1038/s41598-021-89719-x
46. Tett A, Huang KD, Asnicar F, Fehlner-Peach H, Pasolli E, Karcher N, Armanini F, Manghi

P, Bonham K, Zolfo M, et al. The Prevotella copri Complex Comprises Four Distinct Clades Underrepresented in Westernized Populations. Cell Host Microbe. 2019; 26:666–79.e7. http://dx.doi.org/10.1016/j.chom.2019.08.018

47. Pasolli E, Asnicar F, Manara S, Zolfo M, Karcher N, Armanini F, Beghini F, Manghi P, Tett A, Ghensi P, et al. Extensive Unexplored Human Microbiome Diversity Revealed by Over 150,000 Genomes from Metagenomes Spanning Age, Geography, and Lifestyle. Cell. 2019; 176:649–62.e20. http://dx.doi.org/10.1016/j.cell.2019.01.001
48. Human Microbiome Project Consortium. Structure, function and diversity of the healthy human microbiome. Nature. 2012; 486:207–14. http://dx.doi.org/10.1038/nature11234
49. Honkpéhèdji YJ, Adegbite BR, Zinsou JF, Dejon-Agobé JC, Edoa J-R, Zoleko Manego R, McCall M, Mbong Ngwese M, Lotola Mougeni F, Mombo-Ngoma G, et al. Association of low birth weight and polyparasitic infection during pregnancy in Lambaréné, Gabon. Trop Med Int Health. 2021; 26:973–81. http://dx.doi.org/10.1111/tmi.13591
50. Dejon-Agobé JC, Chassem-Lapue C, Nguema-Moure PA, Maloum MN, Lontchi R-AL, Saidou M, Djida Y, Edoa JR, Honkpéhèdji YJ, Zinsou JF, et al. Community surveys of the prevalence, distribution, and coinfection of helminth and protozoan infections in semiurban and rural areas of Gabon, Central Africa. PLoS Negl Trop Dis. 2025; 19:e0013161. http://dx.doi.org/10.1371/journal.pntd.0013161
51. Nguema-Moure PA, Adegbite BR, Nzamba Maloum M, Dejon-Agobé J-C, Laclong Lontchi R-A, Honkpehedji YJ, Manfoumbi Mabicka D-C, Chassem-Lapue C, Sole PW, Ogoula S, et al. Polyparasitic infections: Associated factors and effect on the haemoglobin level of children living in Lambaréné remote and surrounding rural areas from Gabon—A cross-sectional study. Trop Med Infect Dis. 2025; 10:218. http://dx.doi.org/10.3390/tropicalmed10080218
52. Dejon-Agobé JC, Zinsou JF, Honkpehedji YJ, Ateba-Ngoa U, Edoa J-R, Adegbite BR, Mombo-Ngoma G, Agnandji ST, Ramharter M, Kremsner PG, et al. Schistosoma haematobium effects on Plasmodium falciparum infection modified by soil-transmitted helminths in school-age children living in rural areas of Gabon. PLoS Negl Trop Dis. 2018; 12:e0006663. http://dx.doi.org/10.1371/journal.pntd.0006663
53. Lee SC, Tang MS, Lim YAL, Choy SH, Kurtz ZD, Cox LM, Gundra UM, Cho I, Bonneau R, Blaser MJ, et al. Helminth Colonization Is Associated with Increased Diversity of the Gut Microbiota. PLoS Neglected Tropical Diseases. 2014; 8:e2880.

http://dx.doi.org/10.1371/journal.pntd.0002880

54. Toro-Londono MA, Bedoya-Urrego K, Garcia-Montoya GM, Galvan-Diaz AL, Alzate JF. Intestinal parasitic infection alters bacterial gut microbiota in children. PeerJ. 2019; 7:e6200. http://dx.doi.org/10.7717/peerj.6200
55. Chen H, Mozzicafreddo M, Pierella E, Carletti V, Piersanti A, Ali SM, Ame SM, Wang C, Miceli C. Dissection of the gut microbiota in mothers and children with chronic Trichuris trichiura infection in Pemba Island, Tanzania. Parasit Vectors. 2021; 14:62. http://dx.doi.org/10.1186/s13071-021-04580-1
56. Rosa BA, Snowden C, Martin J, Fischer K, Kupritz J, Beshah E, Supali T, Gankpala L, Fischer PU, Urban JF Jr, et al. Whipworm-Associated Intestinal Microbiome Members Consistent Across Both Human and Mouse Hosts. Front Cell Infect Microbiol. 2021; 11:637570. http://dx.doi.org/10.3389/fcimb.2021.637570
57. Costea PI, Hildebrand F, Arumugam M, Bäckhed F, Blaser MJ, Bushman FD, de Vos WM, Ehrlich SD, Fraser CM, Hattori M, et al. Enterotypes in the landscape of gut microbial community composition. Nat Microbiol. 2018; 3:8–16. http://dx.doi.org/10.1038/s41564-017-0072-8
58. Kupritz J, Angelova A, Nutman TB, Gazzinelli-Guimaraes PH. Helminth-Induced Human Gastrointestinal Dysbiosis: a Systematic Review and Meta-Analysis Reveals Insights into Altered Taxon Diversity and Microbial Gradient Collapse. MBio. 2021; 12:e0289021. http://dx.doi.org/10.1128/mBio.02890-21
59. Partida-Rodriguez O, Nieves-Ramirez M, Laforest-Lapointe I, Brown EM, Parfrey L, Valadez-Salazar A, Thorson L, Morán P, Gonzalez E, Rascon E, et al. Exposure to parasitic protists and helminths changes the intestinal community structure of bacterial communities in a cohort of mother-child binomials from a semirural setting in Mexico. mSphere. 2021; 6:e0008321. https://journals.asm.org/doi/10.1128/mSphere.00083-21
60. Raimondi S, Musmeci E, Candeliere F, Amaretti A, Rossi M. Identification of mucin degraders of the human gut microbiota. Sci Rep. 2021; 11:1–10. https://www.nature.com/articles/s41598-021-90553-4
61. Hasnain SZ, Wang H, Ghia J-E, Haq N, Deng Y, Velcich A, Grencis RK, Thornton DJ, Khan WI. Mucin gene deficiency in mice impairs host resistance to an enteric parasitic infection. Gastroenterology. 2010; 138:1763–71. http://dx.doi.org/10.1053/j.gastro.2010.01.045

62. Houlden A, Hayes KS, Bancroft AJ, Worthington JJ, Wang P, Grencis RK, Roberts IS. Chronic Trichuris muris infection in C57BL/6 mice causes significant changes in host Microbiota and metabolome: Effects reversed by pathogen clearance. PLoS One. 2015; 10:e0125945. http://dx.doi.org/10.1371/journal.pone.0125945
63. Wang Y, Xiao S-H, Xue J, Singer BH, Utzinger J, Holmes E. Systems metabolic effects of a necator americanus infection in Syrian hamster. J Proteome Res. 2009; 8:5442–50. http://dx.doi.org/10.1021/pr900711j
64. Li RW, Wu S, Li W, Navarro K, Couch RD, Hill D, Urban JF Jr. Alterations in the porcine colon microbiota induced by the gastrointestinal nematode Trichuris suis. Infect Immun. 2012; 80:2150–7. http://dx.doi.org/10.1128/IAI.00141-12
65. Grove A. The delicate balance of bacterial purine homeostasis. Discov Bact. 2025; 2. http://dx.doi.org/10.1007/s44351-025-00025-7
66. Samuel G, Reeves P. Biosynthesis of O-antigens: genes and pathways involved in nucleotide sugar precursor synthesis and O-antigen assembly. Carbohydr Res. 2003; 338:2503–19. http://dx.doi.org/10.1016/j.carres.2003.07.009
67. Qin J, Hong Y, Morona R, Totsika M. O antigen biogenesis sensitises Escherichia coli K-12 to bile salts, providing a plausible explanation for its evolutionary loss. PLoS Genet. 2023; 19:e1010996. http://dx.doi.org/10.1371/journal.pgen.1010996
68. Parada Venegas D, De la Fuente MK, Landskron G, González MJ, Quera R, Dijkstra G, Harmsen HJM, Faber KN, Hermoso MA. Short chain fatty acids (SCFAs)-mediated gut epithelial and immune regulation and its relevance for Inflammatory Bowel Diseases. Front Immunol. 2019; 10:277. http://dx.doi.org/10.3389/fimmu.2019.00277
69. Yang W, Yu T, Huang X, Bilotta AJ, Xu L, Lu Y, Sun J, Pan F, Zhou J, Zhang W, et al. Intestinal microbiota-derived short-chain fatty acids regulation of immune cell IL-22 production and gut immunity. Nat Commun. 2020; 11:4457. http://dx.doi.org/10.1038/s41467-020-18262-6
70. Solano-Aguilar G, Shea-Donohue T, Madden KB, Quinoñes A, Beshah E, Lakshman S, Xie Y, Dawson H, Urban JF. Bifidobacterium animalis subspecies lactis modulates the local immune response and glucose uptake in the small intestine of juvenile pigs infected with the parasitic nematode Ascaris suum. Gut Microbes. 2018; 9:422–36. http://dx.doi.org/10.1080/19490976.2018.1460014
71. Zaiss MM, Rapin A, Lebon L, Dubey LK, Mosconi I, Sarter K, Piersigilli A, Menin L,

Walker AW, Rougemont J, et al. The intestinal Microbiota contributes to the ability of helminths to modulate allergic inflammation. Immunity. 2015; 43:998–1010. http://dx.doi.org/10.1016/j.immuni.2015.09.012

72. Morton ER, Lynch J, Froment A, Lafosse S, Heyer E, Przeworski M, Blekhman R, Ségurel L. Variation in Rural African Gut Microbiota Is Strongly Correlated with Colonization by Entamoeba and Subsistence. PLoS Genet. 2015; 11:e1005658. http://dx.doi.org/10.1371/journal.pgen.1005658
73. WHO. Soil transmitted helminthiasis. World Health Organization 2023. http://apps.who.int/neglected_diseases/ntddata/sth/sth.html
74. Akue JP, Nkoghe D, Padilla C, Moussavou G, Moukana H, Mbou RA, Ollomo B, Leroy EM. Epidemiology of concomitant infection due to Loa loa and Mansonella perstans in Gabon. PLoS Negl Trop Dis. 2011; 5:e1329. http://dx.doi.org/10.1371/journal.pntd.0001329
75. CADRE DE PLANIFICATION EN FAVEUR DES POPULATIONS SENSIBLES POTENTIELLEMENT AFFECTEES PAR LE PROJET. https://docplayer.fr/64023894-Cadre-de-planification-en-faveur-des-populations-sensibles-potentiellement-affectees-par-le-projet.html
76. Ndoye O, Vantomme P, Others. Living in and from the forests of Central Africa. FAO Non-Wood Forest Products Working Paper [Internet] 2017; Available from: https://www.cabdirect.org/cabdirect/abstract/20173297734
77. Youngblut ND, de la Cuesta-Zuluaga J, Ley RE. Incorporating genome-based phylogeny and functional similarity into diversity assessments helps to resolve a global collection of human gut metagenomes. bioRxiv 2021; 2020.07.16.207845. https://www.biorxiv.org/content/10.1101/2020.07.16.207845v2
78. Verweij JJ, Canales M, Polman K, Ziem J, Brienen EAT, Polderman AM, van Lieshout L. Molecular diagnosis of Strongyloides stercoralis in faecal samples using real-time PCR. Trans R Soc Trop Med Hyg. 2009; 103:342–6. http://dx.doi.org/10.1016/j.trstmh.2008.12.001
79. Kaisar MMM, Brienen EAT, Djuardi Y, Sartono E, Yazdanbakhsh M, Verweij JJ, Supali T, VAN Lieshout L. Improved diagnosis of Trichuris trichiura by using a bead-beating procedure on ethanol preserved stool samples prior to DNA isolation and the performance of multiplex real-time PCR for intestinal parasites. Parasitology. 2017; 144:965–74.

http://dx.doi.org/10.1017/S0031182017000129

80. Verweij JJ, Brienen EAT, Ziem J, Yelifari L, Polderman AM, Van Lieshout L. Simultaneous detection and quantification of Ancylostoma duodenale, Necator americanus, and Oesophagostomum bifurcum in fecal samples using multiplex real-time PCR. Am J Trop Med Hyg. 2007; 77:685–90. https://www.ncbi.nlm.nih.gov/pubmed/17978072
81. Caruccio N. Preparation of next-generation sequencing libraries using Nextera™ technology: simultaneous DNA fragmentation and adaptor tagging by in vitro transposition. Methods Mol Biol. 2011; 733:241–55. http://dx.doi.org/10.1007/978-1-61779-089-8_17
82. Picelli S, Björklund AK, Reinius B, Sagasser S, Winberg G, Sandberg R. Tn5 transposase and tagmentation procedures for massively scaled sequencing projects. Genome Res. 2014; 24:2033–40. http://dx.doi.org/10.1101/gr.177881.114
83. Droop AP. fqtools: an efficient software suite for modern FASTQ file manipulation. Bioinformatics. 2016; 32:1883–4. http://dx.doi.org/10.1093/bioinformatics/btw088
84. Jiang H, Lei R, Ding S-W, Zhu S. Skewer: a fast and accurate adapter trimmer for next-generation sequencing paired-end reads. BMC Bioinformatics. 2014; 15. http://dx.doi.org/10.1186/1471-2105-15-182
85. Ewels P, Magnusson M, Lundin S, Käller M. MultiQC: summarize analysis results for multiple tools and samples in a single report. Bioinformatics. 2016; 32:3047–8. http://dx.doi.org/10.1093/bioinformatics/btw354
86. Wood DE, Lu J, Langmead B. Improved metagenomic analysis with Kraken 2. Genome Biol. 2019; 20:257. http://dx.doi.org/10.1186/s13059-019-1891-0
87. Lu J, Breitwieser FP, Thielen P, Salzberg SL. Bracken: estimating species abundance in metagenomics data. PeerJ Computer Science. 2017; 3:e104. http://dx.doi.org/10.7717/peerj-cs.104
88. Langmead B, Salzberg SL. Fast gapped-read alignment with Bowtie 2. Nat Methods. 2012; 9:357–9. https://www.nature.com/articles/nmeth.1923
89. Core Team R. R: A language and environment for statistical computing. Version 3.6. 0. Vienna, Austria. /ra-language-and-environment-for-statistical-computing. https://www.R-project.org
90. Bolyen E, Rideout JR, Dillon MR, Bokulich NA, Abnet CC, Al-Ghalith GA, Alexander H,

Alm EJ, Arumugam M, Asnicar F, et al. Reproducible, interactive, scalable and extensible microbiome data science using QIIME 2. Nat Biotechnol. 2019; 37:852–7. https://www.nature.com/articles/s41587-019-0209-9

91. Oksanen J, Simpson G, Blanchet FG, Kindt R, Legendre P, Minchin P, O'hara RB, Solymos P, Stevens H, Szöcs E, et al. vegan community ecology package version 2.6-2 April 2022. The Comprehensive R Archive Network Available online: http://cran.r-project .org. 2022. https://github.com/vegandevs/vegan
92. Weiss S, Xu ZZ, Peddada S, Amir A, Bittinger K, Gonzalez A, Lozupone C, Zaneveld JR, Vázquez-Baeza Y, Birmingham A, et al. Normalization and microbial differential abundance strategies depend upon data characteristics. Microbiome. 2017; 5:27. http://dx.doi.org/10.1186/s40168-017-0237-y
93. Nearing JT, Douglas GM, Hayes MG, MacDonald J, Desai DK, Allward N, Jones CMA, Wright RJ, Dhanani AS, Comeau AM, et al. Microbiome differential abundance methods produce different results across 38 datasets. Nat Commun. 2022; 13:342. http://dx.doi.org/10.1038/s41467-022-28034-z
94. Yang L, Chen J. Benchmarking differential abundance analysis methods for correlated microbiome sequencing data. Brief Bioinform. 2023; 24. http://dx.doi.org/10.1093/bib/bbac607
95. Zhu A, Ibrahim JG, Love MI. Heavy-tailed prior distributions for sequence count data: removing the noise and preserving large differences. Bioinformatics. 2019; 35:2084–92. http://dx.doi.org/10.1093/bioinformatics/bty895
96. Korotkevich G, Sukhov V, Budin N, Shpak B, Artyomov MN, Sergushichev A. Fast gene set enrichment analysis. bioRxiv. 2021; 060012. https://www.biorxiv.org/content/10.1101/060012
97. Griffith DM, Veech JA, Marsh CJ. cooccur: Probabilistic Species Co-Occurrence Analysis in R. J Stat Softw. 2016; 69:1–17. https://www.jstatsoft.org/article/view/v069c02
98. McMurdie PJ, Holmes S. phyloseq: an R package for reproducible interactive analysis and graphics of microbiome census data. PLoS One. 2013; 8:e61217. https://journals.plos.org/plosone/article?id=10.1371/journal.pone.0061217
99. Lahti L, Shetty S. Introduction to the microbiome R package. Preprint at https://microbiome.github.io. 2018. https://s3.jcloud.sjtu.edu.cn/899a892efef34b1b944a19981040f55b-oss01/bioconductor/

3.10/bioc/vignettes/microbiome/inst/doc/vignette.html
100. Wickham, François, Henry, Müller. dplyr: A grammar of data manipulation. R package version 04. https://github.com/tidyverse/dplyr, https://dplyr.tidyverse.org
101. Fairbanks. Tidytable: Tidy interface to'data. table'. R package version 05. https://markfairbanks.github.io/tidytable/
102. Pedersen TL. tidygraph: A tidy API for graph manipulation. R package version 1.2. 0. 2020. https://github.com/thomasp85/tidygraph, https://tidygraph.data-imaginist.com.
103. Robinson D. broom: An R Package for Converting Statistical Analysis Objects Into Tidy Data Frames. arXiv [stat.CO]. 2014. http://arxiv.org/abs/1412.3565
104. Antonov M, Csárdi G, Horvát S, Müller K, Nepusz T, Noom D, Salmon M, Traag V, Welles BF, Zanini F. Igraph enables fast and robust network analysis across programming languages. arXiv [cs.SI]. 2023. http://arxiv.org/abs/2311.10260
105. Wickham H. Programming with ggplot2. In: Wickham H, editor. ggplot2: Elegant Graphics for Data Analysis. Cham: Springer International Publishing; 2016. page 241–53. https://doi.org/10.1007/978-3-319-24277-4_12
106. Pedersen TL. ggraph: Grammar of Graph Graphics. Github. https://github.com/thomasp85/ggraph
107. Conway JR, Lex A, Gehlenborg N. UpSetR: an R package for the visualization of intersecting sets and their properties. Bioinformatics. 2017; 33:2938–40. https://academic.oup.com/bioinformatics/article/33/18/2938/3884387
108. Krassowski M. complex-upset: A library for creating complex UpSet plots with ggplot2

Chapter 3: Background on human gut methanogens

3.1. Taxonomy, Ecology, and Role in the Human Gut

Methanogenic archaea are a distinct group of strictly anaerobic microorganisms that produce methane as the end product of anaerobic respiration. They belong to the phylum Euryarchaeota and occur across several orders, including Methanobacteriales, Methanococcales, Methanomassiliicoccales, Methanomicrobiales, Methanopyrales, Methanonatronarchaeales, and Methanosarcinales(Borrel et al., 2020; Sanz, 2011). They are key inhabitants of wetlands, freshwater and marine sediments, peat bogs, rice paddies, and sewage digesters, where they produce methane as a byproduct of the breakdown of organic matter(Conrad, 2007; Thauer et al., 2008; Wagner & Liebner, 2008) (Fig. 3). In these different ecosystems, methanogens can serve as natural sources of methane, which can escape into the atmosphere and contribute to climate change. In general, methanogens grow through three main pathways: (i) hydrogenotrophic methanogenesis, which uses H_2 and CO_2 or formate, (ii) acetoclastic methanogenesis, which splits acetate into methane and CO_2, and (iii) methylotrophic methanogenesis, which uses methanol and methylated compounds(Borrel et al., 2020; Lyu et al., 2018; Thauer et al., 2008), with the hydrogenotrophic methanogenesis being the most widespread across known species.

The methanogens that thrive in geothermal ecosystems, including hot springs, geysers, and hydrothermal vents, such as *Methanothermus* and *Methanothermobacter*, use the highly available CO_2 and H_2 to fuel methane production(Lyu et al., 2018; Stetter et al., 1981), while those found in anaerobic marine environments coexist with sulfate-reducing bacteria, where they compete with them for hydrogen. In these settings, sulfate reducers typically outcompete hydrogenotrophic methanogens, but methanogens persist in these niches because of their flexibility to metabolize non-competitive substrates such as methanol or methylamines(Oremland & Polcin, 1982; Thauer et al., 2008).

Most methanogens are associated with hosts and thrive primarily within the gastrointestinal tracts of ruminants, termites, and other animals, where they constitute a significant portion of >50% of total gut archaea(Janssen & Kirs, 2008; Samuel et al., 2007). In these gut communities, species that use H_2, CO_2, or formate dominate and depend on fermentative bacteria to produce these substrates. Because methanogens consume these bacterial fermentation byproducts, methanogens enhance overall fermentative efficiency by lowering the redox potential. Several

methanogen species colonize humans, including *Methanosphaera stadtmanae*, and members of Methanomassiliicoccales, but *Methanobrevibacter smithii* overwhelmingly dominates(Dridi et al., 2009; Hansen et al., 2011).

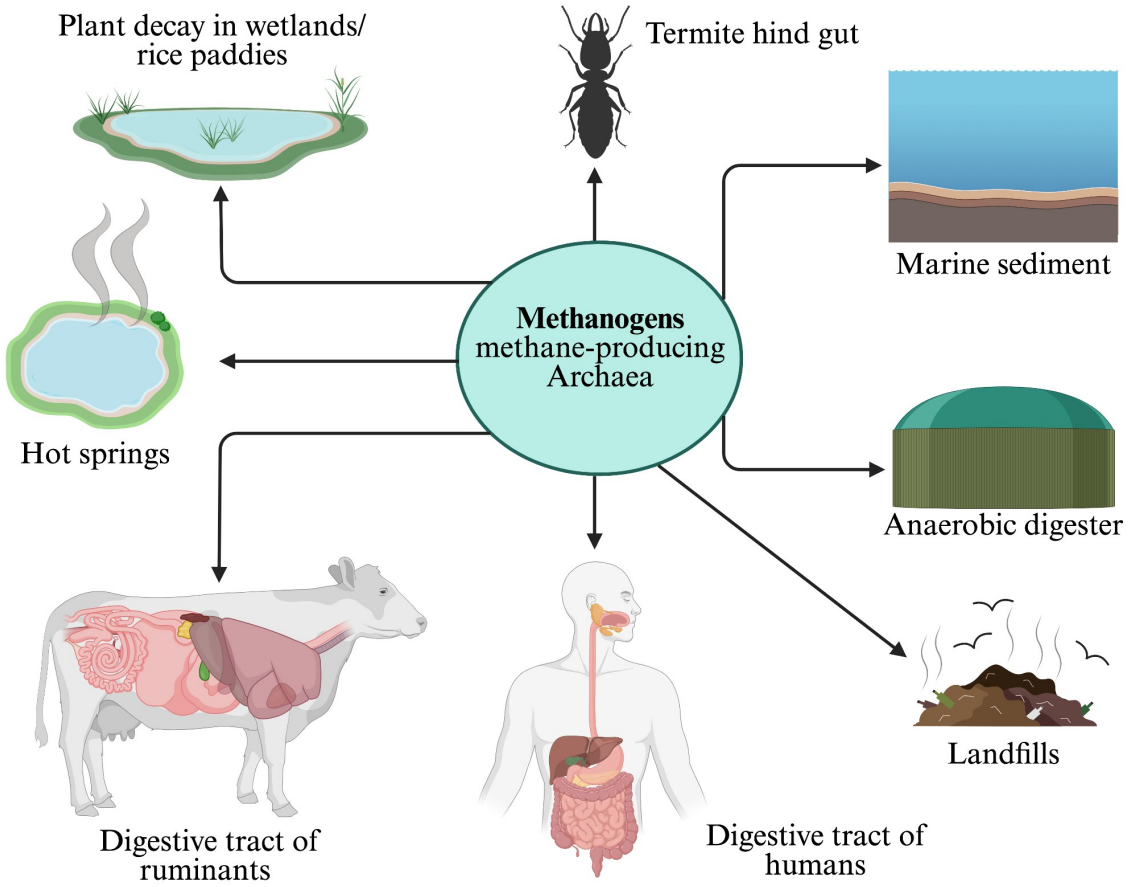

Figure 3. Ecological niches of methanogens.

Methanogenic Archaea thrive in diverse anoxic ecosystems, including wetlands, termite hindguts, marine sediments, anaerobic digesters, landfills, the human digestive tract, the rumen of cattle, and geothermal habitats such as hot springs. Figure adapted from Khanna, 2022(Khanna, 2022) and redrawn using BioRender.com.

3.2. *Methanobrevibacter smithii*: Dominance and prevalence in humans.

Bacteria make up the most diverse and dominant group in the human gut, while archaea constitute only a small part of this community. Among these archaea, methanogens are the most common, with *M. smithii* commonly described as the most abundant, colonizing early in life and found in the majority of healthy individuals. In monogastric hosts such as humans, *M. smithii* mainly colonizes the distal colon, while in ruminants, methanogens dominate the foregut

fermentation chambers. In the human colon, the redox potential is low, the pH is close to neutral, and transit times are long, creating a hospitable niche for methanogens in general and this strictly anaerobic archaeon(Nandhra et al., 2020; Procházková et al., 2023). This region also hosts intense bacterial fermentation, which allows *M. smithii* to sit close to the main hydrogen and carbon dioxide sources, consume these fermentation by-products, and form syntrophic partnerships with neighbouring bacteria while producing methane. The methane produced has long been used in practice by clinicians and researchers, with breath methane measurements used to identify people likely colonized by methanogens and to estimate how common these archaea are in human populations(Triantafyllou et al., 2014). More recently, metagenomic surveys suggest that this species has a prevalence approaching 95% in some cohorts and, in many cases, accounts for more than 90% of archaeal sequence reads(Dridi et al., 2009). Miller and colleagues first described *M. smithii* as a Gram-positive, anaerobic coccobacillus(Miller et al., 1982). Through culture-based studies, researchers could culture *M. smithii* in only about one-third of individuals(Togo et al., 2019; Weaver et al., 1986), mainly because it is challenging to grow this strict anaerobe from fecal material. Advances in molecular methods, including PCR and shotgun metagenomic sequencing, have made it easier to detect *M. smithii* in stool samples.

Some culture-independent studies used PCR targeting the mcrA gene, and reported *M. smithii* in approximately 45–50% of adults(Scanlan et al., 2008). Later assays report it in 80–96% of individuals in diverse cohorts(Dridi et al., 2009; Gaci et al., 2014; Mihajlovski et al., 2010). A recent study in Mali found it in ~41% of healthy children but rarely in severe acute malnutrition(Camara et al., 2021).

However, advances in PCR and sequencing have not only increased detection but also revealed that *M. smithii* is unevenly distributed across populations. Some populations show very high carriage, whereas others have much lower prevalence or abundance, and levels can also shift in specific disease states. Fiber-rich diets and lifestyles seem to matter a lot for populations where *M. smithii* does well. In one Russian study, for instance, although *M. smithii* was not dominant in most samples, people living in rural areas tended to carry more *M. smithii* in their gut than city dwellers, and their traditional diets differed accordingly(Tyakht et al., 2013). Age is another factor that influences *M. smithii* prevalence. In a metagenomic survey using stool samples across three age groups: young adults, older adults, and centenarians, to investigate how gut methanogenic archaea change with age, Mohammadzadeh and colleagues reported a strong association between

age and the prevalence of a high methanogen phenotype, although overall archaeal diversity decreased with age. Centenarians and young adults showed similar methanogen composition, with higher *M. smithii* and lower *M. intestini* levels than in older adults(Mohammadzadeh et al., 2025). This pattern suggests that methanogen colonization can change over the lifespan rather than remaining fixed after early adulthood.

3.3. Genomic organization, metabolic capacities, and ecological role.

M. smithii has a compact, specialized genome that supports hydrogenotrophic methanogenesis (a process which uses H_2 and CO_2 to produce methane in the following reaction: $CO_2 + H_2 \rightarrow CH_4 + 2H_2O$). The *M. smithii* type strain PS genome was sequenced in 2007, revealing a circular chromosome of about 1.85 Mb with about 1,795 predicted protein-coding genes and two rRNA operons. In addition to the complete hydrogenotrophic methanogenesis pathway encoded in its genome (including methyl-CoM reductase, heterodisulfide reductase/[NiFe] hydrogenase complexes, and associated electron-transfer components), it can also use formate to produce methane(Samuel et al., 2007). Also encoded in the PS genome are genes for the biosynthesis of key cofactors, including coenzyme F_{430}, corrinoids, riboflavin (for F_{430} biosynthesis), and coenzyme M. The genome also encodes an ammonium transporter (AmtB) together with two routes for ammonium assimilation: a high-affinity glutamine synthetase–glutamate synthase (GS –GOGAT) system and a lower-affinity glutamate dehydrogenase pathway. In gnotobiotic mice, these genes play a clear role in nitrogen assimilation. When *M. smithii* co-colonizes the gut with *B. thetaiotaomicron*, it up-regulates key ammonium assimilation genes. It competes for a limited ammonium pool, showing that ammonium serves as a primary nitrogen source in the distal gut(Samuel et al., 2007).

Comparative genomics across multiple isolates shows a relatively conserved core genome but a more flexible accessory genome, especially in loci linked to surface structures and metabolism. This variability includes genes for several surface glycan biosynthesis pathways, which allow *M. smithii* to decorate its cell surface with carbohydrate structures resembling host and bacterial glycans in the gut mucosa, as well as a large set of predicted adhesin-like proteins(Hansen et al., 2011; Samuel et al., 2007). These features likely support attachment to the epithelium and to bacterial partners and help stabilize colonization in the distal colon.

Functionally, *M. smithii* acts as a major hydrogen sink in the human gut. It does so by consuming H_2, CO_2, and formate that bacteria release, thereby lowering the redox potential, which

in turn favours bacterial fermentation reactions that produce short-chain fatty acids to run more efficiently. Practical demonstration of the role of *M. smithii* in consuming these fermentation products was observed in gnotobiotic mice experiments by Samuel and Gordon, where mice colonized with *B. thetaiotaomicron* and *M. smithii* produced more acetate and formate and less butyrate and propionate than mice carrying *B. thetaiotaomicron* alone. They absorbed more short-chain fatty acids from the colon(Samuel & Gordon, 2006). More recent in vitro work has elaborated on these partnerships. In a defined co-culture system, Catlett and colleagues grew *B. thetaiotaomicron* together with *M. smithii(Catlett et al., 2022)*. They showed that the archaeon could use the acetate, formate, and hydrogen released by the bacterium as growth substrates. In their co-culture system, Catlett and colleagues showed that *M. smithii* can use the hydrogen and formate produced by *B. thetaiotaomicron* as growth substrates. As the archaeon removed these fermentation products, the metabolic output of *B. thetaiotaomicron* shifted, consistent with relief from end-product inhibition. Notably, Catlett et al. observed that the interaction was not always neutral. When vitamin B_{12} or hematin became limiting, the two organisms together produced more biomass than either could on its own(Catlett et al., 2022). Similarly, pairwise co-cultures with the butyrogenic bacterium *Anaerostipes rhamnosivorans* showed that *M. smithii* promoted butyrate production via interspecies formate/hydrogen transfer, highlighting a syntrophic exchange that stabilizes fermentation end products(Bui et al., 2019).

Ecological links between *M. smithii* and its bacterial partners also include members of the family Christensenellaceae. Christensenellaceae and *M. smithii* often co-occur in human gut metagenomes, and co-culture work shows that *Christensenella spp.* can fuel *M. smithii* syntrophy by supplying hydrogen when the two species are in close physical association(Ruaud et al., 2020). In gnotobiotic mice, supplementing a human microbiota with *Christensenella minuta* reduced host weight gain, pointing to a connection between *Christensenella* and *M. smithii* consortia and host metabolic phenotypes(Goodrich et al., 2014).

Taken together, these experiments highlight the role played by *M. smithii* in shaping gut bacterial fermentation and help explain differences in energy harvest among people.

3.4. Clinical and physiological associations.

M. smithii is widely regarded as a commensal archaeon in the human gut and is not currently considered a direct pathogen. Its abundance and activity have been linked to conditions such as constipation-predominant IBS, obesity-related traits, and altered inflammatory or immune

markers in different study populations(Basseri et al., 2012). The following sections describe the main clinical associations, the data, and the suggested mechanisms.

Constipation and constipation-predominant IBS (IBS-C). The most robust and reproducible association of *M. smithii* is with intestinal motility. Clinical studies consistently show that methane producers exhibit slower intestinal transit and more severe constipation than methane-negative individuals(Kunkel et al., 2011; Triantafyllou et al., 2014). Clinical trial evidence indicates that methane production is directly linked to constipation in IBS. In a randomized, placebo-controlled trial of IBS-C, Pimentel and colleagues treated methane-positive patients with neomycin or placebo and monitored their symptoms alongside breath methane. Neomycin led to a much larger improvement in overall IBS symptoms and constipation scores than placebo, and patients who cleared methane on breath testing showed the highest relief of constipation(Pimentel et al., 2006). These results support a direct link between intestinal methane production and constipation in IBS-C, and they helped establish the concept of intestinal methanogen overgrowth (IMO) as a distinct motility-related disorder(Pimentel et al., 2020).

By consuming H_2, methanogens alter fermentation thermodynamics via shifting bacterial SCFA production. Such alterations can influence host energy harvest and adiposity. Genomic and metagenomic work first suggested a role for methanogens in energy harvesting. Goodrich and colleagues first asked whether a human microbiome enriched in a Christensenellaceae–methanogen consortium affects host weight gain(Goodrich et al., 2014). They added Christensenella minuta to stool from an obese human donor and then transplanted either the amended or the unamended community into germ-free mice. They observed that mice that received the *C. minuta*–amended microbiota gained less weight and produced different short-chain fatty acids than control mice(Goodrich et al., 2014). This result shows that the presence of this microbial combination can affect weight in this mouse model. In human studies, *M. smithii* has also been linked to energy harvest, but the effects are not consistent across populations. In a prospective birth cohort, children who carried *M. smithii*—especially at high fecal counts—had higher weight and BMI z-scores and a greater risk of overweight between 6 and 10 years of age than non-carriers, pointing to a link between early methanogen colonization and childhood weight development even though causality remains unresolved(Mbakwa et al., 2015).

Twin data help connect these microbiome patterns back to host genetics. In the TwinsUK cohort, Goodrich and colleagues identified several "heritable" microbes, meaning taxa whose

abundance variation could partly be explained by host genetic differences. One such group was a consortium built around Christensenellaceae and including the archaeal family Methanobacteriaceae, which contains *M. smithii*. This consortium was more common with higher abundances observed in lean participants than in those with obesity, linking archaeal–bacterial partnerships, host genotype, and body mass(Goodrich et al., 2014). These findings indicate that host genetic background shapes the abundance of methanogens and their bacterial partners and, through this, may influence inter-individual differences in energy handling.

Dirks and colleagues have recently taken this a step closer to the mechanism by re-analysing a tightly controlled randomized crossover feeding study. In that trial, participants were given both a Western-style low-fibre diet and a high-fibre whole-food diet with matched macronutrients. The investigators measured methane production, short-chain fatty acids, and metabolizable energy during each diet phase. On the high-fibre diet, most people absorbed fewer calories overall, but those who produced more methane also took in more energy and had higher levels of short-chain fatty acids in their blood(Dirks et al., 2025). These data suggest that methanogenesis enables a fibre-degrading community to extract additional calories from complex carbohydrates. They also support precision nutrition strategies that tailor diets to a person's microbiota to adjust energy absorption and body weight in the prevention and treatment of obesity(Corbin et al., 2025).

Periodontal disease. Although *M. smithii* is primarily intestinal, related methanogens are now well documented in the mouth, particularly *M. oralis(Pilliol et al., 2024)*. Lepp and colleagues examined subgingival plaque from periodontitis patients and controls using quantitative PCR for archaeal 16S rRNA genes(Lepp et al., 2004). They found archaeal 16S rRNA genes in about one-third of patients with periodontitis, almost exclusively in diseased sites. Archaeal relative abundance rose with pocket depth and clinical attachment loss, then dropped after periodontal therapy as clinical measures improved. They further observed that archaeal communities at these sites were dominated by an M. oralis-like phylotype together with a second *Methanobrevibacter* lineage, and the authors proposed that these methanogens act as hydrogen sinks that enable secondary fermenters to proliferate in deep pockets(Lepp et al., 2004). A later study by Vianna's group examined primary endodontic infections. They made use of archaeal 16S rRNA and mcrA-targeted qPCR to detect methanogens in 5 of 20 infected root canals, with M. oralis-like sequences reaching about 2.5% of the total prokaryotic load in some samples(Vianna et al., 2006). These

findings show that methanogens can inhabit closed endodontic lesions at non-trivial abundance and support the idea that Archaea may participate in oral infections, even though a direct causal role in disease onset has not yet been established.

Neurological conditions. Work on neurological disease has so far pointed to broad gut dysbiosis rather than a specific role for gut methanogens. A recent meta-analysis of fecal shotgun metagenomes in Parkinson's disease by Nishiwaki and colleagues combined six cohorts across Asia, Europe, and North America. The study reported consistent shifts in several bacterial species and pathways—most notably increased *Akkermansia muciniphila* and reduced Roseburia intestinalis and Faecalibacterium prausnitzii—but it did not single out *Methanobrevibacter* or other archaeal lineages as major discriminating taxa between cases and controls(Nishiwaki et al., 2024). Archaea do, however, enter the neurological field through mechanistic work on protein quality control. Archaea proteasomes can degrade aggregation-prone proteins and reduce toxicity in mammalian cells(Yamada et al., 2006). Similarly, Brooks and colleagues demonstrated that an archaeal unfoldase counteracts protein misfolding and protects against retinal degeneration in a mouse model(Brooks et al., 2018), while Sakono and colleagues showed that archaeal prefoldin directly promotes the formation of highly toxic amyloid-β oligomers by stabilizing intermediate species(Sakono et al., 2008). These findings suggest that archaeal proteins have potential neuroprotective properties in heterologous systems. Nevertheless, such results stem from experimental protein studies rather than direct host–microbiome associations, and existing studies have not established a causal or epidemiological link between gut methanogens and Parkinson's disease.

Colorectal cancer. Recent work has highlighted the potential role of methanogens in colorectal cancer. A multi-cohort analysis of more than 2000 metagenomes to characterize how the gut archaeome differs among healthy individuals, patients with adenoma, and patients with colorectal cancer (CRC) found that associations between Archaea and disease were common but highly variable(Li et al., 2025). Key to their findings was an overall within-sample diversity that changed progressively from healthy controls to adenoma to CRC. Also important was their observation of reproducible alterations of specific archaeal species across multiple populations, with *M. smithii* and *M. sp002496065* species enriched in CRC. They also observed that CRC samples were characterized by higher *M. smithii* abundance, frequent co-occurrence with the CRC-

associated bacterium Fusobacterium nucleatum, and a reduced abundance of *Methanosphaera stadtmanae* within the archaeal community(Li et al., 2025).

Abdi and colleagues similarly observed elevated methanogen levels in CRC patients(Abdi et al., 2022). These studies suggest the presence of archaeal dysbiosis and potential microbial interactions in CRC-associated communities. However, evidence remains mainly associative. At present, however, these patterns remain associative. Bu and colleagues recently reviewed archaeal signatures in colorectal cancer and concluded that current data are almost entirely associative. To date, studies have not shown whether methanogens alter gut cell growth, modulate the host response to tumors, or directly affect tumor growth in colorectal cancer(Bu et al., 2025). Additionally, links between methane, short-chain fatty acids, and host biology also remain unclear. Thus, although studies consistently report methanogen enrichment in CRC, the role of methanogens in disease development or progression remains unclear.

Together, these studies indicate that *M. smithii* is not pathogenic but instead associates with distinct host phenotypes through hydrogen scavenging, gas-mediated effects on motility, and trophic interactions with bacterial partners. The best-established clinical role is in constipation and IBS-C, where methane measurement is used diagnostically and targeted therapies can improve symptoms. Other associations, including metabolic traits, CRC, periodontal disease, and Parkinson's disease, remain less consistent and highlight the need for more mechanistic and longitudinal studies.

3.5. Evolutionary dynamics and heritability.

One way to study host–microbe history is to compare the evolutionary trees of gut methanogens and humans. When the trees show matching patterns, it suggests that the methanogens have remained associated with human populations over many generations. Twin studies first indicated that methanogen carriage, including *M. smithii*, has a strong genetic component. In the TwinsUK cohort, Goodrich and colleagues found that monozygotic twins were more likely to carry *M. smithii* than dizygotic twins. They also identified Methanobacteriaceae as part of a cluster of microbes whose abundances are partly shaped by host genotype(Goodrich et al., 2014). Beyond heritability, evolutionary analyses increasingly point to long-term associations between methanogens and their human hosts.

In our recent multi-cohort study spanning Europe, Asia, and Africa, we compared host phylogenies with MAGs from common gut species. We applied the Procrustean Approach to

Cophylogeny (PACo) framework to test for codiversification. Several bacterial and archaeal taxa showed significant cophylogeny signals, and *M. smithii* stood out among the strongest, suggesting a long-term, lineage-specific association between this methanogen and its human hosts(Suzuki et al., 2022). Additionally, signals of codiversification were also recovered from microbial phylogenies based on ancient MAGs assembled from Native American paleofeces, providing independent support for the conclusion that these host–microbe associations extend deep into human evolutionary history(Wibowo et al., 2021).

However, MAGs, while powerful, are inherently incomplete and can limit the resolution of strain-level evolutionary inference. To address this, we expanded our efforts to isolate *Methanobrevibacter* strains. In Chapter 4, I build directly on the codiversification signal detected in the MAG-based study by assessing cophylogeny using *M. smithii* isolates collected from Gabon, Germany, and Vietnam. The use of isolates provides a more complete genomic representation, enabling a stronger test of evolutionary hypotheses and setting the stage for deeper exploration of host–archaea codiversification across geographies.

3.6. Emergence of *Candidatus Methanobrevibacter intestini*.

Evolutionary and genomic work has started to show that not all human gut methanogens are the same, and that closely related lineages can occupy distinct niches in the intestine. This shift in view sets the stage for the recognition of *Candidatus Methanobrevibacter intestini* as a separate species alongside *M. smithii*. Large-scale, genome-resolved metagenomic surveys have overturned the idea that *M. smithii* is the only dominant methanogen in the human gut. Rinke and colleagues examined genomes previously grouped as *M. smithii*. They found a distinct group of strains that shared only ~93–94% average nucleotide identity (ANI) with typical *M. smithii* strains(Rinke et al., 2021). This difference is enough to consider them a separate species. Later, Chibani and colleagues named this lineage *Can Methanobrevibacter intestini(Chibani et al., 2022)*. Beyond genetic differences, *M. intestini* also differs functionally from *M. smithii*. Unlike *M. smithii*, it lacks molybdate transport systems and relies solely on tungsten-dependent methanogenesis.

Work on cultured strains is beginning to reveal the metabolic potential of *M. smithii* and *M. intestini*, suggesting distinct ecological roles for both species in the gut. The first cultured representative of *M. intestini*, strain TLL-48-HuF1(Low et al., 2022), confirmed many predicted similarities with *M. smithii*, but also revealed unique genomic and physiological features. Notably, TLL-48-HuF1 lacks several adhesin-like proteins and molybdate transporter genes, changes that

may alter its attachment to gut bacterial partners and scavenging of cofactors for methanogenesis. More recently, Weinberger and colleagues isolated *M. intestini* alongside another *M. smithii* strain from human feces and compared their growth under identical laboratory conditions. They observed that their *M. intestini* (strain WWM1085) does not accumulate formate when grown with hydrogen and carbon dioxide, whereas the *M. smithii* variant does. However, both isolates produced methane, with differences in metabolite profiles in culture, including higher succinate production in strain WWM1085. These genomic differences supported the formal recognition of *M. intestini* as a distinct species(Weinberger et al., 2025). These observations align with metagenomic co-occurrence patterns, in which *M. smithii* and *M. intestini* exhibit mutual exclusion within individuals.

Yet, our understanding of *M. intestini* is still limited. So far, researchers have cultured only a small number of *M. intestini* strains, all from Asian or European cohorts. No isolate has been reported from Africa, despite metagenomic surveys repeatedly detecting *Methanobrevibacter* lineages at high prevalence and abundance in African gut microbiomes(Borrel et al., 2020; Chibani et al., 2022). As a result, it is hard to know whether current culture-based findings capture the full diversity of *M. intestini* across human populations worldwide. In this thesis, I address this gap by isolating the first *M. intestini* strain from an African population (Chapter 3) and performing comparative pangenomics of newly cultured strains of both *M. smithii* and *M. intestini* (Chapter 4), thereby expanding the known diversity and functional repertoire of these key methanogens.

3.7. Ecological partitioning and evolutionary implications.

Patterns observed for *M. smithii* and *M. intestini* suggest that these two methanogens do not behave similarly in the gut. Although they are closely related, they differ in genomic features and metabolic traits, suggesting the use of overlapping but distinct resources. These differences likely arise from a combination of microbial adaptation and differences in host or environmental conditions.

The cultivation and identification of *M. intestini* show that methanogen diversity in the human gut is broader than previously estimated. Compared with *M. smithii*, *M. intestini* relies on tungsten-dependent methanogenesis, encodes fewer adhesin-related genes, and shows differences in predicted metabolite production. Together, these traits suggest divergence from *M. smithii*, although the effects on host metabolism and immune responses remain to be elucidated.

Patterns of carriage add another layer of separation between these taxa. Studies comparing urban and rural cohorts report higher archaeal abundance in rural or traditional-lifestyle groups than in urban Western populations, where methanogens are often detected at low prevalence(Borrel et al., 2020; Chibani et al., 2022; Tyakht et al., 2013). Age adds a further gradient: recent work shows that *Ca. M. intestini* occupies a central position in archaeal–bacterial networks in adults, while *M. smithii* becomes more dominant in older adults and centenarians(Mohammadzadeh et al., 2025). These trends raise practical questions about how diet, host genetics, and surrounding microbial communities shape methanogen diversity, and how these dynamics may feed back onto host physiology in different settings.

3.8. Future perspectives and knowledge gaps.

Even with recent progress, most data on human-associated methanogens still come from Western cohorts, which make up a small fraction of the global population and often show lower archaeal prevalence than rural or traditional-lifestyle groups(Blake, 2024; Tyakht et al., 2013). As a result, the true global diversity, ecological roles, and functional effects of methanogens remain poorly defined, especially in populations with high archaeal abundance.

Technological advances in metagenomics, pangenomics, and culturomics have already reshaped the field, as exemplified by the recognition and cultivation of *M. intestini*. Expanding these approaches across more diverse populations will be critical to uncovering novel archaeal taxa, clarifying their ecological roles, and understanding how methanogens contribute to human health and disease.

This gap provides the rationale for the present work on methanogens. In the following chapters, I build on these insights in two directions: (i) Chapter 4 describes the first successful isolation and characterization of an African *M. intestini* strain; and (ii) Chapter 5 uses comparative pangenomics to analyze the evolutionary and functional diversification of cultured *M. smithii* and *M. intestini* strains. Together, chapters 4 and 5 demonstrate how *M. smithii* and *M. intestini* dominate the archaeal component of the human gut ecosystem, while revealing insights into their ecology and evolution, as well as their role in host-associated microbial communities.

Chapter 4: Genomic and phenotypic characterization of a human gut *Methanobrevibacter intestini* strain G0370_i3 isolated in Gabon

This chapter is adapted from a manuscript of the same title originally published in Future Microbiology (doi: 10.1080/17460913.2026.2645510).

Only changes to formatting have been made; main figures and tables have been renumbered to ensure consistency with chapter organization.

Authors are listed in publication order:

Mirabeau M. Ngwese[a], Stephen Loum[a], Lara Berg[a], Alexander V. Tyakht[a], Nicholas D. Youngblut[a], Ayola A. Adegnika[b, c, d], Peter G. Kremsner[b,c,d,e], Ruth E. Ley[a, e], and James W. Marsh[a,*]

[a]Department of Microbiome Science, Max Planck Institute for Biology, Tübingen, Germany

[b]Centre de Recherches Médicales de Lambaréné (CERMEL), Lambaréné, Gabon

[c]Institut für Tropenmedizin, Eberhard-Karls-Universität Tübingen, Germany

[d]German Center for Infection Research (DZIF), Tübingen, Germany

[e]Cluster of Excellence EXC 2124 Controlling Microbes to Fight Infections, University of Tübingen, Germany

*: Corresponding author

Manuscript contributions: I contributed to the conceptualization of the study, development of methodology, and writing of the original draft, together with N.D.Y R.E.L, and J.W.M. I performed stool enrichment, DNA extraction, and sequencing of *M. intestini* strain G0370_i3. I conducted growth-curve experiments in collaboration with S.L., while L.B. tested growth of strain G0370_i3 on Sodium formate. I carried out sequence processing and genome assembly alongside J.W.M. I also conducted the formal analyses and generated Figures 1, 3, parts of Figure 4 (4B-D), and Supplementary Figure S4.

Key words: Microbial genome, Developing countries, *Methanobrevibacter intestini,* microbiome, archaea, human archaeome, methanogen

Article Highlights:

- Existing knowledge of *Methanobrevibacter intestini* is derived from a single strain, isolated from the stool of a Western individual (USA). Here, we report the enrichment,

isolation, and preliminary phenotypic characterization of a second strain, G0370_i3, that was isolated from the stool of a rural Gabonese individual.

- Isolation was successful using anaerobic culturing with hydrogen supplementation and antibiotics, followed by clonal purification on solid media and genome sequencing.
- The genome is AT-rich (30.3 % GC), 1.77 Mb in size, and contains 1,808 protein-coding genes. Functional annotations covered 78.5 % of genes, including 1,231 enzymes, 112 transporters, and 27 transcription factors.
- The genome encodes hydrogenotrophic methanogenesis pathways, the methanol coenzyme M methyltransferase (MtaABC) complex for methanol use.
- Genes for 5-Phosphoribosyl-1-Pyrophosphate (PRPP) synthesis, nucleotide salvage, and cell wall precursors suggest adaptation to gut conditions.
- Codon usage shows strong AT bias, with A/U-ending codons preferred and G/C-ending codons underused.
- Phylogenomic analyses place G0370_i3 with WWM1085 and TLL-48-HuF1, distinct from *M. smithii*, supported by high average nucleotide identity (ANI) and digital DNA-DNA hybridization (dDDH) values.
- G0370_i3 survives short oxygen exposure and resumes growth under anaerobic conditions.

The characterization of *M. intestini* from an African source expands our understanding of methanogen diversity, metabolic versatility, and ecological roles within the anaerobic gut environment of humans.

4.1. Abstract

Aims

Methanogens are methane-producing archaea that are present in the human gut. Yet, their adaptation to diverse human lifestyles remains poorly understood. Here, we report the isolation of *Methanobrevibacter intestini* G0370_i3 from the stool of a healthy adult from southern Gabon, Africa, where inhabitants maintain traditional subsistence lifestyles with diets distinct from industrialized populations.

Materials and Methods

M. intestini was enriched from human stool, phenotypically characterized, and sequenced.

Results

G0370_i3 growth relied on the presence of H_2 and CO_2 and could also grow on formate, in contrast to reports for the type strain. The genome encoded pathways for amino acid biosynthesis, cofactor metabolism, and secondary metabolite production. We identified 23 mobile genetic elements and five defense systems, indicating horizontal gene transfer and antiviral defense. No prophage regions were detected. The genome also encoded uridine diphosphate (UDP)-sugar metabolism pathways, indicating capacity for energy storage and cell wall adaptability. Genes encoding adhesin-like proteins suggest capabilities for host interaction. Phenotypically, G0370_i3 is a coccobacillus, grows optimally at 37 °C, and tolerates antibiotics, salt, and oxygen stress.

Conclusions

These findings highlight the stress resilience and selective metabolic capabilities of *M. intestini* and underscore the importance of representing African populations in microbiome research.

4.2. Introduction

Methanogenic Archaea occupy a specialized niche in the human gut, serving as terminal consumers in anaerobic fermentation by converting hydrogen and other end products to methane [1]. This activity influences fermentation thermodynamics, shapes bacterial community composition, and affects energy harvest from dietary substrates [2]. Understanding the diversity and functional variation of these organisms is therefore relevant to broader questions about gut ecosystem function.

Methanobrevibacter smithii has historically been recognized as the predominant methanogenic archaeon in the human intestinal tract, and has been extensively studied for its role in energy metabolism, potential contributions to host adiposity, and interactions with bacterial members of the gut microbiome [3–5]. However, recent taxonomic investigations have revealed greater diversity within the *Methanobrevibacter* genus than previously appreciated [6]. A distinct lineage, initially classified as *Methanobrevibacter_A smithii_A* by the Genome Taxonomy Database (GTDB), has since been formally described as a novel species, *Methanobrevibacter intestini* [7].

Current characterization of *M. intestini* derives from the type strain, isolated from an individual in the USA. This strain is strictly anaerobic, mesophilic, and neutrophilic, growing optimally at 37°C and pH 7 [7]. As a hydrogenotrophic methanogen, H_2/CO_2 is its only validated substrate pair, though genomic analyses suggest capacity for methanol and alcohol utilization [6]. The type strain encodes all enzymes for CO_2-to-CH_4 conversion but lacks the alternative methyl-coenzyme M reductase isoenzymes (mrtABDG) found in *M. smithii*, potentially limiting metabolic flexibility under varying hydrogen partial pressures [8]. Despite encoding formate dehydrogenase genes, the *M. intestini* type strain does not accumulate extracellular formate during H_2/CO_2 growth, in contrast to *M. smithii* [7].

A persistent geographical bias in microbiome research limits our understanding of microbial diversity within underrepresented populations [9]. This gap is particularly significant given substantial variation in microbiome composition and functionality across regions, driven by differences in diet, lifestyle, environmental exposures, and host genetics [10]. Whether the metabolic features observed in the *M. intestini* type strain are conserved across geographically diverse lineages, or represent adaptations specific to Western-associated populations, remains unknown.

Here, we report the isolation and preliminary characterization of *M. intestini* from the stool of a healthy adult living in rural southern Gabon, Central Africa. We conducted genomic, phylogenetic, and morphological analyses to characterize the potential strain-specific properties of this isolate. Our findings provide initial insights into strain-level variation within this species and contribute to a more globally representative understanding of the human gut archaeome.

4.3. Materials and Methods

***Subjects and fecal samples*.** Human faeces were collected from an adult female participant in the Ikobey region of southern Gabon, Central Africa, as part of a broader study as previously described [11]. Gabon has an average elevation of 377 meters above sea level and experiences seasonal variations, but its climate is predominantly tropical. It is regarded as a globally significant, carbon-positive biodiversity hotspot, with rich flora and diverse fauna that are unique to this area. Following informed consent, the participant was provided Fe-Col stool collection kits (Alpha Labs, Eastleigh, UK). The stool sample was transported on ice within 8 hours to the central study facility at the Centre de Recherches Médicales de Lambaréné (CERMEL) Gabon, immediately frozen at -80 °C, and subsequently shipped on dry ice to Germany for long-term storage.

Culture media. Stool samples were enriched and screened for the presence of *M. intestini*. Enrichments were performed in methanogen enrichment (ME) media consisting of minimal media (KH_2PO_4 (4.5 mM), $MgCl_2$ x 6 H_2O (628 µM), NaCl (8.5 mM), NH_4Cl (9.2 mM), $CaCl_2 \times 2{\cdot}H_2O$ (430 µM), Resazurin (25 mg/100 ml: 4 mL), trace minerals SL-10 (1 mL), modified trace elements Wolfe (20 mL)), and bacterial fermentation products, prepared under anaerobic conditions. The minimal media solution was sparged with N_2/CO_2 (80:20 %, 1 bar and 0.5 L/min pressure for each gas) for 40 minutes and autoclaved. After autoclaving at 121 °C for 20 minutes and cooling, we added L-Cysteine-HCl (5 mL), fermentation products (80 mL), and $NaHCO_3$ (47.6 mM) through a 0.22 µm filter in an anaerobic chamber. This media was then supplemented with 1 µg/mL ampicillin, 10 µg/mL erythromycin, 10 µg/mL vancomycin, and 40 mg/L cycloheximide to restrict bacterial growth.

***Methanogen enrichment from faeces*.** The frozen stool sample was thawed and ~1 g was collected using a sterile 3 mm disposable biopsy punch (Kai Europe GmbH) and transferred into a 2 mL tube, which was immediately introduced into an anaerobic glove box (UniLab Pro MBRAUN 20G). Inside the glove box, 1.5 mL of ME medium was added, the sample was briefly vortexed, and centrifuged for 30 s at 10,000 g. One millilitre of the faeces–media slurry was

transferred to a Balch tube containing 9 mL of ME, followed by serial dilutions (1:10, 1:100, 1:1000). Tubes were incubated with an H_2/CO_2 (80/20) headspace pressurized to 1.5 bar at 37 °C with horizontal shaking (100 rpm) for 7 days. After this initial incubation, the headspace gas of each enrichment was exchanged by three vacuum-gas cycles (10 s each) and refilling with H_2/CO_2 (80/20) to 0.5 bar, followed by a final pressurization to 1.5 bar, and incubated for an additional 7 days under identical conditions. Methanogenic activity during enrichment was monitored by methane production, measured weekly as an indicator of growth. For gas chromatography, 200 µL of headspace gas was injected into an SRI 8610C gas chromatograph (6-channel configuration, SRI Instruments Europe GmbH) gas chromatograph equipped with a 0.3 m HaySep-D packed Teflon column maintained at 42 °C, a thermal conductivity detector (TCD) at 111 °C, and a flame ionization detector (FID). Methane concentrations were quantified against a multi-point calibration series. The following concentrations of pure methane were used for the standard curve: 1.75, 3.51, 5.26, 7.02, 10.53, 15.79, 17.54, 24, 50 and 100 %.

Enrichments that showed both visible turbidity and methane production were streaked onto solidified ME media and incubated anaerobically at 37 °C. Distinct colonies appeared after 3–5 days and were repeatedly re-streaked to obtain a pure culture. One colony was picked and designated as strain G0370_i3. Purity was confirmed by microscopy and by sequencing of the 16S rRNA and *mcrA* genes. For long-term storage, the culture was stored at −80 °C in ME medium containing 10 % glycerol. Growth was compared when using either modified brain heart infusion (mBHI) media or ME culture media, with ME observed to be the most optimal. Cells reached high density after 30 hours incubation, with H_2/CO_2 provided as the energy source.

Cellular morphology was assessed using a Carl Zeiss Axioscope A1 light microscope equipped with a Sola light engine® and Zen 3.1 software. Exponential-phase cultures (1 mL) were pelleted (1 min, 10,000 rpm), washed twice in PBS supplemented with 3 % EDTA, and 1.5 µL of the final suspension was applied to glass slides for imaging. Bright-field and UV fluorescence modes were used; methanogen cells were identified by the characteristic blue-green auto-fluorescence of coenzyme F_{420}, which also served as a control for culture purity. Cell sizes were calculated in Fiji [12]. *M. intestini* G0370_i3, was further examined by scanning electron microscopy (SEM). For SEM, 8 mL of exponential-phase culture was pelleted, resuspended in ME medium, and fixed with an equal volume of fixative (8 % formaldehyde, 5 % glutaraldehyde, 0.2 M phosphate buffer). The fixed sample was dehydrated in a graded ethanol series followed by drying with CO_2 in a Polaron critical point dryer (Quorum Technologies, East Sussex, UK).

Finally, cells were sputter coated with a 5 nm thick layer of platinum (CCU-010 Compact coating unit, Safematic GmbH, Bad Ragaz, SWI). Cells were examined with a field emission scanning electron microscope (Regulus 8230; Hitachi High Technologies, Tokyo, Japan) at an accelerating voltage of 10 kV.

Growth and phenotypic experiments. Growth was monitored in the presence of methylated compounds, alcohols, and different sodium chloride (NaCl) concentrations. Starter cultures were grown to mid-exponential phase (optical density $(OD)_{600} \approx 0.1$) and 1 mL was inoculated into 9 mL of fresh ME medium in sealed Balch tubes. Cultures were incubated at 37 °C with shaking at 150 rpm. Unless otherwise indicated, the headspace was H_2/CO_2 (80/20) at 1.5 bar and refreshed daily. OD_{600} was recorded every 2 hours using a MicrobeMeter photometer (Human Technologies Ltd., University of Warwick Science Park, UK).

ME medium was supplemented with trimethylamines (TMA: 1, 5, 10, 50, 100 mM), NaCl (5, 10, 25, 50, 100 mM), 60 mM methanol, or 60 mM isopropanol. Sodium formate experiments included glycylglycine buffer (gly-gly; Carl Roth GmbH) at a 1:1 ratio with 2.8 mM, 44.2 mM, or 200 mM formate, to prevent inhibitory alkalinization. pH ranges from 4.3 to 9.7 were tested in ME medium. All experiments testing substrate utilization (methanol, isopropanol, formate or H_2/CO_2), pH, temperature, and sodium chloride concentrations were performed in three technical replicates. The antibiotics ampicillin (1 μg/mL), erythromycin (10 μg/mL), vancomycin (10 μg/mL), and cycloheximide (40 mg/L) were included in the ME medium during enrichments to suppress bacterial growth. After isolation of *M. intestini* G0370_i3, susceptibility to additional antimicrobials was tested individually in ME medium: novobiocin (100 mg/mL), metronidazole (20 mg/mL), and cetylpyridinium chloride (1 mg/mL). Growth inhibition was assessed based on OD_{600} measurements for up to 96 hours, with cultures showing growth classified as resistant and those with no growth classified as sensitive.

Oxygen tolerance was assessed by first growing cultures anaerobically in Balch tubes with H_2/CO_2 (80/20) at 1.5 bar for 24 hours. Tubes were then exposed to atmospheric oxygen by opening them in a sterile hood for 10, 30, or 60 minutes. Resazurin in the medium served as an oxidation-reduction indicator, turning pink upon oxygen exposure. Tubes were subsequently resealed and flushed with N_2 at ~0.5 L/min for approximately 30 minutes to restore anaerobic conditions, which was confirmed by the colour change of resazurin back to colourless. Cultures were then re-supplemented with H_2:CO_2 gas and incubated for an additional 72 hours while OD_{600}

was monitored. Susceptibility to lysis was evaluated by culturing in the presence of 0.5–3 % sodium dodecyl sulfate (SDS).

***DNA extraction and sequencing*.** Genomic DNA was extracted using phenol:chloroform, treated with RNase A (final concentration ~0.2 mg/mL) for 30 mins at 37 °C, and purified with 0.6× AMPure XP (Beckman Coulter) beads, with final elution in 46 µL. Following sequencing on a PacBio Sequel II sequencer, subreads were demultiplexed with Lima and converted to HiFi reads with CCS v6.4.0. Filtlong v0.2.1 was used to discard reads less than 1 kbp and 5 % of reads with the lowest quality and Trycycler v0.5.5 was used for *de novo* assembly [13,14]. Genomic statistics were calculated with BBMap v39.60 and CheckM2 v1.0.2 was used to estimate assembly completion and contamination [15,16].

***Genome annotation and analysis*.** Open reading frames and functional annotations were predicted with Prokka v1.14.5 [17]. The metabolic pathways and traits of strain G0370_i3 were analysed using the Kyoto Encyclopaedia of Genes and Genomes (KEGG) database via KOfamScan v1.3.0, Traitar3 v3.0.1, MetaPathPredict v1.0, and GapMind v1.0 [18–21]. Defense systems were predicted with DefenseFinder v1.3.0 [22], phage proteins were predicted with Phastest v1.0, mobile genetic elements were predicted with mobileOG-db v1.6 [22–24], and genomic islands were predicted with IslandViewer v4 [25]. Relative synonymous codon usage was calculated for ribosomal proteins using custom scripts.

***Phylogenetic analysis*.** The phylogenetic analysis utilized 16S rRNA sequences extracted with ContEst16S, as well as genome-wide phylogenies predicted using PhyloPhlAn v3.1.1 with 1000 bootstrap replicates for statistical support [26,27]. Additionally, phylogenetic trees were constructed based on the *mcrA* gene (a key marker for methanogens) and 202 conserved marker protein sequences. The resulting trees were visualized using the Interactive Tree Of Life (iTOL) v7 platform to facilitate interpretation [28]. The analysis included 19 representative archaeal genomes from the *Methanobacteriaceae* family obtained from NCBI, along with the genome of *M. intestini* G0370_i3, totalling 20 genomes. To further assess genomic similarity, digital DNA-DNA hybridization (dDDH) was performed using GGDC v3.0 and average nucleotide identity (ANI) and average amino acid identity (AAI) were calculated using fastANI v1.34 and FastAAI v0.0.1, respectively [29–31].

4.4. Results

4.4.1. Genomic analysis

Human faeces collected from the Ikobey region in southern Gabon, Central Africa was used for targeted enrichment of methanogens (Fig. 4.1). We successfully isolated multiple *M. intestini* strains from these samples and selected strain G0370_i3 for phenotypic characterization as a non-Western alternative to the existing type strain (Fig. 4.1). No other methanogens were detected or isolated from the sample from where G0370_i3 was derived.

The complete genome of *M. intestini* G0370_i3 was assembled into a single circular chromosome of 1,995,711 base pairs with no gaps, which is slightly larger than the (incomplete) genome size reported for the *M. intestini* WWM1085 type strain (1,926,345 bp). Comparison of assembly metrics (Supplementary Table 1) shows that G0370_i3 has a single scaffold and contig with an N50 of 2 Mb, whereas WWM1085 is more fragmented, with 16 scaffolds/contigs and an N50 of 240.3 kb. Coverage was higher for G0370_i3 (100× vs 61.4×), while completeness and contamination estimates were comparable between the strains (98.99 % vs 98.95 % completeness; 1.31 % vs 0.94 % contamination).

Genome annotation of G0370_i3 resulted in a total of 1,895 genes, comprising 1,808 protein-coding genes. In contrast, the WWM1085 assembly has 1,875 genes which is likely due to differences in assembly completeness rate. The RNA gene complement included 6 rRNA genes and 77 tRNA genes (Fig. 4.1). A total of 45 pseudogenes were identified, including 32 truncated and 13 fragmented genes, representing approximately 2.4 % of total gene content. The pseudogenes were primarily associated with adhesins, transposases, defense system genes, and hypothetical proteins. Coding regions occupied 90.46 % of the genome, indicating a highly compact genetic architecture with a gene density of 0.95 genes per kilobase. The protein-coding genes have an average length of 976.33 bp (Supplementary Fig. 1), encoding proteins with an average size of 329.57 amino acids. This represents the first complete, closed genome for *M. intestini*, providing an important resource and enabling an in-depth characterization of its genomic and functional potential.

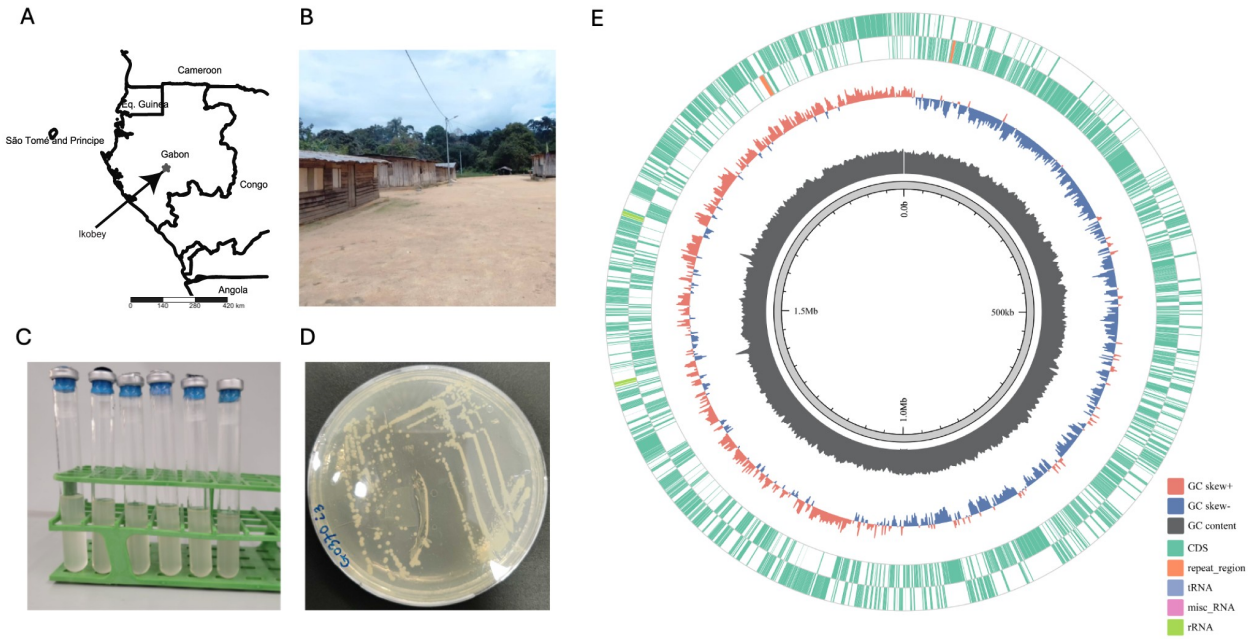

Figure 4.1. **Sampling sites, methanogen cultivation, and genome overview of *M. intestini* G0370_i3.**
(A) Map of Gabon highlighting the sampling sites: Lambaréné, the capital of Moyen-Ogooué province, situated approximately 75 kilometres south of the equator along the Ogooué river; and Ikobey communities, located in the Ngounié province. **(B)** View of the Ikobey village where samples were collected. Photograph taken by Ange Gatien Doumba Ndalemnouly. Licensed under CC BY 4.0. **(C)** Anaerobic cultures of methanogens enriched from human stool. Photograph taken by the author. **(D)** *M. intestini* G0370_i3 colonies on solid media for isolation. Photograph taken by the author. **(E)** Genome map of *M. intestini* G0370_i3. Genome size is shown on the inner circle (grey) and GC content is represented by the grey bar plot. GC skew is shown as the orange (positive) and blue (negative) bar plots. The green outer rings represent coding sequences on the forward strand (inner ring) and reverse strand (outer ring). tRNA, rRNA, misc rRNA, and repeat regions are also shown (blue, light green, pink, orange, respectively).

4.4.2. Low genomic GC content shapes codon usage patterns

A GC content of 30.31 % was observed. A distinct shift in GC skew values was observed around position 1,000,000, likely indicating the origin of replication, with predominantly negative values before this position and positive values after (Fig. 4.1). This asymmetric pattern likely reflects different mutational pressures on leading and lagging strands during DNA replication and suggests a bidirectional replication mechanism typical of archaea and bacteria. Local fluctuations throughout the genome may indicate regions with different functional properties, potentially corresponding to laterally transferred elements or areas under different selective pressures. The AT-rich genomic composition correlated with codon constraints where a pronounced preference for codons ending in A or U was observed, while codons ending in G or C are consistently

underutilized (Supplementary Fig. 2). The amino acids with the strongest bias were arginine, threonine, leucine, and alanine and this codon usage pattern is consistent with what has previously been reported for methanogenic archaea [32]. This bias likely represents adaptation to the available tRNA pool for this species, which in turn optimises translational efficiency and energy conservation.

4.4.3. Mobile genetic elements and genomic islands

A total of 23 mobile genetic elements were annotated in the genome, further suggesting the capacity for horizontal gene transfer. Most of these elements were related to integration/excision events, while eight replication/recombination sites were detected. Seven regions were identified as potential genomic islands based on their aberrant GC content compared to the genome average (Supplementary Fig. 3). These islands ranged in size from 5,000 bp to 15,000 bp and contained between 5 and 14 genes each (Supplementary Table 2). Notably, most islands (10 out of 15) displayed lower GC content (23.62-25.02 %) than the genome average, while 5 islands exhibited higher GC content (35.34-41.12 %). Adhesins, defense system-related genes, transposases, and hypothetical proteins were functionally enriched in the genomic islands (Supplementary Table 2), suggesting that host interaction and anti-phage functions are highly mobile in this strain.

4.4.4. Functional annotation and classification

Of the 1,808 protein-coding genes, 1,420 (78.5 %) were assigned functional annotations, while 388 (21.5 %) were classified as hypothetical proteins with unknown functions (Fig. 4.2). The annotated proteins included 1,231 enzymes, 112 transporters, 27 transcription factors, and 1 two-component system. Analysis of enzyme classes revealed 157 transferases (EC 2), 71 hydrolases (EC 3), 66 oxidoreductases (EC 1), 49 lyases (EC 4), 47 ligases (EC 6), 25 isomerases (EC 5), and 21 translocases (EC 7). Functional categorization identified 75 proteins involved in translation, 73 in transport, 50 in DNA metabolism, 27 in transcription, 10 in signalling, and 7 in membrane-associated functions (Fig. 4.2). No prophage genes were identified, suggesting active viral defense mechanisms.

Five distinct defense systems were identified: Prometheus, Dodola, two restriction-modification systems (RM Type I and RM Type IV), and two CRISPR-Cas systems (CAS Class1 Subtype IB and CAS_Class1 Subtype III A) with two corresponding CRISPR arrays (Fig. 4.2). Only the CRISPR and RM systems were associated with genomic islands (Supplementary Fig. 3), suggesting that the Prometheus, and Dodola systems are evolutionarily conserved anti-phage

systems for this strain. Notably, both Prometheus and Dodola have not been previously identified in archaea.

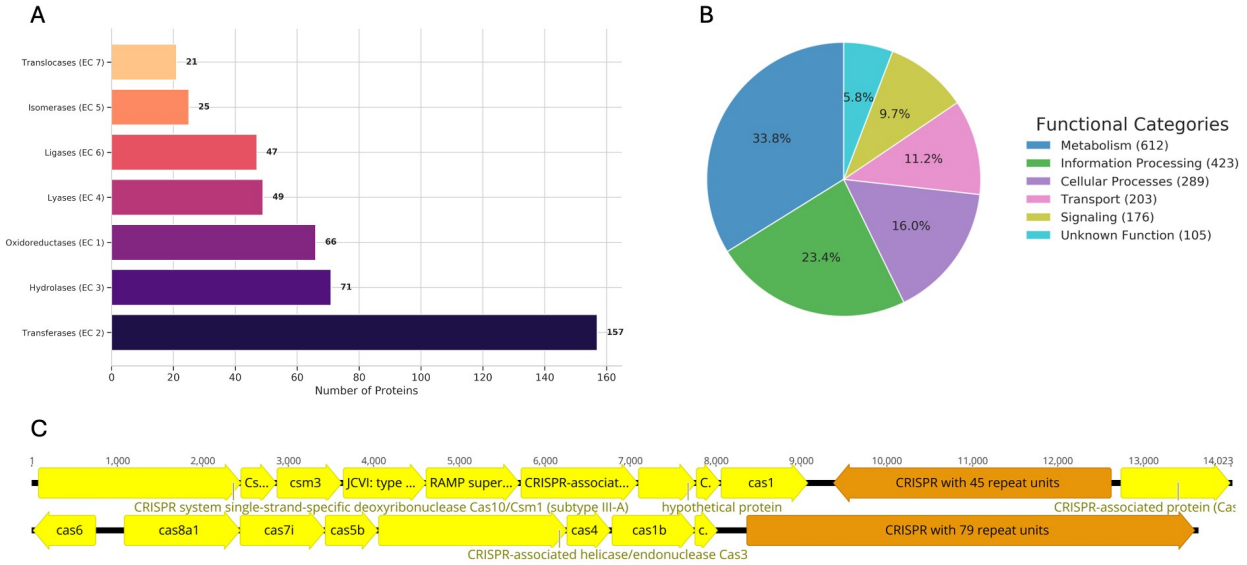

Figure 4.2. Functional prediction for *M. intestini* G0370_i3. A. Number of proteins associated with each enzyme (EC) class. (B) Functional categories for *M. intestini* G0370_i3 proteins. (C) Genomic structures for the CRISPR-Cas systems type III-A (top) and type IB (bottom).

The CRISPR-Cas systems are represented by 15 CRISPR-associated proteins and 124 potential CRISPR arrays. The CRISPR-Cas proteins appear to be organized into two main loci: one spanning position 55,791 to 69,728 (containing the Type III A system components including Cas10/Csm1, Csm3, and Csm4) and another from positions 1,811,246 to 1,819,249 (housing the Type IB system components including Cas8b1/Cst1, Cas7/Cst2/DevR, Cas5b, Cas3, Cas4, Cas1b, and Cas2). The CRISPR arrays predominantly featured repeat sequences of either 28 bp or 32 bp in length, with spacers of 35-40 bp (Fig. 4.2). Notably, both spacers were not present in existing CRISPR spacer databases and blasting each against viral and plasmid databases produced no hits, highlighting the novelty of these CRISPR systems compared to current knowledge [33]. Given the number and novelty of defense systems identified in this strain, a comparative analysis between human gut methanogens would be informative once additional strains are available.

4.4.5. Metabolic prediction

M. intestini G0370_i3 has the genetic determinants for core methanogenic processes, including the *fwd*, *ftr*, and *mcr* operons, pyruvate oxidation, acetyl-coenzyme A metabolism, and

NAD biosynthesis. The genome also encodes the enzymes necessary for hydrogenotrophic methanogenesis, using CO_2 or bicarbonate as electron acceptors and H_2 as electron donors. All seven key enzymes required for the reduction of CO_2 to methane were identified, along with the formate transporter and dehydrogenase (*fdhD*) genes, which are essential for formate to be utilized as a substrate and catalyses the reversible conversion of formate into CO_2. Additionally, genes encoding the three subunits of the methanol coenzyme M-methyltransferase complex (*mtaA*, *mtaB*, *mtaC*) were identified. This complex facilitates methyl transfer from methanol to coenzyme M, forming methyl coenzyme M, a central intermediate in methane biosynthesis [34]. A total of 51 adhesin-like proteins and proteins containing Ig-like domains suggest a diverse surface structure for this species, potentially facilitating host interaction or colonization (Supplementary Table 3). This corresponds with the large number of adhesins observed in other *Methanobrevibacter* species [35].

M. intestini G0370_i3 encoded the biosynthetic capability to synthesize all amino acids with the exception of histidine, consistent with what we observed for the *M. smithii* type strain (Supplementary Table 4). In contrast, WWM1085 was predicted to be incapable of biosynthesizing tryptophan (as well as histidine) but this could be due to the incompleteness of its genome assembly. G0370_i3 was predicted to synthesize cobalamin (vitamin B_{12}), a cofactor essential for methanogenesis, and possessed the genetic capability to produce nicotinamide adenine dinucleotide (NAD), biotin, riboflavin, and coenzyme A, all of which are crucial for various metabolic processes. The presence of a thiamine salvage pathway rather than *de novo* synthesis suggests an adaptation to recover this vital cofactor from the environment, enabling it to conserve energy while ensuring the availability of necessary cofactors for metabolism.

M. intestini G0370_i3 showed capacity for nucleotide processing but not complete *de novo* synthesis. It possessed phosphoribosyl pyrophosphate (PRPP) biosynthesis, which provides a precursor for nucleotide synthesis, and can theoretically convert inosine monophosphate (IMP) to adenine and guanine nucleotides. *M. intestini* G0370_i3 also has pathways for pyrimidine ribonucleotide interconversions but lacks the complete *de novo* purine biosynthesis pathway. This profile suggests a reliance on salvage pathways or environmental sources for some nucleotide components, which is consistent with the energy-efficient metabolic strategy typical of archaea inhabiting nutrient-rich environments like the human gut. *M. intestini* G0370_i3's ability to produce uridine diphosphate (UDP)-glucose and UDP-N-acetylglucosamine, which serve as

precursors for cell wall components, underscores its ability to maintain cellular integrity and adapt to the gut environment.

4.4.6. Phylogenetic analysis

Phylogenetic analyses using whole genome marker genes, 16S rRNA genes, and the *mcrA* functional gene consistently placed *M. intestini* G0370_i3 in a distinct clade alongside *M intestini* WWM1085 and *Methanobrevibacter* sp. strain TLL-48-HuF1, separate from species such as *M. smithii* DSM 861 (Fig. 4.3). TLL-48-HuF1 was isolated from human stool collected in Singapore in 2018 and represents one of the few additional *M. intestini* genome assemblies currently available (NCBI accession: CP081485) [8]. The whole genome tree provided the highest resolution, with strong bootstrap support (85 %) for this clade, while the 16S rRNA gene phylogeny similarly grouped these strains with high bootstrap support (94 %), and the *mcrA* gene phylogeny corroborated this clustering within the *mcrA* I functional group. High ANI values were observed between G0370_i3 and WWM1085 (98.5 %) as well as TLL-48-HuF1 (98.2 %), exceeding the species delineation threshold of ~95–96 %, while a lower ANI value of 93.5 % was found between G0370_i3 and *M. smithii* DSM 861 (Supplementary Table 5). These results, combined with phylogenetic reconstruction and dDDH analyses, strongly support that G0370_i3, WWM1085, and TLL-48-HuF1 represent a unique evolutionary lineage within the *Methanobrevibacter* genus. Furthermore, the ANI range between these *M. intestini* assemblies (98.2-98.5 %) suggest a considerable number of single nucleotide polymorphisms (SNP)s that are likely to contribute to functional variation within this species. These should be investigated in more detail once additional assemblies are available.

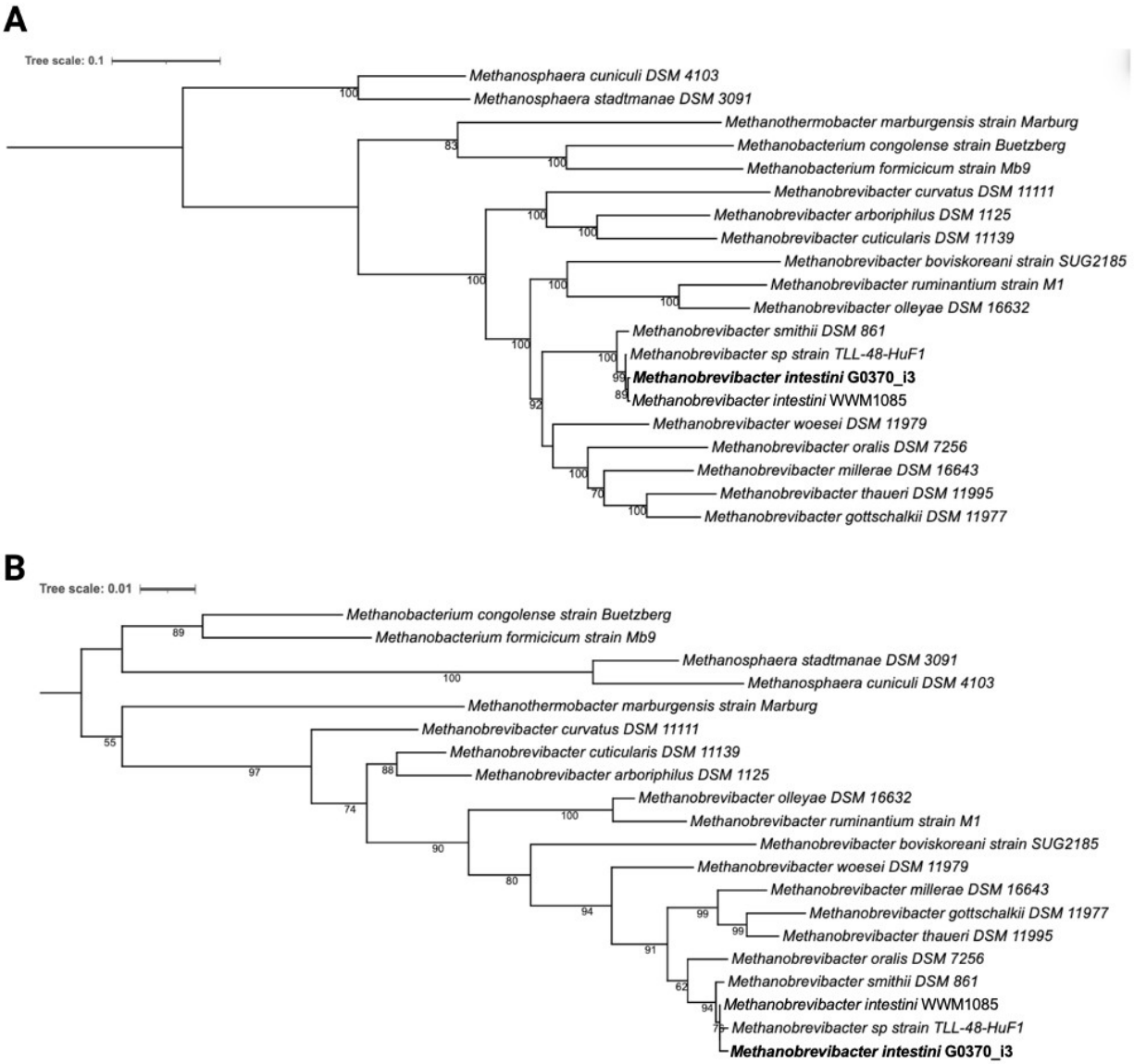

Figure 4.3. Phylogenetic reconstruction of *M. intestini* G0370_i3. (A) Phylogenomic tree based on 202 conserved marker-protein sequences, constructed alongside 19 representative archaeal genomes from the Methanobacteriaceae family. The tree is midpoint rooted, with *M. intestini* G0370_i3 highlighted in black. Bootstrap values greater than 80 are indicated on the tree branches. The scale bar represents the number of amino acid substitutions per site. (B) 16S rRNA gene tree using the same 19 representative Methanobacteriaceae genomes. The tree is midpoint rooted, with *M. intestini* G0370_i3 highlighted in black. Bootstrap values (ranging from 55 to 100) were obtained from 1000 replicates. The scale bar represents the number of nucleotide substitutions per site.

4.4.7. Morphological and physiological characteristics

M. intestini G0370_i3 cells were examined using both fluorescence and scanning electron microscopy, and the cellular morphology were coccobacilli-like (Fig. 4.4). Cell length ranged from 0.61 to 1.67 μm (mean: 1.12 ± 0.26), with a diameter of 0.42 to 0.91 μm (mean: 0.70 ± 0.10), based on measurement from $n = 9$ individual cells. The reported cell dimensions for the *M. intestini* type strain WWM1085 (0.16–0.43 μm in length and 0.29–0.54 μm in width) fall within the lower range of values observed for G0370_i3 [7], indicating that both strains share a similar coccobacillus-like morphology. Single, isolated cells were observed but they predominantly appeared in pairs, although longer chains of more than two cells were observed after extended incubation periods. No cellular appendages such as pili or flagella were observed and all colonies were capable of autofluorescence at 420 nm, corresponding with presence of coenzyme F_{420}, a cofactor that is characteristic of methanogenic archaea (Fig. 4.4).

Growth temperature profiling revealed that growth occurred between 27 °C and 42 °C and was optimal at 37 °C (Fig. 4.4). ANOVA on growth rate (r) revealed a significant temperature effect ($F = 4.04$, $p = 0.015$). Tukey *post-hoc* comparisons indicated that 37 °C supported significantly higher r (0.277 ± 0.012 h^{-1}) and final optical density (*max* OD_{600} = 0.135 ± 0.006) than all other tested temperatures (all FDR adjusted $p < 0.01$). At 27–32 °C, growth rates were markedly slower (r = 0.220–0.315 h^{-1}) with lower yields (max OD_{600} = 0.048–0.089), while moderate growth persisted up to 42 °C (r = 0.111 h^{-1}). No growth was detected at 47 °C, confirming a mesophilic optimum.

Despite the genetic evidence, no growth was detected when *M. intestini* G0370_i3 was cultivated on minimal media supplemented with 60 mM methanol or 2-propanol, suggesting that alternative conditions might activate this metabolic capability (Table 2; Fig. 4. 4). No growth in the presence of trimethylamine (TMA; 1 - 100 mM) was observed (Supplementary Fig. 4). *M. intestini* G0370_i3 tolerated NaCl concentrations between 5 mM and 100 mM without significant loss of fitness (Supplementary Fig. 4), and only a slight reduction in OD_{600} in the presence of 100 mM NaCl compared to the control. Growth rate and final biomass were statistically indistinguishable across this range (ANOVA on r: $F = 5.102$, $p = 0.010$, ANOVA on max OD_{600}: $F = 0.96$, $p = 0.476$). Tukey pairwise comparisons revealed no significant differences among salt concentrations (all FDR adjusted $p > 0.05$). Maximum growth rate occurred at 50 mM NaCl (r =

0.101 h^{-1}), and overall *max* OD_{600} in any tube ranged from 0.320–0.379, confirming broad halotolerance under low-salinity conditions.

Additionally, pH experiments demonstrated observed growth from pH 5.0 to 9.7, with no detectable growth at pH 4.3 (Table 2; Supplementary Fig. 4). ANOVA on growth rate confirmed a highly significant pH effect ($F = 60.92$, $p < 0.001$). Tukey post-hoc comparisons showed that r and max OD_{600} were highest between pH 7.0 and 7.9 ($r = 0.095–0.333$ h^{-1}; *max* $OD_{600} = 0.45–0.64$; all FDR adjusted $p < 0.001$ vs. pH ≤ 5.0 or ≥ 9.0). The optimal growth pH of *M. intestini* G0370_i3 thus spans pH 7.0–7.9, which is slightly broader than that reported for the *M. intestini* WWM1085 type strain (7.0–7.5), but a comparable optimal growth temperature at 37 °C [7]. Growth decreased sharply beyond pH 9.0 ($r \leq 0.125$ h^{-1}, max $OD_{600} < 0.32$).

Further substrate utilization assays confirmed growth on standard H_2/CO_2 medium and on 200 mM sodium formate as the sole electron donor, consistent with genomic predictions. In formate-supplemented cultures, an extended lag phase of ~40 h was observed, followed by exponential growth reaching a max OD_{600} of 0.067, comparable to H_2/CO_2 controls. Growth rate on formate was lower (r = 0.030 h^{-1}) compared to H_2/CO_2 (r = 0.089 h^{-1}), with higher doubling times (≈23 h on formate vs. 7.8 h on H_2/CO_2) and a comparable final OD_{600} (Fig. 4. 4). Growth on formate was additionally confirmed by measuring CH_4 production, which accounted for approximately 10 % of total headspace gas across three technical replicates. Despite the extended lag phase, *M. intestini* G0370_i3 was able to adapt metabolically to formate. This delay likely reflects the time required for genetic and metabolic adaptation to upregulate formate dehydrogenase (FDH) and shift cellular machinery toward formate utilization.

Glycylglycine buffer was included in the medium during formate growth experiments specifically to maintain pH stability, which likely facilitated the observed growth of G0370_i3; the WWM1085 type strain was apparently not tested under buffered conditions [7]. The *M. intestini* WWM1085 type strain similarly encodes the formate transporter and dehydrogenase genes and a multiple sequence alignment between WWM1085 and G0370_i3 for this operon showed 99.7 % sequence identity, with 12 polymorphic sites between them (Fig. 4.4). The differences in pH preference and formate usage likely reflect methodological differences and future experiments incorporating both strains under the same conditions, including RNA-Seq to confirm transcription of the formate utilization operon, will enable further insights and resolve these discrepancies [7].

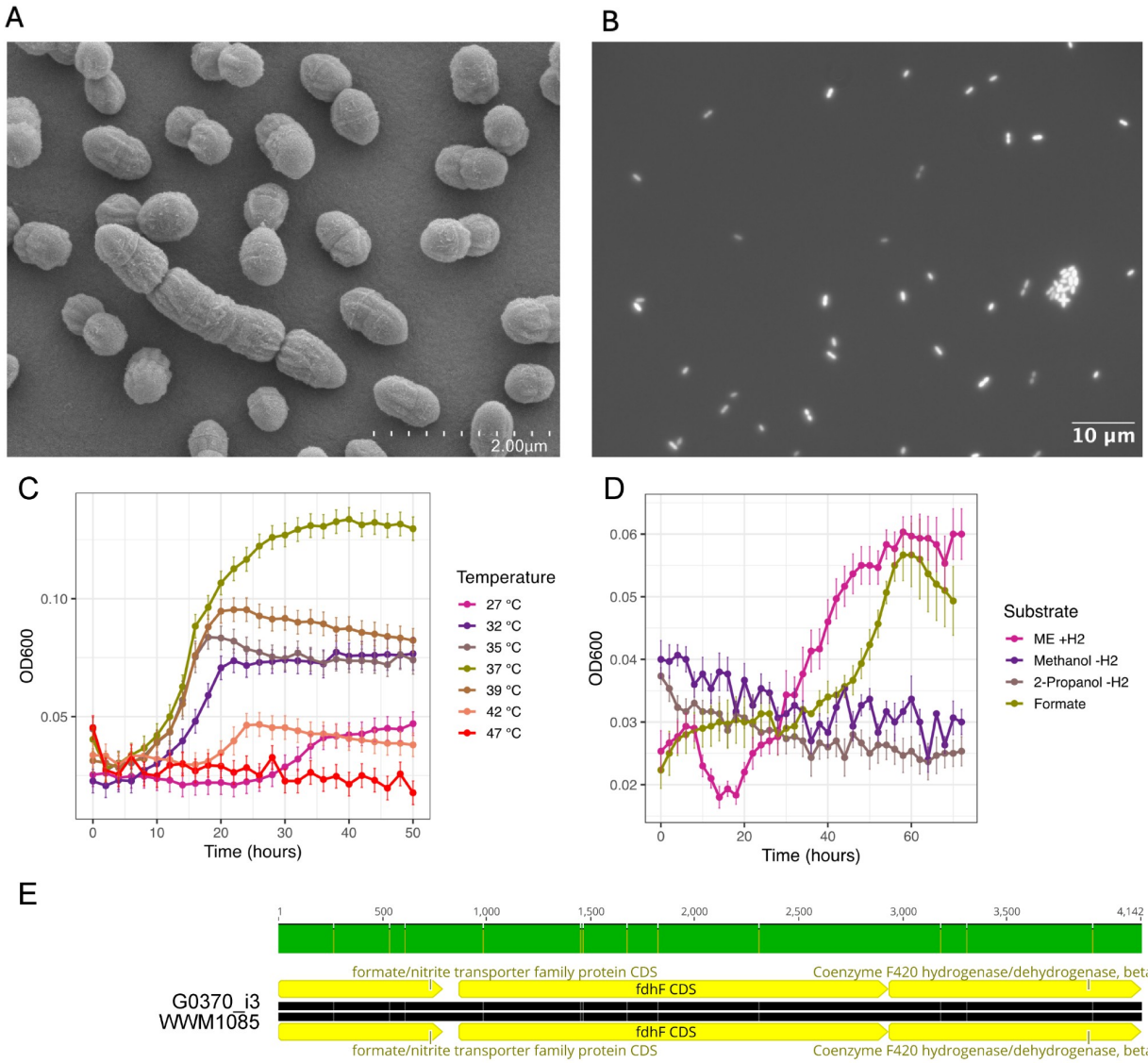

Figure 4.4. Morphological and physiological characterization of *M. intestini* G0370_i3. (A) Scanning electron micrographs showing *M. intestini* G0370_i3 cells as coccobacilli, typically occurring singly, in pairs, or forming short chains (scale bar = 2 µm).
(B) Fluorescence micrograph showing the characteristic blue–green autofluorescence of coenzyme F_{420} under UV illumination (420 nm; scale bar = 10 µm). (C) Growth of *M. intestini* G0370_i3 at different temperatures (27–47 °C). (D) Growth of *M. intestini* G0370_i3 under different substrate conditions: standard ME + H_2/CO_2 (control), 60 mM methanol (–H_2), 60 mM 2-propanol (–H_2), and 200 mM sodium formate (1:1 dilution with glycylglycine buffer). Growth conditions: +H_2 = H_2/CO_2 added to the headspace; –H_2 = N_2/CO_2. For growth curves, points represent mean OD_{600} values (± SEM) from n = 3 technical replicates; error bars denote standard error of the mean (SEM), and lines connect mean values over time. (E) Multiple sequence alignment of the formate utilization operon between *M. intestini* G0370_i3 and WWM1085.

Antibiotics (ampicillin, erythromycin, vancomycin, and cycloheximide) were included in the enrichment medium and did not inhibit growth during isolation, consistent with the resistance to these compounds observed under the tested conditions. Following isolation, susceptibility to additional antimicrobials was individually assessed, with susceptibility classified based on the presence or absence of measurable growth (OD_{600}) over a 96-h period of cultivation. *M. intestini* G0370_i3 exhibited continued growth in the presence of novobiocin, indicating resistance, but showed no growth when exposed to metronidazole (≥ 20 mg/mL) or cetylpyridinium chloride (≥ 1 mg/mL), indicating sensitivity (Table 2). The addition of 0.5–3 % SDS to early log-phase cultures did not affect growth. Short-term exposure to atmospheric oxygen for 10–60 min resulted in only a slight reduction in final biomass, while growth rate and doubling time remained consistent ($r = 0.068–0.075\ h^{-1}$; doubling time 9.3–10.2 h), indicating that G0370_i3 is strictly anaerobic but can tolerate transient oxidative stress (Table 2).

Table 2. Morphological and physiological characteristics of *M. intestini* G0370_i3.

Characteristic	**Strain G0370_i3**
Cell size (length x diameter)	1.12 x 0.7 (µm)
Flagella	-
Optimum growth temperature (°C)	37 (growth range: 27-42) At the optimum: growth rate $r = 0.277\ h^{-1}$, max OD600 = 0.135. Temperature significantly affected growth rate ($p = 0.015$), carrying capacity ($p = 3.96\times10^{-8}$), and maximum OD ($p = 7.93\times10^{-11}$). No growth at 47 °C
pH growth range	5.0 -9.7 No growth detected below pH 5. Optimum pH = 7.0–7.9 with $r = 0.095–0.33\ h^{-1}$, max OD600 = 0.45–0.64. pH significantly affected all growth parameters (all ANOVA $p < 0.001$).
NaCl growth range (mM)	5 - 100 Growth rate $r = 0.09–0.10\ h^{-1}$, doubling time = 7.0–8.0 h, max OD600 = 0.32–0.379. NaCl significantly affected growth rate ($p = 0.010$), but not carrying capacity or maximum OD.
Growth on Formate	Growth observed on formate with ~40 h lag phase. Growth rate $r = 0.03\ h^{-1}$, doubling time = 23 h, max OD600 = 0.067. In ME + H_2/CO_2: $r = 0.089\ h^{-1}$, doubling time = 7.8 h.
Growth on other substrates - Alcohols (methanol and 2-propanol 60 mM) - Trimethylamine (1 -100 mM)	- -

Antimicrobial susceptibility - Erythromycin (10 μg/ml) - Ampicillin (1μg/ml) - Vancomycin (10μg/ml) - Cycloheximide (40 mg/ml) - Novobiocin (100 mg/ml) - Metronidazole (20 mg/ml) - Cetylpyridinium chloride (1mg/ml)	 Resistant Resistant Resistant Resistant Resistant Sensitive Sensitive
Susceptibility to lysis - SDS concentrations (0.5 – 3%)	 Not susceptible
Oxygen tolerance - 10 min to 1-hour O_2 exposure	 Resistant Growth rate = 0.068–0.075 h^{-1}, doubling times = 9.3–10.2 h, max OD600 = 0.26–0.30.

4.5. Discussion

Our analysis of the *M. intestini* strain G0370_i3, isolated from a Central African host, provides new insights into the genomic architecture and metabolic capabilities of this recently described human gut methanogen species. This strain is significant as it was isolated from a non-Western source, a category historically underrepresented in microbiome research [9]. Its detection in this stool sample suggests that *M. intestini* is a common and widespread member of the human gut archaeome, rather than a variant confined to Western industrial populations. To fully understand the geographic distribution and diversity of these methanogens, the isolation and sequencing of additional strains are essential.

The genomic data indicates an organism that is highly adapted to its niche within the human gut. The high coding density and compact genetic architecture indicate that efficient replication and resource utilization are prioritized [36]. This may indicate that *M. intestini* relies on metabolic dependencies that reduce genome maintenance costs, which is typical for symbiotic microorganisms in the gut [37]. The proportion of pseudogenes identified is consistent with what has previously been reported for methanogens [38,39]. Their association with adhesins and defense systems imply frequent adaptation to changing host pressures and phage interactions [5,40]. The proportion of hypothetical proteins identified (21.5 %) underscores a reservoir of uncharacterized functions that are potentially critical for niche-specific processes and highlights our currently limited understanding of gut methanogen function [41]. The assembly of a complete, high-quality

genome for a non-Western *M. intestini* strain provides an important step in this regard. With additional strains, it will allow conserved core functions essential for the methanogen's role in the gut to be identified, as well as variable elements that might reflect local adaptations to specific dietary patterns, host genetics, or other environmental factors.

The observed AT-rich genomic composition for *M. intestini* G0370_i3 is an established feature of genomic evolution under energetic and mutational constraints [42]. This bias is ecologically significant for human gut methanogens, as it reflects an evolutionary trajectory towards minimizing the metabolic cost of nucleotide synthesis, which is particularly advantageous for an organism inhabiting an energy-limited environment like the human gut where competition for resources can be significant. The strong codon usage bias, directly correlated with the AT-rich genome, likely represents evolutionary adaptation for efficient protein synthesis [43]. Similarly, the preference for A/U-ending codons is likely a strategic alignment with the predicted cognate tRNA pool, ensuring rapid and accurate translation [44]. This optimization minimizes ribosomal stalling and translational errors, thereby conserving cellular energy, a critical resource for methanogens whose own metabolism is geared towards energy conservation through methanogenesis [45]. This pattern, consistent across other methanogenic archaea [46], points to a convergent evolutionary solution to the challenge of thriving in anaerobic, competitive ecosystems.

The identification of a significant number of mobile genetic elements and genomic islands in *M. intestini* G0370_i3 provides additional evidence for the dynamic and responsive genome of this strain. Horizontal gene transfer (HGT) allows for rapid adaptation without relying solely on vertical descent and mutation and indicates that the strain exists within a genetically rich and interactive ecosystem, likely exchanging genetic material with other members of the gut microbiota [47]. Correlating with their association with pseudogenes, the enrichment of adhesins within these mobile regions again underscores the importance of host-microbe interaction as a selectable trait. These data suggest the potential for population-specific adaptations within this species.

Anti-phage defense systems are a prominent and dynamic part of this strain’s genome. The localization of CRISPR-Cas and RM systems within genomic islands suggests they represent mobile systems that allow for the horizontal acquisition of new immune capabilities to enable rapid adaptation to new viral threats [48]. RM systems are widespread in bacteria and archaea with a well-established mechanism for anti-phage defense [22]. The organization of the CRISPR

systems into two distinct loci (Type III and Type IB) suggests functional complementarity with Type IB providing DNA-targeted immunity through Cas3-mediated degradation while Type III enables RNA-directed and co-transcriptional DNA cleavage, creating multi-layered protection against diverse mobile genetic elements [49]. The novelty of the spacer sequences, with no matches in existing databases, implies that this strain has been exposed to viruses (phages and possibly archaeal viruses) that are not represented in current repositories.

Conversely, the chromosomally encoded Prometheus, and Dodola systems likely represent a stable, core defensive backbone for this strain. Prometheus functions through an R-loop-dependent mechanism to regulate viral transcription and was identified as part of a broader effort to discover new prokaryotic defense systems via comparative genomics [50]. As a result, its prevalence and distribution in microbial hosts remains to be determined. Similarly, the Dodola defense system is largely uncharacterized and is suggested to be a remnant of larger systems that have since been lost [51]. Nevertheless, the identification of these systems in *M. intestini* G0370_i3 highlights a potentially unique methanogen defense repertoire that warrants deeper investigation when additional strains are available.

The phylogenetic placement of *M. intestini* G0370_i3 confirms its identity as a distinct and coherent evolutionary lineage within the human gut archaeome, separate from the well-characterized species, *M. smithii* [6]. Furthermore, the consistent clustering of strains from geographically disparate regions suggests that *M. intestini* is a widespread, common, and persistent human symbiont. Its presence across continents indicates a successful evolutionary strategy that is not limited to a specific human population or diet, but rather represents a core, cosmopolitan member of the gut methanogen community.

Beyond genomic features, the physiological characteristics of *M. intestini* G0370_i3 contribute to a clearer understanding of how this archaeon may function and persist in the human gut environment. The strain's growth profile across a moderate pH and temperature range is consistent with adaptation to the colonic ecosystem, where physicochemical conditions are relatively stable yet spatially structured [52]. Its ability to withstand transient oxidative exposure also aligns with the dynamic micro-environments of the intestinal mucosa, where brief encounters with oxygen can occur [53]. This resilience likely enables *M. intestini* to maintain metabolic activity near epithelial surfaces where fermentative partners and hydrogen gradients are most pronounced [54].

The ability of G0370_i3 to utilize formate, although expressed only after a prolonged lag phase, is notable. Formate is a common fermentation intermediate in the human gut, and the capacity to shift between hydrogen- and formate-based methanogenesis may expand the ecological niche available to the strain and reduce its dependence on specific syntrophic partners [55]. The extended lag suggests that this metabolic shift is not constitutive but rather induced, implying regulatory flexibility that may allow *M. intestini* to respond to fluctuating substrate availability. Such metabolic flexibility may be advantageous in gut environments where host diet, microbial community composition, and substrate pools vary over time. Although formate utilization was not previously observed in the *M. intestini* type strain, this finding suggests potential for functional diversification within human-associated methanogens [7]. Isolation of additional strains will be needed to determine whether formate utilization is strain-specific or more broadly distributed.

The multidrug resistance profile of *M. intestini* G0370_i3, including resistance to clinically relevant antibiotics, may reflect selective pressures in gut environments periodically exposed to antimicrobial agents [56]. While its sensitivity to biocides like cetylpyridinium chloride suggests vulnerabilities in its cellular structure, its resistance to SDS implies a robust cell envelope [57]. This is potentially an adaptation to withstand bile salts and other membrane-disrupting agents present in the gastrointestinal tract. Furthermore, the strain's characterization as a strict anaerobe capable of withstanding transient oxygen exposure is characteristic of gut residents, enabling resilience against limited oxygen exposures that occur in the gut [58]. The ability to maintain growth kinetics despite short-term oxidative stress implies robust cellular repair mechanisms, allowing it to re-establish its population quickly after transient disturbances.

The isolation, characterization, and sequencing of *M. intestini* G0370_i3 offers opportunities for expanding our understanding of methanogen diversity in the human gut. Experimental validation of its genomically predicted metabolic pathways, especially those unique to this strain, would enhance our understanding of its ecological role. The observed genetic and phenotypic differences between G0370_i3 and WWM1085, especially the ability for G0370_i3 to utilize formate, offers preliminary insights into possible population-specific adaptations. However, given that the WWM1085 genome is currently incomplete and a phenotypic comparison of only two strains is statistically insufficient to draw meaningful conclusions. We present these comparisons as a first step toward understanding intraspecies diversity. Further pan-genome analyses incorporating additional cultured strains from diverse populations, including newly

isolated representatives would provide additional support for identifying population-specific adaptations. Additionally, deeper insight into the methanogen defense system repertoire will be possible. Finally, correlating the prevalence of *M. intestini* with host factors, dietary patterns, and health outcomes through metagenomic analysis will provide further insights into their ecological and functional roles in different human populations.

4.6. Conflicts of interest

The authors have no relevant affiliations or financial involvement with any organization or entity with a financial interest in or financial conflict with the subject matter or materials discussed in the manuscript. This includes employment, consultancies, honoraria, stock ownership or options, expert testimony, grants or patents received or pending, or royalties.

4.7. Author contributions

M.M.N., N.D.Y., R.E.L., and J.W.M. contributed to conceptualization, methodology, writing the original draft, and visualization. M.M.N., S.L., and L.B. carried out all experiments. M.M.N., J.P.K. and J.W.M. performed sequence processing and genome assembly. M.M.N. performed sample processing and data curation. N.D.Y., A.T., R.E.L., and J.W.M. supervised the research. P.G.K., A.A.A. and R.E.L. acquired funding.

4.8. Funding

This manuscript was funded by the Max Planck Society. The funders had no role in study design, data collection and analysis, decision to publish, or preparation of the manuscript.

4.9. Sequencing data

All sequencing data associated with this isolate has been deposited at NCBI with the following accessions: BioProject: PRJNA1216186, BioSample: SAMN46427273, genome accession: CP187956.

4.10. Ethical approvals

This study was conducted in full compliance with ethical principles outlined in the Declaration of Helsinki and relevant international guidelines for research involving human participants. Informed consent was obtained from the participant prior to their inclusion in the study. Ethical approval was granted by Le Comité National d'Ethique du Gabon (The Gabon National Ethics Committee) with protocol number N0025/2017/PR/SG/CNE.

4.11. References

[1] Ley RE, Peterson DA, Gordon JI. Ecological and evolutionary forces shaping microbial diversity in the human intestine. Cell. 2006;124(4):837–848.

*This important review highlights ecological forces, including geography, that shape the gut microbiome.

[2] Thauer RK, Kaster A-K, Seedorf H, et al. Methanogenic archaea: ecologically relevant differences in energy conservation. Nat Rev Microbiol. 2008;6(8):579–591.

**A defining review of methanogenic archaea and their unique metabolic capabilities.

[3] Saengkerdsub S, Ricke SC. Ecology and characteristics of methanogenic archaea in animals and humans. Crit Rev Microbiol. 2014;40(2):97–116.

[4] Ruaud A, Esquivel-Elizondo S, de la Cuesta-Zuluaga J, et al. Syntrophy via interspecies H_2 transfer between *Christensenella* and *Methanobrevibacter* underlies their global cooccurrence in the human gut. MBio. 2020;11(1):e03235-19.

[5] Samuel BS, Hansen EE, Manchester JK, et al. Genomic and metabolic adaptations of *Methanobrevibacter smithii* to the human gut. Proc Natl Acad Sci U S A. 2007;104(25):10643–10648.

**An important study that compares genomic, transcriptomic, and metabolomic features of the major human archaeon, *Methanobrevibacter smithii*.

[6] Chibani CM, Mahnert A, Borrel G, et al. A catalogue of 1,167 genomes from the human gut archaeome. Nat Microbiol. 2022;7(1):48–61.

[7] Weinberger V, Mohammadzadeh R, Blohs M, et al. Expanding the cultivable human archaeome: *Methanobrevibacter intestini* sp. nov. and strain *Methanobrevibacter smithii* "GRAZ-2" from human faeces. Int J Syst Evol Microbiol. 2025;75(4):1–12.

**The first characterization and description of *Methanobrevibacter intestini*

[8] Low A, Lee JKY, Gounot J-S, et al. Mutual exclusion of *Methanobrevibacter* species in the human gut microbiota facilitates directed cultivation of a Candidatus *Methanobrevibacter intestini* representative. Microbiol Spectr. 2022;10(4):e0084922.

[9] Abdill RJ, Adamowicz EM, Blekhman R. Public human microbiome data are dominated by highly developed countries. PLoS Biol. 2022;20(2):e3001536.

[10] Parizadeh M, Arrieta M-C. The global human gut microbiome: genes, lifestyles, and diet. Trends Mol Med. 2023;29(10):789–801.

[11] Suzuki TA, Fitzstevens JL, Schmidt VT, et al. Codiversification of gut microbiota with humans. Science. 2022;377(6612):1328–1332.

[12] Schindelin J, Arganda-Carreras I, Frise E, et al. Fiji: an open-source platform for biological-image analysis. Nat Methods. 2012;9(7):676–682.

[13] Wick RR, Judd LM, Cerdeira LT, et al. Trycycler: consensus long-read assemblies for bacterial genomes. Genome Biol. 2021;22(1):266.

[14] Wick R. Filtlong [Internet]. 2017. Available from: https://github.com/rrwick/Filtlong.

[15] Chklovski A, Parks DH, Woodcroft BJ, et al. CheckM2: a rapid, scalable and accurate tool for assessing microbial genome quality using machine learning. Nat Methods. 2023;20(8):1203–1212.
[16] Bushnell B. BBMap: A Fast, Accurate, Splice-Aware Aligner. 2014.
[17] Seemann T. Prokka: rapid prokaryotic genome annotation. Bioinformatics. 2014;30(14):2068–2069.
[18] Aramaki T. kofam_scan [Internet]. 2019. Available from: https://github.com/takaram/kofam_scan.
[19] Weimann A, Mooren K, Frank J, et al. From genomes to phenotypes: Traitar, the microbial trait analyzer. mSystems. 2016;1(6):e00101-16.
[20] Geller-McGrath D, Konwar KM, Edgcomb VP, et al. Predicting metabolic modules in incomplete bacterial genomes with MetaPathPredict. Elife. 2024;13(e85749):e85749.
[21] Price MN, Deutschbauer AM, Arkin AP. GapMind: automated annotation of amino acid biosynthesis. mSystems. 2020;5(3):1–19.
[22] Tesson F, Hervé A, Mordret E, et al. Systematic and quantitative view of the antiviral arsenal of prokaryotes. Nat Commun. 2022;13(1):2561.
[23] Wishart DS, Han S, Saha S, et al. PHASTEST: faster than PHASTER, better than PHAST. Nucleic Acids Res. 2023;51(W1):W443–W450.
[24] Brown CL, Mullet J, Hindi F, et al. MobileOG-db: A manually curated database of protein families mediating the life cycle of bacterial mobile genetic elements. Appl Environ Microbiol. 2022;88(18):e0099122.
[25] Bertelli C, Laird MR, Williams KP, et al. IslandViewer 4: expanded prediction of genomic islands for larger-scale datasets. Nucleic Acids Res. 2017;45(W1):W30–W35.
[26] Lee I, Chalita M, Ha S-M, et al. ContEst16S: an algorithm that identifies contaminated prokaryotic genomes using 16S RNA gene sequences. Int J Syst Evol Microbiol. 2017;67(6):2053–2057.
[27] Asnicar F, Thomas AM, Beghini F, et al. Precise phylogenetic analysis of microbial isolates and genomes from metagenomes using PhyloPhlAn 3.0. Nat Commun. 2020;11(1):2500.
[28] Letunic I, Bork P. Interactive Tree of Life (iTOL) v6: recent updates to the phylogenetic tree display and annotation tool. Nucleic Acids Res. 2024;52(W1):W78–W82.
[29] Meier-Kolthoff JP, Carbasse JS, Peinado-Olarte RL, et al. TYGS and LPSN: a database tandem for fast and reliable genome-based classification and nomenclature of prokaryotes. Nucleic Acids Res. 2022;50(D1):D801–D807.
[30] Jain C, Rodriguez-R LM, Phillippy AM, et al. High throughput ANI analysis of 90K prokaryotic genomes reveals clear species boundaries. Nat Commun. 2018;9(5114):1–8.
[31] Gerhardt K, Ruiz-Perez CA, Rodriguez-R LM, et al. FastAAI: efficient estimation of genome average amino acid identity and phylum-level relationships using tetramers of universal proteins. Nucleic Acids Res [Internet]. 2025;53(8).

[32] Pal A, Banerjee R, Mondal UK, et al. Deconstruction of archaeal genome depict strategic consensus in core pathways coding sequence assembly. PLoS One. 2015;10(2):e0118245.
[33] Couvin D, Bernheim A, Toffano-Nioche C, et al. CRISPRCasFinder, an update of CRISRFinder, includes a portable version, enhanced performance and integrates search for Cas proteins. Nucleic Acids Res. 2018;46(W1):W246–W251.
[34] Thauer RK. Methyl (alkyl)-coenzyme M reductases: Nickel F-430-containing enzymes involved in anaerobic methane formation and in anaerobic oxidation of methane or of short chain alkanes. Biochemistry. 2019;58(52):5198–5220.
[35] Gupta AB, Seedorf H. Structural and functional insights from the sequences and complex domain architecture of adhesin-like proteins from *Methanobrevibacter smithii* and *Methanosphaera stadtmanae*. Front Microbiol. 2024;15(1463715):1–13.
[36] Frumkin I, Schirman D, Rotman A, et al. Gene architectures that minimize cost of gene expression. Mol Cell. 2017;65(1):142–153.
[37] Moran NA, Ochman H, Hammer TJ. Evolutionary and ecological consequences of gut microbial communities. Annu Rev Ecol Evol Syst. 2019;50(1):451–475.
[38] Lü Z, Lu Y. Complete genome sequence of a thermophilic methanogen, Methanocella conradii HZ254, isolated from Chinese rice field soil. J Bacteriol. 2012;194(9):2398–2399.
[39] Kelly WJ, Pacheco DM, Li D, et al. The complete genome sequence of the rumen methanogen *Methanobrevibacter* millerae SM9. Stand Genomic Sci. 2016;11(1):49.
[40] Benler S, Yutin N, Antipov D, et al. Thousands of previously unknown phages discovered in whole-community human gut metagenomes. Microbiome. 2021;9(1):78.
[41] Jebastin T, Syed Abuthakir MH, Santhoshi I, et al. Unveiling the mysteries: Functional insights into hypothetical proteins from Bacteroides fragilis 638R. Heliyon. 2024;10(11):e31713.
[42] Nguyen DT, Wu B, Xiao S, et al. Evolution of a record-setting AT-rich genome: Indel mutation, recombination, and substitution bias. Genome Biol Evol. 2020;12(12):2344–2354.
[43] Carbone A, Képès F, Zinovyev A. Codon bias signatures, organization of microorganisms in codon space, and lifestyle. Mol Biol Evol. 2005;22(3):547–561.
[44] Zhang W, Foo M, Eren AM, et al. tRNA modification dynamics from individual organisms to metaepitranscriptomics of microbiomes. Mol Cell. 2022;82(5):891–906.
[45] Mand TD, Metcalf WW. Energy conservation and hydrogenase function in methanogenic Archaea, in particular the genus Methanosarcina. Microbiol Mol Biol Rev. 2019;83(4):10.1128/mmbr.00020-19.
[46] Emery LR, Sharp PM. Impact of translational selection on codon usage bias in the archaeon Methanococcus maripaludis. Biol Lett. 2011;7(1):131–135.
[47] Wiedenbeck J, Cohan FM. Origins of bacterial diversity through horizontal genetic transfer and adaptation to new ecological niches. FEMS Microbiol Rev. 2011;35(5):957–976.

[48] Makarova KS, Wolf YI, Snir S, et al. Defense islands in bacterial and archaeal genomes and prediction of novel defense systems. J Bacteriol. 2011;193(21):6039–6056.
[49] Makarova KS, Wolf YI, Alkhnbashi OS, et al. An updated evolutionary classification of CRISPR-Cas systems. Nat Rev Microbiol. 2015;13(11):722–736.
[50] van den Berg DF, Costa AR, Esser JQ, et al. Bacterial homologs of innate eukaryotic antiviral defenses with anti-phage activity highlight shared evolutionary roots of viral defenses. Cell Host Microbe. 2024;32(8):1427-1443.e8.
[51] Beavogui A, Lacroix A, Wiart N, et al. The defensome of complex bacterial communities. Nat Commun. 2024;15(1):2146.
[52] Duncan SH, Louis P, Thomson JM, et al. The role of pH in determining the species composition of the human colonic microbiota. Environ Microbiol. 2009;11(8):2112–2122.
[53] Colgan SP, Campbell EL. Oxygen metabolism and innate immune responses in the gut. J Appl Physiol. 2017;123(5):1321–1327.
[54] Macfarlane M. J. Hopkins G. T. Ma S. Bacterial growth and metabolism on surfaces in the large intestine. Microb Ecol Health Dis. 2000;12(2):64–72.
[55] Kelly WJ, Mackie RI, Attwood GT, et al. Hydrogen and formate production and utilisation in the rumen and the human colon. Anim Microbiome. 2022;4(1):22.
[56] Crits-Christoph A, Hallowell HA, Koutouvalis K, et al. Good microbes, bad genes? The dissemination of antimicrobial resistance in the human microbiome. Gut Microbes. 2022;14(1):2055944.
[57] Mao X, Auer DL, Buchalla W, et al. Cetylpyridinium chloride: Mechanism of action, antimicrobial efficacy in biofilms, and potential risks of resistance. Antimicrob Agents Chemother. 2020;64(8):10.1128/aac.00576-20.
[58] Albenberg L, Esipova TV, Judge CP, et al. Correlation between intraluminal oxygen gradient and radial partitioning of intestinal microbiota. Gastroenterology. 2014;147(5):1055-63.e8.

4.12. Supplementary Tables

Supplementary Table 1: Assembly statistics for *M. intestini* G0370_i3 and WWM1085.

Supplementary Table 2: Genomic coordinates for genomic islands and the genes associated with each island.

Supplementary Table 3: Predicted adhesins in *M. intestini* G0370_i3.

Supplementary Table 4: Predicted amino acid biosynthesis capabilities for *M. intestini* G0370_i3, *M. intestini* WWM1085, and *M. smithii* ATCC 3061.

Supplementary Table 5: Percentage ANI values between each pair of genomes used for phylogenetic tree construction.

4.13. Supplementary Figures

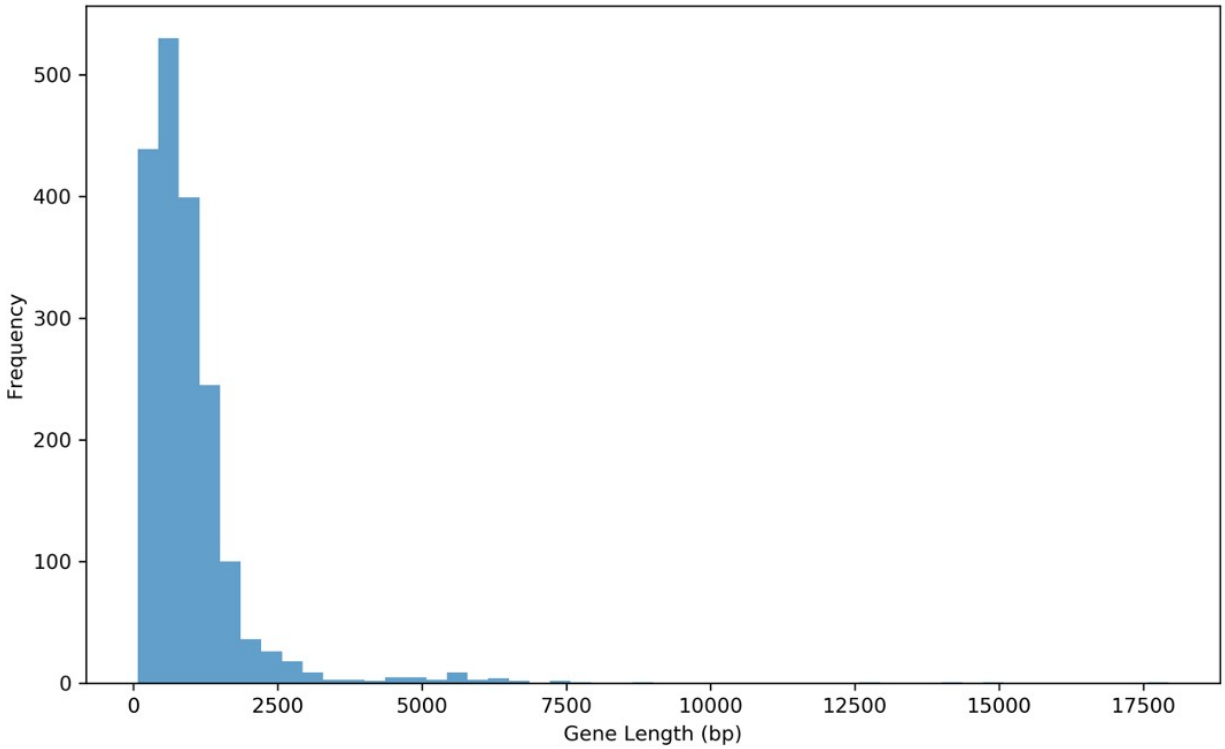

Supplementary Figure S1. Histogram of *M. intestini* G0370_i3 gene length.

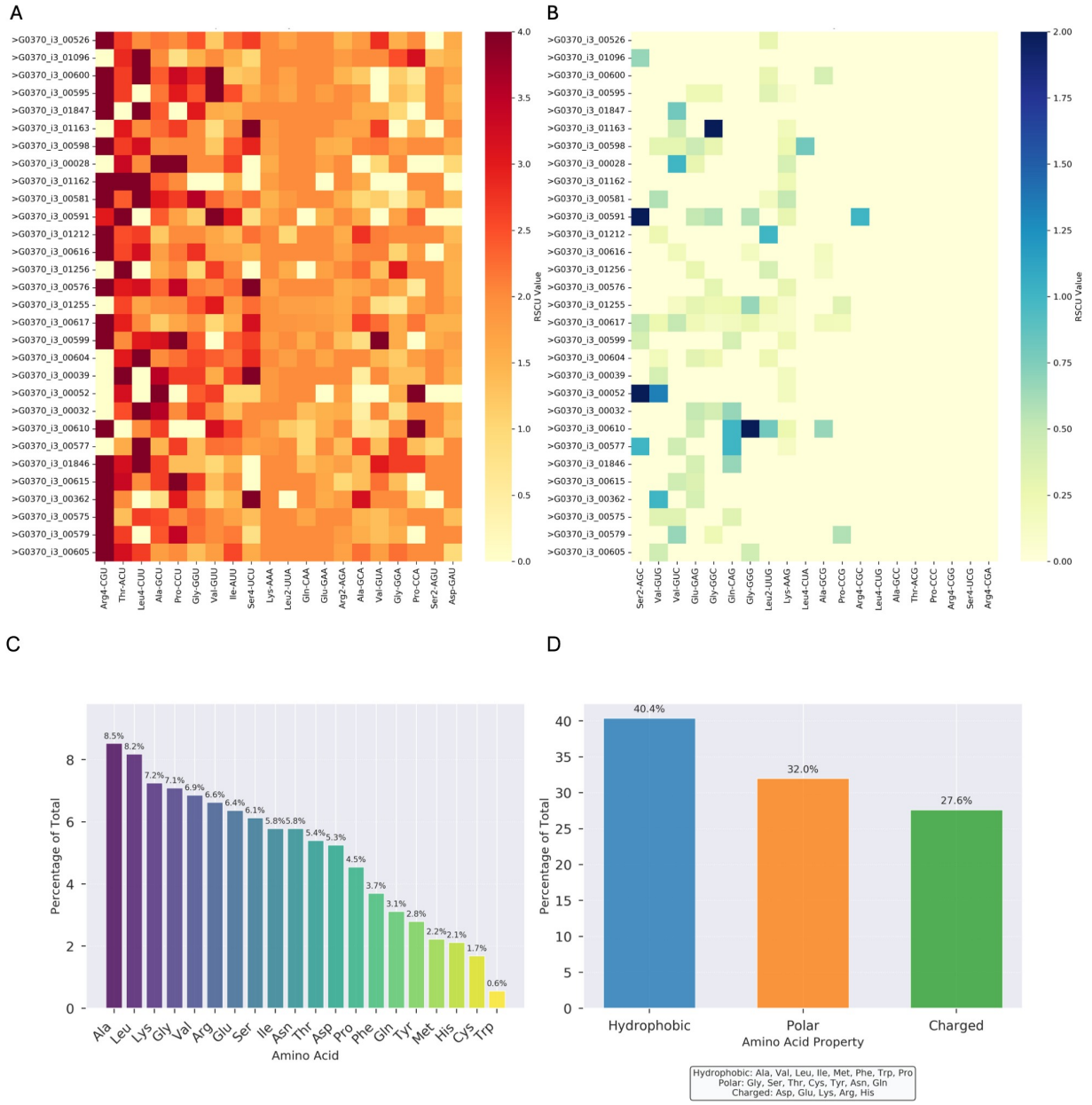

Supplementary Figure S2. (A) Heatmap of the top 20 codons according to their mean RSCU values for *M. intestini* G0370_i3 ribosomal proteins. Codons with usage values greater than 1 are considered to be over-represented (B) Heatmap of the bottom 20 codons according to their mean RSCU values for *M. intestini* G0370_i3 ribosomal proteins. (C) Bar plot of amino acid frequency for *M. intestini* G0370_i3 coding sequences. (D) Bar plot of amino acid types for *M. intestini* G0370_i3.

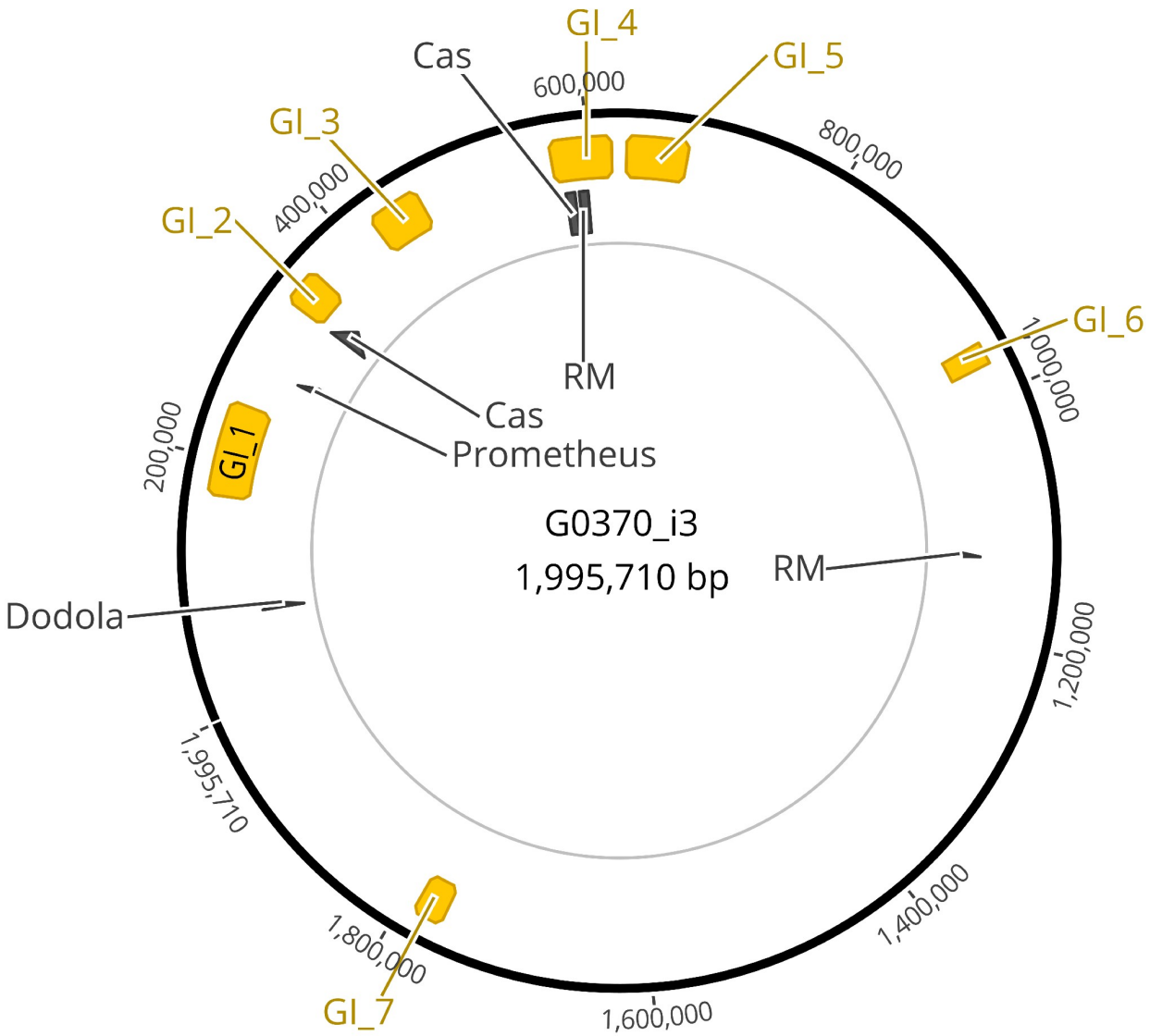

Supplementary Figure S3. Circular genome map for *M. intestini* G0370_i3 showing genomic islands and defense systems.

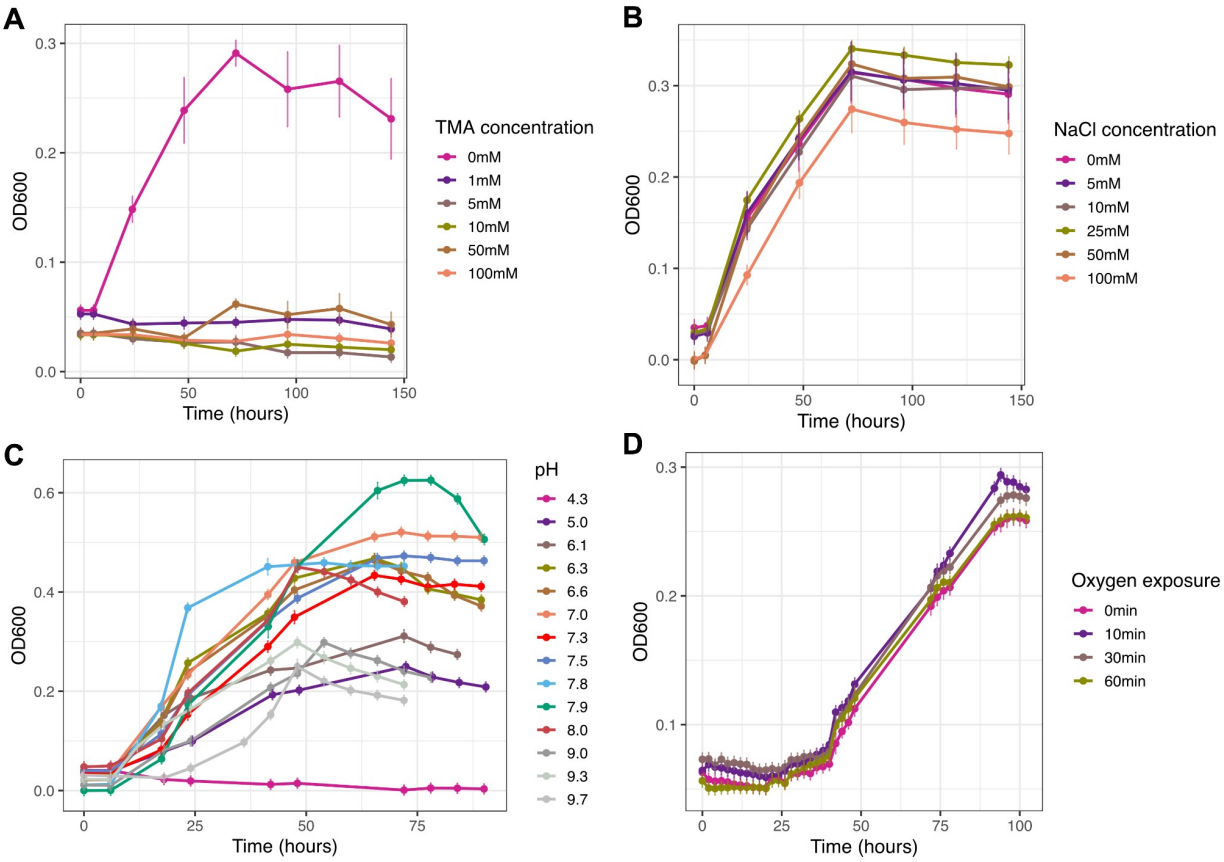

Supplementary Figure S4. Growth characteristics of *Methanobrevibacter* sp. G0370_i3 under different conditions. (A) Growth response to varying concentrations of trimethylamine (TMA) (1-100 mM). (B) Growth under different NaCl concentrations (5 – 100 mM). (C) Determination of optimal growth pH by culturing the strain across a pH range of 4.3 to 9.7. (D) Oxygen tolerance assay showing growth following exposure to atmospheric O_2 for 10–60 min. For all panels, points represent mean OD_{600} values (± SEM) from $n = 3$ technical replicates; error bars indicate SEM, and lines connect mean values over time.

Chapter 5: Strain-resolved metagenomics and phylogenomics of human gut *Methanobrevibacter* spp. reveals Africa–Eurasia biogeographic patterns

This chapter is adapted from a manuscript with the same title that is currently prepared for submission.

Only changes to formatting have been made; main figures and tables have been renumbered to ensure consistency with chapter organization.

Authors are listed in publication order:

Mirabeau M. Ngwese[1,2,3], Lara Berg[1], Jan Philipp Kisker[1], Hagay Enav[1], Inbal Paz[1], Alexander Tyakht[1], Stacey L. Heaver[1], Ayola A. Adegnika[2,3,4], Peter Kremsner[2,3,4,5], Nicholas D. Youngblut[1], Ruth E. Ley[1,5,*], and James W. Marsh[1*]

[1]Department of Microbiome Science, Max Planck Institute for Biology Tuebingen, Tuebingen, Germany

[2]Lambaréné Medical Research Centre (CERMEL), Lambaréné, Gabon

[3]Institute for Tropical Medicine, University of Tuebingen, Tuebingen, Germany

[4]German Centre for Infection Research (DZIF), Tuebingen, Germany

[5]Cluster of Excellence EXC 2124 Controlling Microbes to Fight Infections, University of Tuebingen, Tuebingen, Germany

*: Corresponding authors

Manuscript contributions: I contributed to the conceptualization and methodological design of the study together with N.D.Y, R.E.L, and J.W.M. I performed culturing, DNA extractions, and sequencing of all strains with L.B. and S.L., and carried out sequence processing and genome assembly of all isolates alongside N.D.Y. and J.W.M. I participated in sample collection and processing for the Gabonese dataset, and handled data curation. I conducted Kraken-based taxonomic profiling and formal analysis of the metagenomic datasets with A.V.T. and J.W.M., and performed strain comparisons and pangenomics together with H.E., I.P., and J.W.M. I co-wrote the original manuscript draft with N.D.Y., A.T., R.E.L., and J.W.M., generated visualisations in Figure 4.1, and contributed to Figures 4.2- 4.6, and 4.8, as well as Extended Data Figures 1, 2, and 4.

Running title: Genomic and metagenomic comparisons of *Methanobrevibacter smithii and M. intestini* species cultured from Gabon, Germany and Vietnam reveal species, strain, and biogeographic diversity

Key words: *Methanobrevibacter smithii*, *Methanobrevibacteir intestini*, human gut, methanogen, metagenomics, culturomics, microbiome, non-western microbiome

5.1. Abstract

Methanogenic archaea are key members of the human gut microbiome, yet their global diversity remains underexplored. To better understand the prevalence, abundance, phylogeny, and genomic features of the two predominant methanogen species in the human gut, *Methanobrevibacter smithii* and *Methanobrevibacter intestini*, we combined metagenomic surveys (904 gut microbiomes) with cultivation (209 stool samples yielding 200 methanogen isolates) from Germany, Gabon, and Vietnam. Both species were more prevalent and abundant in Gabon, the least industrialized location, and methanogen abundance correlated with higher bacterial diversity across all populations. Co-occurrence analyses indicated that *M. smithii* occurred either alone or alongside bacterial species enriched for acetogenesis pathways. In contrast, *M. intestini* was rarely found without *M. smithii*. Comparative genomics of cultivated strains revealed 892 novel protein clusters (1,303 proteins) that were largely derived from *M. intestini* genome assemblies isolated in Gabon, suggesting geographically restricted functional repertoires. Both methanogens showed higher genetic similarity within households and countries than between them, suggesting local transmission patterns and geographic population differentiation, with Gabon strains forming a particularly distinct genomic pool. Phylogenomic analysis revealed that both species maintain phylogenetic structures consistent with their geographic distribution and *M. smithii* showed evidence of co-diversification with its human host. *M. smithii* genomic divergence between populations stemmed from hypervariable hotspots containing host-interaction genes, suggesting local adaptation through accessory gene turnover rather than chromosomal rearrangements. Collectively, these results suggest that *M. smithii* and *M. intestini* exhibit geographic population structure, with patterns of genomic diversity consistent with household-level transmission and region-specific selective pressures acting on host-interaction genes.

5.2. Introduction

The human gut archaeome is taxonomically simple yet functionally consequential[1]. In healthy adults, methanogenic Euryarchaeota dominate archaeal communities, typically comprising 90–99% of archaeal sequences, whereas non-methanogenic archaea are detected only sporadically and at low abundance[2–4]. Across populations, gut methanogens exhibit a conserved higher-level taxonomic structure, with members of the order *Methanobacteriales*—particularly the family *Methanobacteriaceae*—predominating, and the genus *Methanobrevibacter* accounting for the majority of archaeal reads in archaeal-positive individuals. Within this framework, *Methanobrevibacter smithii* has emerged as the principal human-associated methanogen and the primary focus of functional, ecological, and evolutionary studies[1].

Evolutionary analyses have suggested a long-term association between *M. smithii* and its human host. Host–methanogen cophylogeny and the recovery of *M. smithii* genomes from ancient coprolites support a history of shared evolutionary trajectories[5,6]. Methanogens are often absent or present at very low abundance in early infancy and increase in prevalence later in life, with strong associations between parental and offspring methane production[7]. These observations imply that while vertical transmission[8] may contribute to long-term host association, household- and ecology-dependent processes play a major role in establishing methanogen colonization.

Methanogens occupy a specialized metabolic niche in the gut by consuming bacterial fermentation byproducts such as hydrogen, formate, and methanol, thereby sustaining fermentative flux and stabilizing short-chain fatty acid production[9–14]. Through these syntrophic interactions, methanogens integrate tightly into bacterial metabolic networks and exert system-level effects on gut metabolism. Experimental and metagenomic studies have shown that *M. smithii* engages in coordinated metabolic interactions with diverse bacterial taxa, including physical association with hydrogen-producing fermenters and co-occurrence with short-chain fatty acid–producing bacteria[15–17]. This central ecological role suggests that even limited variation in methanogen composition or strain biology could have disproportionate functional consequences.

Despite their apparent taxonomic simplicity, methanogen prevalence and abundance vary widely among human populations. Breath-methane surveys and sequencing studies reveal marked geographic differences, with methanogen carriage ranging from ~15% in some East Asian cohorts to >70% in certain rural African populations[7,18]. In Chinese cohorts, geography and urbanization explain a substantial fraction of variation in gut archaeal communities, with rural, higher-fibre

diets often linked to richer and more *Methanobrevibacter*-dominated archaeomes[16]. Host ancestry, familial background, diet, and age further modulate methanogen prevalence, indicating that methanogen colonization and persistence are shaped by multiple interacting factors rather than a single determinant[19–21]. However, the biological basis of this population-level variation—whether driven by differences in exposure, transmission, strain composition, or ecological adaptation—remains poorly understood.

Recent genomic analyses have further revealed previously unrecognized diversity within human-associated *Methanobrevibacter*. Sequences historically classified as *M. smithii* segregate into distinct phylogenetic clades, leading to the formal description of a closely related species, *Methanobrevibacter intestini*[21–24]. Across sampled cohorts, both species are widely distributed, although *M. intestini* typically occurs at lower prevalence and abundance, and in some populations the two species exhibit strong mutual exclusion[22,25,26]. The ecological and evolutionary significance of this species-level partitioning remains unresolved.

Comparative genomic and phenotypic studies indicate that *M. smithii* and *M. intestini* share a conserved hydrogenotrophic methanogenesis machinery but differ in accessory functions, including surface-associated proteins and extracellular vesicle composition[22,26,27]. Emerging evidence suggests that these differences may influence host–microbe interactions, as *M. intestini* vesicles elicit stronger inflammatory responses in intestinal epithelial models[28]. Whether such molecular distinctions translate into population-specific ecological strategies or in vivo functional divergence is unknown. More broadly, it is still unclear whether *M. smithii* and *M. intestini* occupy distinct ecological niches across human populations, whether they partner with different bacterial communities in vivo, and how species- and strain-level diversity within *Methanobrevibacter* feeds back onto host physiology.

Importantly, nearly all existing genomic and culture-based insights into human-associated methanogens derive from European or North American cohorts, which represent a small fraction of global human diversity[29,30]. Although recent large-scale microbiome initiatives have begun to address geographic sampling biases, these efforts have focused primarily on bacterial communities, leaving archaeal diversity comparatively underexplored[31,32]. As a result, the prevalence, strain-level structure, and ecological differentiation of *Methanobrevibacter* species across non-Western populations remain largely uncharacterized.

Together, these findings highlight three unresolved issues: how *Methanobrevibacter* species are distributed across diverse human populations, how their strain-level diversity is structured, and how this diversity relates to ecological interactions in the gut.

Here, we leverage a geographically diverse metagenomic and fecal sample collection spanning Gabon, Vietnam, and Germany[5] to characterize the prevalence, abundance, and co-occurrence patterns of *M. smithii* and *M. intestini*. We further developed a targeted enrichment and isolation strategy that yielded 200 human gut methanogen isolates, representing the largest culture collection assembled to date. By sequencing 91 representative strains and integrating phylogenetic, pangenomic, and lipidomic analyses, we delineate population-specific structure within dominant human gut methanogens and provide a framework for understanding how archaeal diversity and adaptation shape the human gut ecosystem.

5.3. Results

5.3.1. Metagenome analysis reveals *M. smithii* and *M. intestini* niche partitioning and geographic dominance patterns

We analysed 938 human fecal metagenomes, including 819 from our previously published dataset[5] and 119 newly generated for this study (Extended Data Fig. 1). Metagenomes were generated from previous collected fecal samples of adult women and their infants: Gabon (n = 197 adults, 156 infants), Vietnam (n = 197 adults, 156 infants) and Germany (n = 150 adults, 82 infants) (Fig. 5.1A). Within Gabon, samples originated from either Lambaréné (semi-urban; n = 251) or Ikobey (rural; n = 102). In Vietnam, samples originated from Hanoi (urban; n = 100), Hà Tĩnh (semi-rural; n = 96), or Sơn La (rural; n = 157), while samples collected in Germany originated from Tuebingen (urban; n = 232).

Prevalence patterns. We used the Genome Taxonomy Database (GTDB) for taxonomic classification, which classifies these species within the *Methanobrevibacter_A genus*[23]. In our metagenome analysis, *Methanobrevibacter_A* dominated in all three countries. For adults, *Methanobrevibacter_A* prevalence was largely consistent between populations, reaching 95.4 % in Gabon, 96.7 % in Germany, and 86.8 % in Vietnam (Extended Data Fig. 2A). Genus prevalence was slightly lower in infants, reaching 75.6 % in Gabon, 69.5 % in Germany and 66.7 % in Vietnam (Extended Data Fig. 2B). *Methanosphaera* was the second most prevalent genus among adults, and was detected in 35.5 % of samples from Gabon, 29.9 % of samples from Vietnam, and 16.7 % of samples from Germany. In infants, *Thermococcus* was the second-most prevalent genus,

detected in 24.4 % of samples in Gabon, 28.8 % in Vietnam, and 19.5 % in Germany (Extended Data Fig. 2B). Additional genera, including *Methanobrevibacter, Methanococcus*, *Methanobacterium*, *Methanobrevibacter_B*, and *Methanobrevibacter_C,* were detected in both adults and infants at consistently lower prevalences (~1-5 %) (Extended Data Fig. 2A-B). Infants harboured additional, rare genera that were absent from adults, including *CADBMS01*, *Methanocaldococcus*, *Methanothermococcus_A*, *UBA349*, and *Methanofastidiosum* (Extended Data Fig. 2B). The prevalences of these genera were all below 2.5 % (Supplementary Table 1), likely reflecting transient environmental acquisition rather than stable colonization[33].

Within the *Methanobrevibacter_A* genus, *M. smithii* and *M. intestini* were the dominant species overall and were detected in 54.7 % and 41.6 % of adults, and in 40.9 % and 16.0 % of infants, respectively (Fig. 5.1B-C, Extended Data Fig. 2C–D). Other *Methanobrevibacter_A* species were rare: *M. millerae_A* was scarcely present in adults from all three populations (2.0 %, 0.7 % and 2.0 % in Gabon, Germany and Vietnam, respectively) and in infants from Gabon and Vietnam (1.9 % and 1.2 %, respectively) (Extended Data Fig. 2C–D). *M. thaueri*, *M. woesei* and *M. oralis* appeared only in Gabonese (4.6 %, 4.1 %, 1.0 %) and Vietnamese (1.0 %, 1.0 %, 1.5 %) adults, while *M. gottschalkii* was detected exclusively in infants from Vietnam (0.6 %) and Gabon (1.2 %) (Extended Data Fig. 2C–D). Additional methanogen lineages were detected at lower prevalences: *Methanosphaera stadtmanae* and related taxa were detected in 27.4 % of Gabonese adults, 20.3 % of Vietnamese adults, and 6.1 % of German infants (Supplementary Table 1). *Methanobacterium formicicum* occurred sporadically (< 3 %) across all cohorts, while *Methanobrevibacter_A ruminantum_A* was more consistently observed, reaching 20.8 % in Gabonese adults (Supplementary Table 1).

Prevalences of *M. smithii* and *M. intestini* varied by country (Fig. 5.1B–C). *M. smithii* was the most common overall but occurred least often in Germany (31.3 %, 18.3 % of adults and infants, respectively), more frequently in Vietnam (42.6 % and 39.7 %), and most frequently in Gabon (75.1 % and 53.8 %). These differences were statistically significant for both adults (H = 74.6, adjusted p = 6.3e-17, BH-corrected) and in infants (H = 28.2, adjusted p = 1.5e-6, BH-corrected). *M. intestini* prevalences were lower in each country compared to *M. smithii* but showed a similar geographical gradient where its prevalence in Gabon (69.0 % and 26.3 %) was higher than Vietnam (23.3 % and 12.8 %), which was higher than Germany (20.0 % and 2.4 %). These

differences were also statistically significant in both adults (H = 117.8 adjusted p = 5.3e-26) and infants (H = 24.7, adjusted p = 4.4e-6; all BH-corrected).

We tested whether mother-infant pairs were more likely to share *M. smithii* and *M. intestini* colonization status than expected by chance. Using a permutation-based approach applied to presence-absence colonization data across each country cohort, we observed no statistically significant within-family associations (all $\varphi < 0.15$, adjusted $p > 0.5$). The highest concordance was observed for *M. intestini* in Gabon ($\varphi = 0.12$, adjusted $p = 0.54$), followed by *M. smithii* in Germany ($\varphi = 0.13$, adjusted $p = 0.54$), but neither deviated from random expectations. These findings indicate that, at the presence-absence level, mother-infant pairs do not exhibit greater concordance than expected by chance, suggesting that colonization by these species is shaped by shared environmental exposures or stochastic processes rather than by vertical transmission.

An additional taxon consistently appeared in our metagenomic profiles, provisionally named *Methanobrevibacter_A sp900766745* in GTDB release 202 and *Methanocatella sp900766745* in release 226 (Supplementary Table 1). Initial estimates suggested this taxon was highly prevalent and abundant, often exceeding *M. smithii*: in our adult samples it accounted for nearly half of all Methanobacteriota reads, while in some infant samples it reached 100 % prevalence. Country-level comparisons showed its substantial contributions to *Methanobrevibacter_A* reads in Gabon (~25 %), Germany (~67 %), and Vietnam (~52 %). However, upon validation by mapping the individual metagenomic reads to the representative *M. sp900766745* reference genome (GCA_902463315.1), most covered regions were unusually short (often < 20 bp) and the few longer regions (~600-700 bp) were classified as diverse gut bacteria rather than methanogens. This suggested that the reference assembly was highly chimeric; a conclusion supported by NCBI's suppression of this reference genome due to contamination concerns. To investigate further, we constructed a 16S rRNA phylogenetic tree that included representative species for all archaea that have previously been shown to be associated with the human gut[22], alongside three assemblies for the taxon in question (Extended Data Fig. 3). This tree indicated that, nevertheless, this taxon is likely to be a genuine, novel methanogen species. Yet, the corrupted reference assembly is causing misalignment of bacterial reads, leading to substantial overestimation of its true abundance. Consequently, we excluded this species from our analysis, and previous reports of this methanogen's prevalence and abundance should be interpreted with caution[34–36].

Relative abundance patterns. We next examined relative abundances of *M. smithii* and *M. intestini* in our samples. Benjamini–Hochberg–adjusted pairwise Wilcoxon rank-sum tests in adults showed that the median abundance of both species was higher in Gabon than in Vietnam (*M. smithii*: adjusted p = 1.08e-12; *M. intestini*: adjusted p = 1.49e-25) and Germany (*M. smithii*: adjusted p = 3.21e-15; *M. intestini*: adjusted p = 8.34e-20) (Fig. 5.1D-E). In addition, Vietnam had a higher median abundance than Germany for *M. smithii* (adjusted p = 4.79e-2), whereas the Vietnam–Germany comparison was not statistically significant for *M. intestini* (adjusted p = 0.76) (Fig. 5.1D–E). Similarly, in infants, median abundances were significantly higher in Gabon than in Vietnam (*M. smithii*: adjusted p = 4.32e-3; *M. intestini*: adjusted p = 7.47e-4) and Germany (*M. smithii*: adjusted p = 4.39e-7; *M. intestini*: adjusted p = 1.23e-5) (Fig. 5.1F-G). Between Vietnam and Germany, however, median *M. smithii* abundances were significantly higher in Vietnam for both species in infants (*M. smithii*: adjusted p = 1.56e-3; *M. intestini*: adjusted p = 8.49e-3) (Fig. 5.1F–G). As expected, when comparing adults and infants, median abundances were significantly higher in adults for both methanogen species (Extended Data Fig. 2E-F).

To explore finer-scale geographic variation, we compared median abundances between rural (Ikobey) and semi-urban (Lambaréné) Gabonese sites (Fig. 5.1H-K). *M. smithii* abundances did not significantly differ between Ikobey and Lambaréné for both adults and infants (Fig. 5.1H-I). In contrast, *M. intestini* was significantly more abundant in rural Ikobey than in semi-urban Lambaréné for both adults (Wilcoxon rank-sum test, BH-adjusted p = 0.0004) and infants (Wilcoxon rank-sum test, BH-adjusted p = 8.75e-11) (Fig. 5.1J-K). Similar to the country-level comparisons, median abundances were significantly higher for adults compared to infants for both species (Extended Data Fig. 2G-H). Although significant, these urban-rural differences in Gabon were far smaller than the between-country contrasts. No significant within-country differences were observed between the three Vietnamese sampling sites (Hanoi, Hà Tĩnh, and Sơn La). For both *M. smithii* and *M. intestini*, median relative abundances were uniformly low for each location ($\leq$ 0.001 %), and pairwise comparisons yielded no significant differences after FDR correction (adjusted $p > 0.6$ for adults; adjusted $p > 0.05$ for infants).

Methanogen abundance is positively correlated with microbiome diversity.

Next, we tested whether *M. smithii* and *M. intestini* abundance correlated with microbiome diversity. The Shannon Diversity Index (SDI) for whole microbiomes varied by location and age (Fig. 5.1L-M), broadly tracking the methanogen relative abundance gradients we observed

between countries. Gabonese adults exhibited significantly higher microbiome diversity according to median SDI compared to Vietnam and Germany (pairwise Wilcoxon test with BH correction: Gabon vs. Germany, adjusted p = 2.1e-11; Gabon vs. Vietnam, adjusted p < 2.22e-16) (Fig. 5.1L). This difference was also consistent for other alpha-diversity metrics (Faith's phylogenetic diversity and observed richness; all adjusted p < 5e-04) (Extended Data Fig. 4A-B). Germany showed significantly higher median SDI compared to Vietnam (adjusted p = 0.0062) (Fig. 5.1L), but this comparison was not significant for Faith's PD (adjusted p = 0.68) and observed richness (adjusted p = 0.41) metrics (Extended Data Fig. 4A-B).

For infants, microbiome median SDI was significantly higher in Gabonese infants compared to both German and Vietnamese infants (Gabon vs. Germany, adjusted p = 2.9e-10; Gabon vs. Vietnam, adjusted p = 1.7e-13), while differences between Germany and Vietnam were not significant (adjusted p = 0.9; all BH-corrected; Fig. 5.1M). This was consistent for Faith's PD (Gabon vs. Germany, adjusted p = 5.9e-10; Gabon vs. Vietnam, adjusted p = 2.8e-05) and observed richness (Gabon vs. Germany, adjusted p = 1.6e-11, Gabon vs. Vietnam, adjusted p = 7.2e-06) (Extended Data Fig. 4C-D). Additionally, Vietnam showed significantly higher Faith's PD (adjusted p = 0.021) and observed richness (adjusted p = 0.0051) compared to Germany (Extended Data Fig. 4C-D).

We then investigated whether microbiome alpha-diversity tracked with methanogen abundance, as has been previously reported[37]. Linear regression analysis confirmed that the relative abundance of both *M. smithii* and *M. intestini* was positively associated with SDI, while sampling location also contributed significantly (*M. smithii*: p = 0.002; *M. intestini*: p = 0.001; Supplementary Table 2). When stratifying by age group, higher methanogen abundance in adults remained strongly associated with higher SDI (*M. smithii*: p = 0.004; *M. intestini*: p = 0.002), whereas age had a minimal effect and did not improve model fit (likelihood ratio test, p > 0.1). In infants, by contrast, methanogen relative abundance was not significantly associated with SDI.

M. smithii and *M. intestini* co-occur and bacterial co-associations suggest metabolic interdependencies.

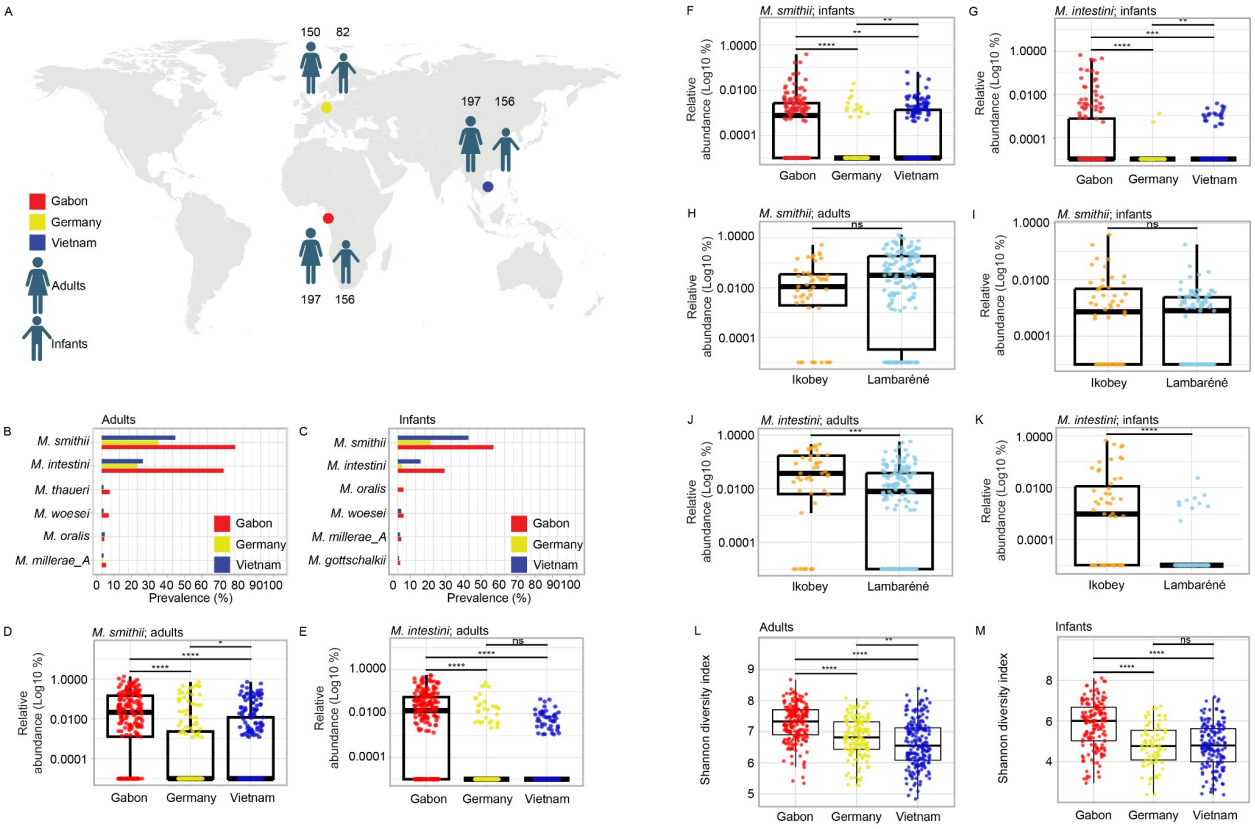

Figure 5.1: Prevalence and abundance of *M. smithii* and *M. intestini* across human populations in Gabon, Germany, and Vietnam.
A. Geographic location of sampling sites in Gabon (red), Germany (yellow), and Vietnam (blue). Icons indicate the numbers of adult and infant metagenomic samples collected at each site. **B**. Prevalence of *Methanobrevibacter_A* spp. in adult gut metagenomes by country (n = 544). **C**. Prevalence of *Methanobrevibacter_A* spp. in infant gut metagenomes by country (n = 394). Only species with a prevalence ≥ 0.1% are shown in **B** and **C** (red: Gabon; yellow: Germany; blue: Vietnam). **D–G**. Relative abundances of *M. smithii* (**D, F**) and *M. intestini* (**E, G**) in adults (**D, E**) and infants (**F, G**) by country. **H–K**. Relative abundances of *M. smithii* (**H, I**) and *M. intestini* (**J, K**) in adults (**H, J**) and infants (**I, K**) from the two Gabonese populations: Ikobey (rural, orange) and Lambaréné (semi-urban, sky blue). **L–M**. Shannon alpha diversity in adults (**L**) and infants (**M**) by population. Relative abundances are expressed as percentages on a log10 scale following the addition of a pseudo-count of 1×10^{-7} to preserve zeros. Taxonomic classification was performed using Kraken2, and statistical comparisons were made using the Wilcoxon test (**** $p < 0.001$, *** $p < 0.01$, ** $p < 0.05$).

Co-occurrence patterns for M. smithii and M. intestini. In adults, both species frequently co-occurred across all three populations, with the highest proportion of samples where both were observed in Gabon (*n* = 134; 89.4 %), followed by Germany (*n* = 29; 60.4 %) and Vietnam (*n* = 84; 54.8 %) (Fig. 5.2A). These co-occurrences were statistically significant, with odds ratios (ORs)

of 224.9 in Gabon (95 % CI: 49.3-1026.8, adjusted p < 2.33e-29), 164.3 in Germany (95 % CI: 21.0-1283.5, adjusted p < 6.39e-18), and 274.2 in Vietnam (95 % CI: 16.5-4556.4, adjusted p < 3.88e-19), and strong effect sizes as indicated by phi coefficients (φ) ranging from 0.64 to 0.81 (Fig. 5.2B). When only considering samples in which both species co-occurred, the relative abundances of both methanogens were also positively correlated, although the strength of correlation varied by country: Gabon (Spearman's ρ = 0.16, adjusted p = 0.086), Germany (ρ = 0.10, adjusted p = 0.62), and Vietnam (ρ = 0.92, adjusted p < 1e-28; BH-corrected). When both species co-occurred, *M. smithii* was significantly more likely to be the dominant methanogen, with dominance ORs of 2.1 in Gabon (95 % CI: 1.5-3.0) and 3.1 in Germany (95 % CI: 1.3-7.4), while in Vietnam *M. smithii* was exclusively dominant in all 46 co-occurrence cases (OR = 93, 95 % CI: 5.7-1509.1) (Fig. 5.2C).

In contrast, infant populations demonstrated weaker co-occurrence associations, a lower proportion of samples containing both species were observed (Gabon: n = 91, 37.32 %; Germany: n = 16, 6.2 %, Vietnam: n = 65, 26.2 %) (Fig. 5.2D). These associations were statistically significant for Gabon (OR = 6.3, adjusted p < 2.04e-5) and Vietnam (OR = 11.5, adjusted p < 2.04e-5), while German infants showed no significant association between methanogen species (adjusted p = 0.24) (Fig. 5.2E). The relative abundances of both methanogens were positively correlated for the Gabon samples (ρ = 0.55, adjusted p = 0.0019), while no significant association was detected in Vietnamese infants (ρ = 0.38, adjusted p = 0.14; BH-corrected). In German infants, correlations could not be estimated due to an insufficient number of samples with co-occurring species (n = 1). Species dominance patterns also differed in infants compared to adults, where 22/34 (64.7 %) co-occurrence cases showed *M. intestini* as the dominant methanogen in Gabonese infants (OR = 0.55, 95 % CI: 0.27-1.10), while *M. smithii* remained dominant in Vietnamese infants, similar to what was observed for adults (OR = 3.25, 95 % CI: 1.1-9.97) (Fig. 5.2F).

Together, these results suggest an age-dependent ecological coupling, where *M. smithii* and *M. intestini* are almost always found together in adults, while they co-occur less often in infants but still more than expected. Whenever both methanogens co-occur, adults generally favour *M. smithii*, but infants trend toward *M. intestini* dominance, especially in Gabon.

Co-occurrences with bacterial taxa and functions. We identified microbial taxa whose relative abundances were significantly correlated with each methanogen species (Kendall's τ; FDR < 0.05). We observed that *M. smithii* was positively associated with four bacterial species:

UMGS75 sp900538885 (phylum Bacillota, family CAG-313), *Blautia_A sp900547615* (phylum Bacillota, family Lachnospiraceae), *Blautia_A luti* (phylum Bacillota, family Lachnospiraceae), and *RUG410 sp900553115* (phylum Pseudomonadota, family CAG-239) (Fig. 5.2G). A positive association between *M. smithii* and *UMGS75 sp900538885* has been previously reported[25]. Additional positive associations with Christensenellaceae were observed, but these did not pass our filtering thresholds indicating that Christensenellaceae–methanogen interactions may be context-dependent and comparatively subtle in these populations. Species negatively correlated with *M. smithii* were *CAG-1024 sp000432015* (phylum Bacillota, family Clostridiaceae), *Eubacterium_G sp902766735* (phylum Bacillota, family Lachnospiraceae), *PeH17 sp000435055* (phylum Bacillota, family Clostridiaceae), *CAG-448 sp003150135* (phylum Bacillota, family Oscillospiraceae), *Phil1 sp001940855* (phylum Bacillota, family Christensenellaceae), *Amulumruptor sp900547825* (phylum Bacteroidota, family Porphyromonadaceae) (Fig. 5.2G).

Only four taxa: *M. smithii* itself and three uncultured bacterial species (*UBA9502 sp003506385* (phylum Bacillota, family Lachnospiraceae), *UMGS1668 sp004556975* (phylum Bacillota, family Ruminococcaceae), and *RUG410 sp900553115* (phylum Pseudomonadota, family CAG-239) showed positive associations with *M. intestini* (Fig. 5.2H). Negatively associated taxa with *M. intestini* included *UMGS1889 sp900556055* (phylum Bacillota, family Oscillospiraceae), *CAG-452 sp000434035* (phylum Bacillota, family Clostridiaceae), *CAG-272 sp000433515* (phylum Bacteroidota, family unclassified), *Holdemania massiliensis* (phylum Bacillota, family Erysipelotrichaceae), *Dysosmobacter sp900770295* (phylum Bacillota, family Oscillospiraceae), *Faecalibacterium prausnitzii* (phylum Bacillota, family Oscillospiraceae), *UBA737 sp002451855* (phylum Bacillota, family Oscillospiraceae), and *RUG472 sp900545265* (phylum Bacillota, family unclassified) (Fig. 5.2H).

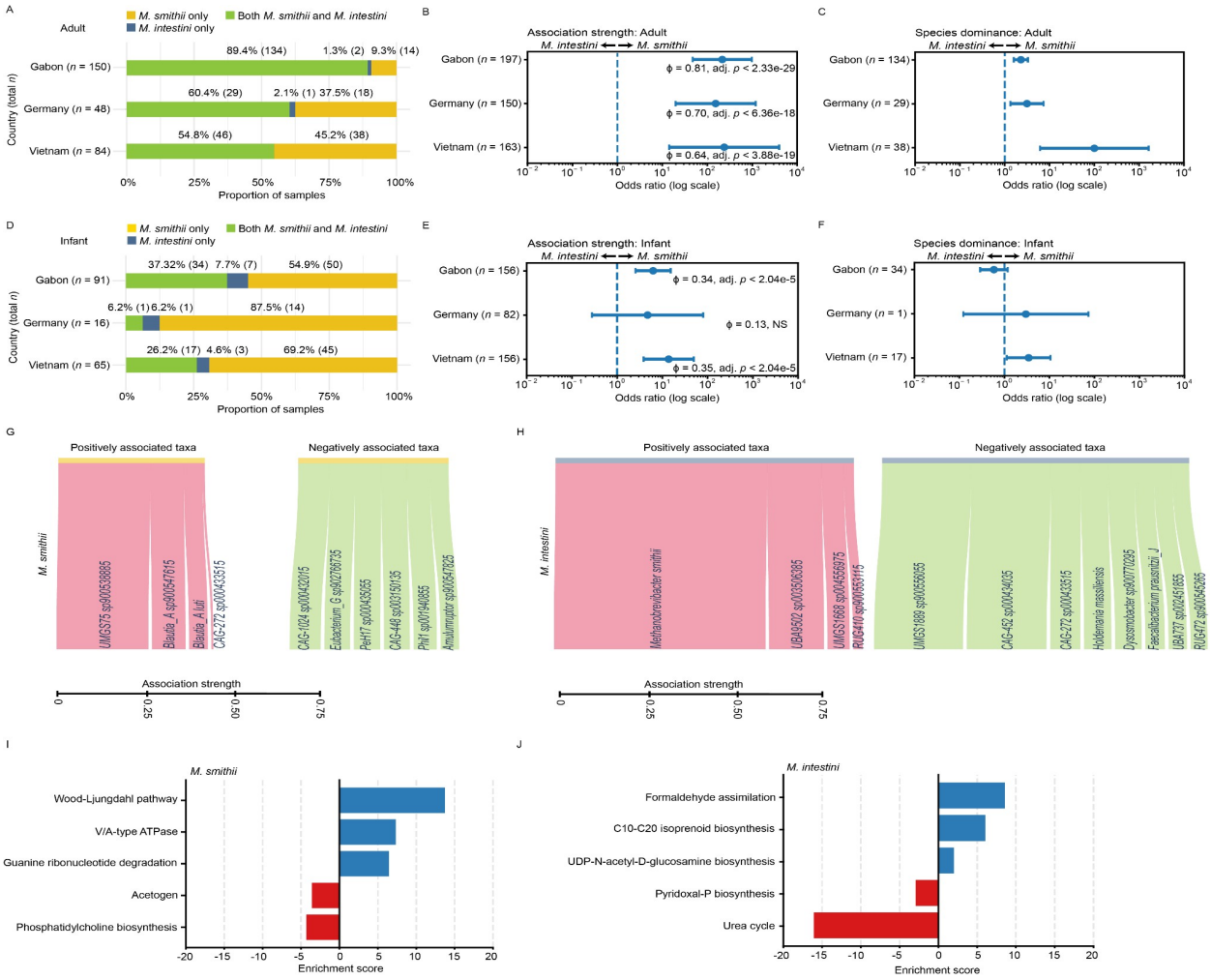

Figure 5.2: Methanogen-methanogen and methanogen-bacteria co-occurrence patterns. **A.** Occurrence and co-occurrence of *M. smithii* and *M. intestini* in adult samples from Gabon, Germany, and Vietnam. Horizontal stacked bars show samples positive for only *M. smithii*, only *M. intestini*, or both taxa; percentages and counts are indicated. Sample sizes (n) refer to methanogen-positive samples. **B.** Strength of *M. smithii–M. intestini* co-occurrence in adults, shown as odds ratios (ORs) with 95% confidence intervals (CIs) on a log scale; the dashed line indicates no association (OR = 1). φ coefficients and Benjamini–Hochberg (BH)-adjusted P values are shown. Sample sizes refer to all samples per country. **C.** Dominance of *M. smithii* versus *M. intestini* among co-occurring adult samples (OR > 1 indicates *M. smithii* dominance; OR < 1 indicates *M. intestini* dominance). **D–F.** Corresponding analyses for infant samples: occurrence and co-occurrence (**D**), co-occurrence strength (**E**), and species dominance (**F**). Bar colours, sample-size definitions, and statistical annotations are as described for panels **A–C**. **G–H.** Significant positive and negative intra- and inter-domain associations for *M. smithii* (**G**) and *M. intestini* (**H**), inferred using SPIEC-EASI from Kraken2-derived taxonomic profiles; bacterial taxa were filtered to a prevalence ≥20%. **I–J.** Enrichment of metabolic functions among bacterial and archaeal taxa associated with *M. smithii* (**I**) and *M. intestini* (**J**). Bars represent Rao test statistics from logistic regression models; blue and red indicate positive and negative enrichment, respectively.

Functional enrichment of the combined genomes from taxa indicated positively associated with *M. smithii* showed an overrepresentation of genes encoding the Wood–Ljungdahl (acetyl-CoA) pathway, V/A-type ATPases, and guanine ribonucleotide degradation functions (Fig. 5.2I), indicating the genetic capability for acetogenesis from $H_2 + CO_2$, which may reflect competition for these substrates. However, both *M. smithii* and *M. intestini* contain genes for acetate assimilation, and previous culture experiments have demonstrated that *M. smithii* can utilize acetate for growth[38], suggesting a balance between $H_2 + CO_2$ competition and acetate cross-feeding. The negatively associated taxa were enriched for acetogenic taxa (Fig. 5.2I), as previously reported in adult cohorts[21], supporting a competition dynamic.

The collective gene set of the organisms positively associated with *M. intestini* was significantly enriched for ribulose-monophosphate, isoprenoid biosynthesis, and UDP-N-acetyl-D-glucosamine (FDR < 0.01) (Fig. 5.2J). These pathways are functionally related to formaldehyde assimilation, membrane construction, and glycosylation and cell signaling[39–41]. Alternatively, negatively associated taxa were enriched for urea-cycle–related functions and pyridoxal-5-phosphate (PLP; vitamin B_6) biosynthesis[42] (FDR < 0.01) (Fig. 5.2J).

5.3.2. A culture and sequence collection of *M. smithii* and *M. intestini* strains from Gabon, Vietnam, and Germany.

We next established a strain and sequence collection to enable in-depth genetic and phylogenetic analyses of these methanogens. We selected 193 adult samples and 16 infant samples for enrichment based on sample availability and quantity (n = 209). Of these, 36 were from Germany, 97 from Vietnam, and 76 from Gabon (61 from adults and 15 from infants; Table 3). For infants, samples were selected predominantly from the rural Ikobey region in Gabon, especially as *M. intestini* was more prevalent here based on metagenomic profiling. This infant subset included seven infants whose mothers were also included in the adult stool enrichment dataset, as well as two additional family sets: one composed of two siblings and their mother, and another composed of three siblings and their mother.

Table 3: Summary of cultured strains and assembled genomes before and after dereplication (ANI = 99.99) across sampling locations.

		Gabon	Germany	Vietnam	Total
Stool enrichments	Total	76	36	97	209
	infant	15	1	0	16
Methanogen positive samples	Total	54	13	37	104
	infant	14	0	0	14
	Unique (Post dereplication; adults)	43	12	33	88
	Unique (Post dereplication; infant)	5	0	0	5
Isolation rate (%)		71	36	38	49
Methanogen strains	Total	99	38	63	200
	Unique (Post dereplication)	46	12	33	91
M. smithii	Total	54	30	59	143
	infant	2	0	0	2
	Unique (Post dereplication; adults)	23	9	29	52
	Unique (Post dereplication; infant)	2	0	0	2
M. intestini	Total	45	8	0	53
	infant	12	0	0	12
	Unique (Post dereplication; adults)	23	3	0	26
	Unique (Post dereplication; infant)	3	0	0	3
M. oralis	Total	0	0	4	4
	infant	0	0	0	0

	Unique (Post dereplication; adults)	0	0	4	4
	Unique (Post dereplication; infant)	0	0	0	0

We developed a strategy to efficiently enrich and isolate methanogens from stool (Fig. 5.3A; Extended Data Fig. 1). The 209 samples were serially diluted in a rich medium supplemented with an antimicrobial cocktail and H_2/CO_2 (80:20; v/v), which were monitored for methane production (see Materials and Methods). Methane-positive cultures were spread onto solid media and screened for coenzyme F_{420} auto-fluorescence; fluorescent colonies were sub-cultured to isolate clonal populations (Fig. 5.3A). In total, 200 putative methanogens were clonally isolated from 104 stool samples (of 209; 49.7 %). Isolation success differed significantly by region (H = 16.19, H = 2, p = 0.0003), with Gabon yielding the highest recovery rate (n = 54/76, 71.1 %, 95 % CI: 59.5–80.9 %), followed by Vietnam (n = 37/97, 38.1 %, 95 % CI: 29–49 %), and Germany (n = 13/36, 36.1 %, 95 % CI: 22-52 %). Gabon's isolation rate was significantly higher than both Germany (adjusted p = 0.0006) and Vietnam (adjusted p = 0.0075), while the difference between Germany and Vietnam was not significant (adjusted p = 0.1588).

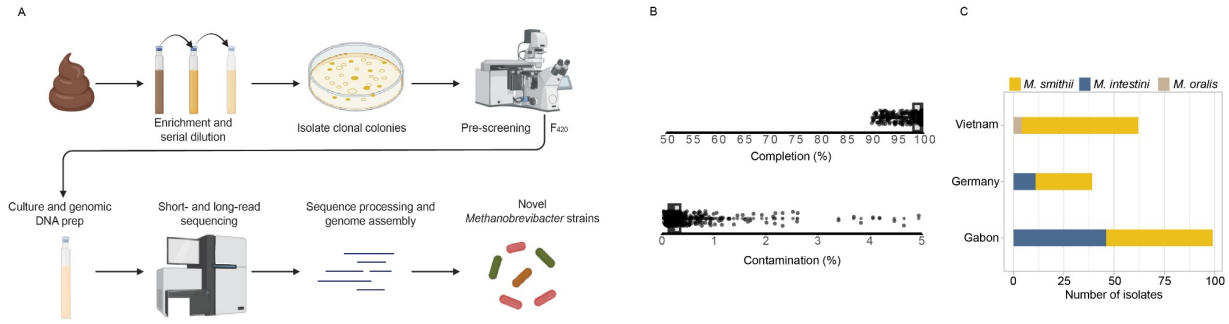

Figure 5.3: Targeted enrichment, isolation, and sequencing of human-associated methanogens.
A. Overview of the enrichment and isolation workflow for methanogens from human stool samples. Stool suspensions were serially diluted in selective medium containing antibiotics and an antifungal under an H_2/CO_2 atmosphere. Putative methanogens were identified by methane production and F_{420} fluorescence, cultured, and subjected to DNA extraction followed by short- and long-read sequencing. **B.** Quality metrics of cultured methanogen genome assemblies showing completeness and contamination estimates; all genomes were ≥90% complete and <5% contaminated. **C.** Numbers of cultured strains of *M. smithii* (yellow), *M. intestini* (blue), and *M. oralis* (beige) recovered from Gabon, Germany, and Vietnam.

DNA from all 200 putative methanogens was extracted and shotgun-sequenced. Genome assemblies showed a completeness level of 90 % or higher and a contamination level of 5 % or lower (Fig. 5.3B). Taxonomic profiling of the genome assemblies revealed *M. smithii* as the dominant species isolated from all three countries (n = 140; 70 %), followed by *M. intestini* (n = 56; 28 %) and *Methanobrevibacter oralis* (n = 4, 2 %) (Fig. 5.3C). Species distributions were strongly associated with geographic origin (H = 39.74, H = 4, $p < 0.001$): *M. smithii* dominated among isolates from Vietnam (98.3 %), with significant overrepresentation (standardized residual = 5.50) compared to Gabon (53.5 %) and Germany (76.9 %). In contrast, we did not isolate *M. intestini* from Vietnamese samples; *M. intestini* was significantly overrepresented in isolates from Gabon (84.9 %, standardized residual = 5.84); only 15.1 % of *M. intestini* isolates were derived from the samples from Germany. This regional specificity was statistically significant ($p = 0.015$), with the odds of isolating *M. intestini* from Gabon being 3.05 times higher than from Germany (95 % CI: 1.32–7.81).

5.3.3. Human population history shapes the phylogeny of *M. smithii*

After clustering genomes at 99.99 % ANI to retain only unique strains, 91 high-quality genome assemblies remained (*M. smithii*: n = 61, *M. intestini*: n = 26, *M. oralis*: n = 4; Supplementary Table 3). The four *M. oralis* genome assemblies were excluded from further analysis, resulting in a final set of 87 genomes. To assess the phylogenetic structure of these species, we inferred a maximum-likelihood phylogeny from an alignment of conserved, core genes predicted to be under neutral selection. This included all *M. smithii* and *M. intestini* assemblies in our dataset, the corresponding type strains (ATCC 35061 and WWM1085), and additional publicly available genomes[25]. The resulting phylogeny produced two maximally supported monophyletic clades (96-98 % bootstrap support, 1000 replicates) differentiating *M. smithii* from *M. intestini* lineages and corroborating previous phylogenetic findings that *M. intestini* represents a distinct species within the *Methanobrevibacter_A* genus[22] (Fig. 5.4A).

Within the *M. smithii* clade, long internal branches and multiple well-supported sublineages suggested deeper population structure and greater strain diversity compared to *M. intestini* (Fig. 5.4A). The comparatively shorter internal branches observed for *M. intestini* potentially imply more recent diversification (> 95 % bootstrap support at major nodes). Both species harboured phylogenetically distinct sublineages that corresponded to geographic origin.

Within *M. smithii*, strains from Vietnam formed a cohesive, well-supported subclade, suggesting possible regional transmission chains or founder effects in this population. Similarly, most strains from Gabon formed a single subclade (n = 18), while the remaining Gabonese strains (n = 4) occupied a smaller, more distinct subclade. In contrast, the *M. intestini* clade was dominated by Gabonese isolates, which formed well-supported subclades that were phylogenetically distinct from a separate subclade composed primarily of German/Austrian strains (and the USA type strain) (Fig. 5.4A).

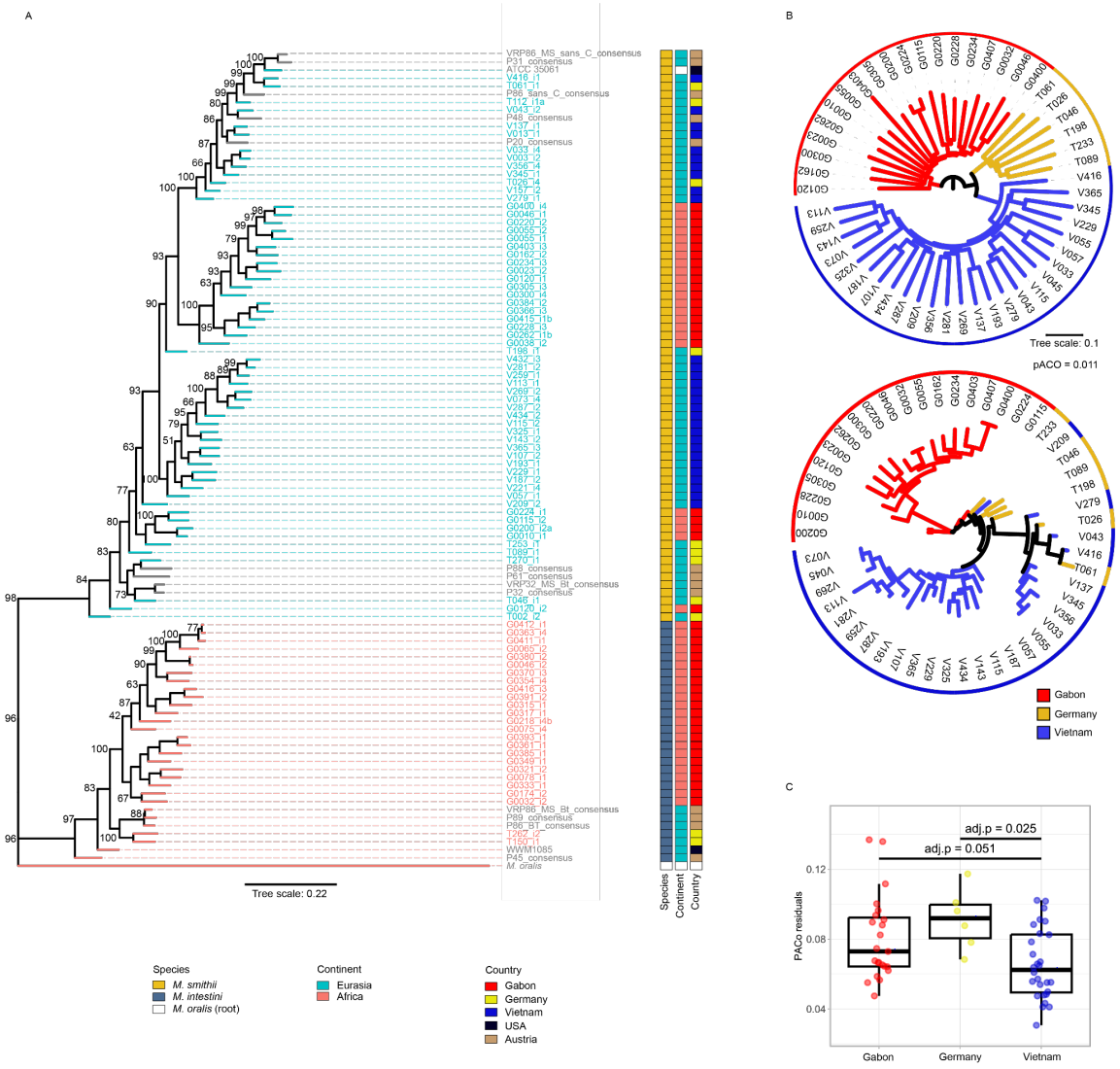

Figure 5.4: Phylogenetic differentiation of *M. smithii* and *M. intestini* lineages and host-associated cophylogeny of *M. smithii*.

A. Phylogenetic tree of *M. smithii* and *M. intestini* genomes, including the type strains *M. smithii* ATCC35061 and *M. intestini* WWM1085, rooted with *M. oralis*. Branch lengths were square-root

transformed and rescaled to a total tree height of 1 (scale bar indicates transformed distance units). Tip labels and terminal branches are colour-coded by species, with genomes from this study shown in light blue (*M. smithii*) and salmon (*M. intestini*), and publicly available genomes in grey. Internal node labels indicate bootstrap support. Outer annotation rings denote species (*M. smithii*: dark yellow, *M. intestini*: dark blue, *M. oralis*: white), continent of origin (Eurasia: light blue; Africa: salmon), and country of origin (Gabon: red, Germany: yellow, Vietnam: blue, USA: black, Austria: brown). **B.** Host–microbe cophylogeny analysis using the Procrustean Approach to Cophylogeny (PACo). The upper tree represents human host genotypes (~33,000 SNPs) and the lower tree the *M. smithii* phylogeny based on 202 single-copy core genes. Both midpoint-rooted trees include matched host–microbe pairs (n = 51) from Gabon, Germany, and Vietnam. Nodes are labelled by individual IDs and strain names and coloured by country. The global PACo fit and permutation-based P value are indicated. **C.** PACo residuals grouped by country. Statistical comparisons were performed using the Kruskal–Wallis test with multiple-testing correction; adjusted P values are shown.

We then investigated evidence for cophylogeny between both *M. smithii* and *M. intestini* and their hosts. For this analysis, we applied the Procrustean Approach to Cophylogeny (PACo) to compare a previously obtained host phylogeny that was constructed from ~33,000 SNPs[5] with an *M. smithii* phylogeny based on 202 single-copy core genes. Each *M. smithii* strain was isolated from the stool of a genotyped individual (n = 51), which allowed us to analyse matched host-microbe pairs from Gabon, Germany, and Vietnam. PACo revealed a significant global fit between the host and *M. smithii* phylogenies (Procrustes $m^2 = 0.3442$, permutation $p < 0.001$), indicating overall congruence in phylogenies (Fig. 5.4B). To evaluate whether the strength of this congruence differed across populations, we compared PACo residuals between the three countries (lower values indicate stronger congruence). Residuals differed significantly by country (Kruskal–Wallis $H = 9.04$, d.f. = 2, $p = 0.011$; Fig. 5.4C). Given the limited phylogenetic depth of the German samples, country-level pairwise inference was restricted to Vietnam and Gabon. In this comparison, residuals were significantly higher in Gabon than in Vietnam (Wilcoxon rank-sum test, adjusted $p = 0.028$), indicating stronger host–microbe phylogenetic congruence in the Vietnamese cohort. German samples are shown for completeness but were excluded from pairwise statistical testing.

Compared to *M. smithii*, the number of *M. intestini* strains with host genomic data was small: the vast majority were from Gabon (n = 22), with none from Vietnam and only a few from Germany. Of these, only 15 Gabonese strains had corresponding human SNP data, so all analyses were restricted to Gabon. PACo analysis revealed significant global congruence between host and

M. intestini phylogenies (Procrustes $m^2 = 0.379$, permutation $p = 0.003$), with generally low residuals (median = 0.142, interquartile range = 0.112–0.162), indicating a strong overall fit.

5.3.4. *M. smithii* and *M. intestini* are genetically distinct, and geography structures strain level diversity.

Comparison of the genomes in our dataset revealed distinct genetic differences between *M. smithii* and *M. intestini*. The genomes of *M. smithii* were significantly smaller (mean: 1.81 ± 0.04 Mbp, range: 1.68-1.89 Mbp) compared to those of *M. intestini* (mean: 2.03 ± 0.08 Mbp, range: 1.92-2.36 Mbp; adjusted $p < 0.001$; Fig. 5.5A). This was reflected in differences in gene content, where *M. intestini* isolates harboured a greater number of coding genes (mean: 1917 ± 85.93 vs. 1769.64 ± 39.00, adjusted $p < 0.001$; Fig. 5.5B), and these coding genes were, on average, longer than those found in *M. smithii* (946.74 ± 22.70 bp vs. 909.24 ± 18.10 bp, adjusted $p < 0.001$; Fig. 5.5C). Despite this expansion, *M. intestini* exhibited a significantly lower coding density (the proportion of its genome that encodes proteins) (0.9 vs. 0.88, adjusted $p = 0.013$; Fig. 5.5D), which may indicate increased regulatory complexity within this species.

M. smithii had a lower median percentage of hypothetical proteins compared to *M. intestini* (Fig. 5.5E) and the total number of coding sequences and the number of hypothetical proteins for both groups (Fig. 5.5F), suggesting that the proportion of proteins with unknown functions remains relatively constant for each species. Furthermore, both *M. smithii* and *M. intestini* possessed AT-rich genomes, with *M. smithii* showing a significantly higher GC content (31 %) compared to *M. intestini* (30 %) (Fig. 5.5G; Supplementary Table 3). Their amino acid usage patterns were similar, and both species preferentially use AT-rich codons, correlating with their low GC content (Supplementary Table 4). Both *M. smithii* and *M. intestini* genome sizes differed according to geography, with African isolates possessing significantly larger genomes than their Eurasian counterparts (2.03 ± 0.04 Mbp vs. 1.86 ± 0.04 Mbp, $p < 0.001$; Fig. 5.5H-I; Supplementary Table 3). This implies that African isolates may possess a broader functional repertoire, while Eurasian isolates may be more functionally streamlined.

To determine the novelty of the genes in our isolate catalogue, we collected publicly available, high-quality methanogen MAGs (560 *M. smithii* and *M. intestini* assemblies with > 90 % completeness, < 5 % contamination; Supplementary Table 5) and clustered the combined amino acid sequences for both datasets. We identified 1,303 novel proteins corresponding to 909 protein clusters in our collection that are absent from existing *M. smithii* and *M. intestini* assemblies (Fig.

5.5J). Of these clusters, 675 (74.3 %) were exclusive to methanogens isolated from Gabon samples and 530 (58.3 %) were specifically associated with *M. intestini* (Fig. 5.5J).

Notably, all *M. intestini* isolates from Gabon included novel gene clusters, while none were associated with the two *M. intestini* isolates from Germany. Together this indicates that (1) our isolate catalogue has captured significant undiscovered methanogen functional repertoires; (2) methanogen gene content might be linked to geography; and (3) *M. intestini* is currently under-represented in existing reference databases. Rarefaction analysis of both species showed that gene discovery was nearing a plateau, especially for *M. smithii*, indicating that the remaining unidentified genes are likely to be low-frequency variants (Fig. 5.5K).

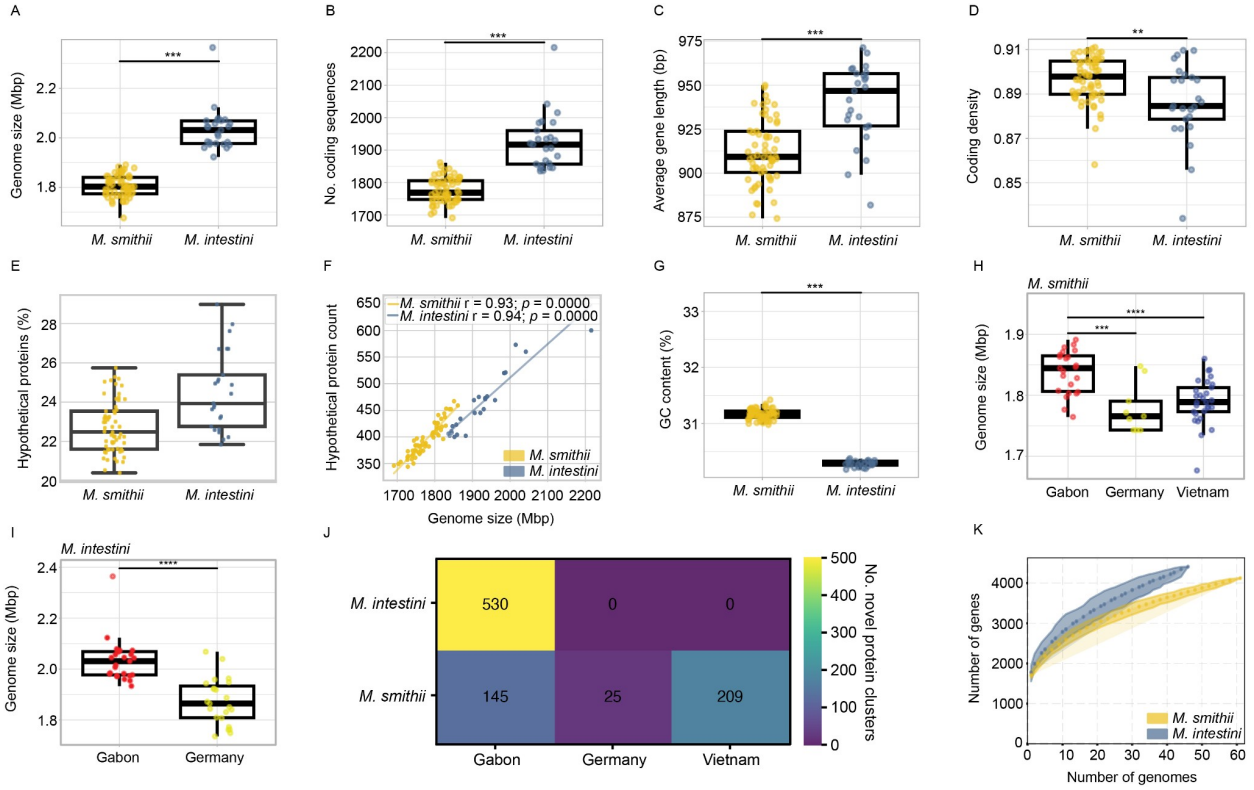

Figure 5.5: Genomic comparisons between *M. smithii* and *M. intestini* at the species and population level.
A. Box plots comparing median genome sizes between sequenced *M. smithii* and *M. intestini* strains. **B.** Box plots comparing the number of coding sequences observed between sequenced *M. smithii* and *M. intestini* strains. **C.** Box plots comparing the average gene lengths between sequenced *M. smithii* and *M. intestini* strains. **D.** Box plots comparing genome coding density between sequenced *M. smithii* and *M. intestini* strains. **E.** Box plots comparing the percentage of hypothetical proteins detected between sequenced *M. smithii* and *M. intestini* strains. **F.** Scatter plot showing the linear relationship between the number of hypothetical proteins and genome size for both species. The straight lines represent linear regression models fitted separately to each

species' data, demonstrating that both species exhibit strong positive trends. **G.** Box plot showing percentage GC content for both species. **H.** *M. smithii* genome sizes between assemblies from Gabon, Germany, and Vietnam. **I.** *M. intestini* genome sizes between assemblies from Gabon, Germany, and Vietnam. **J.** Heatmap showing the number of novel protein clusters derived from Gabon, Germany, and Vietnam that were detected in our dataset compared to publicly available *M. smithii* and *M. intestini* assemblies. **K.** Rarefaction curve showing the relationship between the number of genome assemblies and gene discovery for both methanogen species. The shaded regions represent confidence intervals calculated during resampling. Statistics was performed for all plots using the Wilcoxon test (**** $p < 0.001$, *** $p < 0.01$, ** $p < 0.05$).

5.3.5. Methanogen genetic diversity indicates strain-sharing and population-specific genetic diversity.

Given the availability of *M. intestini* isolate sequences from mother–infant and sibling pairs in Ikobey, Gabon ($n = 18$), we investigated whether *M. intestini* strains were shared within families. We compared strain similarity within households versus between households using average nucleotide identity (ANI) values. This revealed that genetically similar strains were significantly more common within households than between them (Fig. 5.6A). Specifically, 41.7 % of strain pairs within the same household (5 out of 12 comparisons) showed high similarity, compared to only 8.51 % of strain pairs from different households (12 out of 141 comparisons). A permutation test of the difference in proportions yielded an observed difference of 0.3316 against a near-zero null mean (0.00113) with a null SD of 0.0912 and a two-sided $p = 0.0066$, providing strong evidence that the observed enrichment is unlikely under random relabelling. These findings indicate that *M. intestini* isolates with highly similar genomes are preferentially found within the same household, supporting either frequent transmission between family members or shared environmental exposures that select for similar strains.

We then examined genetic diversity of both methanogen species at the geographic population level using pairwise ANI comparisons. Both species showed a clear geographic signal: within-country comparisons had consistently higher median ANI than cross-country comparisons, with the largest drops observed for pairs spanning the widest geographic contrasts ($p <$ 1e-300 for *M. smithii*; $p =$ 6.7e-41 for *M. intestini*; Mann-Whitney U test). Effect sizes were large (Cliff's $\delta \approx 0.76$ for *M. smithii*, $\delta \approx 0.85$ for *M. intestini*). For *M. smithii*, within-country median ANIs were high: Vietnam 99.148 % ($n = 847$; SD 0.390), Gabon 98.951 % ($n = 727$; SD 0.529), and Germany 98.854 % ($n = 226$; SD 0.471) (Fig. 5.6B). Between-country medians were lower, with the Gabon pairings showing the greatest divergence: Gabon–Germany 98.047 % ($n = 692$; SD 0.319), Gabon–Vietnam 98.188 % ($n = 1331$; SD 0.155), and Germany–Vietnam 98.734 % ($n = 766$; SD 0.207)

(Fig. 5.6C). The Germany–Vietnam comparison thus showed the smallest cross-country drop in ANI, suggesting greater genomic similarity between these two populations. Several between-country distributions were right-skewed (Fig. 5.6C), consistent with a long tail of near-identical cross-country pairs that likely reflects occasional widespread or recently shared strains. For *M. intestini*, within-country medians were 98.971 % in Gabon (n = 337; SD 0.305) and 99.019 % in Germany (n = 5; SD 0.564) (Fig. 5.6D). Notably, dispersion was generally larger within countries than across country pairs (e.g., for *M. smithii*, within-country SDs ≈ 0.39–0.53 vs. cross-country SDs ≈ 0.16–0.32), indicating that local populations harbour a broader range of genomic similarity while cross-country comparisons cluster more narrowly around lower ANI values.

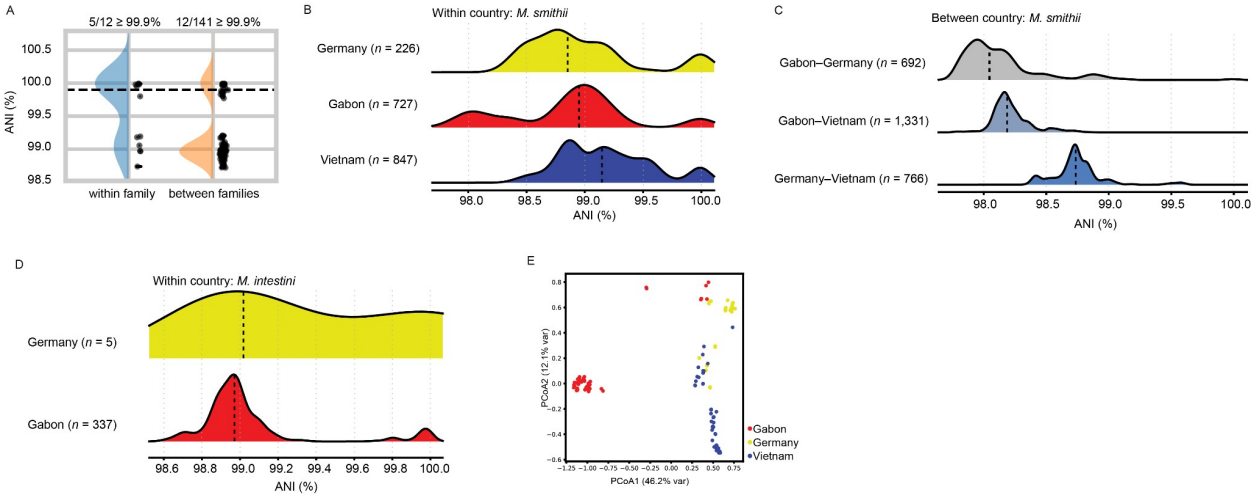

Figure 5.6: Strain-sharing and population-specific genetic diversity.
A. Raincloud plot of pairwise average nucleotide identity (ANI) among *M. intestini* genomes, stratified by comparison group (within-family versus between-family). Half-violins show Gaussian kernel density estimates and black points represent individual genome pairs. The dashed horizontal line indicates the highly similar strain threshold (99.9% ANI); text above each group shows the number of comparisons exceeding this threshold (k/N). B–D. Ridgeline distributions of pairwise ANI values. **B.** *M. smithii* within-country comparisons. **C.** *M. smithii* between-country comparisons. **D.** *M. intestini* within-country comparisons. Each ridge represents a Gaussian kernel density estimate, with dashed vertical lines indicating median ANI values; labels indicate the comparison group and sample size (n). **E.** Principal coordinates analysis (PCoA) of genome distances (100 − ANI) for *M. smithii*. Each point represents one genome, coloured by country of origin. Axes show the percentage of variance explained by PCoA1 and PCoA2.

To visualize the overall structure of genomic divergence, we performed PCoA on 100−ANI for *M. smithii*. The ordination revealed country-associated clustering consistent with the pairwise statistics. PCoA1 (46.2 % of variance) separated Gabon genomes from those of Germany and Vietnam (Fig. 5.6E), confirming that the dominant axis of genomic dissimilarity distinguishes

Gabon from non-Gabon populations. PCoA2 (12.1 %) captured finer structure within the non-Gabon set. Germany and Vietnam substantially overlapped along PCoA1 (Fig. 5.6E), consistent with the relatively high ANI observed between these countries and suggesting recent cross-border movement or shared ancestry. Vietnam displayed a vertically elongated, partly bimodal distribution along PCoA2, indicating within-country substructure that corresponds to the broader dispersion observed in the ridgeline plots. These results point to strong biogeographic differentiation of *M. smithii*, with Gabon forming the most genetically distinct population and Germany–Vietnam showing the closest inter-country relationship.

5.3.6. Hypervariable genomic regions partition *M. smithii* genomes by geography.

To investigate the relative contributions of mutation and recombination to genomic diversity in *M. smithii*, we analysed the relationship between sequence divergence and syntenic conservation across 140 genome assemblies. We quantified sequence divergence using ANI and structural rearrangements using average pairwise synteny score (APSS)[43]. Our analysis revealed a strong positive correlation between ANI and APSS scores (Fig. 5.7A), indicating that mutation and structural changes occur concordantly in *M. smithii* populations. The data exhibited a hierarchical pattern consistent with isolation-by-distance: within-individual comparisons showed the highest ANI and APSS values, followed by progressively lower values for within-province and within-country comparisons. This nested population structure supports a model of predominantly local transmission with limited long-range gene flow. The parallel decay of both metrics suggests that genomic diversity has accumulated through a combination of point mutations (affecting ANI) and larger-scale genomic rearrangements (affecting APSS). The concordance between ANI and APSS argues against a model dominated solely by clonal divergence, instead supporting a scenario where both mutational and recombinational processes shape genomic architecture in proportion to evolutionary distance[44].

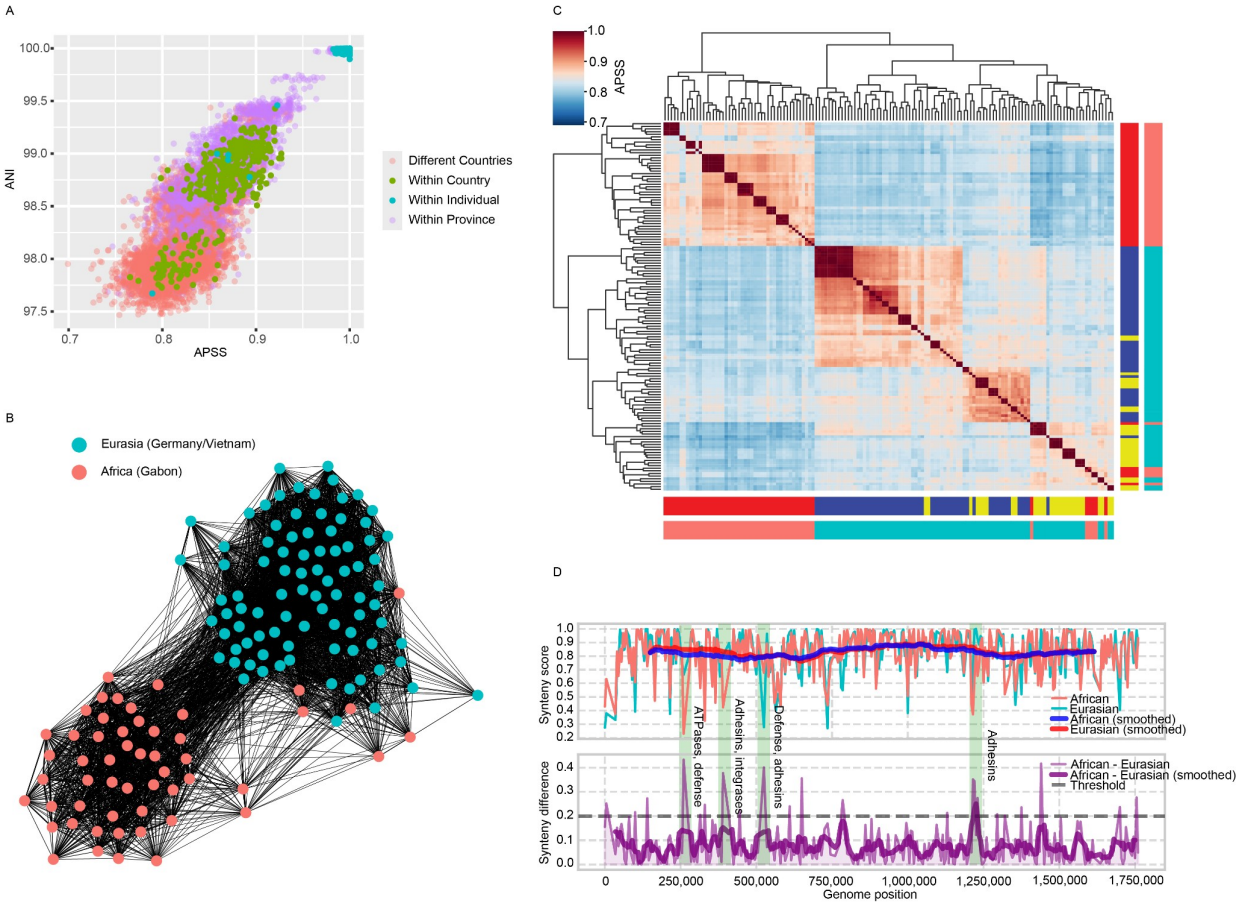

Figure 5.7. Genomic structural variation tracks geography.
A. Two-dimensional scatterplot of ANI versus average pairwise synteny score (APSS) for 140 *M. smithii* assemblies. Points are coloured according to the comparison scale: within individual (blue), within province (purple), within country (green), and between countries (salmon). **B.** Fruchterman–Reingold force-directed network of 143 *M. smithii* genomes, using synteny scores as edge weights. Genomes with higher synteny similarity are positioned closer together. **C.** Hierarchical clustering of pairwise whole-genome synteny scores showing separation of African (salmon) and Eurasian (light blue) isolates and country-level groupings (Gabon: red; Germany: yellow; Vietnam: blue). **D.** Genome-wide synteny comparison across the ~1.8 Mb *M. smithii* genome between African and Eurasian groups. The upper panel shows absolute synteny scores along genome position, and the lower panel shows differences between groups (African − Eurasian). Shaded regions indicate genomic intervals with divergent synteny patterns and associated functional annotations, including ATPases, defense systems, adhesins, and integrases.

To determine if genome synteny also shapes population-specific clustering, we constructed a Fruchterman–Reingold graph with edges weighted by APSS. The network revealed two primary clusters corresponding to African (Gabon) and Eurasian (Germany, Vietnam) strains, indicating that *M. smithii* genomic architecture is shaped by geography (Fig. 5.7B). Hierarchical clustering on APSS distances further supported geographic structuring, where additional sub-

clustering within the Eurasian module that broadly tracked Germany–Vietnam groupings was observed (Fig. 5.7C). The tight intra-regional connectivity and sparse inter-regional bridges in these visualizations are consistent with the isolation-by-distance pattern observed in the correlation analysis: gene flow occurs predominantly within geographic regions, with only occasional long-range dispersal or admixture connecting distant populations.

We then identified hypervariable regions driving the APSS differences in the 1.75 Mb *M. smithii* chromosome by calculating the per-region average synteny scores. Synteny scores remained uniformly high across the chromosome, indicating no large-scale rearrangements differentiate the lineages (Fig. 5.7D). Instead, divergence was concentrated to four hypervariable hotspots at ~250, 500, 750 and 1,400 kb that coincide with annotated islands enriched for adhesins, defense systems, ATPases/integrases, and other mobile or surface-exposed functions (fold-enrichment > 2, FDR < 0.02; Fig. 5.7D). These localized troughs, together with the otherwise conserved backbone, point to turnover of accessory cassettes and host-interaction genes that is likely driven by selection and horizontal transfer as the primary drivers of regional differentiation. Taken together, these data support a model of largely clonal, yet geographically structured populations whose core genomes are stable, while adaptive, locale-specific variation arises in a limited set of flexible genomic islands. At this stage, we cannot carry out an equivalent analysis for *M. intestini* due to the absence of sufficient samples across populations in our dataset.

5.3.7. Pangenome analysis reveals distinct metabolic adaptations and adhesin diversification between *M. smithii* and *M. intestini* methanogens.

To explore the functional genetic differences resulting from speciation and regional adaptation, we conducted a pangenome analysis using the translated coding sequence (CDS) annotations for both species. The combined *M. smithii–M. intestini* pangenome analysis revealed that the two species share 1,982 core genes, representing approximately 36 % of their total gene repertoire, while the remaining accessory genes account for the majority of the genetic divergence underlying their speciation[25]. Statistical testing indicated that *M. smithii* accessory genes are significantly enriched for molybdate transport genes compared to *M. intestini*, suggesting that molybdate utilization is unique to this species (Fig. 5.8A, Supplementary Table 6). Genomic analysis confirmed that the molybdate transport genes (*modA* and *modB*) genes were exclusively present in all *M. smithii* isolates compared to *M. intestini* isolates in our catalogue and Tajima's D analysis indicated these genes were also under strong negative selection (Supplementary Table 7).

This indicates that molybdate utilization is an evolutionarily conserved, essential biological function for this species, as previously suggested[22]. Both species encoded tungsten-dependent formylmethanofuran dehydrogenase isoenzymes suggesting that *M. intestini* is restricted to tungsten-dependent pathways for hydrogenotrophic methanogenesis, while *M. smithii* can potentially utilize both tungsten and molybdate and likely dominates in environments with fluctuating molybdenum/tungsten ratios. No genes under positive selection were identified for *M. smithii*, which, together with its smaller genome size compared to *M. intestini*, suggests that *M. smithii* occupies a stable ecological niche with minimal pressure for further adaptation.

Compared to *M. smithii*, *M. intestini* showed significant enrichment of maltose-O-acetyltransferase, membrane-associated proteins, glycosyltransferases, and a mannosyltransferase (Fig. 5.8A). This suggests that *M. intestini* has evolved unique outer surface structures compared to *M. smithii* which may enable distinct interactions with its environment and neighbouring microbes, potentially differentiating its ecological niche from that of *M. smithii*[25]. Furthermore, 2-oxoglutarate synthase, 2-oxoacid oxidoreductase (ferredoxin), and formylmethanofuran--tetrahydromethanopterin N-formyltransferase were under strong positive selection in *M. intestini* genomes, likely to enhance its ability to utilize alternative carbon sources, participate in unique electron transfer reactions, or optimize methanogenesis pathways to respond to environmental or host-driven selective pressures[45] (Supplementary Table 7).

To analyse the strain-level gene repertoire for *M. smithii* and *M. intestini*, a pangenome was created for each species. All *M. smithii* assemblies from our collection were included ($n = 61$), while the *M. intestini* pangenome additionally incorporated publicly available high-quality assemblies derived from Western locations, including UK, France, Austria, USA, Sweden, Italy, and Germany (Supplementary Table 8). This resulted in 23 additional *M. intestini* MAGs that were combined with the 21 Gabon and two Germany *M. intestini* assemblies in our catalogue ($n = 44$). Principal component analysis showed distinct clustering of the accessory pangenome according to geography for *M. smithii* (Fig. 5.8B) and clustering according to Eurasian (Western) and African (Gabon; non-Western) assemblies for *M. intestini* (Fig. 5.8C). This suggests that both species have evolved distinct accessory genes potentially driven by adaptation to geographic-specific factors. For both species, random forest analysis indicated that putative adhesins (Ig-like domain repeat protein, bacterial Ig-like domain, Ig-like domain-containing protein, adhesin-like protein), microbial defense systems (CRISPR-associated protein, type I restriction modification DNA

specificity domain protein) and a vitamin B_{12} biosynthesis gene (encoding cobaltochelatase subunit CobN) were the main drivers of accessory genome clustering according to geography (Fig. 5.8D). Alternatively, transposases (transposase, transposase DDE domain protein), phosphopantetheine adenylyltransferase, and the aforementioned maltose-O-acetyltransferase gene were the top features additionally discriminating African (non-Western) from Eurasian (Western) *M. intestini* assemblies according to their accessory pangenomes (Fig. 5.8E). The geographic partitioning of these accessory functions is consistent with our synteny-based comparisons and suggest that both *M. smithii* and *M. intestini* populations have acquired and/or retained distinct accessory gene repertoires potentially shaped by region-specific ecological or host-associated selection pressures.

The *cobN* gene encodes a subunit of cobaltochelatase, which catalyses a key step in corrinoid (vitamin B_{12}) biosynthesis[46]. A closer examination of this locus revealed distinct geographic patterns between each methanogen species. In *M. smithii*, *cobN* was present in 100 % of assemblies (n = 61), but copy number showed significant geographic structuring (Kruskal–Wallis H = 29.35, adjusted p = 8.46e-7) (Fig. 5.8F). Gabonese genomes maintained significantly lower copy numbers (mean = 1.11, median = 1.0, range 1–2) compared to both German (mean = 1.75, median = 2.0) and Vietnamese populations (mean = 2.24, median = 2.0, range 1–5) (Fig. 5.8F). *Post-hoc* pairwise comparisons confirmed that Gabonese populations differed significantly from both German (Mann–Whitney U = 27.00, adjusted p = 2.3e-3) and Vietnamese populations (U = 28.50, adjusted p = 5.5e-7), while Germany and Vietnam showed similar median values despite Vietnam's greater variance. For *M. intestini*, by contrast, geographic differentiation occurred at the level of gene presence rather than copy number. Only a single non-Western assembly (Gabon; 4.8 %; 1/21) harboured the *cobN* gene, compared to 87.5 % (21/24) of Western population assemblies (Fig. 5.8G), yielding a highly significant association between geographic origin and gene presence (H = 26.49, adjusted p = 8.46e-7). Among the *M. intestini* assemblies where *cobN* was present, copy number showed no significant geographic variation (Kruskal–Wallis adjusted p = 0.501).

Differences in the maltose O-acetyltransferase gene locus was identified as an additional example of region-specific functional diversity, specifically for *M. intestini.* This enzyme catalyzes the transfer of an acetyl group from acetyl-CoA to the 6-hydroxyl position of glucosyl residues in maltooligosaccharides to modulate antigenicity and host immune recognition across diverse bacteria[47]. Within our dataset, a locus encoding a putative maltose O-acetyltransferase was

consistently syntenic with a predicted large adhesin/adhesin-like protein in *M. intestini* genomes that originated from the African samples (Fig. 5.8H). Neither the maltose O-acetyltransferase locus nor the adjacent adhesin homolog was detected in *M. intestini* assemblies from other geographic sources in our collection or the publicly available MAGs. This indicates a geographically patterned accessory gene block that could differentially modulate cell-surface properties and adhesion phenotypes. This is the first evidence for this enzyme in an archaeal lineage.

The accessory pangenome data indicates that both methanogen species prioritize adhesin diversification, likely to facilitate microbial partnerships or the rapid adaptation to ecological niches without altering core metabolic functions[19,48]. A survey of the total adhesin content of both species indicated substantial diversity both within and between species (Fig. 5.8I), with *M. intestini* encoding significantly more adhesins per genome compared to *M. smithii* (Fig. 5.8J). Analysis of potential horizontal gene transfer (HGT) events revealed that adhesins were significantly enriched in bi-directional exchange patterns between methanogen species (data not shown), supporting their frequent transmission to likely facilitate niche adaptation. While the median number of adhesions per genome was consistent between African and Eurasian samples for *M. smithii* (Fig. 5.8K), in *M. intestini*, Eurasian isolates contained significantly fewer adhesin genes compared to their African counterparts (Fig. 5.8L). The bimodal adhesin distribution for African strains suggests the existence of ongoing evolutionary processes driving subpopulations within Gabonese human gut environments (Fig. 5.8M).

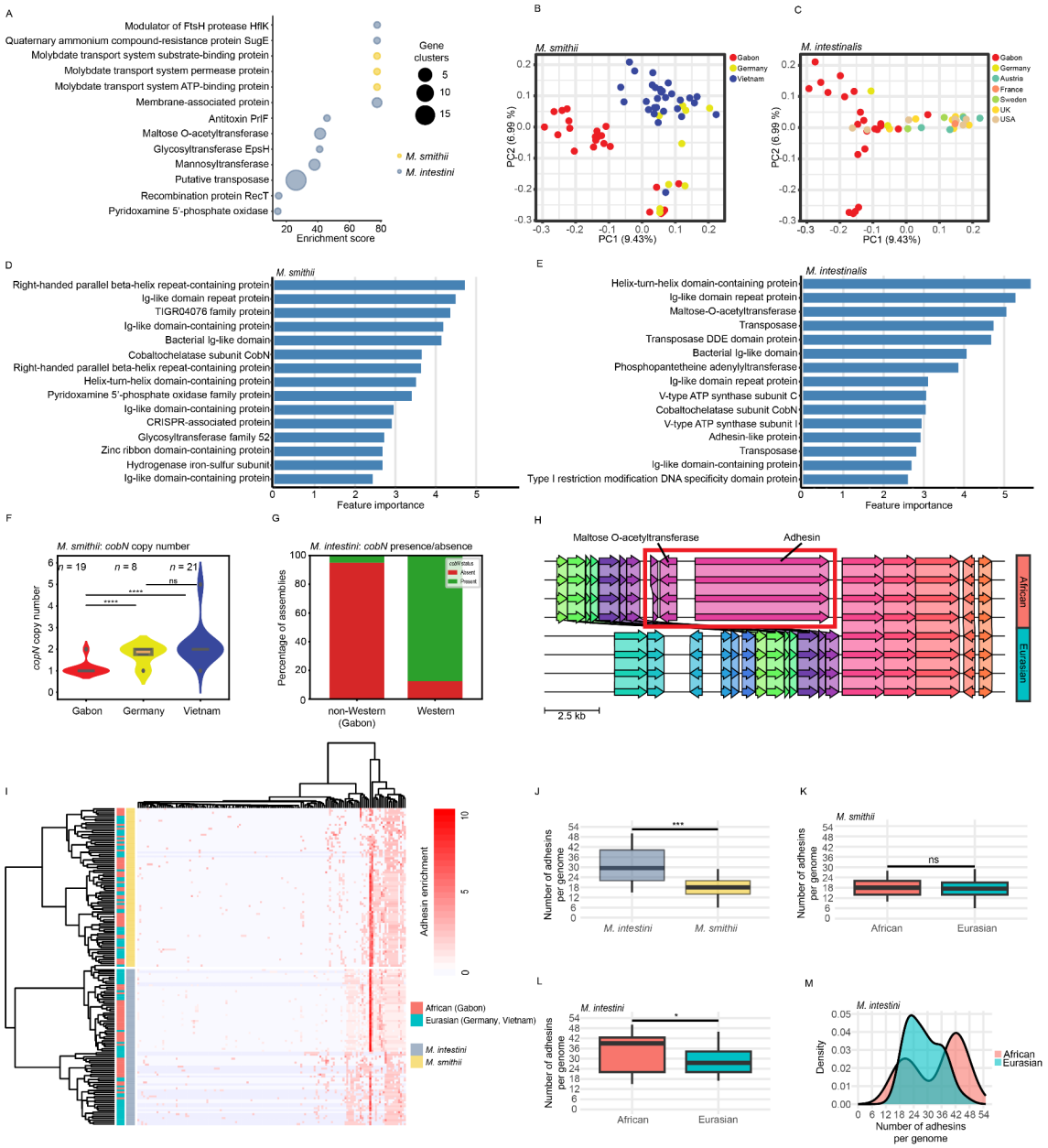

Figure 5.8: Pangenome analysis of *M. smithii* and *M. intestini* isolates from Gabon, Germany, and Vietnam.

A. KEGG functional enrichment of metabolic pathways in *M. smithii* and *M. intestini*. Dot size indicates the number of gene clusters assigned to each pathway, and colour denotes species-specific enrichment. Only significantly enriched pathways (adjusted $P < 0.05$) are shown. **B–C.** Principal component analysis (PCA) of accessory gene presence/absence profiles for *M. smithii* (**B**) and *M. intestini* (**C**). Strains are coloured by population origin or country of origin, respectively. D–E. Random Forest feature importance identifying accessory genes contributing to differentiation between African and Eurasian populations of *M. smithii* (**D**) and *M. intestini* (**E**). **F–**

G. Distribution of the *cobN* gene across populations. **F.** *cobN* copy number in *M. smithii* genomes from Gabon, Germany, and Vietnam. **G.** Proportion of *M. intestini* genomes containing *cobN* in non-Western (Gabon) and Western populations. **H.** Genomic context of the maltose-*O*-acetyltransferase locus in representative *M. intestini* genomes, showing co-localization with an adhesin gene in African but not Eurasian strains. **I–M.** Geographic and species-level variation in adhesin repertoires. **I.** Heatmap of adhesin gene enrichment across *M. smithii* and *M. intestini* populations. **J–L.** Comparison of adhesin gene counts between species (**J**), and between African and Eurasian populations of *M. smithii* (K) and *M. intestini* (**L**). **M.** Distribution of adhesin gene counts across populations. Statistical comparisons were performed using Wilcoxon tests (**** $P < 0.001$, *** $P < 0.01$, ** $P < 0.05$).

5.3.8. Lipid profiling reveals a shared lipid diversity in *M. intestini* and *M. smithii.*

Given that outer membrane structures were largely driving methanogen species and strain-level differences, we quantified 41 lipid species in 8 lipid classes across 12 representative *M. smithii* ($n = 5$) and *M. intestini* ($n = 7$) isolates using both positive and negative ionization modes. All 41 lipid species were present in both methanogen species, with comparable relative abundances between lipid classes. These included the core lipid dialkyl glycerol diethers (DGDs), as well as fatty acids (FAs), and DGDs with the following headgroups: one or two hexose groups (glycosyldiradylglycerols, Hex-DGD and Hex(2)DGD), phosphatidylinositol (PI-DGD), phosphatidylserine (PS-DGD), phosphatidic acid (PA-DGD), and phosphatidylthreonine (PT-DGD) or phosphatidylhomoserine (PHS-DGD), which are structural isomers that could not be definitely distinguished by their ion spectra (Supplementary Table 9).

Overall, of the lipid species within each class of lipid, fully saturated DGD 40:0 backbones were most abundant. The minor abundance of unsaturated lipid species in some lipid classes (e.g., PI-DGD:1-8) likely reflects incomplete saturation of isoprenoid chains during DGD synthesis. While PI-DGD and PS-DGD lipids are commonly described in methanogens, the presence of a threonine or homoserine headgroup in PT-DGD or PHS-DGD does not seem to have been previously reported; such a headgroup may be uncommon in archaea or have been undetected in previous studies for technical reasons. Also surprising for the archaea, some FAs were detected at a relatively low intensity; given the FA profile (FA 16:0, 18:0, and 18:1), these possibly originated from eukaryote-derived components in the culturing medium and were not synthesized by the archaea themselves. The overall conservation of lipid classes among all 12 representatives of both *M. smithii* and *M. intestini* suggest that this lipid profile may be advantageous specifically in the context of survival in the gut niche.

5.4. Discussion

We conducted a geographically and demographically stratified analysis of *M. smithii* and *M. intestini* in Gabon, Germany, and Vietnam, using metagenomic, pangenomic, phylogenomic, and lipidomic data. As part of this work, we generated the first geographically stratified culture and genome resource for these human gut methanogens, substantially expanding the number and diversity of available isolates and genomes for both species[29].

Across these populations, we observed that (1) both methanogens were more prevalent and abundant in less-industrialized Gabon; (2) *M. smithii* and *M. intestini* frequently co-occurred; (3) phylogenies of both species showed geographic structuring; (4) *M. smithii* exhibited strong cophylogeny with human hosts, whereas *M. intestini* showed weaker geographic differentiation; and (5) genomic divergence, especially in hypervariable regions enriched for host-interaction genes, contributed to regional population structure.

Methanogen prevalence patterns in our study broadly match prior reports of geographic and demographic structuring in the human archaeome[1,20]. *M. smithii* and *M. intestini* were common in all three cohorts, with *M. smithii* consistently more prevalent and abundant, as described in earlier work[3]. Rather than forming a uniform "core" archaeal microbiota, both species showed geography- and age-dependent variation: prevalences were highest in Gabon, intermediate in Vietnam, and lowest in Germany, echoing earlier observations of higher methanogen carriage in rural African populations than in Western cohorts[18,49–52].

Diet likely contributes to these differences, although we did not measure diet directly. The high prevalences seen in Gabon are compatible with previous findings that high-resistant-starch, lower-animal-fat diets in rural African communities are associated with abundant and diverse methanogens[20,53,54]. Such diets promote colonic fermentation and hydrogen production, which can support hydrogenotrophic methanogens[55]. The intermediate prevalences in Vietnam may reflect transitional dietary patterns, as traditional plant-rich diets increasingly incorporate more "modern" elements[56]. Conversely, lower prevalences in Germany are consistent with Western-style dietary patterns characterized by lower fibre intake and altered fermentation dynamics that are considered less favourable for methanogen establishment[57].

Within Gabon, we observed species-specific variation that cannot be explained by geography alone. *M. intestini*, but not *M. smithii*, was significantly more abundant in the rural Ikobey community than in semi-urban Lambaréné, despite ongoing dietary transitions in both

settings[58]. This pattern suggests that additional factors—such as antimicrobial exposure, sanitation, co-occurring fermentative bacteria, or host demography—shape *M. intestini* ecology in ways that differ from *M. smithii*[22,59].

Age further modulated methanogen patterns. We detected both species in infants, but at lower frequencies than in adults, consistent with progressive methanogen establishment during early life[60,61]. In infants, microbiome diversity mostly tracked age, whereas in adults, methanogen abundance correlated with diversity independent of site. Co-occurrence between *M. smithii* and *M. intestini* was also weaker and more variable in infants, including instances where *M. intestini* dominated. We did not detect strong mother–infant concordance, which argues against frequent vertical transmission above our detection threshold and instead aligns with reports that gut methanogens often colonize later in infancy[62–64]. Household-linked strain similarity for *M. intestini* in our data, together with previous evidence for household clustering of *Methanobrevibacter* strains[19,65], supports a model of predominantly local, close-contact transmission.

Contrary to earlier reports of mutual exclusion between *M. smithii* and *M. intestini*[26], we observed frequent co-occurrence and positively correlated abundances in adults across all three populations. The rarity of *M. intestini* in the absence of *M. smithii* suggests that *M. smithii* may help define community contexts in which *M. intestini* can persist, although our data do not distinguish whether this reflects direct ecological dependence or shared environmental requirements.

Species-specific associations with bacterial taxa suggest a potential mechanistic basis for gut methanogen co-occurrence and niche differentiation. We observed that *M. smithii* co-occurred with bacteria enriched for the Wood–Ljungdahl pathway, a metabolic route used by acetogens to produce acetate from H_2 and CO_2[66]. Both acetogens and methanogens utilize the same substrates (H_2/CO_2), creating potential for both competition and cross-feeding. Genomic predictions have indicated that *M. smithii* can assimilate acetate via an incomplete TCA cycle[19], thus, our data suggests a dual interaction: acetogens may serve as carbon providers (via acetate) while simultaneously competing with *M. smithii* for electron donors. Consistent with this interpretation, *M. smithii* showed negative correlations with other acetogenic taxa, suggesting that competitive dynamics may constrain which acetogens can stably coexist with this methanogen. Previous work has demonstrated that acetogens and methanogens can coexist despite substrate overlap, which was proposed to reflect differences in thermodynamic thresholds for H_2 utilization[67]. Given our

observations, *M. smithii* may exploit its lower H_2 threshold to outcompete certain acetogens while benefiting from acetate produced by others. However, direct experimental validation of these interactions is necessary.

In contrast, *M. intestini* exhibits a narrower set of positively associated partners, which are enriched for pathways involved in C_1 metabolism, ether-linked lipids, and cell-wall precursors, suggesting greater dependence on specific metabolic inputs from co-resident bacteria. In addition, inverse relationships between *M. intestini* and ureolytic or vitamin B_6-producing taxa, whose activities draw on overlapping nitrogen pools and reducing power[68], are consistent with potential competitive interactions.

In adults, higher *Methanobrevibacter* abundance was associated with greater microbiome alpha diversity, in line with syntrophic models where archaeal consumption of fermentation products supports diverse fermentative consortia[17,37,69]. Prior work has shown that *M. smithii* can redirect bacterial fermentation and nitrogen use to favour saccharolytic, fibre-adapted bacteria[15], and that *Methanobrevibacter* prevalence often coincides with complex co-occurrence networks[34,70]. In our data, Gabon was both methanogen-rich and highly diverse, whereas Germany and Vietnam showed similar intermediate diversity despite comparable methanogen levels, indicating that methanogens alone do not determine diversity states. This pattern is consistent with archaeome catalogues in which lifestyle and regional microbial source pools shape both archaeal gene content and strain structure[22].

Taken together, these ecological patterns are consistent with *M. smithii* occupying a broader range of fermentative contexts, while *M. intestini* appears more restricted. This difference does not map simply onto genome size: *M. smithii* has a smaller, streamlined genome yet shows wider distribution and more flexible co-occurrence patterns than *M. intestini*. One possible interpretation, consistent with previous work[5,71], is that long-term host association has favoured a compact core genome in *M. smithii* that functions across many gut environments, whereas *M. intestini* retains an expanded accessory genome geared toward more specific syntrophic configurations. Our data alone cannot distinguish among these scenarios, so experimental tests in co-culture or gnotobiotic models will be needed.

Our phylogenetic and cophylogenetic analyses show that *M. smithii* is a geographically structured human commensal. Its deeper internal branching and regionally clustered sublineages agree with previous evidence for an open pan-genome and population-specific accessory gene

pools[19,29], and echo cross-mammalian patterns in which *Methanobrevibacter* clades display host specificity and long host association rather than free mixing[72,73]. The significant congruence between human and *M. smithii* phylogenies across African and Eurasian cohorts[5] suggests that host history and geography have jointly shaped *M. smithii* diversification, likely filtered further by local lifestyle. By contrast, *M. intestini* showed shallower branching and weaker geographic structure, consistent with a lineage that is globally distributed but less differentiated.

We also observed hierarchical geographic structure within both species, consistent with predominantly local transmission. Household-level clustering of *M. intestini* strains, together with distinct country- and continent-level clusters, suggests isolation by distance, as reported in large-scale archaeome catalogues[22,29]. For *M. smithii*, German and Vietnamese genomes overlapped, whereas Gabonese genomes formed a separate cluster, suggesting more recent connectivity between Eurasian cohorts and a more distinct regional reservoir in Gabon. *M. intestini* exhibited weaker but still detectable regional structure, suggesting partially segregated populations maintained by local transmission.

At the sequence level, *M. smithii* populations showed a strong correlation between average nucleotide identity and genome synteny, indicating that point mutations and structural rearrangements accumulate together within geographically structured lineages. The most divergent genomic regions were enriched for adhesins, mobile-element–associated functions, and defense genes, categories that are expected to be shaped by local host immunity, phages and archaeal viruses, and co-occurring microbes[74,75]. This pattern suggests that, while the core genome retains a phylogeographic signal, a flexible set of accessory loci underpins fine-scale adaptation to regional host–microbiome contexts.

Comparisons of accessory gene content provide a functional view on these patterns. At the genus level, the shared core genome defines both species as hydrogenotrophic methanogens, while the accessory genome contributes most of the observed divergence[71]. In *M. smithii*, retention of a highly conserved molybdate transport system, together with the capacity to use both molybdenum and tungsten as cofactors, is consistent with a metabolically flexible commensal that can cope with fluctuating trace-metal availability[76]. In *M. intestini*, by contrast, the accessory genome is enriched for genes involved in cell-surface modification (for example, glycosyl- and mannosyl-transferases) and in metabolic fine-tuning, and we detect signatures of positive selection on loci involved in alternative carbon use. These findings fit with our ecological observations of a narrower set of

bacterial partners and more restricted prevalence, but direct functional studies will be required to determine whether these genomic differences translate into distinct metabolic strategies in vivo.

Within each species, African and Eurasian strains of *M. smithii* and *M. intestini* formed distinct clusters based on accessory gene content, indicating that population divergence extends beyond core genome differences to include the gain and loss of functionally relevant genes. This gene-level structure agrees with our synteny patterns and supports prior evidence that *Methanobrevibacter*_A evolution is shaped strongly at the host–microbe interface rather than in core metabolism[72]. Regionally structured loci, such as cobN presence in *M. smithii* and cobN presence together with adhesin repertoire shifts in *M. intestini*, indicate that corrinoid-related and surface-associated functions differ between African and Eurasian populations[77].

A further example is the discovery of a maltose O-acetyltransferase gene, the first reported in any archaeon, found exclusively in African *M. intestini* isolates within a syntenic block adjacent to an adhesin gene. Given that bacterial acetylation of surface sugars can modulate immune recognition and microbial adhesion[78], this locus is consistent with a specialized mechanism for interfacing with local host or microbial environments that was not detected in the German and Vietnamese lineages. More broadly, adhesins emerged as a likely major substrate for rapid adaptation[71]: the significantly larger repertoire in African *M. intestini* populations, together with evidence of bidirectional horizontal gene transfer between species, suggests that biogeographic structure may be maintained through recurrent gene gain, loss, local amplification, and inter-species exchange. Conversely, the marked reduction in adhesin number and diversity in Eurasian strains is compatible with reductive evolution and/or shifting ecological demands in less complex, fiber-poor Western guts[79], although the specific underlying selective regimes remain to be characterized. These patterns provide genomic support for our metagenomic observations of methanogen reduction in more industrialized/Western settings. They imply that this is not only a quantitative decline, but also a qualitative erosion of the adaptive functions that likely enable long-term persistence within human hosts. However, these functional consequences are largely inferential and the development of genetic systems for human methanogens will enable these mechanistic perspectives to be explored in more detail.

Both species converge on a membrane architecture dominated by saturated C40 diether lipids[80,81], a core physiological trait that underpins their ability to persist in the gut. This lipid composition provides the low proton permeability essential for energy-efficient methanogenesis

while maintaining sufficient fluidity for growth at body temperature, thereby minimizing energetic costs under fluctuating fermentative conditions. The retention of specific lipid headgroups, such as inositol and serine, likely enhances resistance to host bile salts, supporting survival during transit through and residency in the intestinal milieu. The discovery of phosphatidylthreonine, a headgroup rare outside eukaryotes, further hints at horizontal gene transfer or convergent evolution to fine‐tune membrane surface properties and host interactions. Together, this shared, gut‐tuned lipidome provides a biophysical foundation for methanogen colonization strategies, coupling proton-tight, bile-resistant membranes to robust resilience in the colonic ecosystem.

M. smithii and *M. intestini* exemplify how microbial speciation, adaptation, and host-microbe cophylogeny converge to shape the dominant archaeal component of the human gut ecosystem. Their evolution has likely been shaped by a hierarchy of selection pressures, potentially driven by human migration and adaptation to modern lifestyles and diets. Our findings highlight gut methanogens as sensitive biogeographic markers that not only track human history but also functionally adapt to local host environments. Future research disentangling the regulation of their accessory genomes and the functional consequences of regional strain variation will deepen our understanding of the human gut archaeome's contribution to human health and disease.

5.5. Materials and Methods

Culture media. Methanogen Enrichment (ME) media was used for all liquid cultures. This consisted of KH_2PO_4 (4.5 mM), $MgCl_2 \times 6\ H_2O$ (628 μM), NaCl (8.5 mM), NH_4Cl (9.2 mM), $CaCl_2 \times 2{\cdot}H_2O$ (430 μM), Resazurin (25 mg/100 ml: 4 ml), trace minerals SL-10 (1 ml), modified trace elements Wolfe (20 ml), and bacterial fermentation products, prepared under anaerobic conditions. The minimal media solution was sparged with N_2/CO_2 (80:20 %, 1 bar and 0.5 L/min pressure for each gas) for 40 minutes and autoclaved. After autoclaving at 121 °C for 20 minutes and cooling, we added L-cysteine-HCl (5 ml), fermentation products (80 ml), and $NaHCO_3$ (47.6 mM) through a 0.22 μm filter in an anaerobic chamber. The media was then supplemented with 1 μg/ml ampicillin, 10 μg/ml erythromycin, 10 μg/ml vancomycin, and 40 mg/L cycloheximide to restrict bacterial growth.

Isolation and enrichment of methanogens from human stool

Serial dilutions. Using existing stool samples(Suzuki et al., 2022) from adult females living in Gabon (Ngounié and Moyen-Ogooué provinces, n = 76), Vietnam (Sonla, Hanoi and Hatinh, n = 97), and Germany (Baden-Württemberg, n = 36), we generated a comprehensive

culture collection of human gut-derived methanogens. For each stool sample, ~1 g of frozen stool was extracted and transferred into 2 ml Eppendorf tubes containing 1 ml of ME media. This produced a faeces-media slurry which was briefly centrifuged (30 s at 3000 RPM). One ml of supernatant was used to make serial dilutions with 9 ml of ME media in 18 mm by 150 mm Balch tubes. Three serial dilutions were made for each sample (1:10, 1:100 and 1:1000). The headspace of the Balch tubes was filled with H_2:CO_2 at a flow of 80:20 (%) atmosphere and a pressure of 1-1.6 bar. All serial dilutions were incubated for up to 14 days at 37 °C, in a rotary shaker (Infors AG CH-4103 Miniton) at 150 RPM.

Methane measurements. Methane production was measured in all tubes every seven days using an SRI 8610C gas chromatograph (Torrance, USA). This instrument was equipped with a packed column at 42 °C (0.3-m HaySep-D packed Teflon; Restek, Bellefonte, PA, USA), a thermal conductivity detector (TCD) at 111 °C, and a flame ionization detector (FID). Before analysing the sample gasses, a series of pure methane (99.9 %) tests were conducted at concentrations of 1.75 %, 3.51 %, 5.26 %, 7.02 %, 10.53 %, 15.79 %, 17.54 %, 24 %, 50 %, and 100 % to establish a standard curve. The gasses produced and consumed were estimated from the total pressure in the Balch tubes and the percent concentration was estimated using standard equations obtained from standard curves that were generated using pure gasses (CH_4, CO_2, and H_2).

Isolation of clonal colonies. Once methane was detected in any of the tubes, the culture was transferred by spread plating onto anoxic ME solid agar. The plates were then placed in anaerobic jars, the headspace was filled with H_2:CO_2 at an 80:20 ratio and a pressure of 1.6 bar, incubated at 37 °C. Plates were examined for growth after 3-7 days. Once colonies appeared, a fluorescent microscope (Axioscope A1, Zeiss) was used to identify auto-fluorescent colonies at a wavelength of 420 nm. Auto-fluorescent colonies were sub-cultured onto solid ME agar and incubated at 37 °C until additional colonies formed. Clonal, isolated colonies were picked and used to inoculate liquid ME media for the preparation of glycerol stocks and DNA extractions.

DNA extraction, library preparation and sequencing. For short-read sequencing, five ml cultures were centrifuged at 4,100 × *g* for 15-20 mins and the pellet was resuspended with 50 µL nuclease-free water. This solution was used as the input for DNA extraction with a DNeasy PowerSoil Pro kit (Qiagen, Redwood City, California). Genomic DNA libraries were constructed using the Nextera protocol with the Tn5 enzyme[61]. Extracted DNA was diluted to 5 ng/µL, tagmented with Tn5 transposase, and amplified using paired-barcoded primers for 12 cycles.

Libraries were pooled and quantified with a Qubit (Thermo Fisher, Waltham, Massachusetts) before being size selected on a BluePippin (Sage Science, Beverly, Massachusetts) for 300-700 base pairs. The resulting libraries were then sequenced with 2 × 150 paired-end on an Illumina MiSeq, NextSeq2000 and HiSeq3000 sequencers. For long-read sequencing, DNA was extracted using the Qiagen MagAttract HMW DNA Kit (Qiagen, Waltham, Massachusetts) and quantified with a Qubit. Only samples with DNA concentrations exceeding 30 ng/μL were utilized for library preparation. The Nanopore SPRI size selection protocol for DNA fragments of > 1.5–2 kb was used to obtain high molecular weight DNA. The size distributions of DNA fragments were visualized using the Agilent Femto Pulse system (Agilent Technologies, Santa Clara, California). Libraries were prepared using the Rapid Barcoding kit 96 (SQK-RBK 110.96), and sequencing was carried out with a Nanopore MiniON Mk1B using the MinKNOW software and compatible flow cells. The resulting Illumina and Nanopore reads were used to generate hybrid assemblies.

Sequence assembly, taxonomic profiling, and functional annotation. Raw sequences were validated with fqtools v.2.0(Droop, 2016) and de-duplicated with BBtools clumpify v37.78 (https://github.com/bbushnell/BBTools). Adapters were trimmed and read quality was assessed with Skewer v0.2.2 (https://sourceforge.net/projects/skewer) and BBtools bbduk (https://github.com/bbushnell/BBTools). Reads mapping to the *Homo sapiens* hg19 assembly were filtered using BBtools bbmap v39.52 (https://github.com/bbushnell/BBTools). Quality control reports for all reads were generated with fastqc v0.11.7 (https://github.com/s-andrews/FastQC) and multiQC v1.5a[82]. Reads were assembled per-sample with Unicycler v0.5.0 (https://github.com/rrwick/Unicycler). CheckM2 v1.0.2[83] was used to assess completeness and contamination; assemblies that were less than 90 % complete and with greater than 5 % contamination were filtered out. Genome statistics including GC content, N50, and number of contigs were predicted using BBmap stats v39.52 (https://github.com/bbushnell/BBTools). Genome sizes were calculated using the formula:
Taxonomic classifications were assigned using GTDB-Tk r214[84]. Coding sequences were predicted with Prokka v1.14.5[85] using the *M. smithii* type strain as the initial annotation source (https://www.ncbi.nlm.nih.gov/datasets/genome/GCF_000016525.1/). Average nucleotide identities (ANI) were calculated with FastANI v1.34[86]. Gene functions were predicted with eggNOG-mapper v2.1.12[87] and kofam_scan v1.3.0 (https://github.com/takaram/kofam_scan), while pathways and phenotypic characteristics were predicted with MetaPathPredict[88], Gapmind[89],

and Traitar v3.0.1[90]. Antimicrobial resistance genes were predicted using Abricate v1.1.0 (https://github.com/tseemann/abricate). antiSMASH v7[91] and BiG-SCAPE v1.1.9[92] were used to identify Biosynthetic Gene Clusters (BGC). Adhesins were predicted using DeepTMHMM v1.0.42 (https://services.healthtech.dtu.dk/services/DeepTMHMM-1.0/).

Metagenomic sequencing and cross-domain microbial association networks. Gut metagenomic data from all three populations were generated as previously described[5]. Microbial taxonomic profiles were derived from Kraken2 v2.1.2[93] using a comprehensive, customized database encompassing bacteria and archaea. Species-level abundances were estimated using Bracken v2.6.0[94]. To mitigate biases introduced by variable sequencing depth, samples were subsampled to an even depth of 1 million reads prior to downstream analyses. This threshold was chosen based on distributional read depth assessments, ensuring sufficient representation of taxonomic diversity across all samples. For relative abundance plots using a logarithmic scale, a pseudo-count of 1.0e−7 was added to each abundance value to allow log transformation. Species with a prevalence below 0.1 % across all populations were excluded from the prevalence analysis.

To investigate ecological interactions between methanogenic archaea and bacteria, we constructed cross-domain microbial association networks using SpiecEasi v1.1.2[95]. For each sample group (adults and infant), we filtered species-level abundance tables to retain bacterial taxa and two target archaeal species, *Methanobrevibacter_A smithii* and *Methanobrevibacter_A intestini*, present in at least 20 % of samples. Analyses were conducted on absolute (non-rarefied) read counts to preserve underlying covariance structure essential for network inference. SpiecEasi was run using the Meinshausen–Bühlmann neighborhood selection method (method = "mb"), with nlambda = 20 and lambda.min.ratio = 1e−2. Model selection employed the Stability Approach to Regularization Selection (StARS) with a threshold of 0.05 to ensure robust edge selection. The resulting networks included both positive and negative associations, interpreted as potential co-occurrence and mutual exclusion relationships, respectively.

Co-abundance networks between methanogens and bacteria were visualized using Sankey diagrams. To focus on biologically meaningful associations, a minimum absolute association strength (the SpiecEasi metric for determining significant co-occurrence) cutoff of 0.05 was applied to filter the data. The filtered associations were separated into positive (co-occurring) and negative (mutually exclusive) subsets for independent visualization. Sankey diagrams were constructed using the Plotly library, with bacterial species positioned as source nodes on the left

and methanogen species as target nodes on the right. Link widths were normalized globally across all plots using min-max scaling to a range of 1-100, ensuring visual comparability between positive and negative association diagrams. Statistical enrichment analysis of KEGG metabolic pathways across microbial assemblies was performed using a generalized linear modelling approach implemented in R. A binomial generalized linear model (GLM) with logit link function was fitted to test for differential pathway occurrence across assemblies. The Rao score test was applied to assess the significance of assembly-level differences, generating an enrichment score and corresponding *p*-value for each pathway. To account for multiple testing across all analysed pathways, false discovery rate (FDR) correction was implemented using Storey's *q*-value method, with the proportion of true null hypotheses (π_0) estimated using a smoothing approach across a range of lambda values (0.05 to 0.95). Pathways were ranked by enrichment score, with higher scores indicating greater differential occurrence across assemblies.

Codon usage. Codon usage for total and ribosomal protein genes was predicted from the putative coding sequences produced by Prodigal v2.6.3[96]. First, ribosomal proteins were classified by screening amino acid sequences from all assemblies for PFAM domains associated with microbial ribosomal proteins. Nucleotide sequences for all predicted coding sequences were then separated into ribosomal and non-ribosomal sets for each assembly and the Relative Synonymous Codon Usage (RSCU) was calculated for each using coRdon v1.26.0 (https://github.com/BioinfoHR/coRdon). Expression levels were predicted based on codon usage by comparing the ribosomal protein nucleotide sequences to the non-ribosomal protein sequences and calculating the Codon Adaptation Index (CAI) and Measure Independent of Length and Composition-based Expression Level Predictor (MELP) using coRdon. The top 5 % genes according to the CAI index were classed as highly expressed.

Phylogenetic analysis

Maximum likelihood (ML) phylogenetic analyses were conducted using IQ-TREE v3.0.1 (https://github.com/iqtree/iqtree2) to resolve the evolutionary relationships among the *Methanobrevibacter_A* strains. A phylogenomic tree was inferred from a concatenated alignment of protein sequences of core genes under neutral selection (see below), including the *M. smithii* type strain and an *M. oralis* outgroup. The final alignment consisted of 13,110 amino acid sites. The best-fit model of protein evolution was determined using ModelFinder[97] and selected based on the Bayesian Information Criterion (BIC). Branch support was assessed using 1,000 ultrafast

bootstrap replicates. The -bnni flag was used to perform an additional optimization step to reduce the risk of artifacts from severe model violations in the bootstrap trees.

Pangenome construction and functional enrichment analysis. Pangenome analysis was performed to investigate methanogen gene content with and between both species. Gene presence/absence patterns were determined using Roary v3.11.2[98], and subsequent analyses were conducted in R v4.0. The pangenome was stratified with core genes defined as those present in ≥ 95 % of genomes, shell genes as those with 15-95 % frequency, and cloud genes representing the rare accessory genome (< 15 %). Principal Component Analysis (PCA) was applied to visualize genomic relationships between isolates, with k-means clustering employed to identify discrete genomic groups. Random Forest machine learning (randomForest package v4.7) was implemented to identify gene clusters discriminating between both k-means-derived clusters and Eurasian/African isolation sources, with feature importance quantified. For population structure analysis, core genes were aligned using the AlignTranslation algorithm in DECIPHER v3.0.0, and neutrally evolving genes (Tajima's D between -2 and 2, calculated using pegas v1.3[99]) were concatenated for subsequent analyses. Hierarchical Bayesian Analysis of Population Structure (RhierBAPS) v1.1.4[100] was applied to neutral core gene alignments to detect population structure without selective bias. Phylogenetic reconstruction was performed using a neighbor-joining algorithm on maximum likelihood distances of concatenated neutral core genes (phangorn R package v2.11.1[101]), with evolutionary lineages and isolation sources visualized using ggtree v3.12.0[102].

Synteny analyses. SynTracker v1.4.0[43] was used to analyse genome synteny. Synteny scores were calculated based on pairwise comparisons of 100 genomic regions against the reference genome of each species. To compare *M. intestini* strains between related and unrelated hosts, we first removed self-comparisons and integrated host metadata (country, household, age group) to classify each genome pair as related (from the same household, including mother–child or sibling pairs), unrelated (from different households), or siblings (related infants). Comparisons were grouped as “related” or “unrelated” and annotated by sampling location to assess whether household members harboured more syntenic strains than random pairs.

To identify regions with asymmetric conservation between groups, divergence ratios were calculated by dividing Group 1 synteny scores by Group 2 synteny scores, with a small epsilon value (1 × 10e-10) added to prevent division by zero. These ratios were subsequently $\log_2$-transformed to create a symmetric scale where positive values indicate higher conservation in

Group 1 and negative values indicate higher conservation in Group 2. Values near zero represent similar conservation levels between groups, while values approaching ± 1 indicate two-fold differences in synteny conservation. Statistical differences in synteny scores between related and unrelated individuals were tested using a two-sided Wilcoxon rank-sum test. SynTrackerVis v1.0.8 was used to generate synteny plots (https://github.com/leylabmpi/SynTrackerVis/).

Cophylogeny analysis

The congruence between human host phylogeny and *M. smithii* strain phylogeny, was assessed using a Procrustean Approach to Cophylogeny (PACo) from the paco v0.4.2 R package[103]. The host phylogeny was based on genome-wide SNP distances from human stool donors, while the *M. smithii* phylogeny was derived from a core gene alignment of 202 single-copy marker genes from isolated strains. A binary association matrix was constructed based on 1:1 or 1:many mappings between human donors and their corresponding *M. smithii* isolates. Pairwise patristic distances were calculated using the cophenetic.phylo() function from the ape v5.8-1 package[104]. PACo was run using Cailliez correction for negative eigenvalues, and significance was assessed using 1000 permutations. PACo residuals were extracted to evaluate variation in phylogenetic congruence across geographic regions (Gabon, Germany, Vietnam), followed by non-parametric statistical tests.

Lipid quantification

Sample preparation. Representative methanogen strains with comparable genome sizes were selected from the three countries (Gabon, Germany, and Vietnam). Cultures were grown to mid-log phase in 50 ml ME media under anaerobic conditions. Cells were harvested by centrifugation at 4,000 × *g* for 10 min, and the supernatant was discarded. The pellets were washed 3–5 times with 10 ml PBS, each time resuspending the cells and centrifuging at 4,000 × *g* for 10 min. After the final wash, cells were suspended in 2 ml PBS and transferred to pre-weighed 2 ml tubes. From each sample, 1.8 ml was used for lipid analysis. Excess PBS was removed, and pellets were stored at -80 °C until extraction.

Lipid extraction, analysis, and quality control. Lyophilized cell pellets were extracted using a butanol:methanol (45:40:15 v/v) mixture. Internal standards were included to ensure quantification accuracy, consisting of Trp-13C11, 15:0-18:1-d7-PI, 18:1-d7 Lyso-PC, and 14:0-16:1-14:0-D5-TG at a final concentration of 0.3 µg/ml. The extraction solvent was prepared by

mixing 69.9 ml butanol/methanol (1:1) with 92.4 µL of the internal standard mix. The extraction volume was adjusted to 1 ml per 10 mg of dried cells. The cell suspension was vortexed thoroughly, incubated on a shaker for 1 hour, and sonicated for 10 min at 40 °C. Following sonication, samples were centrifuged at 13,000 × *g* for 15 min, and the supernatant was carefully transferred to autosampler vials.

LC-MS/MS. LC-MS/MS analysis was performed following the method described by Barone et al. 2024[105]. Samples were analysed using both negative and positive ionization modes, with injection volumes of 40 µL (negative mode) and 20 µL (positive mode). Separation was performed using a C-18 column (150 mm × 3 mm) with mobile phases: Solvent A: water + 0.1 % formic acid. Solvent B: acetonitrile + 0.1 % formic acid. The flow rate was 0.6 ml/min, and lipid detection was performed in a mass range of 200–600 m/z with data-dependent acquisition at 2 Hz frequency and fragmentation energy of 30–40 eV. A calibration curve was generated using lipid standard mixtures at concentrations ranging from 0.1 to 10 µg/ml. A pooled quality control (QC) sample was prepared by mixing aliquots from all experimental samples. QC samples were analysed every 10 injections to monitor instrument performance. Blank samples (solvent only) were included to detect background contamination. Quantification was performed using Compass Data Analysis (Bruker, v5.2) and Skyline (MacCoss Lab Software), normalizing lipid intensities to internal standards to account for sample-to-sample variability.

Statistical analyses. Statistical analyses were performed using R v4 with packages including stats, epitools, ggplot2, and dplyr. Species distribution across geographic locations was assessed using Pearson's chi-square test of independence, with Fisher's exact test applied as a more robust alternative given some low cell counts. *Post hoc* analysis employed standardized residuals to identify significant deviations from expected frequencies, with values exceeding 1.96 considered statistically significant. Pairwise comparisons between regions were conducted using two-sample proportion tests with continuity correction to evaluate specific geographic differences in species prevalence. ORs with 95 % confidence intervals were calculated to quantify the likelihood of isolating specific methanogen species across geographic locations, with appropriate modifications applied for zero-count cells. Statistical significance was established at $p < 0.05$ for all analyses. Data visualization included stacked bar charts and mosaic plots to illustrate species distribution patterns. All statistical outputs, including contingency tables, test results, and

visualizations, were systematically documented and stored in a dedicated directory to ensure reproducibility of findings.

5.6. Acknowledgements

We are grateful to the field research team and laboratory personnel of CERMEL-Gabon and members of the Department of Microbiome Science at the MPI for Biology, in particular Silke Dauser, Sophie Maisch and Stephen Loum, for technical support. We also thank Victor Schmidt and Liam Fitzstevens for their contribution to population-scale sampling, sample processing, DNA extractions, and metagenomic sequencing. This work was funded by the Max Planck Society.

5.7. Author Contributions

M.M.N., N.D.Y., A.T., R.E.L., and J.W.M. contributed to conceptualization, methodology, writing the original draft, and visualization. M.M.N., A.T., and J.W.M. performed metagenome profiling. S.L.H. and D.L.V. conducted lipid profiling. M.M.N. and L.B. analysed growth curves. M.M.N., N.D.Y., and J.W.M. performed sequence processing and genome assemblies. M.M.N., H.E., I.P., and J.W.M. conducted strain comparisons and pangenomics. M.M.N., S.L., L.B., and J.P.K. performed strain cultivation. J.C.D.-A., J.F.Z., B.R.A., J.L.F., V.T.S., A.A.A., and M.M.N. conducted field investigations. M.M.N. performed sample processing and data curation. N.D.Y., A.T., R.E.L., and J.W.M. supervised the research. P.G.K. and R.E.L. acquired funding.

Competing Interest Statement

The authors declare that there are no conflicts of interest related to this work

Sequencing Data

All sequencing data associated with these isolates are currently being deposited at NCBI.

5.8. *Data Availability*

The raw metagenomic sequencing data used in this study are available from the European Nucleotide Archive (ENA) under the accession numbers PRJEB46788 and PRJEB93776. Sequencing data from unique cultured strains have been deposited in the ENA under accession number PRJEB93776. The raw mass spectrometry data are available at: https://massive.ucsd.edu/ProteoSAFe/private-dataset.jsp?task=16b6b117e185482db397b160c6bc9a5f

Code Availability

No custom software or novel code was generated for this study. All R notebooks used for data processing and analysis are publicly available in the github repository: https://github.com/leylabmpi/global-methanogen-strain-diversity

Supplementary Data Table Captions

Supplementary Table 1. Population-level prevalence and relative abundance of Methanobacteriota species in adults and infants. For each species, prevalence (percentage of individuals carrying the species) and mean and median relative abundance were calculated at the population level for adult and infant cohorts, with samples originating from Gabon, Germany, and Vietnam.

Supplementary Table 2. Linear regression models evaluating associations between methanogen abundance and gut microbial diversity. Summary of regression coefficients, standard errors, confidence intervals, and *p*-values for models assessing the relationship between *M. smithii* and *M. intestini* relative abundances and Shannon diversity. Results are shown for the combined dataset (adults + infants) and for age-stratified models (adults only and infants only).

Supplementary Table 3. Genome assembly statistics for all isolates sequenced in this study.

Supplementary Table 4. Relative synonymous codon usage (RSCU) values for each codon for all *M. smithii* and *M. intestini* assemblies**.**

Supplementary Table 5. Genome assembly statistics for additional methanogen MAGs used in this study.

Supplementary Table 6. KEGG and COG20 functional annotations of genes significantly enriched in *M. smithii* or *M. intestini* including enrichment scores and Benjamini-Hochberg-adjusted *p*-values**.**

Supplementary Table 7. Tajima's D estimates of core genes under positive, negative, or neutral selection**.**

Supplementary Table 8. Genome assembly statistics for additional publicly available high-quality assemblies of *M. intestini* derived from Western locations**.**

Supplementary Table 9. Quantified archaeal lipids detected across samples, including lipid names, chemical classes, ionization modes, and intensity values**.**

Extended Data Figures

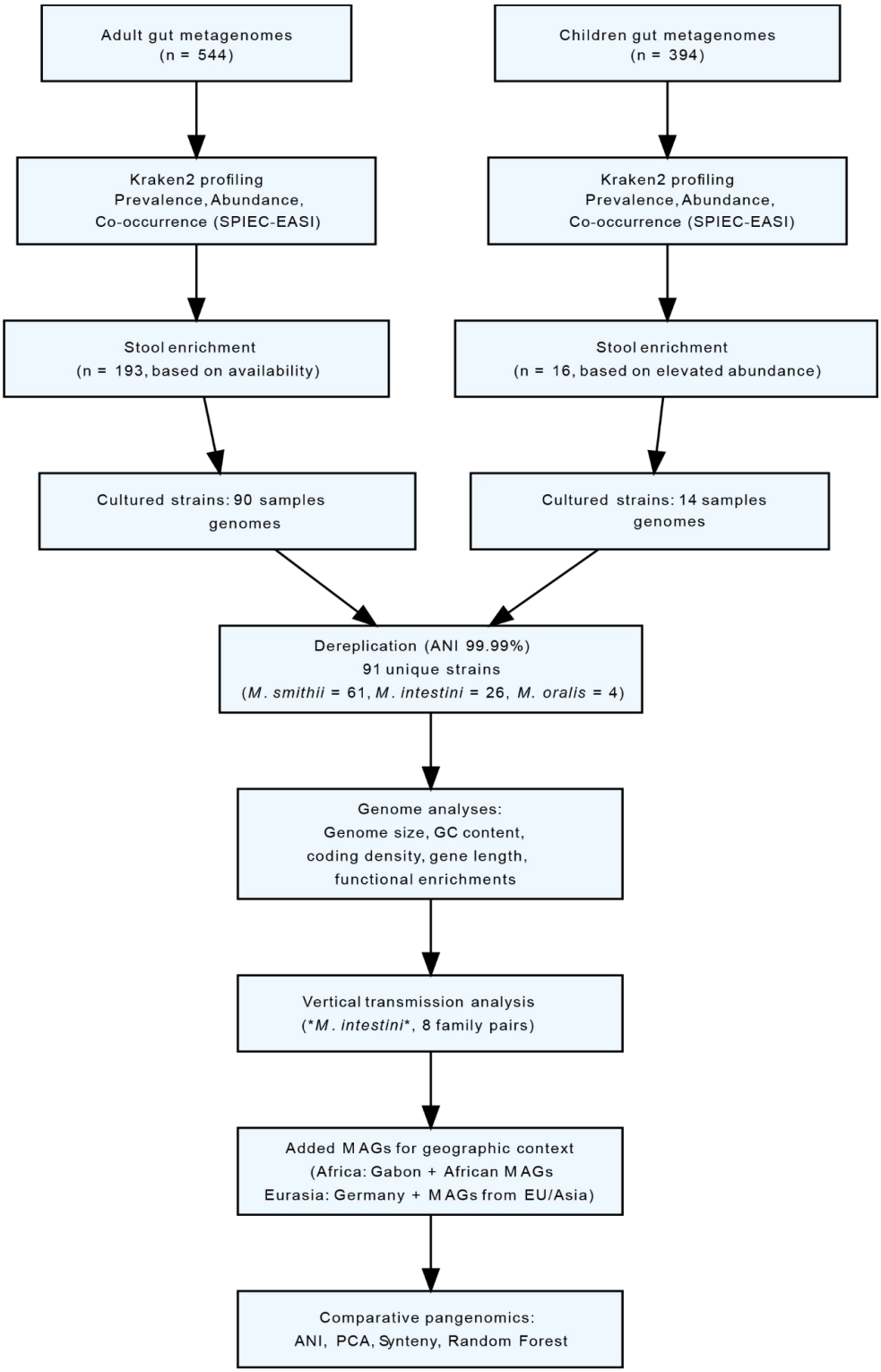
Adult gut metagenomes
(n = 544)
Children gut metagenomes
(n = 394)
Kraken2 profiling
Prevalence, Abundance,
Co-occurrence (SPIEC-EASI)
Kraken2 profiling
Prevalence, Abundance,
Co-occurrence (SPIEC-EASI)
Stool enrichment
(n = 193, based on availability)
Stool enrichment
(n = 16, based on elevated abundance)
Cultured strains: 90 samples
genomes
Cultured strains: 14 samples
genomes
Dereplication (ANI 99.99%)
91 unique strains
(M. smithii = 61, M. intestini = 26, M. oralis = 4)
Genome analyses:
Genome size, GC content,
coding density, gene length,
functional enrichments
Vertical transmission analysis
(*M. intestini*, 8 family pairs)
Added MAGs for geographic context
(Africa: Gabon + African MAGs
Eurasia: Germany + MAGs from EU/Asia)
Comparative pangenomics:
ANI, PCA, Synteny, Random Forest

Extended Data Fig. 1. Pipeline of sample collection, processing, methanogen enrichment, isolation, and sequencing.

Metagenomic profiling of adult and infant stool samples was followed by targeted culturing and dereplication of methanogen strains. Cultured genomes and publicly available MAGs were used for comparative genomic and pangenome analyses.

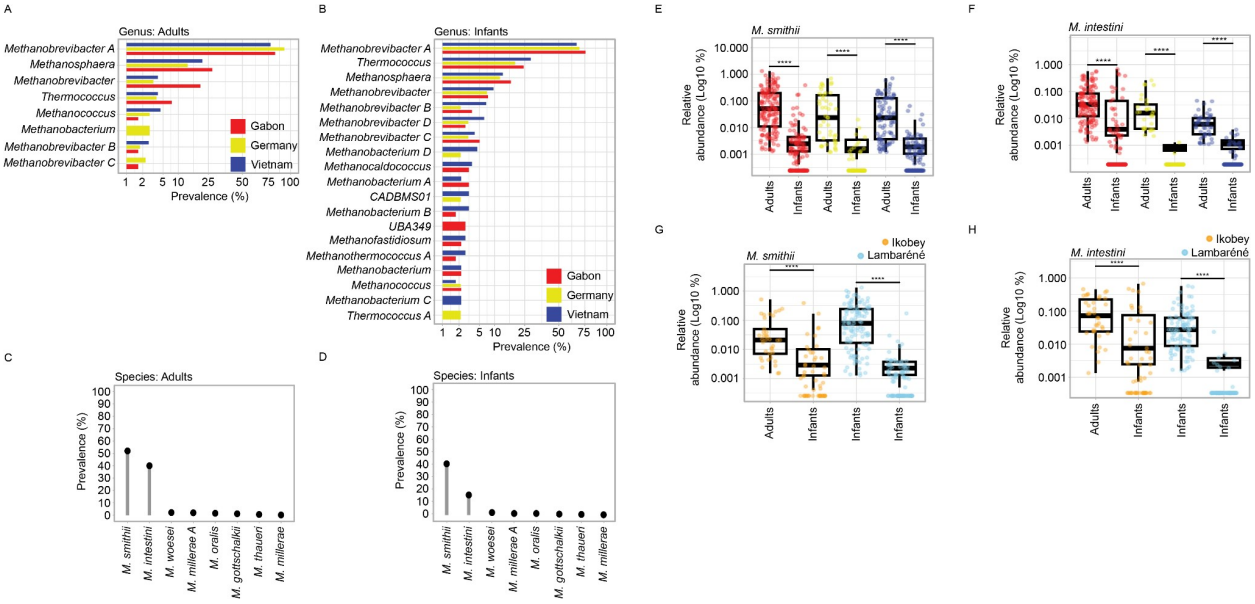

Extended Data Fig. 2. Expanded prevalence and abundance analyses of methanogen genera and *Methanobrevibacter_A* species across populations.

A–B. Genus-level prevalence of methanogens within the phylum *Methanobacteriota* in adult (**A**) and infant (**B**) gut metagenomes from Gabon (red), Germany (yellow), and Vietnam (blue). **C–D.** Species-level prevalence of *Methanobrevibacter_A* spp. across adult (**C**) and infant (**D**) samples. **E–F.** Relative abundances of *M. smithii* (**E**) and *M. intestini* (**F**) in adults and infants across Gabon, Germany, and Vietnam. **G–H.** Relative abundances of *M. smithii* (**G**) and *M. intestini* (**H**) in adults and infants from the two Gabonese populations: Ikobey (rural, orange) and Lambaréné (semi-urban, sky blue). Boxplots show log-transformed abundances. Statistical comparisons were performed using Wilcoxon tests (ns = not significant; * $P < 0.05$, ** $P < 0.01$, *** $P < 0.001$, **** $P < 0.0001$).

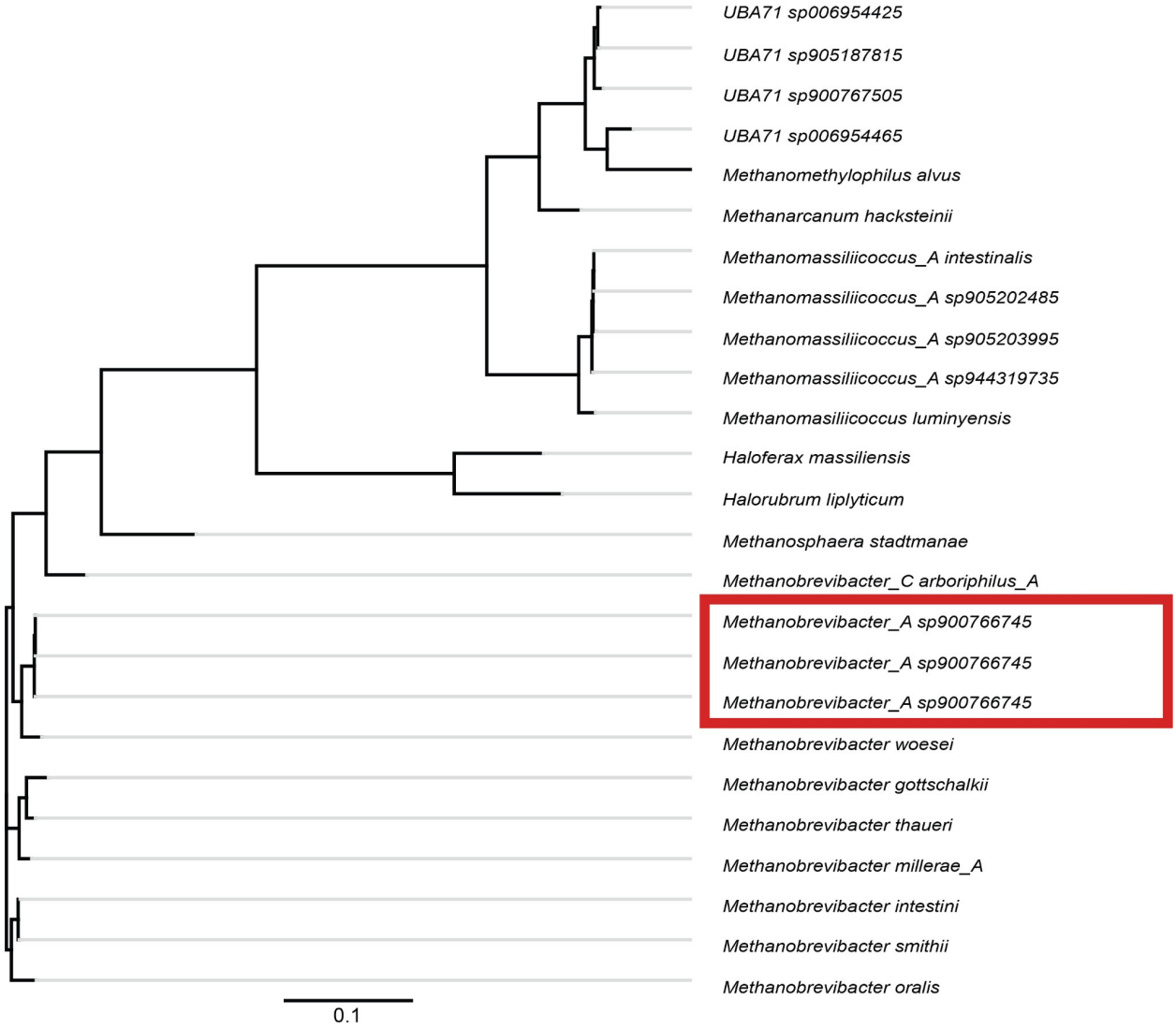

Extended Data Fig. 3. Phylogenetic placement of a putative novel methanogen across countries and age groups.

16S rRNA gene Maximum Likelihood phylogenetic tree including representative archaeal taxa previously detected in the human gut and three assemblies corresponding to the provisional taxon *Methanobrevibacter_A sp900766745* (GTDB r202; *Methanocatella sp900766745* in r226). The red rectangle highlights the clade containing *sp900766745* in relation to *M. smithii* and *M. intestini*.

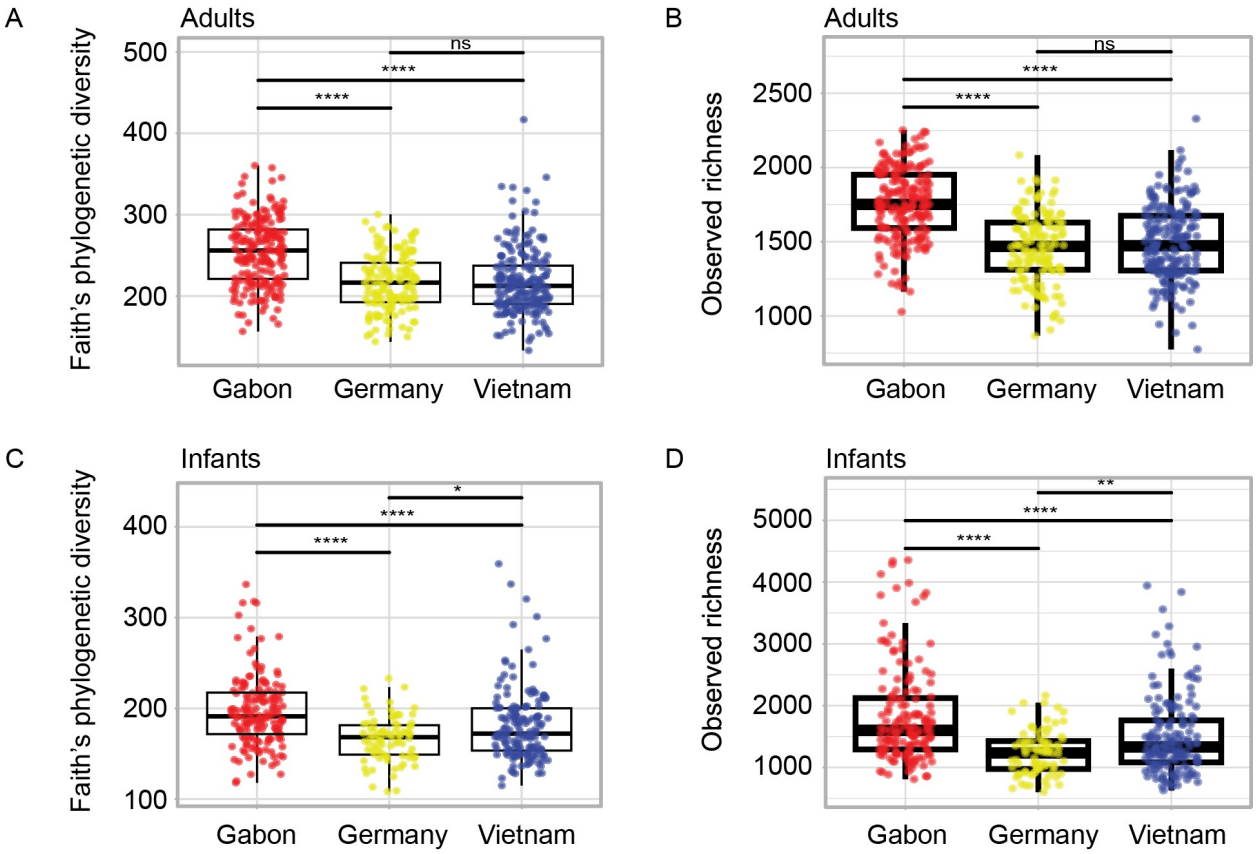

Extended Data Fig. 4. Alternative microbiome alpha diversity metrics across countries and age groups.
A–B. Alpha diversity of adult gut microbiomes measured by Faith's phylogenetic diversity (PD; **A**) and observed species richness (**B**) across Gabon (red), Germany (yellow), and Vietnam (blue). **C–D.** Corresponding alpha diversity measures in infant gut microbiomes: Faith's PD (**C**) and observed species richness (**D**). Boxplots show medians and interquartile ranges, with individual samples displayed as jittered points. Pairwise Wilcoxon rank-sum tests were performed between countries (Gabon vs. Germany, Gabon vs. Vietnam, and Germany vs. Vietnam); significance levels indicate FDR-adjusted P values (ns = not significant; * $P < 0.05$, ** $P < 0.01$, *** $P < 0.001$, **** $P < 0.0001$).

5.9. References

1. Borrel, G., Brugère, J.-F., Gribaldo, S., Schmitz, R. A. & Moissl-Eichinger, C. The host-associated archaeome. *Nat. Rev. Microbiol.* **18**, 622–636 (2020).

2. Borrel, G. *et al.* Genomics and metagenomics of trimethylamine-utilizing Archaea in the human gut microbiome. *ISME J.* **11**, 2059–2074 (2017).

3. Dridi, B., Henry, M., El Khéchine, A., Raoult, D. & Drancourt, M. High prevalence of *Methanobrevibacter smithii* and *Methanosphaera stadtmanae* detected in the human gut using an improved DNA detection protocol. *PLoS One* **4**, e7063 (2009).

4. Hoegenauer, C., Hammer, H. F., Mahnert, A. & Moissl-Eichinger, C. Methanogenic archaea in the human gastrointestinal tract. *Nat. Rev. Gastroenterol. Hepatol.* **19**, 805–813 (2022).

5. Suzuki, T. A. *et al.* Codiversification of gut microbiota with humans. *Science* **377**, 1328–1332 (2022).

6. Wibowo, M. C. *et al.* Reconstruction of ancient microbial genomes from the human gut. *Nature* **594**, 234–239 (2021).

7. Morii H., Oda K., Suenaga Y. & Nakamura T. Low methane concentration in the breath of Japanese. *J. UOEH* **25**, 397–407 (2003).

8. Sereme, Y. *et al.* Meconial *Methanobrevibacter smithii* suggests intrauterine methanogen colonization in preterm neonates. *Curr. Res. Microb. Sci.* **2**, 100034 (2021).

9. Thauer, R. K. & Shima, S. Biogeochemistry: methane and microbes: Biogeochemistry. *Nature* **440**, 878–879 (2006).

10. Abell, G. C. J., Conlon, M. A. & McOrist, A. L. Methanogenic archaea in adult human faecal samples are inversely related to butyrate concentration. *Microb. Ecol. Health Dis.* **18**, 154–160 (2006).

11. Berghuis, B. A. *et al.* Hydrogenotrophic methanogenesis in archaeal phylum Verstraetearchaeota reveals the shared ancestry of all methanogens. *Proc. Natl. Acad. Sci. U. S. A.* **116**, 5037–5044 (2019).

12. Dirks, B. *et al.* Methanogenesis associated with altered microbial production of short-chain fatty acids and human-host metabolizable energy. *ISME J.* **19**, (2025).

13. Djemai, K., Drancourt, M. & Tidjani Alou, M. Bacteria and methanogens in the human microbiome: A review of syntrophic interactions. *Microb. Ecol.* **83**, 536–554 (2022).

14. Fricke, W. F. *et al.* The genome sequence of *Methanosphaera stadtmanae* reveals why this human intestinal archaeon is restricted to methanol and H2 for methane formation and ATP synthesis. *J. Bacteriol.* **188**, 642–658 (2006).

15. Catlett, J. L. *et al.* Metabolic synergy between human symbionts Bacteroides and *Methanobrevibacter*. *Microbiol. Spectr.* **10**, e0106722 (2022).

16. Bai, X. *et al.* Landscape of the gut archaeome in association with geography, ethnicity, urbanization, and diet in the Chinese population. *Microbiome* **10**, 147 (2022).

17. Ruaud, A. *et al.* Syntrophy via Interspecies H2 transfer between Christensenella and *Methanobrevibacter* underlies their global cooccurrence in the human gut. *MBio* **11**, e03235–19 (2020).

18. Hudson, M. J., Tomkins, A. M., Wiggins, H. S. & Drasar, B. S. Breath methane excretion and intestinal methanogenesis in children and adults in rural Nigeria. *Scand. J. Gastroenterol.* **28**, 993–998 (1993).

19. Hansen, E. E. *et al.* Pan-genome of the dominant human gut-associated archaeon, *Methanobrevibacter* smithii, studied in twins. *Proc. Natl. Acad. Sci. U. S. A.* **108 Suppl 1**, 4599–4606 (2011).

20. Nava, G. M. *et al.* Hydrogenotrophic microbiota distinguish native Africans from African and European Americans: Diet and colonic hydrogenotrophs. *Environ. Microbiol. Rep.* **4**, 307–315 (2012).

21. Mohammadzadeh, R. *et al.* Age-related dynamics of predominant methanogenic archaea in the human gut microbiome. *BMC Microbiol.* **25**, 193 (2025).

22. Chibani, C. M. *et al.* A catalogue of 1,167 genomes from the human gut archaeome. *Nat. Microbiol.* **7**, 48–61 (2022).

23. Parks, D. H. *et al.* GTDB: an ongoing census of bacterial and archaeal diversity through a phylogenetically consistent, rank normalized and complete genome-based taxonomy. *Nucleic Acids Res.* **50**, D785–D794 (2022).

24. Weinberger, V. *et al.* Expanding the cultivable human archaeome: *Methanobrevibacter* intestini sp. nov. and strain *Methanobrevibacter smithii* 'GRAZ-2' from human faeces. *Int. J. Syst. Evol. Microbiol.* **75**, 006751 (2025).

25. Duller, S. *et al.* Targeted isolation of *Methanobrevibacter* strains from fecal samples expands the cultivated human archaeome. *Nat. Commun.* **15**, 7593 (2024).

26. Low, A. *et al.* Mutual exclusion of *Methanobrevibacter* species in the human gut Microbiota facilitates directed cultivation of a Candidatus *Methanobrevibacter* intestini representative. *Microbiol. Spectr.* **10**, e00849–22 (2022).

27. Baquero, D. P. *et al.* Biogenesis of DNA-carrying extracellular vesicles by the dominant human gut methanogenic archaeon. *Nat. Commun.* **16**, 5093 (2025).

28. Weinberger, V. *et al.* Proteomic and metabolomic profiling of extracellular vesicles produced by human gut archaea. *Nat. Commun.* **16**, 5094 (2025).

29. Almeida, A. *et al.* A unified catalog of 204,938 reference genomes from the human gut microbiome. *Nat. Biotechnol.* **39**, 105–114 (2021).

30. Blake, K. S. Missing microbiomes: global underrepresentation restricts who research will benefit. *J. Clin. Invest.* **134**, e183884 (2024).

31. Abdill, R. J. *et al.* Integration of 168,000 samples reveals global patterns of the human gut microbiome. *Cell* **188**, 1100–1118.e17 (2025).

32. Maghini, D. G. *et al.* Expanding the human gut microbiome atlas of Africa. *Nature* **638**, 718–728 (2025).

33. Suárez-Martínez, C., Santaella-Pascual, M., Yagüe-Guirao, G. & Martínez-Graciá, C. Infant gut microbiota colonization: influence of prenatal and postnatal factors, focusing on diet. *Front. Microbiol.* **14**, 1236254 (2023).

34. Candeliere, F., Sola, L., Raimondi, S., Rossi, M. & Amaretti, A. Good and bad dispositions between archaea and bacteria in the human gut: new insights from metagenomic survey and co-occurrence analysis. *Synth. Syst. Biotechnol.* **9**, 88–98 (2024).

35. Li, T. *et al.* Multi-cohort analysis reveals altered Archaea in colorectal cancer fecal samples across populations. *Gastroenterology* **168**, 525–538.e2 (2025).

36. Woh, P. Y. *et al.* Reevaluation of the gastrointestinal methanogenic archaeome in multiple sclerosis and its association with treatment. *Microbiol. Spectr.* **13**, e0218324 (2025).

37. Wang, T. *et al.* Methanogen levels are significantly associated with fecal Microbiota composition and alpha diversity in healthy adults and irritable bowel syndrome patients. *Microbiol. Spectr.* **10**, e0165322 (2022).

38. Pilliol, V. *et al.* Culturing clinical *Methanobrevibacter smithii* using GG medium in a minimal anaerobe atmosphere. *J. Microbiol. Methods* **207**, 106704 (2023).

39. Niu, F.-X., Lu, Q., Bu, Y.-F. & Liu, J.-Z. Metabolic engineering for the microbial production of isoprenoids: Carotenoids and isoprenoid-based biofuels. *Synth. Syst. Biotechnol.* **2**, 167–175 (2017).

40. Wyllie, J. A., McKay, M. V., Barrow, A. S. & Soares da Costa, T. P. Biosynthesis of uridine diphosphate N-Acetylglucosamine: An underexploited pathway in the search for novel antibiotics? *IUBMB Life* **74**, 1232–1252 (2022).

41. Yasueda, H., Kawahara, Y. & Sugimoto, S. Bacillus subtilis yckG and yckF encode two key enzymes of the ribulose monophosphate pathway used by methylotrophs, and yckH is required for their expression. *J. Bacteriol.* **181**, 7154–7160 (1999).

42. Cellini, B. *et al.* Pyridoxal 5'-phosphate-dependent enzymes at the Crossroads of host-microbe tryptophan metabolism. *Int. J. Mol. Sci.* **21**, 5823 (2020).

43. Enav, H., Paz, I. & Ley, R. E. Strain tracking in complex microbiomes using synteny analysis reveals per-species modes of evolution. *Nat. Biotechnol.* **43**, 773–783 (2025).

44. Torrance, E. L., Diop, A. & Bobay, L.-M. Homologous recombination shapes the architecture and evolution of bacterial genomes. *Nucleic Acids Res.* **53**, (2025).

45. Li, B., Steindel, P., Haddad, N. & Elliott, S. J. Maximizing (electro)catalytic CO2 reduction with a ferredoxin-based reduction potential gradient. *ACS Catal.* **11**, 4009–4023 (2021).

46. Rodionov, D. A., Vitreschak, A. G., Mironov, A. A. & Gelfand, M. S. Comparative genomics of the vitamin B12 metabolism and regulation in prokaryotes. *J. Biol. Chem.* **278**, 41148 –41159 (2003).

47. Leggio, L. L., Degan, F. D., Poulsen, P., Andersen, S. M. & Larsen, S. The structure and specificity of Escherichia coli maltose acetyltransferase give new insight into the LacA family of acyltransferases. *Biochemistry* **42**, 5225–5235 (2003).

48. Gupta, A. B. & Seedorf, H. Structural and functional insights from the sequences and complex domain architecture of adhesin-like proteins from *Methanobrevibacter smithii* and *Methanosphaera stadtmanae*. *Front. Microbiol.* **15**, 1463715 (2024).

49. Reese, A. T. *et al.* Effects of domestication on the gut microbiota parallel those of human industrialization. *Elife* **10**, e60197 (2021).

50. Stewart, J. A., Chadwick, V. S. & Murray, A. Carriage, quantification, and predominance of methanogens and sulfate-reducing bacteria in faecal samples. *Lett. Appl. Microbiol.* **43**, 58–63 (2006).

51. Tian, C. *et al.* Industrialization drives the gut microbiome and resistome of the Chinese populations. *mSystems* **10**, e01372–24 (3 2025).

52. Weaver, G. A., Krause, J. A., Miller, T. L. & Wolin, M. J. Incidence of methanogenic bacteria in a sigmoidoscopy population: an association of methanogenic bacteria and diverticulosis. *Gut* **27**, 698–704 (1986).

53. Mntambo, N., Arumugam, T., Pramchand, A., Pillay, K. & Ramsuran, V. A review of global patterns in gut Microbiota composition, health and disease: Locating South Africa in the conversation. *Microorganisms* **13**, 2831 (2025).

54. Murga-Garrido, S. M. *et al.* Alterations of the gut microbiome associated to methane metabolism in Mexican children with obesity. *Children (Basel)* **9**, 148 (2022).

55. Ou, J. *et al.* Diet, microbiota, and microbial metabolites in colon cancer risk in rural Africans and African Americans 1 , 2 , 3 , 4. *Am. J. Clin. Nutr.* **98**, 111–120 (2013).

56. Vu, L. H. & Nguyen, A. N. The nutrition transition in Vietnam: evidence from national household survey data 2012–2020. *Crit. Public Health* **36**, (2026).

57. Corbin, K. D. *et al.* Host-diet-gut microbiome interactions influence human energy balance: a randomized clinical trial. *Nat. Commun.* **14**, 3161 (2023).

58. Lokmer, A. *et al.* Response of the human gut and saliva microbiome to urbanization in Cameroon. *Sci. Rep.* **10**, 2856 (2020).

59. Hoffmann, C. *et al.* Archaea and fungi of the human gut microbiome: correlations with diet and bacterial residents. *PLoS One* **8**, e66019 (2013).

60. Mihajlovski, A., Doré, J., Levenez, F., Alric, M. & Brugère, J.-F. Molecular evaluation of the human gut methanogenic archaeal microbiota reveals an age-associated increase of the diversity. *Environ. Microbiol. Rep.* **2**, 272–280 (2010).

61. Vanderhaeghen, S., Lacroix, C. & Schwab, C. Methanogen communities in stools of humans of different age and health status and co-occurrence with bacteria. *FEMS Microbiol. Lett.* **362**, fnv092 (2015).

62. Neumann, C. J. *et al.* First-year dynamics of the anaerobic microbiome and archaeome in infants' oral and gastrointestinal systems. *mSystems* **10**, e0107124 (2025).

63. Polag, D., Leiß, O. & Keppler, F. Age dependent breath methane in the German population. *Sci. Total Environ.* **481**, 582–587 (2014).

64. van de Pol, J. A. A. *et al.* Gut Colonization by Methanogenic Archaea Is Associated with Organic Dairy Consumption in Children. *Front. Microbiol.* **8**, 355 (2017).

65. Hildebrand, F. *et al.* Dispersal strategies shape persistence and evolution of human gut bacteria. *Cell Host Microbe* **29**, 1167–1176.e9 (2021).

66. Ragsdale, S. W. & Pierce, E. Acetogenesis and the Wood-Ljungdahl pathway of CO(2) fixation. *Biochim. Biophys. Acta* **1784**, 1873–1898 (2008).

67. Dar, S. A., Kleerebezem, R., Stams, A. J. M., Kuenen, J. G. & Muyzer, G. Competition and coexistence of sulfate-reducing bacteria, acetogens and methanogens in a lab-scale anaerobic bioreactor as affected by changing substrate to sulfate ratio. *Appl. Microbiol. Biotechnol.* **78**, 1045 –1055 (2008).

68. Rodionov, D. A. *et al.* Micronutrient requirements and sharing capabilities of the human gut microbiome. *Front. Microbiol.* **10**, 1316 (2019).

69. Bui, T. P. N. *et al.* Mutual metabolic interactions in co-cultures of the intestinal Anaerostipes rhamnosivorans with an acetogen, methanogen, or pectin-degrader affecting butyrate production. *Front. Microbiol.* **10**, 2449 (2019).

70. Saengkerdsub, S. & Ricke, S. C. Ecology and characteristics of methanogenic archaea in animals and humans. *Crit. Rev. Microbiol.* **40**, 97–116 (2014).

71. Samuel, B. S. *et al.* Genomic and metabolic adaptations of *Methanobrevibacter smithii* to the human gut. *Proc. Natl. Acad. Sci. U. S. A.* **104**, 10643–10648 (2007).

72. Poehlein, A., Schneider, D., Soh, M., Daniel, R. & Seedorf, H. Comparative genomic analysis of members of the genera Methanosphaera and *Methanobrevibacter* reveals distinct clades with specific potential metabolic functions. *Archaea* **2018**, 1–9 (2018).

73. Volmer, J. G., McRae, H. & Morrison, M. The evolving role of methanogenic archaea in mammalian microbiomes. *Front. Microbiol.* **14**, 1268451 (2023).

74. Deschamps, M. *et al.* Genomic signatures of selective pressures and introgression from archaic hominins at human innate immunity genes. *Am. J. Hum. Genet.* **98**, 5–21 (2016).

75. Gupta, V. K., Paul, S. & Dutta, C. Geography, ethnicity or subsistence-specific variations in human microbiome composition and diversity. *Front. Microbiol.* **8**, 1162 (2017).

76. Zhang, Y., Rump, S. & Gladyshev, V. N. Comparative genomics and evolution of molybdenum utilization. *Coord. Chem. Rev.* **255**, 1206–1217 (2011).

77. Degnan, P. H., Taga, M. E. & Goodman, A. L. Vitamin B12 as a modulator of gut microbial ecology. *Cell Metab.* **20**, 769–778 (2014).

78. Lei, C., Wang, T., Wang, J., Tan, Y. & Deng, Z. Commensal bacterial glycosylation at the interface of host-bacteria interactions. *Gut Microbes* **17**, 2545421 (2025).

79. Maldonado-Gomez, M. X. *et al.* A diverse set of solubilized natural fibers drives structure-dependent metabolism and modulation of the human gut microbiota. *MBio* **16**, e0047025 (2025).

80. Chugunov, A. O., Volynsky, P. E., Krylov, N. A., Boldyrev, I. A. & Efremov, R. G. Liquid but durable: molecular dynamics simulations explain the unique properties of archaeal-like membranes. *Sci. Rep.* **4**, 7462 (2014).

81. Łapińska, U. *et al.* Systematic comparison of unilamellar vesicles reveals that archaeal core lipid membranes are more permeable than bacterial membranes. *PLoS Biol.* **21**, e3002048 (2023).

82. Ewels, P., Magnusson, M., Lundin, S. & Käller, M. MultiQC: summarize analysis results for multiple tools and samples in a single report. *Bioinformatics* **32**, 3047–3048 (2016).

83. Chklovski, A., Parks, D. H., Woodcroft, B. J. & Tyson, G. W. CheckM2: a rapid, scalable and accurate tool for assessing microbial genome quality using machine learning. *Nat. Methods* **20**, 1203–1212 (2023).

84. Chaumeil, P.-A., Mussig, A. J., Hugenholtz, P. & Parks, D. H. GTDB-Tk v2: memory friendly classification with the genome taxonomy database. *Bioinformatics* **38**, 5315–5316 (2022).

85. Seemann, T. Prokka: rapid prokaryotic genome annotation. *Bioinformatics* **30**, 2068–2069 (2014).

86. Jain, C., Rodriguez-R, L. M., Phillippy, A. M., Konstantinidis, K. T. & Aluru, S. High throughput ANI analysis of 90K prokaryotic genomes reveals clear species boundaries. *Nat. Commun.* **9**, 5114 (2018).

87. Cantalapiedra, C. P., Hernández-Plaza, A., Letunic, I., Bork, P. & Huerta-Cepas, J. eggNOG-mapper v2: functional annotation, orthology assignments, and domain prediction at the metagenomic scale. *Mol. Biol. Evol.* **38**, 5825–5829 (2021).

88. Geller-McGrath, D. *et al.* Predicting metabolic modules in incomplete bacterial genomes with MetaPathPredict. *Elife* **13**, e85749 (2024).

89. Price, M. N., Deutschbauer, A. M. & Arkin, A. P. GapMind: automated annotation of amino acid biosynthesis. *mSystems* **5**, e00291–20 (2020).

90. Weimann Aaron *et al.* From Genomes to Phenotypes: Traitar, the Microbial Trait Analyzer. *mSystems* **1**, 10.1128/msystems.00101–16 (2016).

91. Blin, K. *et al.* antiSMASH 7.0: new and improved predictions for detection, regulation, chemical structures and visualisation. *Nucleic Acids Res.* **51**, W46–W50 (2023).

92. Navarro-Muñoz, J. C. *et al.* A computational framework to explore large-scale biosynthetic diversity. *Nat. Chem. Biol.* **16**, 60–68 (2020).

93. Wood, D. E., Lu, J. & Langmead, B. Improved metagenomic analysis with Kraken 2. *Genome Biol.* **20**, 257 (2019).

94. Lu, J., Breitwieser, F. P., Thielen, P. & Salzberg, S. L. Bracken: estimating species abundance in metagenomics data. *PeerJ Comput. Sci.* **3**, e104 (2017).

95. Kurtz, Z. D. *et al.* Sparse and compositionally robust inference of microbial ecological networks. *PLoS Comput. Biol.* **11**, e1004226 (2015).

96. Hyatt, D. *et al.* Prodigal: prokaryotic gene recognition and translation initiation site identification. *BMC Bioinformatics* **11**, 119 (2010).

97. Kalyaanamoorthy, S., Minh, B. Q., Wong, T. K. F., von Haeseler, A. & Jermiin, L. S. ModelFinder: fast model selection for accurate phylogenetic estimates. *Nat. Methods* **14**, 587–589 (2017).

98. Page, A. J. *et al.* Roary: rapid large-scale prokaryote pan genome analysis. *Bioinformatics* **31**, 3691–3693 (2015).

99. Paradis, E. pegas: an R package for population genetics with an integrated-modular approach. *Bioinformatics* **26**, 419–420 (2010).

100. Tonkin-Hill, G., Lees, J. A., Bentley, S. D., Frost, S. D. W. & Corander, J. RhierBAPS: An R implementation of the population clustering algorithm hierBAPS. *Wellcome Open Res.* **3**, 93 (2018).

101. Schliep, K. P. phangorn: phylogenetic analysis in R. *Bioinformatics* **27**, 592–593 (2011).

102. Yu, G., Smith, D. K., Zhu, H., Guan, Y. & Lam, T. T.-Y. Ggtree: an r package for visualization and annotation of phylogenetic trees with their covariates and other associated data. *Methods Ecol. Evol.* **8**, 28–36 (2017).

103. Balbuena, J. A., Míguez-Lozano, R. & Blasco-Costa, I. PACo: a novel procrustes application to cophylogenetic analysis. *PLoS ONE* vol. 8 e61048 Preprint at https://doi.org/10.1371/journal.pone.0061048 (2013).

104. Paradis, E. & Schliep, K. ape 5.0: an environment for modern phylogenetics and evolutionary analyses in R. *Bioinformatics* **35**, 526–528 (2019).

105. Mirretta Barone, C. *et al.* Spatially resolved lipidomics shows conditional transfer of lipids produced by Bacteroides thetaiotaomicron into the mouse gut. *Cell Host Microbe* **32**, 1025–1036.e5 (2024).

Chapter 6. General Discussion and Perspectives

6.1. Integrative overview.

This thesis set out to investigate the ecological and evolutionary forces that shape the human gut microbiome, with a particular focus on parasite–microbiome interactions and the diversity, distribution, and adaptation of methanogenic archaea. The work presented here draws on three interlinked chapters. Chapter 2 combined qPCR detection of STH parasites with metagenomic analyses and network inference, while chapters 4 and 5 described cultivation-based methods and comparative genomics of *Methanobrevibacter* to elaborate on the microbial processes that shape methanogen diversity and evolution across different populations. The key finding of this body of work is that the ecological context is crucial in microbiome studies. Across the studies and datasets described here, Geography, lifestyle, and local transmission dynamics usually explained more variation than individual-level factors such as age or household clustering. This context-dependence showed in both the links between STH infections and the microbiome and in the distribution of methanogens across populations. By focusing on populations rarely included in microbiome studies, the thesis underscores the importance of more globally inclusive sampling and of adopting a multi-layer perspective to connect microbial ecology with geography.

6.2. Parasitic infections as ecological and methodological modulators (Chapter 2).

In Chapter 2, I established a proof-of-concept for detecting STH directly from untargeted shotgun metagenomic sequence data. I showed that from such sequence data, signals from bacterial, archaeal, and eukaryotic parasites can be retrieved and quantified without the need for additional diagnostics, such as PCR or microscopy, for STH parasites. Within the Gabonese cohort, I observed apparent differences in STH prevalence between study sites. Rural Ikobey consistently showed a higher prevalence than semi-urban Lambaréné. This contrast likely reflects differences in environmental exposure, sanitation, and access to deworming treatment, although my analysis did not explicitly incorporate these variables.

Participant age influenced STH prevalence in predictable ways, with older school-age children carrying a higher number of infections, particularly in Ikobey. However, when I compared explanatory factors, geographic location accounted for more variation in infection patterns than either age or household-level clustering.

Building on this, I next looked at how STH richness (the number of STH species per individual) relates to gut microbiome composition. In addition to STH richness, I included other

factors, such as age and sampling location, in the linear models to assess the percentage of variance in microbiome composition explained by each factor. I observed only a modest association between STH richness and microbiome alpha diversity (measured by Shannon entropy and Faith's phylogenetic diversity), and this pattern became evident only when I separated the data by site and age group (adults versus children). As detailed in chapter two, age and location had a much more apparent influence on microbiome composition, in agreement with previous observations and suggesting that the microbiomes of different populations respond more strongly to diet, local lifestyle, and environmental exposures than to parasite richness alone. Overall, the findings suggest that where people live matters more than how many helminth species they carry, and that parasite-related microbiome patterns only really stand out once I account for that underlying variation.

Age-related patterns were likewise context-dependent. While adults in many endemic settings exhibit reduced parasite burdens(Andereck et al., 2014; Gurmassa et al., 2024), adults in the different African sites, especially in the Ikobey community of the Gabonese population studied here, showed unexpectedly high prevalence for several species. Although the Ikobey community is less well studied than the other locations in this study, factors such as uneven STH treatment coverage, livelihood-related soil exposure, and interruptions to mass drug administration programmes likely contribute to the observed differences. These observations highlight the need to interpret parasitism within its local ecological and public health context rather than relying solely on age-based expectations.

Co-infections were common among participants, especially in the rural Ikobey community, compared to the semi-urban Lambaréné. People who carried one STH species often carried others as well, pointing to shared environmental conditions and everyday habits that promote repeated exposure. Because most microbiome studies focus on single STH-species infections to characterise how they associate with microbiome community compositions, the frequent multi-infections in this cohort make it challenging to tease apart the individual effects of each parasite on the gut microbial community. Mixed infections can generate combined or even opposing influences on the microbiome that observational data cannot easily separate. Together, these observations reinforce the view of STHs as components of a broader ecological disturbance rather than isolated exposures.

Despite these complexities, several microbial patterns were consistent. People with STH parasites tended to show slight increases in microbial α-diversity, in line with other human studies(Lee et al., 2014; Toro-Londono et al., 2019), and they also showed reproducible shifts in

community composition. In STH-infected individuals, Clostridia and mucin-associated taxa tended to increase, whereas members of Bifidobacteriaceae were more enriched in those without parasites. These patterns suggest broad functional adjustments in the microbiome, with different species within the same family responding differently to STH infection. As described in chapter two, such variability makes it challenging to identify bacterial species as biomarkers of STH infection. The recovery of *Methanobrevibacter* within adult co-occurrence networks also suggests that archaeal lineages may participate in these ecological shifts, even if mechanisms remain unresolved.

A final theme concerns methodological advancement. Microscopy and qPCR are still widely used to detect and quantify STH parasites, but they need substantial laboratory infrastructure, which is not readily available in most resource-limited settings. Additionally, qPCRs do not scale well for large-scale multi-pathogen screening. In contrast, metagenomic sequencing offers a single, unified approach that can simultaneously identify bacteria, protozoa, viruses, archaea, and helminths from a single stool sample. This thesis provides one of the first systematic comparisons between qPCR-based and metagenomic quantification for human STHs. Although metagenomics is less sensitive at low infection intensities, several patterns were encouraging, particularly the utility of genome coverage, alongside read counts, as a more reliable indicator to quantify infection. My findings suggest that metagenomics could become a reliable complementary tool for detecting and quantifying both bacteria and parasites in a single analysis. Because parasite reads are much rarer than bacterial ones, developing shared standard protocols, such as validated genomes, harmonized workflows, and potentially global guidelines endorsed by institutions like the WHO, could make it easier to integrate metagenomics into future studies of STH epidemiology.

The work further illustrates how parasitic infections act as context-dependent modulators of the gut ecosystem and demonstrates the value of metagenomics for studying helminths in regions where parasitology and microbiome research remain limited. As sequencing costs continue to fall, even resource-constrained countries may soon be able to apply joint-parasite-microbiome profiling to monitor STH burden and assess the impact of mass drug administration programmes.

6.3. Cultivation and taxonomic resolution of human gut methanogens (Chapter 4).

Chapter 4 extends the study from metagenomic analysis in Chapter 2 to hands-on cultivation and genomic characterization of gut methanogens. I employed a targeted approach to enrich for methanogens using stool samples. Using this approach, I isolated a new methanogen species, *Methanobrevibacter* intestini strain G0370_i3, from a Gabonese adult stool sample. While other studies have isolated several strains of this species, this is the first human-derived *M. intestini* genome from Central Africa. When using the whole genome sequence to infer the genomic and phylogenetic differences between this strain, *M. smithii*, and other methanogen strains, we find a clear separation from *M. smithii*, while the strain clusters with other cultured *M. intestini* strains, reinforcing the species-level distinction proposed only recently in the literature(Duller et al., 2024; Low et al., 2022; Weinberger et al., 2025). The strain G0370_i3 described in this chapter adds an important piece to the picture of *M. intestini* diversity and expands our understanding of human gut methanogens worldwide. Its recovery also underscores that slow-growing, technically demanding methanogens remain underrepresented in culture collections, particularly from populations whose traditional diets and lifestyles may support distinct lineages.

Beyond defining the taxonomic position of this isolate, the chapter also lays the genomic and phenotypic groundwork for broader comparative work. These data serve as the basis for the analyses in Chapter 5, which bring together isolates and metagenomes from Gabon, Germany, and Vietnam to explore diversity at a large scale.

6.4. Comparative genomics, ecology, and evolution of methanogens (Chapter 5).

Building on the targeted cultivation work of Chapter 4, Chapter 5 expanded the scale of investigation to include multiple isolates of *M. smithii* and *M. intestini* obtained from Gabon, Germany, and Vietnam. Together, these isolates form one of the most extensive and geographically balanced culture collections of human gut methanogens reported so far, offering a rare opportunity to compare strain diversity across geographies. To do this, we combined whole-genome sequences from cultured isolates with shotgun metagenomic data to assess species prevalence, diversity, and evolutionary relationships. This combined approach revealed key ecological and evolutionary trends in both *M. smithii* and *M. intestini* that overlap those described in Chapter 2. For example, we again observed geography-linked differences between the rural Ikobey and semi-urban Lambaréné, with higher STH prevalence and higher *M. intestini* abundance in the Ikobey cohort. At the same time, the genomic data highlighted features specific to

methanogens, including species-level differences in molybdate transport genes between *M. smithii* and *M. intestini*.

Our isolate-level phylogenies uncovered substantial strain-level diversity in *M. smithii*, with deep internal branching and regionally clustered sublineages among cultured isolates. Furthermore, principal component analysis of accessory gene content showed population-specific profiles, with variation in adhesin-related genes among the main features separating groups. Similar geographically structured patterns have been described for other gut microbes at the strain level, indicating that such population structure is a common feature of host-associated microbiota(Schloissnig et al., 2013; Truong et al., 2017). The cultured strains also allowed us to explore coevolutionary patterns at much higher resolution than metagenome-assembled genomes (MAGS) typically provide. Because all of our isolates have genome completeness exceeding 90%, they provide clearer evolutionary signals than typical MAGs. Codiversification is a process in which the host (in this case, humans) and symbiont (in this case, *M. smithii*) lineages diversify in parallel over evolutionary timescales, producing non-random congruence between their phylogenetic histories(Suzuki et al., 2022).

Methanogens evolved as ancient anaerobes and have long inhabited mammalian gut ecosystems. They occur throughout the human lifespan, although the precise duration of their association with humans remains unclear. Existing studies show that methanogens rarely occur in early infancy, increase in prevalence during the first years of life, and become common in school-aged children and adults, suggesting that childhood colonization can persist for decades(Gaci et al., 2014; Mihajlovski et al., 2010; Nkamga et al., 2017; van de Pol et al., 2017; Vanderhaeghen et al., 2015). This long-term host association provides enough evolutionary time and vertical or pseudo-vertical transmission (e.g., within families, within populations) for *M. smithii* lineages to track the human host lineages. Although due to limited within-country coverage of our *M. smithii* strain collections that could allow us to test codiversification within countries, using the *M. smithii* strain phylogeny together with the corresponding human host tree, we detected partial congruence between branches, consistent with parallel evolution and with codiversification signals previously reported for gut microbes and humans(Suzuki et al., 2022). Although we would have liked to test for similar host-microbe codiversification in *M. intestini* across all three populations, the available dataset included too few cultured strains from two of the three populations, preventing meaningful comparisons.

When examining abundance patterns, *M. intestini* appeared consistently less prevalent than *M. smithii* and declined sharply along gradients of urbanization and industrialization. For instance, its abundance was considerably higher in rural Ikobey than in semi-urban Lambaréné. These differences likely reflect lifestyle and dietary contrasts between the two communities and suggest that *M. intestini* may represent a lineage best adapted to traditional, high-fibre diets and less industrialized lifestyles. The mechanisms underlying this gradient remain unclear, but the pattern itself argues against earlier views of methanogens as uniform, low-diversity commensals and instead shows that their ecology responds strongly to differences in lifestyle and diet across populations.

Methanogen carriage in the cohort proved age- and context-dependent rather than universal. Adults carried methanogens more often than children, and there was no strong concordance in methanogen presence between mothers and their infants, arguing against simple, ubiquitous vertical transmission(Camara et al., 2021; Togo et al., 2019). At the same time, given limitations in sequencing depth and culture sensitivity, it may miss low-level early colonization. However, the pattern aligns with reports that gut methanogens often establish later in infancy or childhood. At the same time, cultured *M. smithii* strains from people living in the same community were highly similar, consistent with circulation from shared local sources or community environments rather than strict inheritance of identical strains within families(Asnicar et al., 2017).

Taken together with the geographic and lifestyle differences described earlier, these findings indicate that diet, host development, and cultural context are more likely to influence archaeal colonization and persistence. Chapter 5, therefore, uses methanogens as a case study of how human–microbe relationships are shaped by both evolution and ecology. Pangenome analysis highlighted significant differences in metabolic capacity and genome content of both *M. smithii* and *M. intestini*. For example, *M. smithii* genomes are enriched for molybdate transport genes, such as modA and modB, whereas *M. intestini* lacks these loci and instead shows enrichment for predicted glycosyltransferases and other membrane-associated functions. These differences point to distinct resource use and cell-surface architectures in the two species, supporting the idea that *M. smithii* and *M. intestini* occupy related but not identical niches and may respond differently to dietary environments(Low et al., 2022; Weinberger et al., 2025). At the same time, the population structure and codiversification signals observed for *M. smithii* raise questions about how closely some archaeal lineages have tracked human population history and how dependent they have

become on specific hosts. The prevalence and abundance patterns observed here also echo the conclusions from Chapter 2: geography and lifestyle significantly shape biological variation in both datasets, and pooling data from diverse groups too broadly can blur these population-specific signals.

Viewed together, Chapters 4 and 5 show that human-associated methanogens are diverse, evolving, and ecologically structured members of the gut ecosystem. Cultivation, comparative genomics, and biogeographic analyses provide complementary ways to study these archaea, revealing long-standing evolutionary associations alongside the effects of contemporary environmental and cultural pressures.

6.5. Broader implications and future perspectives.

Taken together, the parasite- and methanogen-focused studies presented in this thesis converge on several overarching themes that extend beyond the individual chapters. First, the work underscores the value of geographically inclusive sampling. Many of the biological insights presented here, such as metagenomic detection of helminths and the recovery of a novel *M. intestini* isolate, were only possible because the research incorporated populations that remain sparsely represented in global microbiome datasets. These results emphasize the broader need to ensure equity in sampling and in the construction of reference genome databases.

Second, the findings show that local conditions play a central role in shaping human-associated microorganisms. Local epidemiology, diet, lifestyle, and degree of urbanization strongly influenced patterns of parasite prevalence, parasite–microbiome relationships, and distributions of *M. smithii* and *M. intestini*. This illustrates why analyses that pool data across populations can obscure meaningful variation unless stratification by geography or environment is explicitly incorporated.

Third, the combined use of metagenomics, cultivation, and comparative genomics demonstrates how evolutionary history and present-day ecology intersect. Signals of long-term association in *M. smithii*, the distinct distribution of *M. intestini*, and the ecological structuring of parasite–microbiome interactions all point to dynamic relationships between humans and their microbial partners. These observations invite broader reflection on how modernization and lifestyle change may alter not only bacterial diversity but also the archaeal and parasitic components of the gut ecosystem.

Taken together, the results highlight the need for broader methanogen cultivation, richer comparative genomic datasets, and multi-kingdom approaches that situate archaea within the wider gut ecological network.

6.6. Concluding remarks.

The work in this thesis demonstrates that human gut microbial communities are influenced by well-known factors such as age and geography, as well as STH parasites. Despite the cross-sectional nature of the data, a key observation is the higher prevalence of STH in the rural Ikobey community of Gabon than in the semi-urban Lambaréné, which could serve as baseline data to inform governmental and public health interventions, such as deworming through MDA, and to strengthen local epidemiological surveillance.

The Ikobey community gained renewed significance when we studied methanogens and identified it as a potential hotspot for *M. intestini*, with a higher prevalence than in semi-urban Lambaréné. We further confirmed this pattern through cultivation, recovering more isolates of this species from the Ikobey community than from Lambaréné, which suggests a possible decline in *M. intestini* as the population transitions to an industrialized lifestyle.

6.7. General References

Abdi, H., Kordi-Tamandani, D. M., Lagzian, M., & Bakhshipour, A. (2022). Archaeome in Colorectal Cancer: High Abundance of Methanogenic Archaea in Colorectal Cancer Patients. *International Journal of Cancer Management*, *15*(4). https://doi.org/10.5812/ijcm-117843

Adegnika, A. A., Lötsch, F., Mba, R. M. O., & Ramharter, M. (2015). Update on treatment and resistance of human trichuriasis. *Current Tropical Medicine Reports*, *2*(4), 218–223.

Andereck, J. W., Kipp, A. M., Ondiek, M., & Vermund, S. H. (2014). Helminth prevalence among adults in rural Kenya: a stool survey for soil-transmitted helminths and schistosomiasis in Nyanza province. *Transactions of the Royal Society of Tropical Medicine and Hygiene*, *108*(12), 804–809.

Anderson, R. M., & Schad, G. A. (1985). Hookworm burdens and faecal egg counts: an analysis of the biological basis of variation. *Transactions of the Royal Society of Tropical Medicine and Hygiene*, *79*(6), 812–825.

Arndt, M. B., John-Stewart, G., Richardson, B. A., Singa, B., van Lieshout, L., Verweij, J.

J., Sangaré, L. R., Mbogo, L. W., Naulikha, J. M., & Walson, J. L. (2013). Impact of helminth diagnostic test performance on estimation of risk factors and outcomes in HIV-positive adults. *PloS One*, *8*(12), e81915.

Asnicar, F., Manara, S., Zolfo, M., Truong, D. T., Scholz, M., Armanini, F., Ferretti, P., Gorfer, V., Pedrotti, A., Tett, A., & Segata, N. (2017). Studying vertical microbiome transmission from mothers to infants by strain-level metagenomic profiling. *mSystems*, *2*(1). https://doi.org/10.1128/mSystems.00164-16

Basseri, R. J., Basseri, B., Pimentel, M., Chong, K., Youdim, A., Low, K., Hwang, L., Soffer, E., Chang, C., & Mathur, R. (2012). Intestinal methane production in obese individuals is associated with a higher body mass index. *Gastroenterology & Hepatology*, *8*(1), 22–28.

Bhaskaran, N., Quigley, C., Paw, C., Butala, S., Schneider, E., & Pandiyan, P. (2018). Role of short chain fatty acids in controlling Tregs and immunopathology during mucosal infection. *Frontiers in Microbiology*, *9*, 1995.

Blake, K. S. (2024). Missing microbiomes: global underrepresentation restricts who research will benefit. *The Journal of Clinical Investigation*, *134*(14), e183884.

Borrel, G., Brugère, J.-F., Gribaldo, S., Schmitz, R. A., & Moissl-Eichinger, C. (2020). The host-associated archaeome. *Nature Reviews. Microbiology*, *18*(11), 622–636.

Brady, M. A., Hooper, P. J., & Ottesen, E. A. (2006). Projected benefits from integrating NTD programs in sub-Saharan Africa. *Trends in Parasitology*, *22*(7), 285–291.

Brooker, S., Clements, A. C. A., & Bundy, D. A. P. (2006). Global epidemiology, ecology and control of soil-transmitted helminth infections. *Advances in Parasitology*, *62*, 221–261.

Brooks, C., Snoberger, A., Belcastro, M., Murphy, J., Kisselev, O. G., Smith, D. M., & Sokolov, M. (2018). Archaeal unfoldase counteracts protein misfolding retinopathy in mice. *The Journal of Neuroscience: The Official Journal of the Society for Neuroscience*, *38*(33), 7248–7254.

Bui, T. P. N., Schols, H. A., Jonathan, M., Stams, A. J. M., de Vos, W. M., & Plugge, C. M. (2019). Mutual metabolic interactions in co-cultures of the intestinal Anaerostipes rhamnosivorans with an acetogen, methanogen, or pectin-degrader affecting butyrate production. *Frontiers in Microbiology*, *10*, 2449.

Bu, J., Zhu, X., & Zhang, H. (2025). Methanogens in colorectal cancer: Association or

causation? *Gastroenterology*, *169*(2), 372–373.

Camara, A., Konate, S., Tidjani Alou, M., Kodio, A., Togo, A. H., Cortaredona, S., Henrissat, B., Thera, M. A., Doumbo, O. K., Raoult, D., & Million, M. (2021). Clinical evidence of the role of *Methanobrevibacter smithii* in severe acute malnutrition. *Scientific Reports*, *11*(1), 5426.

Catlett, J. L., Carr, S., Cashman, M., Smith, M. D., Walter, M., Sakkaff, Z., Kelley, C., Pierobon, M., Cohen, M. B., & Buan, N. R. (2022). Metabolic synergy between human symbionts Bacteroides and *Methanobrevibacter*. *Microbiology Spectrum*, *10*(3), e0106722.

Cheesbrough, M. (2005). Parasitilogical Test. In *District Laboratory Practice in Tropical Countries* (pp. 178–306). Cambridge University Press.

Chibani, C. M., Mahnert, A., Borrel, G., Almeida, A., Werner, A., Brugère, J.-F., Gribaldo, S., Finn, R. D., Schmitz, R. A., & Moissl-Eichinger, C. (2022). A catalogue of 1,167 genomes from the human gut archaeome. In *Nature Microbiology* (Vol. 7, Issue 1, pp. 48–61). https://doi.org/10.1038/s41564-021-01020-9

Conrad, R. (2007). Microbial ecology of methanogens and methanotrophs. In *Advances in Agronomy* (Vol. 96, pp. 1–63). Elsevier.

Corbin, K. D., Igudesman, D., Smith, S. R., Zengler, K., & Krajmalnik-Brown, R. (2025). Targeting the gut microbiota's role in host energy absorption with precision nutrition interventions for the prevention and treatment of obesity. *Nutrition Reviews*, *83*(10), 1928–1943.

Dirks, B., Davis, T. L., Carnero, E. A., Corbin, K. D., Smith, S. R., Rittmann, B. E., & Krajmalnik-Brown, R. (2025). Methanogenesis associated with altered microbial production of short-chain fatty acids and human-host metabolizable energy. *The ISME Journal*, *19*(1). https://doi.org/10.1093/ismejo/wraf103

Donnelly, S., O'Neill, S. M., Stack, C. M., Robinson, M. W., Turnbull, L., Whitchurch, C., & Dalton, J. P. (2010). Helminth cysteine proteases inhibit TRIF-dependent activation of macrophages via degradation of TLR3. *The Journal of Biological Chemistry*, *285*(5), 3383–3392.

Dridi, B., Henry, M., El Khéchine, A., Raoult, D., & Drancourt, M. (2009). High prevalence of *Methanobrevibacter smithii* and *Methanosphaera stadtmanae* detected in the human gut using an improved DNA detection protocol. *PloS One*, *4*(9), e7063.

Duller, S., Vrbancic, S., Szydłowski, Ł., Mahnert, A., Blohs, M., Predl, M., Kumpitsch, C., Zrim, V., Högenauer, C., Kosciolek, T., Schmitz, R. A., Eberhard, A., Dragovan, M., Schmidberger, L., Zurabischvili, T., Weinberger, V., Moser, A. M., Kolb, D., Pernitsch, D., … Moissl-Eichinger, C. (2024). Targeted isolation of *Methanobrevibacter* strains from fecal samples expands the cultivated human archaeome. *Nature Communications*, *15*(1), 7593.

Easton, A. V., Oliveira, R. G., Walker, M., O'Connell, E. M., Njenga, S. M., Mwandawiro, C. S., Webster, J. P., Nutman, T. B., & Anderson, R. M. (2017). Sources of variability in the measurement of Ascaris lumbricoides infection intensity by Kato-Katz and qPCR. *Parasites & Vectors*, *10*(1), 256.

Easton, A. V., Quiñones, M., Vujkovic-Cvijin, I., Oliveira, R. G., Kepha, S., Odiere, M. R., Anderson, R. M., Belkaid, Y., & Nutman, T. B. (2019). The impact of anthelmintic treatment on human gut Microbiota based on cross-sectional and pre- and postdeworming comparisons in western Kenya. *mBio*, *10*(2). https://doi.org/10.1128/mBio.00519-19

Fenwick, A. (2006). New initiatives against Africa's worms. *Transactions of the Royal Society of Tropical Medicine and Hygiene*, *100*(3), 200–207.

Fu, Y., Zhang, K., Yang, M., Li, X., Chen, Y., Li, J., Xu, H., Dhakal, P., & Zhang, L. (2023). Metagenomic analysis reveals the relationship between intestinal protozoan parasites and the intestinal microecological balance in calves. *Parasites & Vectors*, *16*, NA.

Gaci, N., Borrel, G., Tottey, W., O'Toole, P. W., & Brugère, J.-F. (2014). Archaea and the human gut: new beginning of an old story. *World Journal of Gastroenterology: WJG*, *20*(43), 16062–16078.

Gazzinelli-Guimaraes, P. H., & Nutman, T. B. (2018). Helminth parasites and immune regulation. *F1000Research*, *7*. https://doi.org/10.12688/f1000research.15596.1

Glover, M., Colombo, S. A. P., Thornton, D. J., & Grencis, R. K. (2019). Trickle infection and immunity to Trichuris muris. *PLoS Pathogens*, *15*(11), e1007926.

Goodrich, J. K., Waters, J. L., Poole, A. C., Sutter, J. L., Koren, O., Blekhman, R., Beaumont, M., Van Treuren, W., Knight, R., Bell, J. T., Spector, T. D., Clark, A. G., & Ley, R. E. (2014). Human genetics shape the gut microbiome. *Cell*, *159*(4), 789–799.

Grainger, J. R., Smith, K. A., Hewitson, J. P., McSorley, H. J., Harcus, Y., Filbey, K. J., Finney, C. A. M., Greenwood, E. J. D., Knox, D. P., Wilson, M. S., Belkaid, Y., Rudensky, A. Y., & Maizels, R. M. (2010). Helminth secretions induce de novo T cell Foxp3

expression and regulatory function through the TGF-β pathway. *The Journal of Experimental Medicine*, *207*(11), 2331–2341.

Gurmassa, B. K., Gari, S. R., Solomon, E. T., Goodson, M. L., Walsh, C. L., Dessie, B. K., & Alemu, B. M. (2024). Prevalence and risk factors of soil transmitted helminths among vegetable farmers of Akaki river bank, Addis Ababa, Ethiopia. *BMC Infectious Diseases*, *24*(1), 961.

Hansen, E. E., Lozupone, C. A., Rey, F. E., Wu, M., Guruge, J. L., Narra, A., Goodfellow, J., Zaneveld, J. R., McDonald, D. T., Goodrich, J. A., Heath, A. C., Knight, R., & Gordon, J. I. (2011). Pan-genome of the dominant human gut-associated archaeon, *Methanobrevibacter* smithii, studied in twins. *Proceedings of the National Academy of Sciences of the United States of America*, *108 Suppl 1*, 4599–4606.

Hasnain, S. Z., Evans, C. M., Roy, M., Gallagher, A. L., Kindrachuk, K. N., Barron, L., Dickey, B. F., Wilson, M. S., Wynn, T. A., Grencis, R. K., & Thornton, D. J. (2011). Muc5ac: a critical component mediating the rejection of enteric nematodes. *The Journal of Experimental Medicine*, *208*(5), 893–900.

Herbert, D. R., Yang, J.-Q., Hogan, S. P., Groschwitz, K., Khodoun, M., Munitz, A., Orekov, T., Perkins, C., Wang, Q., Brombacher, F., Urban, J. F., Jr, Rothenberg, M. E., & Finkelman, F. D. (2009). Intestinal epithelial cell secretion of RELM-beta protects against gastrointestinal worm infection. *The Journal of Experimental Medicine*, *206*(13), 2947–2957.

Houlden, A., Hayes, K. S., Bancroft, A. J., Worthington, J. J., Wang, P., Grencis, R. K., & Roberts, I. S. (2015). Chronic Trichuris muris infection in C57BL/6 mice causes significant changes in host Microbiota and metabolome: Effects reversed by pathogen clearance. *PloS One*, *10*(5), e0125945.

Janssen, P. H., & Kirs, M. (2008). Structure of the archaeal community of the rumen. *Applied and Environmental Microbiology*, *74*(12), 3619–3625.

Jenkins, T. P., Rathnayaka, Y., Perera, P. K., Peachey, L. E., Nolan, M. J., Krause, L., Rajakaruna, R. S., & Cantacessi, C. (2017). Infections by human gastrointestinal helminths are associated with changes in faecal microbiota diversity and composition. *PloS One*, *12*(9), e0184719.

Katz, N., Chaves, A., & Pellegrino, J. (1972). A simple device for quantitative stool thick-

smear technique in Schistosomiasis mansoni. *Revista Do Instituto de Medicina Tropical de Sao Paulo*, *14*(6), 397–400.

Keiser, J., & Utzinger, J. (2008). Efficacy of current drugs against soil-transmitted helminth infections: systematic review and meta-analysis: Systematic review and meta-analysis. *JAMA: The Journal of the American Medical Association*, *299*(16), 1937–1948.

Khanna, K. (2022). How Methanogenic Archaea Contribute to Climate Change. *American Society for Microbiology*. https://asm.org/articles/2022/may/how-methanogenic-archaea-contribute-to-climate-cha

Kirstahler, P., Aarestrup, F. M., & Pamp, S. J. (2022). Detection of Parasites in Microbiomes using Metagenomics. In *bioRxiv* (p. 2022.03.27.485979). https://doi.org/10.1101/2022.03.27.485979

Kunkel, D., Basseri, R. J., Makhani, M. D., Chong, K., Chang, C., & Pimentel, M. (2011). Methane on breath testing is associated with constipation: a systematic review and meta-analysis. *Digestive Diseases and Sciences*, *56*(6), 1612–1618.

Kupritz, J., Angelova, A., Nutman, T. B., & Gazzinelli-Guimaraes, P. H. (2021). Helminth-induced human gastrointestinal dysbiosis: A systematic review and meta-analysis reveals insights into altered taxon diversity and microbial gradient collapse. *mBio*, *12*(6), e0289021.

Lammie, P. J., Fenwick, A., & Utzinger, J. (2006). A blueprint for success: integration of neglected tropical disease control programmes. *Trends in Parasitology*, *22*(7), 313–321.

Lee, S. C., Tang, M. S., Lim, Y. A. L., Choy, S. H., Kurtz, Z. D., Cox, L. M., Gundra, U. M., Cho, I., Bonneau, R., Blaser, M. J., Chua, K. H., & Loke, P. 'ng. (2014). Helminth colonization is associated with increased diversity of the gut microbiota. *PLoS Neglected Tropical Diseases*, *8*(5), e2880.

Lepp, P. W., Brinig, M. M., Ouverney, C. C., Palm, K., Armitage, G. C., & Relman, D. A. (2004). Methanogenic Archaea and human periodontal disease. *Proceedings of the National Academy of Sciences of the United States of America*, *101*(16), 6176–6181.

Li, T., Coker, O. O., Sun, Y., Li, S., Liu, C., Lin, Y., Wong, S. H., Miao, Y., Sung, J. J. Y., & Yu, J. (2025). Multi-cohort analysis reveals altered Archaea in colorectal cancer fecal samples across populations. *Gastroenterology*, *168*(3), 525–538.e2.

Lokmer, A., Cian, A., Froment, A., Gantois, N., Viscogliosi, E., Chabé, M., & Ségurel, L. (2019). Use of shotgun metagenomics for the identification of protozoa in the gut microbiota

of healthy individuals from worldwide populations with various industrialization levels. *PloS One*, *14*(2), e0211139.

Low, A., Lee, J. K. Y., Gounot, J.-S., Ravikrishnan, A., Ding, Y., Saw, W.-Y., Tan, L. W. L., Moong, D. K. N., Teo, Y. Y., Nagarajan, N., & Seedorf, H. (2022). Mutual exclusion of *Methanobrevibacter* species in the human gut Microbiota facilitates directed cultivation of a Candidatus *Methanobrevibacter* intestini representative. *Microbiology Spectrum*, *10*(4), e00849–22.

Lyu, Z., Shao, N., Akinyemi, T., & Whitman, W. B. (2018). Methanogenesis. *Current Biology: CB*, *28*(13), R727–R732.

Mahanty, S., & Nutman, T. B. (1995). Immunoregulation in human lymphatic filariasis: the role of interleukin 10. *Parasite Immunology*, *17*(8), 385–392.

Maizels, R. M., & McSorley, H. J. (2016). Regulation of the host immune system by helminth parasites. *The Journal of Allergy and Clinical Immunology*, *138*(3), 666–675.

Maizels, R. M., Smits, H. H., & McSorley, H. J. (2018). Modulation of host immunity by helminths: The expanding repertoire of parasite effector molecules. *Immunity*, *49*(5), 801–818.

Mbakwa, C. A., Penders, J., Savelkoul, P. H., Thijs, C., Dagnelie, P. C., Mommers, M., & Arts, I. C. W. (2015). Gut colonization with methanobrevibacter smithii is associated with childhood weight development: Gut Archaea and Weight Development in Children. *Obesity (Silver Spring, Md.)*, *23*(12), 2508–2516.

Mbong Ngwese, M., Prince Manouana, G., Nguema Moure, P. A., Ramharter, M., Esen, M., & Adégnika, A. A. (2020). Diagnostic techniques of soil-transmitted helminths: Impact on control measures. *Tropical Medicine and Infectious Disease*, *5*(2), 93.

McKeand, J. B. (1998). Molecular diagnosis of parasitic nematodes. *Parasitology*, *117 Suppl*, S87–S96.

McSorley, H. J., Blair, N. F., Smith, K. A., McKenzie, A. N. J., & Maizels, R. M. (2014). Blockade of IL-33 release and suppression of type 2 innate lymphoid cell responses by helminth secreted products in airway allergy. *Mucosal Immunology*, *7*(5), 1068–1078.

Mihajlovski, A., Doré, J., Levenez, F., Alric, M., & Brugère, J.-F. (2010). Molecular evaluation of the human gut methanogenic archaeal microbiota reveals an age-associated increase of the diversity. *Environmental Microbiology Reports*, *2*(2), 272–280.

Miller, T. L., Wolin, M. J., Conway de Macario, E., & Macario, A. J. (1982). Isolation of *Methanobrevibacter smithii* from human feces. *Applied and Environmental Microbiology*, *43*(1), 227–232.

Mohammadzadeh, R., Mahnert, A., Shinde, T., Kumpitsch, C., Weinberger, V., Schmidt, H., & Moissl-Eichinger, C. (2025). Age-related dynamics of predominant methanogenic archaea in the human gut microbiome. *BMC Microbiology*, *25*(1), 193.

Molyneux, D. H., Hotez, P. J., & Fenwick, A. (2005). "Rapid-impact interventions": how a policy of integrated control for Africa's neglected tropical diseases could benefit the poor. *PLoS Medicine*, *2*(11), e336.

Mules, T. C., Vacca, F., Cait, A., Yumnam, B., Schmidt, A., Lavender, B., Maclean, K., Noble, S.-L., Gasser, O., Camberis, M., Le Gros, G., & Inns, S. (2024). A small intestinal helminth infection alters colonic mucus and shapes the colonic mucus microbiome. *International Journal of Molecular Sciences*, *25*(22). https://doi.org/10.3390/ijms252212015

Nandhra, G. K., Mark, E. B., Di Tanna, G. L., Haase, A.-M., Poulsen, J., Christodoulides, S., Kung, V., Klinge, M. W., Knudsen, K., Borghammer, P., Andersen, K. O., Fynne, L., Sutter, N., Schlageter, V., Krogh, K., Drewes, A. M., Birch, M., & Scott, S. M. (2020). Normative values for region-specific colonic and gastrointestinal transit times in 111 healthy volunteers using the 3D-Transit electromagnet tracking system: Influence of age, gender, and body mass index. *Neurogastroenterology and Motility: The Official Journal of the European Gastrointestinal Motility Society*, *32*(2), e13734.

Nishiwaki, H., Ueyama, J., Ito, M., Hamaguchi, T., Takimoto, K., Maeda, T., Kashihara, K., Tsuboi, Y., Mori, H., Kurokawa, K., Katsuno, M., Hirayama, M., & Ohno, K. (2024). Meta-analysis of shotgun sequencing of gut microbiota in Parkinson's disease. *NPJ Parkinson's Disease*, *10*(1), 106.

Nkamga, V. D., Henrissat, B., & Drancourt, M. (2017). Archaea: Essential inhabitants of the human digestive microbiota. *Human Microbiome Journal*, *3*, 1–8.

Oremland, R. S., & Polcin, S. (1982). Methanogenesis and sulfate reduction: competitive and noncompetitive substrates in estuarine sediments. *Applied and Environmental Microbiology*, *44*(6), 1270–1276.

Pilliol, V., Mahmoud Abdelwadoud, B., Aïcha, H., Lucille, T., Gérard, A., Hervé, T., Michel, D., Ghiles, G., & Elodie, T. (2024). *Methanobrevibacter* oralis: a comprehensive

review. *Journal of Oral Microbiology*, *16*(1), 2415734.

Pimentel, M., Chatterjee, S., Chow, E. J., Park, S., & Kong, Y. (2006). Neomycin improves constipation-predominant irritable bowel syndrome in a fashion that is dependent on the presence of methane gas: subanalysis of a double-blind randomized controlled study. *Digestive Diseases and Sciences*, *51*(8), 1297–1301.

Pimentel, M., Saad, R. J., Long, M. D., & Rao, S. S. C. (2020). ACG clinical guideline: Small intestinal bacterial overgrowth: Small intestinal bacterial overgrowth. *The American Journal of Gastroenterology*, *115*(2), 165–178.

Procházková, N., Falony, G., Dragsted, L. O., Licht, T. R., Raes, J., & Roager, H. M. (2023). Advancing human gut microbiota research by considering gut transit time. *Gut*, *72*(1), 180–191.

Reynolds, L. A., Finlay, B. B., & Maizels, R. M. (2015). Cohabitation in the intestine: Interactions among helminth parasites, bacterial Microbiota, and host immunity. *The Journal of Immunology*, *195*(9), 4059–4066.

Rinke, C., Chuvochina, M., Mussig, A. J., Chaumeil, P.-A., Davín, A. A., Waite, D. W., Whitman, W. B., Parks, D. H., & Hugenholtz, P. (2021). A standardized archaeal taxonomy for the Genome Taxonomy Database. *Nature Microbiology*, *6*(7), 946–959.

Rooney, J., Northcote, H. M., Williams, T. L., Cortés, A., Cantacessi, C., & Morphew, R. M. (2022). Parasitic helminths and the host microbiome - a missing "extracellular vesicle-sized" link? *Trends in Parasitology*, *38*(9), 737–747.

Rosa, B. A., Supali, T., Gankpala, L., Djuardi, Y., Sartono, E., Zhou, Y., Fischer, K., Martin, J., Tyagi, R., Bolay, F. K., Fischer, P. U., Yazdanbakhsh, M., & Mitreva, M. (2018). Differential human gut microbiome assemblages during soil-transmitted helminth infections in Indonesia and Liberia. *Microbiome*, *6*(1), 33.

Ruaud, A., Esquivel-Elizondo, S., de la Cuesta-Zuluaga, J., Waters, J. L., Angenent, L. T., Youngblut, N. D., & Ley, R. E. (2020). Syntrophy via Interspecies H2 transfer between Christensenella and *Methanobrevibacter* underlies their global cooccurrence in the human gut. *mBio*, *11*(1), e03235–19.

Sakono, M., Zako, T., Ueda, H., Yohda, M., & Maeda, M. (2008). Formation of highly toxic soluble amyloid beta oligomers by the molecular chaperone prefoldin: Formation of amyloid beta oligomers by prefoldin. *The FEBS Journal*, *275*(23), 5982–5993.

Sakti, H., Nokes, C., Hertanto, W. S., Hendratno, S., Hall, A., Bundy, D. A., & Satoto. (1999). Evidence for an association between hookworm infection and cognitive function in Indonesian school children. *Tropical Medicine & International Health: TM & IH*, *4*(5), 322–334.

Samuel, B. S., & Gordon, J. I. (2006). A humanized gnotobiotic mouse model of host-archaeal-bacterial mutualism. *Proceedings of the National Academy of Sciences of the United States of America*, *103*(26), 10011–10016.

Samuel, B. S., Hansen, E. E., Manchester, J. K., Coutinho, P. M., Henrissat, B., Fulton, R., Latreille, P., Kim, K., Wilson, R. K., & Gordon, J. I. (2007). Genomic and metabolic adaptations of *Methanobrevibacter smithii* to the human gut. *Proceedings of the National Academy of Sciences of the United States of America*, *104*(25), 10643–10648.

Sanz, J. L. (2011). Methanogens. In *Encyclopedia of Astrobiology* (pp. 1037–1038). Springer Berlin Heidelberg.

Satoguina, J. S., Weyand, E., Larbi, J., & Hoerauf, A. (2005). T regulatory-1 cells induce IgG4 production by B cells: role of IL-10. *The Journal of Immunology*, *174*(8), 4718–4726.

Scanlan, P. D., Shanahan, F., & Marchesi, J. R. (2008). Human methanogen diversity and incidence in healthy and diseased colonic groups using mcrA gene analysis. *BMC Microbiology*, *8*, 79.

Schloissnig, S., Arumugam, M., Sunagawa, S., Mitreva, M., Tap, J., Zhu, A., Waller, A., Mende, D. R., Kultima, J. R., Martin, J., Kota, K., Sunyaev, S. R., Weinstock, G. M., & Bork, P. (2013). Genomic variation landscape of the human gut microbiome. *Nature*, *493*(7430), 45–50.

Stetter, K. O., Thomm, M., Winter, J., Wildgruber, G., Huber, H., Zillig, W., Jané-Covic, D., König, H., Palm, P., & Wunderl, S. (1981). Methanothermus fervidus, sp. nov., a novel extremely thermophilic methanogen isolated from an Icelandic hot spring. *Zentralblatt Für Bakteriologie, Mikrobiologie Und Hygiene. 1. Abt. Originale. C, Allgemeine, Angewandte Und ökologische Mikrobiologie*, *2*(2), 166–178.

Su, C., Su, L., Li, Y., Long, S. R., Chang, J., Zhang, W., Walker, W. A., Xavier, R. J., Cherayil, B. J., & Shi, H. N. (2018). Helminth-induced alterations of the gut microbiota exacerbate bacterial colitis. *Mucosal Immunology*, *11*(1), 144–157.

Suzuki, T. A., Fitzstevens, J. L., Schmidt, V. T., Enav, H., Huus, K. E., Mbong Ngwese, M.,

Grießhammer, A., Pfleiderer, A., Adegbite, B. R., Zinsou, J. F., Esen, M., Velavan, T. P., Adegnika, A. A., Song, L. H., Spector, T. D., Muehlbauer, A. L., Marchi, N., Kang, H., Maier, L., … Ley, R. E. (2022). Codiversification of gut microbiota with humans. *Science (New York, N.Y.)*, *377*(6612), 1328–1332.

Taniuchi, M., Verweij, J. J., Noor, Z., Sobuz, S. U., van Lieshout, L., Petri, W. A., Jr, Haque, R., & Houpt, E. R. (2011). High throughput multiplex PCR and probe-based detection with Luminex beads for seven intestinal parasites. *The American Journal of Tropical Medicine and Hygiene*, *84*(2), 332–337.

ten Hove, R. J., van Esbroeck, M., Vervoort, T., van den Ende, J., van Lieshout, L., & Verweij, J. J. (2009). Molecular diagnostics of intestinal parasites in returning travellers. *European Journal of Clinical Microbiology & Infectious Diseases: Official Publication of the European Society of Clinical Microbiology*, *28*(9), 1045–1053.

Thauer, R. K., Kaster, A.-K., Seedorf, H., Buckel, W., & Hedderich, R. (2008). Methanogenic archaea: ecologically relevant differences in energy conservation. *Nature Reviews. Microbiology*, *6*(8), 579–591.

Togo, A. H., Grine, G., Khelaifia, S., des Robert, C., Brevaut, V., Caputo, A., Baptiste, E., Bonnet, M., Levasseur, A., Drancourt, M., Million, M., & Raoult, D. (2019). Culture of methanogenic Archaea from human colostrum and milk. *Scientific Reports*, *9*(1), 18653.

Toro-Londono, M. A., Bedoya-Urrego, K., Garcia-Montoya, G. M., Galvan-Diaz, A. L., & Alzate, J. F. (2019). Intestinal parasitic infection alters bacterial gut microbiota in children. *PeerJ*, *7*, e6200.

Triantafyllou, K., Chang, C., & Pimentel, M. (2014). Methanogens, methane and gastrointestinal motility. *Journal of Neurogastroenterology and Motility*, *20*(1), 31–40.

Truong, D. T., Tett, A., Pasolli, E., Huttenhower, C., & Segata, N. (2017). Microbial strain-level population structure and genetic diversity from metagenomes. *Genome Research*, *27*(4), 626–638.

Turner, J.-E., Stockinger, B., & Helmby, H. (2013). IL-22 mediates goblet cell hyperplasia and worm expulsion in intestinal helminth infection. *PLoS Pathogens*, *9*(10), e1003698.

Tyakht, A. V., Kostryukova, E. S., Popenko, A. S., Belenikin, M. S., Pavlenko, A. V., Larin, A. K., Karpova, I. Y., Selezneva, O. V., Semashko, T. A., Ospanova, E. A., Babenko, V. V., Maev, I. V., Cheremushkin, S. V., Kucheryavyy, Y. A., Shcherbakov, P. L., Grinevich, V.

B., Efimov, O. I., Sas, E. I., Abdulkhakov, R. A., … Govorun, V. M. (2013). Human gut microbiota community structures in urban and rural populations in Russia. *Nature Communications*, *4*(1), 2469.

van de Pol, J. A. A., van Best, N., Mbakwa, C. A., Thijs, C., Savelkoul, P. H., Arts, I. C. W., Hornef, M. W., Mommers, M., & Penders, J. (2017). Gut Colonization by Methanogenic Archaea Is Associated with Organic Dairy Consumption in Children. *Frontiers in Microbiology*, *8*, 355.

Vanderhaeghen, S., Lacroix, C., & Schwab, C. (2015). Methanogen communities in stools of humans of different age and health status and co-occurrence with bacteria. *FEMS Microbiology Letters*, *362*(13), fnv092.

van Lieshout, L., & Roestenberg, M. (2015). Clinical consequences of new diagnostic tools for intestinal parasites. *Clinical Microbiology and Infection: The Official Publication of the European Society of Clinical Microbiology and Infectious Diseases*, *21*(6), 520–528.

Verweij, J. J., Blangé, R. A., Templeton, K., Schinkel, J., Brienen, E. A. T., van Rooyen, M. A. A., van Lieshout, L., & Polderman, A. M. (2004). Simultaneous detection of Entamoeba histolytica, Giardia lamblia, and Cryptosporidium parvum in fecal samples by using multiplex real-time PCR. *Journal of Clinical Microbiology*, *42*(3), 1220–1223.

Verweij, J. J., Brienen, E. A. T., Ziem, J., Yelifari, L., Polderman, A. M., & Van Lieshout, L. (2007). Simultaneous detection and quantification of Ancylostoma duodenale, Necator americanus, and Oesophagostomum bifurcum in fecal samples using multiplex real-time PCR. *The American Journal of Tropical Medicine and Hygiene*, *77*(4), 685–690.

Vianna, M. E., Conrads, G., Gomes, B. P. F. A., & Horz, H. P. (2006). Identification and quantification of archaea involved in primary endodontic infections. *Journal of Clinical Microbiology*, *44*(4), 1274–1282.

Wagner, D., & Liebner, S. (2008). Global warming and carbon dynamics in permafrost soils: Methane production and oxidation. In *Soil Biology* (pp. 219–236). Springer Berlin Heidelberg.

Weaver, G. A., Krause, J. A., Miller, T. L., & Wolin, M. J. (1986). Incidence of methanogenic bacteria in a sigmoidoscopy population: an association of methanogenic bacteria and diverticulosis. *Gut*, *27*(6), 698–704.

Weinberger, V., Mohammadzadeh, R., Blohs, M., Kalt, K., Mahnert, A., Moser, S.,

Cecovini, M., Mertelj, P., Zurabishvili, T., Arora, B., Wolf, J., Shinde, T., Madl, T., Habisch, H., Kolb, D., Pernitsch, D., Hingerl, K., Metcalf, W., & Moissl-Eichinger, C. (2025). Expanding the cultivable human archaeome: *Methanobrevibacter* intestini sp. nov. and strain *Methanobrevibacter smithii* "GRAZ-2" from human faeces. *International Journal of Systematic and Evolutionary Microbiology*, *75*(4), 006751.

WHO. (2015). *Investing to Overcome the Global Impact of Neglected Tropical Diseases: Third WHO Report on Neglected Diseases* (pp. P1–P191). WHO Press.

WHO. (2018). *Guideline: Preventive Chemotherapy to Control Soil-Transmitted Helminth Infections in At-Risk Population Groups*. World Health Organization.

WHO. (2023). *Soil-transmitted helminth infections*. https://www.who.int/news-room/fact-sheets/detail/soil-transmitted-helminth-infections

Wibowo, M. C., Yang, Z., Borry, M., Hübner, A., Huang, K. D., Tierney, B. T., Zimmerman, S., Barajas-Olmos, F., Contreras-Cubas, C., García-Ortiz, H., Martínez-Hernández, A., Luber, J. M., Kirstahler, P., Blohm, T., Smiley, F. E., Arnold, R., Ballal, S. A., Pamp, S. J., Russ, J., … Kostic, A. D. (2021). Reconstruction of ancient microbial genomes from the human gut. *Nature*, *594*(7862), 234–239.

Wolff, M. J., Broadhurst, M. J., & Loke, P. 'ng. (2012). Helminthic therapy: improving mucosal barrier function. *Trends in Parasitology*, *28*(5), 187–194.

Yamada, S.-I., Niwa, J.-I., Ishigaki, S., Takahashi, M., Ito, T., Sone, J., Doyu, M., & Sobue, G. (2006). Archaeal proteasomes effectively degrade aggregation-prone proteins and reduce cellular toxicities in mammalian cells. *The Journal of Biological Chemistry*, *281*(33), 23842–23851.

Zou, Y., Pu, L., Guo, A., Li, Y., Liu, Y., Wang, Y., Ding, Y., Du, X., Guo, X., Zhang, S., Cai, X., & Wang, S. (2025). Helminth reshapes host gut microbiota and immunoregulation by deploying an antimicrobial program of innate immunity. *Gut Microbes*, *17*(1), 2496447.

Appendix

Laboratory reagents

Table 4: Laboratory reagents used in this study

Reagent	Manufacturer	Catalogue Number
Agar	VWR International GmbH	9002-18-0
Ampicillin	Carl Roth GmbH	69-52-3
Brain Heart Infusion	Becton Dickinson Pty Ltd	237500
$CaCl_2$	Carl Roth GmbH	A119.1
$CaCl_2$ $2H_2O$	Carl Roth GmbH	5239.2
Chloroform isoamylalcohol (24:1)	Sigma Aldrich GmbH	25666-100ML
$CoCl_2$ $6H_2O$	Alfa Aesar	61500222
$CuCl_2$ $2H_2O$	Carl Roth GmbH	CN82.1
Cycloheximide	VWR International GmbH	66-81-9
EDTA	Carl Roth GmbH	8043.2
Erythromycin	Sigma Aldrich GmbH	114-0708
$FeCl_2$	VWR International GmbH	7705-08-0
Glycylglycine	Carl Roth GmbH	HN74.4
H_3BO_3	Carl Roth GmbH	6943.1
HCl	Carl Roth GmbH	4625.2
KH_2PO_4	Carl Roth GmbH	3904.1
L-Cyteine HCL	Carl Roth GmbH	7048-04-6

B-mercaptoethanol	Sigma Aldrich GmbH	60-24-2
$MgCl_2$ $6H_2O$	Carl Roth GmbH	2189.2
$MnCl_2$	Acros Organics	A0367050
$MnCl_2$ $4H_2O$	Carl Roth GmbH	T881.3
Na_2MoO_4 $2H_2O$	Carl Roth GmbH	0274.1
Na_2SeO_3	Sigma Aldrich GmbH	10102-18-8
$NaCH_3COO$	Carl Roth GmbH	127-09-3
NaCl	Carl Roth GmbH	3957.1
$NaWO_4$ $2H_2O$	Acros Organics	A0365962
NH_4Cl	Carl Roth GmbH	K298.1
$NiCl_2$ $6H_2O$	Carl Roth GmbH	7791-20-0
Phenol: Chloroform isoamylalcohol (25:24:1)	Carl Roth GmbH	A156.3
Resazurin	Sigma Aldrich GmbH	MKBV7955V
Vancomycin	Carl Roth GmbH	1404-93-9
Yeast Extract (BD)	Becton Dickinson Pty Ltd	DIFC212750
$ZnCl_2$	Alfa Aesar	61600242

Laboratory materials

Table 5: Laboratory materials used in this study

Material	**Manufacturer**	**Catalogue Number**
3mm biopsy punch	Bako	33-32-P/25
Agani 23G x 1¼”	Terumo	210315
Agani 27G x ¾”	Terumo	201230
Balch Tube	Ochs Glasgeraetebau	102048
Bunsen burner	Greiner	-

Butyl rubber stoppers	Bellco	BELC2048-11800
Cryo tubes	VWR	479-6840
CryzoTraq™ 5ml 2D Barcoded Cryogenic Vial	Ziath	ZTS-5ECT
Duran® pressure plus 1000ml	Merk	Z674419
Duran® pressure plus 250ml	Merck	Z674397
Duran® pressure plus 500ml	Merk	Z674400
Eppendorf reaction tube 1.5ml	Eppendorf	0030121023
Eppendorf reaction tube 2ml	Eppendorf	0030121686
Falcon™ 15ml	Falcon™	11507411
Falcon™ 50ml	Falcon™	10788561
Glass beads	Sigma Aldrich GmbH	G8772-500G
Injekt®-F 10ml	Braun	20L12C8
Injekt®-F 1ml	Braun	21F24C8
Injekt®-F 20ml	Braun	20L05C8
Injekt®-F 2ml	Braun	21E24C8
Injekt®-F 5ml	Braun	21C15C8
Petri dish 10cm	Sigma Aldrich GmbH	CLS430599
Pipet 1000µl	Eppendorf	3123000063
Pipet 10µl	Eppendorf	3123000020
Pipet 2.5µl	Eppendorf	3123000012
Pipet 200µl	Eppendorf	3123000055
Pipet 20µl	Eppendorf	3123000039

Pipet tips 1000µl	Eppendorf	0030000919
Pipet tips 10µl	Eppendorf	0030000870
Pipet tips 200µl	Eppendorf	0030000870
Whatman™ PURADISC™	GE Healthcare	10462205

Laboratory instruments

Table 6: Laboratory instruments used in this study

Material	**Manufacturer**	**Catalogue Number**
Anaerobic Jars	Raff Grund	S10373
Axio Scope A1	Carl Zeiss	430035-9040-000
Centrifuge 5427 R	Eppendorf	5409000010
Freezer -20°C	Liebherr	Lgex 3410
Freezer -80°C	Fisher scientific	17014127
Heraeus Multifuge X3R	Thermo Fisher Scientific	50117498-6
Ice machine	Scotsman	AF103 VE water
Laboratory Glove Box, UNIlab Pro	MBRAUN	-
MicrobeMeter	Human Technologies	-
Minitron S-II255I	Infora	-
Sola light engine®	AHF AG	-
SRI 8610C Gas Chromatograph	SRI Instruments	-
Thermomixer C	Eppendorf	5382000015